



FUNCTIONAL MATERIALS
& NANOTECHNOLOGIES

Abstract book

Virtual Vilnius, Lithuania,
23 - 26 November, 2020

ACKNOWLEDGEMENTS

The organizers would like to thank the following companies and institutions for generous support.

Sponsors



Taylor & Francis Group
an **informa** business



**LIGHT
CONVERSION**

Partners



TABLE OF CONTENTS

Conference Committees	5
Scientific Programme	6
List of Oral Presentations	7
List of Posters.....	10
Plenary & Invited Abstracts	15
Oral Abstracts.....	32
Poster Abstracts.....	71
Index	183

WELCOME WORD



Dear Colleagues,

FM&NT-2020 will be held in Vilnius, Lithuania, on November 23 – 26, 2020. We warmly welcome all participants and guests who will attend the 13th international conference Functional Materials and Nanotechnologies 2020 – FM&NT2020. The FM&NT conference series was started in 2006 by scientists of the Institute of Solid State Physics, University of Latvia. Since 2013 FM&NT conferences turned over a new page – becoming a common conference of all three Baltic countries. Now it is being organized periodically by the ISSP of University of Latvia, University of Tartu, and Vilnius University. This conference bringing together researchers from the Baltic states and whole world. The warm and open atmosphere of this scientific conference has turned it into event where people from rather different research fields meet under the common name functional materials and nanotechnology. It is particularly important for early stage scientists who are looking for new knowledge and contacts with other researchers to build up own network. We are happy that succeeded bringing graduate students from Baltic and other countries together. In year 2015, FM&NT conference for first time was in Vilnius. Now, after five years, it's time to “visit” Lithuania again. The conference topics include: Optical materials; Nanocomposites and ceramics; Thin films and coatings; Energy harvesting and storage; Electronic and photonic devices and yet more. The invited speakers from countries closer and further from Lithuania will review a state of art studies in different hot topics. We hope that continuation of the tradition that FM&NT conferences take place each year in different Baltic states will strengthen international cooperation of scientists from all Baltic states and researchers from other countries and increases visibility of research achievements. We invite researchers to take part in this beautiful conference! Due to the ongoing pandemic, we had to cancel the physical conference in Vilnius, Lithuania but nevertheless, we are very pleased to announce that the conference will be organized on November 23-25 as the first all-virtual version of this meeting in order to share our research and stay connected during these insecure times. We are therefore particularly grateful for your contribution to and the participation in the experiment of executing the FM&NT conference as a first full online event in this series. Being aware that scientific exchange and the personal interaction with colleagues and friends is fundamentally important for our profession, an online conference is an important alternative these times. As for any conference, the success of the event depends mostly on the quality of presentations and the commitment of its participants. We hope to offer you a comfortable and exciting online conference environment to enable a successful, inspiring and productive meeting.

Conference Chair

Prof. Jūras Banys

A handwritten signature in blue ink, which appears to be "J. Banys". The signature is fluid and cursive, written over a light blue horizontal line.

CONFERENCE COMMITTEES

International Steering Committee

Prof. Andris Sternbergs, Institute of Solid State Physics, University of Latvia, Latvia
– Chairman

Prof. Jūras Banys, Lithuania

Prof. Antonio Bianconi, Italy

Prof. emeritus Niels Egede Christensen, Denmark

Prof. Robert Evarestov, Russia

Prof. Claes-Göran Granqvist, Sweden

Prof. Marco Kirm, Estonia

Dr. Jiri Kulda, France

Dr. Toomas Plank, Estonia

Dr. Martins Rutkis, Latvia

Local organising committee

Prof. J. Banys (**Chairman**)

Prof. R. Grigalaitis

Dr. M. Kinka

Dr. E. Palaimienė

Dr. Š. Svirskas

Dr. A. Plyushch

Dr. I. Zamaraitė

Dr. S. Balčiūnas

Programme committee

Prof. J. Banys – Chairman

Prof. R. Grigalaitis

Prof. M. Kirm

Dr. A. Sternbergs

Dr. V. Samulionis

Dr. M. Kinka

Dr. E. Palaimienė

Dr. A. Plyushch

SCIENTIFIC PROGRAMME

FM&NT-2020 Programme

November 23 (Monday)

9:00	
10:00	
11:00	
12:00	
13:00	
14:00	Opening
15:00	Session P1 P1 Mangirdas Malinauskas
16:00	Session S1 I1 Sigitas Tamulevičius S1-1 Daniel Vieira S1-2 Ivan Venevtsev S1-3 Andrejs Cesnokovs S1-4 Baiba Berzina S1-5 Kęstutis Staliunas S1-6 Lina Grineviciute
17:00	Session S2 I2 Laima Trinkler S2-1 Ekaterina Vagapova S2-2 Juhan Saaring S2-3 Vitali Nagirnyi S2-4 Ramūnas Nedzinskas S2-5 Ott Rebane
18:00	Break
19:00	Poster session I

November 24 (Tuesday)

9:00	Session P2 P2 Gerd Buntkowsky
10:00	Break
11:00	Session S3 I3 Aldona Balčiūnaitė S3-1 Alexander Vetcher S3-2 Konstantin Glukhov S3-3 Marco Kirm
12:00	Session S4 I4 Robert Evarestov S4-1 Roberts Eglitis S4-2 Yuri Mastrikov S4-3 Amirullah M.Mamedov
13:00	Lunch
14:00	Session S5 I5 Qin Wang S5-1 Andris Šutka S5-2 Anatoly Kravtsov S5-3 Tsung-Ming Tsai
15:00	Session S6 I6 Karol Frohlich S6-1 Vidmantas Gulbinas S6-2 Linas Vilčiauskas S6-3 Simona Pūkienė
16:00	Break
17:00	Session S7 I7 Gunnar Nurk S7-1 Anatoli I.Popov
18:00	Session S8 I8 Gintautas Tamulaitis S8-1 Tigran Akopdzhanyan S8-2 Kęstutis Arlauskas
19:00	Break Poster session II

November 25 (Wednesday)

9:00	Session P3 P3 Mattias Hammar
10:00	Break
11:00	Session S9 I9 Anders Hallen S9-1 Patrik Scajev S9-2 Nikita Derets S9-3 Tatjana Dedova
12:00	Session S10 I10 Andrei Salak S10-1 Ekaterina Politova S10-2 João Cardoso S10-3 Yulian Vysochanskii
13:00	Lunch
14:00	Session S11 I11 Aleksandr Lushchik S11-1 Vytautas Klimavičius S11-2 Evgenij Artsiukh
15:00	Session S12 I12 Jiri Kulda S12-1 Jan Dec S12-2 Vladimir Shur S12-3 Roman Burkovsky
16:00	Break Poster session III
17:00	Closing
18:00	
19:00	

LIST OF ORAL PRESENTATIONS

P1 Mangirdas Malinauskas	Laser 3D Mesoscale Printing: From Renewable Organics to Crystalline Inorganics
I1 Sigitas Tamulevičius	2D Nanoparticle Based Nanostructures – Technology and Applications
S1-1 Daniel Vieira	Continuous corrosion protection via layered double hydroxide UV-degradation
S1-2 Ivan Venevtsev	Influence of In and Ga dopants on structural and scintillating properties of ZnO nanopowders and optical ceramics
S1-3 Andrejs Cesnokovs	Role of interstitial oxygens in Ir-doped ZnO
S1-4 Baiba Berzina	Persistent luminescence properties of doped AlN
S1-5 Kęstutis Staliūnas	Fano Resonances in Nanostructured Thin Films
S1-6 Lina Grineviciute	Deposition of multilayer optical coatings on corrugated surfaces for 2D photonic crystals formation
I2 Laima Trinkler	Luminescence of LiGaO ₂ crystal – mechanisms and potential application
S2-1 Ekaterina Vagapova	Site-selective laser spectroscopy of Nd ³⁺ doped b modification of calcium triphosphate
S2-2 Juhan Saaring	Ultrafast Cross-Luminescence in BaGeF ₆ and K ₂ GeF ₆
S2-3 Vitali Nagirnyi	Up-conversion luminescence in Yb doped Li ₆ Y(BO ₃) ₃ single crystals
S2-4 Ramūnas Nedzinskas	Structural analysis and photoluminescence spectroscopy of rock-salt ZnMgO thin films with high ZnO content
S2-5 Ott Rebane	Photonic solutions for monitoring of pathogen decontamination efficiency
P2 Gerd Buntkowsky	Solid-State-NMR Characterization of functional Materials
I3 Aldona Balčiūnaitė	Formation and investigation of different catalysts for alkaline fuel cells
S3-1 Alexander Vetcher	Metal powder materials with nanomodified oxide coatings and their technical application
S3-2 Konstantin Glukhov	Magnetic ordering in multilayered compounds of M ₁ M ₂ P ₂ X ₆ (M ₁ , M ₂ – Mn, Fe, Cr, Cu; X – S, Se) type
S3-3 Marco Kirm	Challenges in the development of Commercial Analytical Research Organisations in the Baltic Sea region
I4 Robert Evarestov	First-principles study of pressure-induced insulator-to-metal transition in 2D layered compound FePS ₃
S4-1 Roberts Eglitis	Ab initio calculations of ReO ₃ (001) as well as ABO ₃ perovskite (001), (011) and (111) nano-surfaces, interfaces and defects therein
S4-2 Yuri Mastrikov	Modelling of oxygen reduction reaction at solid oxide fuel cell cathode
S4-3 Amirullah M.Mamedov	Slater Insulator Phase of A ₂ (A=Li, Na)IrO ₃ : first principal calculations

I5 Qin Wang	Graphene based nanostructures and nanoparticles for sensing applications
S5-1 Andris Šutka	Revealing polymer contact electrification mechanisms and designing triboelectric nanogenerators
S5-2 Anatoly Kravtsov	Reduction of impurity sources in Si crystal growth system with electron gun beam heating
S5-3 Tsung-Ming Tsai	Characterization of ZnMgO Based Solar-blind Photodetector with Supercritical Fluid Treatment
I6 Karol Frohlich	Preparation and performance of photoanode with thin RuO ₂ - and IrO ₂ -RuO ₂ -based oxide electrocatalysts for water splitting
S6-1 Vidmantas Gulbinas	Organic solar cells: from light absorption to electric power
S6-2 Linas Vilčiauskas	Towards the Understanding of NASICON Structured Systems for the Na-ion Energy Storage
S6-3 Simona Pūkienė	Electro-optical characteristics of NIR light emitting sources
I7 Gunnar Nurk	Operando NAP-HT-XPS and impedance spectroscopy study of pulsed laser deposited Ni-Ce _{0.9} Gd _{0.1} O ₂ -d solid oxide fuel cell electrode
I7a Maxim Ananyev	Surface defect chemistry and ionic transport in oxides with perovskite related structure
S7-1 Anatoli I. Popov	Radiation-Induced Point Defects and Processes in Ionic Oxides – where we are standing now and what we understand better
I8 Gintautas Tamulaitis	Response time as the key functional property of future scintillation materials
S8-1 Tigran Akopdzhanyan	Synthesis of AlON powders and ceramics and their optical and luminescent properties
S8-2 Kęstutis Arlauskas	Synthesis and Photophysical Features of Several (2,4-dinitrophenyl)hydrazones from Various Alicyclic Mono- and Diketones
P3 Mattias Hammar	Nanostructured semiconductor optoelectronics
I9 Anders Hallen	Silicon Carbide Material Development for Semiconductor Power Devices
S9-1 Patrik Scajev	Extension of Spectral Sensitivity of GeSn IR Photodiode after Laser Annealing
S9-2 Nikita Derets	Thermomechanical response of main-chain liquid crystal elastomers with different degrees of crosslinking
S9-3 Tatjana Dedova	Enhanced Photocatalytic Activity of ZnO Nanorods by Surface Treatment with HAuCl ₄ : Synergic Effects Through an Electron Scavenging, Plasmon Resonance and Surface Hydroxylation
I10 Andrei Salak	Field-assisted formed nanostructures of multifunctional 2-D anion exchangers
S10-1 Ekaterina Politova	Structure, ferroelectric and local piezoelectric properties of lead-free KNN- based perovskite ceramics
S10-2 João Cardoso	Phase transitions in the BiFe _{1-x} CrxO ₃ multiferroics
S10-3 Yulian Vysochanskii	Ferroelectricity induced by germanium dopants in quantum paraelectrics in Pb ₂ P ₂ (S,Se) ₆
I11 Aleksandr Lushchik	Accumulation and annealing of structural defects in wide-gap metal oxides under intense radiation of different types
S11-1 Vytautas Klimavičius	DNP enhanced solid-state NMR and its application to investigate novel catalyst

S11-2 Evgenij Artsiukh	Estimation of the degree of antisite disordering of magnetoactive ions in Sr ₂ FeMoO _{6-δ} by means of the intensity of the X-ray peak (101)
I12 Jiri Kulda	What is hidden in the background of Bragg diffraction. Diffuse scattering and PDF analysis not only with neutrons
S12-1 Jan Dec	100 years with ferroelectricity
S12-2 Vladimir Shur	Growth of dendrite domains and superfast domain shape transformation in ferroelectrics
S12-3 Roman Burkovsky	Triggered incommensurate transitions

* *P* – Plenary; *I* – Invited; *S* – Session.

LIST OF POSTERS

P1_1	Olga Demidenko	Corrosion resistance of V4A stainless steel in different seawaters conditions
P1_2	Ligita Valeikiene	Study of Alkaline earth metal substitution effects in sol-gel derived mixed-metal oxides and Mg _{2-x} M _x /Al ₁ (M = Ca, Sr, Ba) layered double hydroxides
P1_3	Sholpan Giniyatova	Synthesis and characteristic of ZnSe ₂ O ₅ nanocrystals
P1_4	Alexander Vetcher	Magnetic properties of materials based on FeNi-50, FeSi and ASC100.29 iron powders with nanomodified coatings
P1_5	Kaspars Kaprans	Nanostructured porous hybrid network of nitrogen-doped carbon as an anode for Li-ion batteries
P1_6	Gintarė Plečkaitytė	Hydro(solvo)thermal synthesis of NASICON-type materials for Na-ion batteries
P1_7	Gintarė Rimkutė	Research toward development of reiterated third generation biosensors using thermally reduced graphene oxide fractions
P1_8	Guntars Vaivars	CO ₂ Adsorption on Copper Catalyst as Enhanced by Ion Liquid
P1_9	Deimante Vaitukaityte	Cross-linkable fluorene-based enamines as hole transporting materials for perovskite solar cells
P1_10	Povilas Luizys	Synthesis and characteristics of organic semiconductors with one, two, three and four carbazolyl chromophores
P1_11	Sarune Daskeviciute	Carbazole-terminated isomeric hole transporting materials for perovskite solar cells
P1_12	Aistė Ilčiukaitė	NEW FLUORENE DERIVATIVES AS HOLE TRANSPORTING MATERIALS FOR EFFICIENT PEROVSKITE SOLAR CELLS
P1_13	Gleb Gorokhov	Method of laser structuring of multiwall nanotube arrays for terahertz applications
P1_14	Roberts Oliņš	Electrochemical exfoliation – streamline method for synthesis of nitrogen doped graphene
P1_15	Žygimantas Vosylius	Scalable Solar Simulators Based on Arrays of Light-Emitting Diodes
P1_16	Guntars Vaivars	Swelling of composite sulfonated polyetheretherketone (SPEEK)/ZrO ₂ membranes in electrolytes
P1_17	Juris Prikulis	Colloidal noble metal nanoparticles deposited on ZnO nanowires
P1_18	Alexander Molnar	Ferroelectric based multi-type energy-harvesting device to power a mobile medical telemetry system
P1_20	Peteris Lesnicenoks	Electrochemical CO ₂ conversion: a method of electrode formation and its composition impact on products
P1_21	Vasili Rubanik	Preparation of Titanium Nickelide Coatings by Hypersonic Metallization
P1_22	Gints Kucinskis	Na ₂ FeP ₂ O ₇ /C cathode for sodium-ion batteries: preparation and electrochemical properties
P1_23	Liva Germane	Prediction of triboelectric series based on polymer physico-chemical properties

P1_24	Monica Susana Campos Covarrubias	Microstructure properties of formed doped barium cerate thin film formed on different alloy substrates
P1_25	Dalius Gudeika	1,8-Naphthalimide-based derivatives for potential optoelectronic devices
P1_26	Leonid Fetisov	Magnetoelectric effect in a planar composite ferromagnet-piezoelectric-meander structure
P1_27	Vytautas Kavaliauskas	Novel Hydrophobic Deep Eutectic Solvents Based on Fluorinated Hydrogen Bond Donors
P1_28	Mantas Norkus	One-Step Phosphor in Glass Synthesis and Characterization
P1_29	Madara Leimane	Low temperature sol-gel synthesis of transparent nanoporous silicon dioxide glass
P1_30	Artis Linarts	Increase in Polymer Triboelectrification by Transition from a Glassy to Rubbery State
P1_31	Maksims Jurinovs	Nanocellulose filled acrylated epoxidized soybean oil inks for UV-assisted 3D printing
P1_32	Sergejs Beluns	Biobased low density and high porosity lignocellulose composite materials from wood and hemp waste
P1_33	Aleksander Prudnik	Electromagnetic shielding material based on porous alumina membranes filled with nickel and carbon-containing needle-punched textile
P2_1	Andrius Pakalniskis	Preparation and investigation of bulk Bi ₃ Fe ₅ O ₁₂
P2_2	Oleg Kiprijanovič	Barkhausen type Pulses during Generation the High Voltage Pulse by PZT Igniters
P2_3	Ekaterina Mikhaleva	Large barocaloric effect at ferroelectric phase transitions in ammonium hydrogen sulfate
P2_4	Fedor Fedulov	Influence of the Ni-PZT composite structure dimensions on characteristics of the magnetoelectric effect
P2_5	Alexander Molnar	The effect of changes in chemical composition and uniaxial compression on the phase transition of CuInP ₂ S ₆ crystals
P2_6	Lyubov Kharkhalis	Structural instability and electron-phonon interaction in the CuInS(Se) ₂ semiconductor-ferroelectrics
P2_7	Alexander A. Grabar	Photorefractive parameters of Sn ₂ P ₂ S ₆ crystals modified by doping, co-doping, and indiffusion
P2_8	Andrew Horvat	Stability and nanocrystalline structure investigation of Se-based chalcogenide glasses
P2_9	Arnoldas Solovjovas	DIELECTRIC PROPERTIES OF THE RELAXOR FERROELECTRIC (1-x)Pb(Zn _{1/3} Nb _{2/3})O ₃ - xPbTiO ₃
P2_10	Miks Jurjans	Electromechanical properties in (0.8Na _{0.5} Bi _{0.5} TiO ₃ -0.2BaTiO ₃)-CaTiO ₃ Solid solutions
P2_11	Edita Palaimiene	Dielectric Investigations of Ba _{0.17} Ca _{0.83} TiO ₃ Ceramic
P2_12	Tomas Kudrevičius	Tape casting and dielectric characteristics of NBYT thick films
P2_13	Liga Bikse	ROLE OF THERMAL TREATMENT IN SURFACE MORPHOLOGY OF NBT-BASED CERAMICS

P2_14	Halyna Klym	Microstructure and free-volume defects in the doped BaTiO ₃ ceramics
P2_15	Yulian Vysochanskii	Dielectric and pyroelectric properties of Sn ₂ P ₂ S ₆ ferroelectrics with double – loop switching
P2_16	Yulian Vysochanskii	Layered GeP ₂ S ₆ , GeP ₂ Se ₆ , GeP ₂ Te ₆ , SnP ₂ S ₆ , SnP ₂ Se ₆ polar crystals with by pressure or chemical composition induced semiconductor – metal transition
P2_17	Aleksey Pashchenko	Influence of Compacting Pressure on the Dielectric Properties of Bismuth Iron Oxide Multiferroic
P2_18	Ramūnas Diliautas	Preparation of BiFe _{1-x} Mn _x O ₃ solid solutions via low temperature sol-gel synthesis route
P2_19	Dovydas Karoblis	Synthesis and characterization of YMnO ₃ -GdMnO ₃ solid solutions via sol-gel method
P2_20	Anatoli I.Popov	In-plane lattice parameters and structural transitions on SrTiO ₃ (001) surface at low temperatures
P2_21	Andrei Karabanov	Synthesis, structure, and dielectric properties of XPbBr ₃ (X=MA, FA, Cs) and Cs ₂ AgBiBr ₆ perovskite single crystals
P2_22	Marija Dunce	Influence of sintering temperature on NBT ceramics
P2_23	Yuri Mastrikov	First principles modelling of water adsorption and dissociation on flat and faceted SrTiO ₃ surfaces
P2_24	Yuri Mastrikov	Band gap engineering of SrTiO ₃ photocatalyst for sunlight-driven water splitting: ab initio simulations
P2_25	Zafer Ozer	Second Harmonic Generation in Generalized Ferroelectric Superlattices
P2_26	Zafer Ozer	Phononic Crystals with Archimedean-like Tiling: Band Structure and Transformation of Sound
P2_27	Husnu Koc	Influence of the Phase Transition on the Mechanical, Electronic and Optical Properties of Sn ₂ P ₂ X ₆ Compounds
P2_28	Igor Djerdj	Rational Sol-Gel-Based Synthesis Design and Magnetic and Dielectric Properties Study of Selected Nanocrystalline Double and Triple Perovskites
P2_29	Andrius Aukštuolis	Charge carriers transport properties in PCPDTBT thin film transistor structures
P2_30	Marina Tretjak	Low frequency noise and resistivity characteristics of epoxy composites with variety of onion-like carbon
P2_31	Tomas Šalkus	Electrical conductivity of superionic (Ag _x Cu _{1-x}) ₇ GeS ₅ I and (Ag _x Cu _{1-x}) ₇ GeSe ₅ I mixed crystals
P2_32	Darya Meisak	The manganese ferrite effect on dielectric properties of MWCNT-based epoxy resin composites
P2_33	R. Merijs-Meri	DEVELOPMENT, CHARACTERISATION AND MODELING OF MECHANICAL PROPERTIES OF THE POLYPROPYLENE COMPOSITES WITH RENEWABLE FILLERS
P2_34	Edita Palaimiene	Dielectric/electric properties of the silver-PDMS nanocomposite

P2_35	Halyna Klym	Adsorption and desorption processes in the modified MgAl ₂ O ₄ ceramics
P2_36	Sintija Eglite	Electro-thermal properties of cross-linked carbon black (CB) and ethylene-vinyl acetate (EVA) composite
P2_37	Povilas Bertasius	Fine Tuning of Electrical Transport and Dielectric Properties of Epoxy/Carbon Nanotubes Composites via Magnesium Oxide Additives
P2_38	Vilma Kavaliukė	Impedance spectroscopy study of some Argyrodite crystals
P2_39	Saulius Daugėla	Temperature dependent structural changes of Na ₂ Mn ₃ (P ₂ O ₇) ₂ phase in NaLiMnP ₂ O ₇ mixed phase compound
P2_40	Erik Cizmar	Multiferroic perovskite BiFeO ₃ -BiZn _{0.5} Ti _{0.5} O ₃ system with the morphotropic phase boundary
P3_1	Greta Inkrataitė	Coats of Cerium, Boron and/or Magnesium Doped Garnets on Different Pallets and Their Luminescence Properties for Scintillators Application
P3_2	Janis Cipa	Improving dosimetric properties of AlN by doping with rare earth metals.
P3_3	Aida Maratova	Effect of a low-temperature deformation on Ex luminescence of KI single crystals
P3_4	Aleksandrs Dutovs	Templated synthesis and optical properties of multilayer porous anodized aluminium oxide – zinc oxide nanostructures for biosensing applications
P3_5	Zhakyp Karipbayev	Structure and luminescent properties of YAG: Ce synthesized ceramic phosphors in radiation fields
P3_6	Rihards Ruska	Luminescence of doped AlN powders
P3_7	Aleksejs Zolotarjovs	Luminescence of undoped ZnO and ZnO:In nanopowders
P3_8	Saulius Miasojedovas	Luminescence properties of ZnMgO with different magnesium composition
P3_9	Julija Grigorjevaite	Luminescence and upconversion luminescence properties of K ₂ Yb _{0.2} Bi _{0.8-x} (PO ₄)(MoO ₄): x Er ³⁺
P3_10	Ernests Einbergs	Chromium doped alumina usability in dosimetry
P3_11	Laurits Puust	Phase Stability and Luminescence Properties of ZrO ₂ :Pr ³⁺ and ZrO ₂ :Pr ³⁺ ,Nb ⁵⁺ Nanophosphors
P3_12	Artūrs Zariņš	In-situ luminescence measurements for advanced ceramic breeder pebbles under the influence of X-rays and \hat{I}^2 -rays
P3_13	Faina Muktepavela	Nanoindentation and fracture characteristics of doped ZnO:In and ZnO: Ga luminescent ceramics
P3_14	Nina Mironova-Ulmane	Fine structure of luminescence spectra of RE ³⁺ ions in single crystals Gd ₃ Ga ₅ O ₁₂
P3_15	Ruta Aukstakojyte	Structural Characterization of Thermally Reduced Graphene Oxide in the Presence of Malonic Acid and Phosphorus Pentoxide

P3_16	Vidmantas Kalendra	EPR SPECTROSCOPY OF MANGANESE DOPED FERROELECTRIC $[\text{NH}_4][\text{Zn}(\text{HCOO})_3]$ FORMATE FRAMEWORK
P3_17	Andris Antuzevics	X-ray defect formation in rare-earth ion doped oxyfluoride glasses
P3_18	Haralds Ozols	Cr^{3+} Paramagnetic probe in LaOCl
P3_19	Jekabs Cirulis	Gadolinium ion incorporation in calcium fluoride oxyfluoride glass ceramics.
P3_20	Gatis Priedītis	Thermal annealing of oxygen-related structural defects in fast-neutron-irradiated aluminium oxide crystals
P3_21	Andris Antuzevics	Paramagnetic defects in neutron irradiated Al_2O_3
P3_22	George Chikvaidze	FTIR spectra of neutron irradiated CVD diamonds
P3_23	Anatoli I.Popov	Case analysis of self-trapped hole V_k center mobility in metal fluorides and fluoroperovskites
P3_24	Natalia Porotnikova	LAMOX functional materials as promising oxygen-ion electrolytes
P3_25	Jevgenijs Gabrusenoks	LATTICE DYNAMICS CALCULATIONS FOR MgO AND $\text{Mg}_{1-x}\text{Zn}_x\text{O}$ SOLID SOLUTIONS
P3_26	Ainars Knoks	Theoretical calculation and spectroscopic measurements of electrocatalytic Cu and Cu/C thin films for CO_2 reduction
P3_27	Sergei Piskunov	First-principles calculations and spectral characterization of $\text{Zn}_{(1-x)}\text{Mg}_x\text{O}$ epilayers
P3_28	Anna Bystrova	Engineering of surface electrical charge of HAp due to its structural imperfections
P3_29	Kirils Surovovs	Modelling of the pedestal growth of silicon crystals
P3_30	Valerii Karpov	First-principles calculations on stability, electronic and phonon properties of monolayers and nanotubes based on gallium monochalcogenides
P3_31	Anuar Aldongarov	Effect of the dipole moment on the formation of trap states in CdS and CdSe quantum dots
P3_33	Davis Zavickis	CHARACTERIZATION OF Co ION OXIDATION STATE AND LOCAL STRUCTURAL DISTORTIONS IN BaCoO_{3-x}
P3_34	Lyubov Kharkhalis	Theoretical simulation of electron-phonon interaction in the indium selenides from the first principles
P3_35	Tetiana Babuka	Electronic and vibrational properties of $\text{TlIn}(\text{S}_{0.75}\text{Se}_{0.25})_2$ crystal: theoretical and experimental study
P3_36	Artyom Plyushch	Conductivity and percolation in carbon nanotubes filled materials: numerical simulations
P3_37	Amirullah M.mamedov	KNbO_3 Based Space-Time Crystal and Dispersion Near Dirac Point
P3_38	Dmitry Bocharov	Ab initio molecular dynamics simulations of transition metal dichalcogenides
P3_39	Iryna Doroshenko	Spectroscopic study of water clusters in nanostructured materials
P3_40	Zhiger Ubaev	Radiation defects in a NaCl matrix with lowered lattice symmetry due to light cation doping and elastic uniaxial deformation

Plenary & Invited Abstracts

Laser 3D Mesoscale Printing: From Renewable Organics to Crystalline Inorganics

E. Skliutas, S. Varapnickas, E. Aleksandravičius, D. Gailevičius,
S. Rekštytė, and M. Malinauskas

Laser NanoPhotonics Group, Laser Research Center, Physics Faculty, Vilnius University, Saulėtekio Ave. 10, Vilnius, Lithuania, EU

mangirdas.malinauskas@ff.vu.lt

The ultrafast laser assisted mesoscale lithography will be introduced by presenting its technological principles, current *state-of-the-art* and potential in 3D printing of diverse materials ranging from biocompatible, biodegradable and renewable organics to amorphous, ceramic and crystalline inorganics [1-3]. Its applications towards prototyping and producing bio-medical implants, micro-optics and nano-photonics as well as creating micro-fluidic sensors will be shown [4-5]. Furthermore, the possibility to employ the technique for precision additive manufacturing out of plant-based resins and pure inorganics will be demonstrated [6,7]. Finally, some unique functional properties of selected prototypes will be provided in detail [8-10].

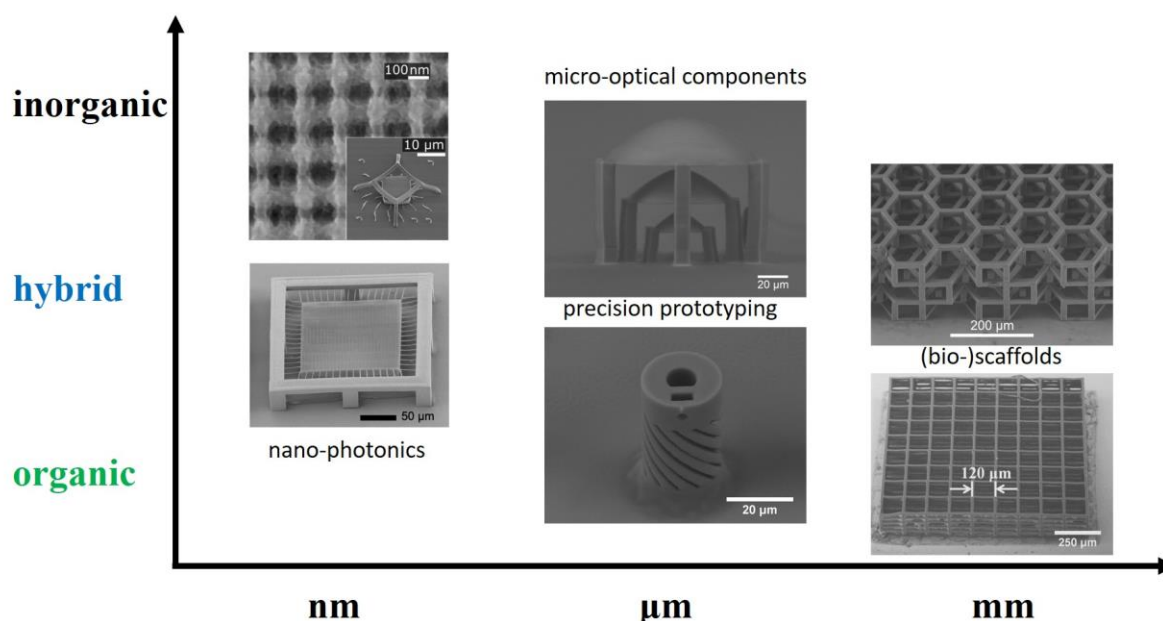


Figure 1. The output of laser 3D mesoscale lithography results in merging nanometer, micrometer and millimetre sized objects out of wide spectrum of materials ranging from pure organic to completely inorganic substances. Insets demonstrate the benchmark objects for nano-photonics, micro-optic, and bio-medical applications.

A financial support from the EU ERDF, through the INTERREG BSR Programme, (ECOLABNET project (#R077)) is kindly acknowledged.

- [1] M. Malinauskas, A. Žukauskas, S. Hasegawa, Y. Hayasaki, V. Mizeikis, R. Buividas, and S. Juodkazis, Ultrafast laser processing of materials: from science to industry, *Light: Sci. Appl.* **5**, e16133 (2016).
- [2] L. Jonušauskas, S. Juodkazis, and M. Malinauskas, Optical 3D printing: bridging the gaps in the meso-scale, *J. Opt.* **20**, 053001, (2018).
- [3] L. Jonušauskas, D. Gailevičius, S. Rekštytė, T. Baldacchini, S. Juodkazis, M. Malinauskas, Mesoscale Laser 3D Printing, *Opt. Express* **27**(11), 15205-15221 (2019).
- [4] J. Mačiulaitis, S. Rekštytė, M. Bratchikov, R. Gudas, M. Malinauskas, A. Pocevičius, A. Ūsas, A. Rimkūnas, V. Jankauskaitė, V. Grigaliūnas, R. Mačiulaitis, Customization of Direct Laser Lithography-based 3D Scaffolds for Optimized *in Vivo* Outcome, *Appl. Surf. Sci.* **487**, 692-702 (2019).
- [5] S. Rekštytė, D. Paipulas, M. Malinauskas, and V. Mizeikis, Microactuation and sensing using reversible deformations of laser-written polymeric structures, *Nanotechnology*, **28**(12), 124001 (2017).
- [6] M. Lebedevaitė, J. Ostrauskaitė, E. Skliutas, M. Malinauskas, Photoinitiator free resins composed of plant-derived monomers for optical 3D μ -printing, *Polymers* **11**(1), 11 (2019).
- [7] E. Skliutas, M. Lebedevaitė, S. Kašėtaitė, S. Rekštytė, S. Lileikis, J. Ostrauskaitė, and M. Malinauskas, Biobased resin for optical 3D printing from macro- to nano-scales, *Nat. Commun.*, **submitted** (2020).
- [8] A. Butkutė, L. Čekanavicius, G. Rimšelis, D. Gailevičius, V. Mizeikis, A. Melninkaitis, T. Baldacchini, L. Jonušauskas, M. Malinauskas, Optical Damage Thresholds of Microstructures Made by Laser 3D Nanolithography, *Opt. Lett.* **45**(1), 13-16 (2020).
- [9] D. Gailevičius, V. Padolskytė, L. Mikoliūnaitė, S. Šakirzhanovas, S. Juodkazis, and M. Malinauskas, Additive-Manufacturing of 3D Glass-Ceramics down to Nanoscale Resolution, *Nanoscale Horiz.* **4**, 647-651 (2019).
- [10] S. Varapnickas *et al.*, Glassy Free-Form Micro-Optics Realized *via* Laser 3D Nanolithography and Calcination, **in preparation** (2020).

Solid-State-NMR Characterization of functional Materials

Gerd Buntkowsky

Institute of Physical Chemistry, Technical University Darmstadt, Alarich-Weiss-Str. 8, D-64287 Darmstadt, Germany

gerd.buntkowsky@chemie.tu-darmstadt.de

Recent results about standard and dynamic nuclear polarization (DNP) enhanced solid-state nuclear magnetic resonance (NMR) spectroscopy on nanostructured and functional materials are reported. The first example reports studies on materials based on crystalline nanocellulose (CNC) or microcrystalline cellulose (MCC), which are used as support material for functionalization or in combination with heterocyclic molecules as ion conducting membranes. The second example reports studies on mixed metal oxides such as V-Mo-W oxides, which are employed as heterogeneous catalyst in bulk-scale production of basic chemicals. The third example reports solid-state NMR studies of lead-free perovskite materials, which are employed as environmentally benign substitution materials for conventional lead-based electronics materials. These materials are discussed in terms of their application and physico-chemical characterization by solid-state NMR techniques, combined with gas-phase NMR and quantum-chemical modelling on the density functional theory (DFT) level. Moreover, the analytic power of the combination of these techniques with DNP for the identification of low-concentrated carbon and nitrogen containing surface species in natural abundance is discussed.

Nanostructured Semiconductor Optoelectronics

Mattias Hammar

Department of Electrical Engineering, Royal Institute of Technology, 16440 Kista, Sweden

hammar@kth.se

The increasing request for internet and advanced networking services as well as other high-end photonics applications put enormous requirements on versatile and high-performance optical components. Nanostructuring may here play an important and enabling role since it allow for precise tuning and optimization of the optoelectronic device properties. However, due to manufacturing complexity and variability it has proven difficult for such device technologies to meet requirements on high-volume fabrication and to reach real-world applications. Here, we review some photonics device developments at our laboratory where nanostructuring is used for extended performance or manufacturability beyond what is achievable with conventional technologies.

At first, we discuss the fabrication of 1.55- μm photonic crystal-confined vertical-cavity surface-emitting lasers in two different configurations, either by direct integration on silicon, resulting in ultra-shallow devices with potential applications in CMOS photonics [1-3], or a bulk InP device designed for very-large area singlemode operation [4]. In the latter case, a major challenge relates to the precise tuning of the metal-organic vapor-phase epitaxy (MOVPE) growth conditions to form perfectly encapsulated cavities in the InP matrix [4].

In a different development, we consider quantum dot (QD)-based single-photon telecommunication-wavelength emitters in the GaAs-system. Using graded InGaAs buffer layer we realize InAs QDs in an In-rich InGaAs metamorphic matrix grown on GaAs substrate and observe narrow and bright micro-photoluminescence emission lines from isolated QDs around 1.55 μm at low temperature [5]. By tuning the MOVPE growth conditions, almost perfectly symmetrical QDs can be realized for minimized fine-structure splitting [6]. These QDs offer an interesting alternative approach to InAs/InP QDs for the realization of single-photon emitters for fiber-based quantum networks for the telecommunication regime.

Besides optical communication, we also address work related to detectors for long-wavelength infrared (LWIR; 8-12 μm) imaging. Such detector elements are presently predominantly realized in the mercury-cadmium-telluride (MCT) system, which offers high performance but suffers from difficult growth and materials properties and thereby high cost, and AlGaAs/GaAs quantum-well infrared photodetectors (QWIPs), which offers excellent manufacturing properties over large wafers and thereby low cost but at compromised performance levels. Here we report on the development of interband quantum dot photodetectors based on spatially indirect transitions in the In(Ga)Sb QD/InAs type-II system to combine the excellent performance of MCT detectors with the manufacturing properties of QWIPs. This approach resembles that of strained-layer quantum-well InAs/GaSb superlattice detectors but with relaxed epitaxial growth complexity [7] and performance advantages due to inherent type II QD properties [8].

- [1] Transfer-printed stacked nanomembrane lasers on silicon, H. Yang, D. Zhao, S. Chuwongin, J.-H. Seo, W. Yang, Y. Shuai, J. Berggren, M. Hammar, Z. Ma, and W. Zhou, *Nature Photonics*, 6, 615–620 (2012)
- [2] Printed Large-Area Single-Mode Photonic Crystal Bandedge Surface-emitting Lasers on Silicon, D. Zhao, S. Liu, H. Yang, Z. Ma., C. Reuterskiöld-Hedlund, M. Hammar, and W. Zhou, *Scientific Reports*, 6, 18860 (2016)
- [3] Buried tunnel junction current injection for InP-based nanomembrane photonic crystal surface emitting lasers on Silicon, C. Reuterskiöld Hedlund, S.-C. Liu, D. Zhao, W. Zhou, and M. Hammar, *Physica Status Solidi A*, 1900527 (2019)
- [4] Buried InP/Air hole Photonic Crystal Surface Emitting Lasers, C. Reuterskiöld Hedlund, J. Martins De Pina, A. Kalapala, S. Yeom, W. Zhou., and M. Hammar, *Compound Semiconductor Week, CSW'2020*, May 17-21, Stockholm, Sweden
- [5] A stable wavelength-tunable triggered source of single photons and cascaded photon pairs at the telecom C-band, K.D. Zeuner, M. Paul, T. Lettner, C. Reuterskiöld Hedlund, L. Schweickert, S. Steinhauer, L. Yang, J. Zichi, M. Hammar, K.D. Jöns and Val Zwiller, *Appl. Phys. Lett.* 112, 173102 (2018)
- [6] An on-demand entangled photon pair source for deployed fiber-based quantum networks, K.D. Zeuner, K.D. Jöns, L. Schweickert, C. Reuterskiöld Hedlund, C. Nuñez Lobato, T. Lettner, K. Wang, E. Schöll, S. Steinhauer, M. Hammar, and V Zwiller, arXiv preprint arXiv:1912.04782
- [7] A performance assessment of type-II interband In_{0.5}Ga_{0.5}Sb QD photodetectors, O. Gustafsson, A. Karim, C. Asplund, Q. Wang, T. Zabel, S. Almqvist, J.Y. Andersson, and M. Hammar, *Infrared Physics & Technology* 61, 319 (2013)
- [8] Auger recombination in In(Ga)Sb/InAs quantum dots, T. Zabel, C. Reuterskiöld Hedlund, O. Gustafsson, A. Karim, J. Berggren, Q. Wang, C. Ernerheim-Jokumsen, J. Weissenrieder, M. Göthelid, and M. Hammar, *Appl. Phys. Lett.* 106 (1), 013103 (2015)

2D Nanoparticle Based Nanostructures – Technology and Applications

Sigitas Tamulevičius, Mindaugas Juodėnas, Domantas Peckus, Tomas Tamulevičius

Institute of Materials Science, Kaunas University of Technology, Baršausko st. 59, Kaunas LT51423, Lithuania

Sigitas.Tamulevicius@ktu.lt

The optical properties metals such as gold (Au), silver (Ag) and copper (Cu) are interesting because they support collective excitations of free electrons called surface plasmons (SPs). SPs generate strong electromagnetic (EM) fields that enable various electro-optical applications in molecular sensing, medical therapy, solar cells, photodetectors, surface-enhanced Raman spectroscopy substrates, ultrafast optical switches, opto-mechanical devices, photocatalysis, nano-antennas and metamaterials [1].

In our research we present optical and opto- mechanical properties of Ag nanocubes (NCs) and Au bipyramids (BPs) synthesized using colloidal chemistry methods [2]. We expand range of the available plasmonic properties to the UV region using Al NPs and compare them with corresponding properties of the noble metallic nanoparticles.

Plasmonic metal nanoparticles arranged in a periodic array can generate a surface lattice plasmon resonance with an extremely high Q-factor. We used the capillary force assisted particle assembly technique [3] to assemble nearly defect-free $>1 \text{ cm}^2$ hexagonal lattices of wet-synthesized Ag cuboctahedra with edge lengths of $123 \pm 2 \text{ nm}$ and a center-to-center spacing of 600 nm. These arrays are large enough to be measured with conventional UV-Vis spectroscopy, which revealed a surface lattice resonance extinction peak with a quality factor 28.6 at orthogonal illumination and up to 62.1 at higher illumination angles. Analysis of the plasmonic modes showed the possibility of the nanoparticles in our arrays to be excited into both in-plane and out-of-plane surface lattice resonance states. The combination of the combination of high aspect ratios of the particles and precise patterning allows us to achieve the highest Q-factors even at normal incidence and an asymmetric environment. The ease of generating ultra-narrow resonances that are still accessible to the surrounding environment should make applications such as nanolasing and biosensing a lot easier.

[1] Tamulevičius, Sigitas; Meškiniš, Šarūnas; Tamulevičius, Tomas; Rubahn, Horst-Günter. Diamond like carbon nanocomposites with embedded metallic nanoparticles // Reports on Progress in Physics. Bristol : 2018, Vol. 81, iss. 2, art. 024501, p. 1-31. DOI: 10.1088/1361-6633/aa966f.

[2] Peckus, Domantas; Rong, Hongpan; Stankevičius, Lukas; Juodėnas, Mindaugas; Tamulevičius, Sigitas; Tamulevičius, Tomas; Henzie, Joel. Hot electron emission can lead to damping of optomechanical modes in core-shell Ag@TiO₂ nanocubes // Journal of Physical Chemistry C. 2017, vol. 121, iss. 43, p. 24159-24167. DOI: 10.1021/acs.jpcc.7b06667

[3] Virganavičius, Dainius; Juodėnas, Mindaugas; Tamulevičius, Tomas; Schiff, H.; Tamulevičius, Sigitas. Investigation of transient dynamics of capillary assisted particle assembly yield // Applied surface science. 2017, vol. 406, p. 136-143. DOI: 10.1016/j.apsusc.2017.02.100.

Luminescence of LiGaO₂ crystal – mechanisms and potential application

L.Trinkler¹, A.Trukhin¹, J.Cipa¹, V.Pankratov¹, B.Berzina¹, Mitch M.C.Chou²,

1- Institute of Solid State Physics, University of Latvia, Kengaraga St.8, Riga, Latvia

2- Center of Crystal Research, Department of Materials and Optoelectronic Science, National Sun Yat-sen University, Kaohsiung, Taiwan

laima.trinklere@cfi.lu.lv

Lithium metagallate LiGaO₂ (LGO) is a wide band ($E_g \sim 6$ eV) material with a wurtzite-derived structure. Noncentrosymmetric lattice of LGO determines peculiarities of luminescence processes in this material, such as presence of polarized luminescence, dependence of luminescence and its excitation spectra on orientation of a crystal and presence of pyroelectric luminescence. The present study reports on luminescence mechanisms in nominally pure LGO crystal grown by the Taiwan author, revealed in photoluminescence (PL), thermoluminescence (TL) and pyroelectric luminescence (PEL). The spectral, kinetic, polarization measurements were implemented under UV, X-ray and synchrotron excitation.

PL emission spectrum consists of several main luminescence bands: 280 nm (4.4 eV), 340 nm (3.65 eV), 540 (2.3 eV) and 700 nm (1.77 eV). The 280 nm emission band is excited in the band-to-band region and in an exciton band in the 200-210 nm region (around 6.0 eV), revealing fine structure, which depends on crystal orientation. Other emission bands have their own excitation bands in the energy gap region, besides all of them are excited in the band-to-band region [1].

The complex study of dependence of spectral properties on intensity of the excitation light and kinetic measurements allowed conclusion that all the PL emission bands of LGO are due to donor-acceptor pair (DAP) recombination, furthermore, the DAPs responsible for the 280 nm band are characterized with the random distribution of the separation distance. Additional information about the recombination process in LGO is obtained from polarization measurements, confirming the complex structure of emission and excitation bands due to anisotropic structure of LGO crystal. Conclusion about the atomistic nature of the DAPs causing the 280 and 340 nm bands: Ga-O and Li_i-O, correspondingly, is based on comparison with the PL of Al₂O₃-Ga and Al₂O₃-Li crystals [2].

We have found that LGO produces the TL response after irradiation with X-rays and UV light in as a sequence of several TL peaks the 80-400 K temperature range. Peculiarities of the UV light-induced TL glow curve and emission spectra speak in favour of delocalized character of the recombination process, causing TL.

For the first time in LGO we have observed PEL - spontaneous light emission from a crystal with the noncentrosymmetric lattice, which occurs when the crystal temperature is varied [3]. In LGO the pyroelectric effect was observed in the form of repeated fast luminescence pulses both at increase and decrease of temperature in the 60-400 K temperature range. Comparison of PEL spectral and kinetic characteristics with those of UV-induced PL and TL allows proposal of the mechanism of the spontaneous PEL, as well as estimation of nonuniform distribution character of the luminescence centres in the LGO crystal.

Besides of the current application of LGO as a substrate for semiconductor epilayers the results of the comprehensive study allows proposal of the additional spheres for possible application of this material such as TL dosimetry and pyroelectric temperature detection.

[1] L.Trinkler, A.Trukhin, B.Berzina, V.Korsaks, P.Ščaev, R.Nedzinskas, S.Tumėnas, M.M.C.Chou, L.Chang, C-A.Li, Luminescence properties of LiGaO₂ crystal. *Optical materials*, 69, pp. 449-459, (2017).

[2] L.Trinkler, A.Trukhin, M.Chou, Comparison of luminescence in LiGaO₂, Al₂O₃-Ga and Al₂O₃-Li crystals. *Latvian journal of physics and technical sciences*, 6, pp. 4-12, (2018).

[3] L.Trinkler, A.Trukhin, J.Cipa, B.Berzina, V.Korsaks, Mitch M.C. Chou, Chu-An Li, Spectral and kinetic characteristics of pyroelectric luminescence in LiGaO₂. *Optical Materials*, 94, pp.15–20, (2019).

The present research has been sponsored from the Latvian Sciences Council Grant No. lzp-2018/1-0361.

Formation and investigation of different catalysts for alkaline fuel cells

A. Balčiūnaitė

Department of Catalysis, Center for Physical Sciences and Technology, Saulėtekio av. 3, LT-10257, Vilnius, Lithuania

aldona.balciunaite@ftmc.lt

The need for electrical energy and transportation systems is rising globally and fuel cells are one of the renewable electricity sources. This study is related to the intensively developing research in the field of fuel cells and nanomaterials and is devoted to the search for new effective materials, which can be used for the development and design of direct alkaline fuel cells.

Herein we propose low-cost and simple approaches for the fabrication of efficient catalysts for direct borohydride hydrogen peroxide ($\text{NaBH}_4\text{-H}_2\text{O}_2$) fuel cells. This work includes the discussion of:

- the use of different support (Ti or Cu) for the fabrication of catalysts;
- the synthesis of catalysts using different methods: electrochemical, electroless metal deposition, and galvanic displacement techniques;
- the characterization of the prepared catalysts and investigation of their electrocatalytic properties;
- the performance of the different catalysts in direct $\text{NaBH}_4\text{-H}_2\text{O}_2$ fuel cell test.

The surface morphology, structure, and composition of the prepared catalysts have been characterized using field-emission scanning electron microscopy (FESEM), inductively coupled plasma optical emission spectroscopy (ICP-OES), whereas the electrocatalytic activity of catalysts has been investigated by cyclic voltammetry and chrono-techniques. The performance of direct $\text{NaBH}_4\text{-H}_2\text{O}_2$ single fuel cell tests has been carried out by employing the prepared catalysts as the anode.

First-principles study of pressure-induced insulator-to-metal transition in 2D layered compound FePS₃

Robert A. Evarestov¹ and Alexei Kuzmin²

¹ Department of Quantum Chemistry, Saint Petersburg State University, Russian Federation

² Institute of Solid State Physics, University of Latvia, Latvia

e-mail: r.evarestov@spbu.ru

Iron thiophosphate (FePS₃) belongs to the newly emerged family of van der Waals (vdW) 2D layered materials and currently attracts much attention due to its remarkable physicochemical and magnetic properties [1]. It has a band gap of 0.5-1.6 eV and exhibits an Ising-type antiferromagnetic ordering below the Néel temperature of about 120 K, which remains down to the monolayer limit [2]. Very recently, it has been experimentally discovered that high pressure can be used to tune FePS₃ properties [3, 4]. It was found by X-ray diffraction that FePS₃ has two high-pressure phases (HP-I and HP-II) in the range from 0 to 35 GPa with the transitions occurring at about 4 and 14 GPa [3, 4]. Moreover, the second transition is accompanied by the loss of magnetic ordering and the band gap collapse, resulting in a metallic state [3, 4]. Recent ab initio calculations [5] have well supported the experimental findings, however, they have not explained the origin of the insulator-to-metal transition (IMT) at 14 GPa in details.

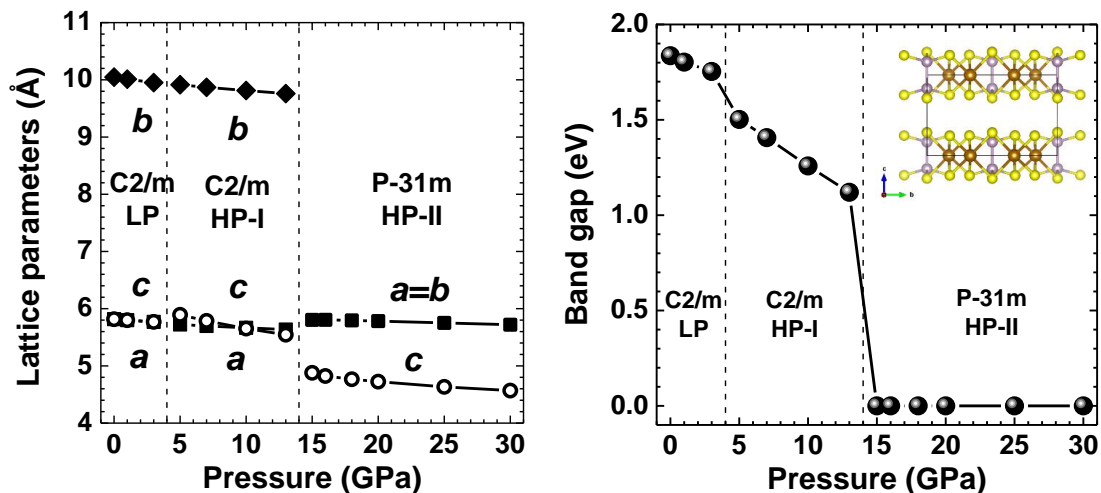


Figure 1 Calculated pressure dependence of the lattice parameters and the band gap for FePS₃.

In this study, we have used first-principles calculations within the periodic linear combination of atomic orbitals (LCAO) method with hybrid Hartree-Fock-DFT B3LYP functional to understand the mechanism of the ITM in FePS₃. Our calculations reproduce correctly the IMT at ~15 GPa, which is accompanied by a reduction of the unit cell volume and the band gap (Figure 1). The detailed analysis of the projected density of states suggests that in low pressure (LP) and HP-I phases the top of the valence bands is formed mainly by the 3d(Fe) and 3p(S) states, whereas the bottom of the conduction band originates mainly from the 3d(Fe), 3p(P), and 3p(S) states. The increase of pressure induces displacements of phosphorus atoms along the *c*-axis direction that affects strongly the contribution of the 3p(P) states around the Fermi level and leads to a collapse of the band gap in the HP-II phase.

[1] F. Wang, T.A. Shifa, P. Yu, P. He, Y. Liu, F. Wang, Z. Wang, X. Zhan, X. Lou, F. Xia, J. He, New frontiers on van der Waals layered metal phosphorous trichalcogenides, *Adv. Funct. Mater.* 28, 1802151 (2018).

[2] J.-U. Lee, S. Lee, J. H. Ryoo, S. Kang, T. Y. Kim, P. Kim, C.-H. Park, J.-G. Park, H. Cheong, Ising-type magnetic ordering in atomically thin FePS₃, *Nano Lett.* 16, 7433-7438 (2016).

[3] C. R. S. Haines, M. J. Coak, A. R. Wildes, G. I. Lampronti, C. Liu, P. Nahai-Williamson, H. Hamidov, D. Daisenberger, S. S. Saxena, Pressure-induced electronic and structural phase evolution in the van der Waals compound FePS₃, *Phys. Rev. Lett.* 121, 266801 (2018).

[4] Y. Wang, J. Ying, Z. Zhou, J. Sun, T. Wen, Y. Zhou, N. Li, Q. Zhang, F. Han, Y. Xiao, et al., Emergent superconductivity in an iron-based honeycomb lattice initiated by pressure-driven spin-crossover, *Nature Commun.* 9, 1914 (2018).

[5] Y. Zheng, X.-x. Jiang, X.-x. Xue, J. Dai, Y. Feng, Ab initio study of pressure-driven phase transition in FePS₃ and FePSe₃, *Phys. Rev. B* 100, 174102 (2019).

Graphene based nanostructures and nanoparticles for sensing applications

Qin Wang

Department of Smart Hardware, Research Institutes of Sweden AB (RISE)

Box 1070, SE-16440 Kista, Sweden

qin.wang@ri.se

Abstract

Sensors are widely used in our daily life, and further development and improvement of current sensing technologies are continually demanded. They are driven by applications and markets in various areas including good health and wellbeing, green energy, sustainable cities, as well as promotion of industry innovation and infrastructure worldwide. As atomically thick monolayer with remarkable optoelectronic tunability, graphene and its derived materials have shown unique potential as a tunable platform to enable new functionalities of various desired sensors.

This talk presents an overview of the graphene-related R&D work at RISE with focus upon three objectives for sensing applications: graphene materials, including large area graphene, chemically synthesized graphene oxide (GO), reduced graphene oxide (RGO) and graphene quantum dots (or carbon nano particles); design and fabrication of the graphene devices, especially on their multiplexed sensing capability for detection of different targets on a miniature integrated chip; and analyses of sensing mechanisms. The challenges faced by the current graphene-based sensors along with some of the probable solutions and their future opportunities will be also briefly addressed.

Two sensor examples are highlighted. One of them is the development of cost-effective onsite crime-scene analysis tools for detection of narcotics/explosives and age determination of biological traces. The idea is to bridge science fiction and reality for crime scene investigation by joint effort from the sensor technology researchers and forensic scientists. Another work is graphene-based plasmonic structures to sense CO₂ and/or alcohol in IR regimes. It is well known that it is challenging to define nano structures in large areas, but the work has proceeded at a good pace and also benefits from collaborations with the Institute of Solid-State Physics (ISSP), Latvia, within the frame of the EU CAMART2 project, <https://www.camart2.com/>. The outcome of the work will help to provide joint offer(s) within the Riga-Stockholm (RIX-STO) collaboration and technology transfer platform to industrial and academic partners.

RIX-STO involves all aspects of the activities within CAMART² relevant for the research, technology transfer, education and investments. The RIX-STO aims to increase the scientific collaboration between research partners from Latvia and Sweden but also to develop collaboration with other countries, to promote the mobility of students and researchers between partner organisations, and to encourage the sharing of research infrastructure and maximize the impact on the industrial growth in the region.



Qin, Wang received Licentiate and Ph.D. degrees in solid state physics at Lund University in Sweden, in 1996 and 1999, respectively. Her research fields at Lund focused on electron transport physics in nanoelectronic devices based on quantum dots and quantum wires.

Now she is a senior expert at RISE and an adjunct Professor at KTH working on high performance optoelectronic devices/sensors based on various nano materials including graphene for imaging, life-science and optical communication applications.

Preparation and performance of photoanode with thin RuO₂- and IrO₂-RuO₂-based oxide electrocatalysts for water splitting

**K. Fröhlich^{1,2}, M. Mikolášek³, P. P. Sahoo¹, K. Hušková^{1,2}, P. Ondrejka³,
V. Řeháček³, L. Harmatha³**

1- CEMEA SAS, Dúbravská cesta 5807/9, 841 04, Bratislava, Slovakia

2- Institute of Electrical Engineering SAS, Dúbravská cesta 9, 841 04, Bratislava, Slovakia

3- Institute of Electronics and Photonics, Slovak University of Technology, Ilkovičova 3, 812 19 Bratislava, Slovakia

Main author address: karol.frohlich@savba.sk

Water splitting to oxygen and hydrogen under sun light using a semiconductor photoanode has attracted lot of interest since its discovery [1]. Many types of photoelectrochemical cells were studied and developed up to now. Unfortunately, water splitting is still not ready for practical application because of insufficient performance of the materials used.

We report on properties of a metal-insulator-semiconductor photoanode for water splitting comprising a thin RuO₂ and RuO₂-IrO₂ films as a top catalytic layers. RuO₂ and IrO₂ offer low resistivity, high optical transparency, work function as well as high catalytic efficiency [2]. RuO₂ and IrO₂ films with the thickness 5 nm were grown using liquid injection metal organic chemical vapour deposition, MOCVD [3]. Thin SiO₂ layer was prepared by ozone treatment of the Si-n substrate at 300 °C. RuO₂/SiO₂/n-Si photoanode exhibited a photovoltage of 0.5 V and was able to generate photocurrent with a density up to 10 mA/cm² at a thermodynamic water oxidation potential (1.23 V vs. reversible hydrogen electrode, RHE) in H₂SO₄, pH=0 solution. Slightly lower photovoltages and photocurrents were achieved in Na₂SO₄, (pH=6), and KOH (pH=14) solutions.

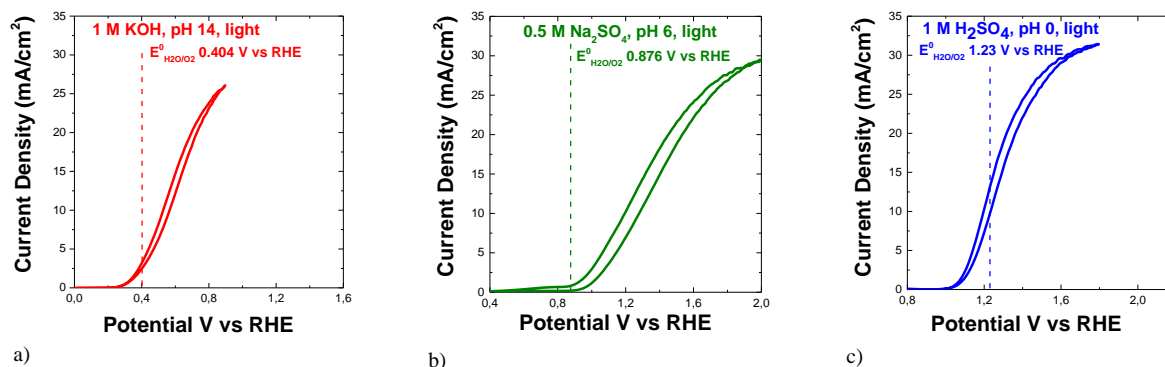


Figure 1 Cyclic voltammograms of the RuO₂/SiO₂/n-Si photoanode in a) 1M KOH, b) 0.5 M Na₂SO₄ and c) 1M H₂SO₄ solutions.

Stability of the RuO₂/SiO₂/n-Si photoanode was examined in 1 M H₂SO₄, 0.5 M Na₂SO₄ and 1 M KOH solutions. The RuO₂/SiO₂/n-Si photoanode in the 1M H₂SO₄ solution showed current density of 10 mA/cm² under applied voltage of 1.23 V vs. RHE. Degradation occurred after 1.5 h operation. Higher applied voltage 1.5 V (0.27 V above the thermodynamic water splitting potential) resulted in faster degradation. The RuO₂/SiO₂/n-Si photoanode was found to be more stable in the KOH solution. Using applied voltage of 0.674 V vs. RHE (0.27 V above the thermodynamic water splitting potential) in 1M KOH resulted in current density of 2 mA/cm² after 10 h. The current density decreases to 1.4 mA/cm² v after 24 h. It is shown, that stability of the photoanode can be further increased by alloying RuO₂ with IrO₂.

This study was performed during the implementation of the project Building-up Centre for advanced materials application of the Slovak Academy of Sciences, ITMS project code 313021T081 supported by Research & Innovation Operational Programme funded by the ERDF. The research was funded also by APVV (project APVV-17-0169).

- [1] Fujishima, A.; K. Honda, K. Electrochemical Photolysis of Water at a Semiconductor Electrode. *Nature* **1972** 238, 37-38.
- [2] M. Mikolášek, K. Fröhlich, K. Hušková, J. Racko, V. Rehacek, F. Chymo, M. Tapajna, L. Harmatha, Silicon based MIS photoanode for water oxidation: A comparison of RuO₂ and Ni Schottky contacts, *Appl. Surface Science*, 461, pp. 48-53, (2018).
- [3] K. Fröhlich, V. Cambel, D. Machajdík, P. K. Baumann, J. Lindner, M. Schumacher, H. Juergensen, Low-temperature growth of RuO₂ films for conductive electrode applications, *Mater. Science Semicond. Processing*, 5, 173-177 (2003).

***Operando* NAP-HT-XPS and impedance spectroscopy study of pulsed laser deposited Ni-Ce_{0.9}Gd_{0.1}O_{2-d} solid oxide fuel cell electrode**

Gunnar Nurk¹, Kuno Kooser^{2,4}, Ove Korjus¹, Rait Kanarbik¹, Samuli Urpelainen³, Tanel Käämbre², Urmas Joost², Mati Kook², Margus Kodu², Priit Möller¹, Indrek Kivi¹, Mihkel Vestli¹, Jean-Jacques Gallet⁵, Edwin Kukk⁴, Enn Lust¹

1-University of Tartu Institute of Chemistry, Ravila 14a Street, Tartu 50411, Estonia

2-University of Tartu, Institute of Physics, W. Ostwald Str. 1, 50411 Tartu, Estonia

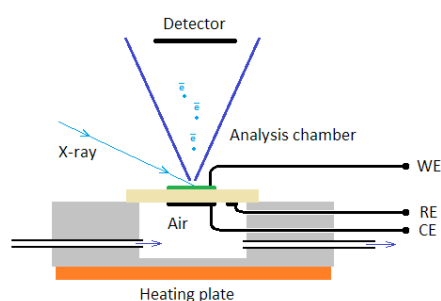
3-Lund University, MAX IV Laboratory, Box 118, 22100 Lund, Sweden

4-University of Turku, Department of Physics and Astronomy, 20014 Turku, Finland

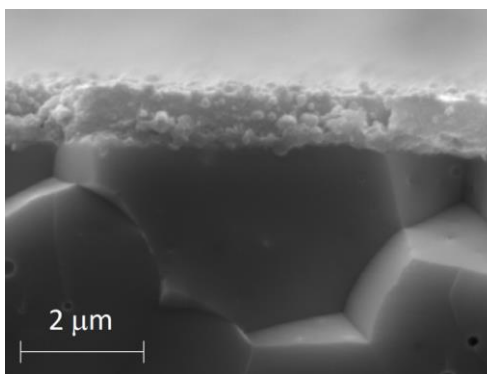
5-Synchrotron-Soleil, L'orme des Merisiers, Saint Aubin—BP48 91192, Gif-sur-Yvette Cedex, France

gunnar.nurk@ut.ee

Detailed chemical information from electrode surfaces at operating conditions is essential for rational development of solid oxide cell (SOC) electrodes but so far, because of harsh operating conditions very little is known about mechanistic aspects of surface reactions as well as surface thermodynamics at SOC electrodes under electrochemical reaction conditions [1,2]. Spectroelectrochemistry, i.e. spectroscopic (x-ray absorption, x-ray photoelectron spectroscopy (XPS) and Raman spectroscopy) characterization of operating electrode at electrochemically controlled conditions is very promising approaches for characterization of surface properties like oxidation states, surface polarization, surface coverage with adsorbate, etc. at real or almost real working conditions. In previous studies single chamber (SC) two-electrode *in situ* near ambient pressure (NAP) XPS has been applied to monitor different aspects of some SOFC electrode materials [3]. This study present results of *operando* high temperature (HT)-NAP-XPS spectroelectrochemical measurements of pulsed lased deposited thin film Ni- Ce_{0.9}Gd_{0.1}O_{2-δ} electrode using novel three electrode dual-chamber spectroelectrochemical cell, at H₂ and CO environments and at different cell loads at 650 °C.



(a)



(b)

Figure 1. (a) A schematic drawing of the dual-chamber three-electrode HT-NAP-XPS spectroelectrochemical cell and (b) SEM micrograph of the studied Ni-GDC PLD anode.

Change on redox state of surface Ni and Ce atoms has been observed as a function of chemical nature of used fuel. Chemical nature of electrode surface is dominantly defined by gas environment – chemical nature and concentration of gas. Changes in oxidation state of electrode surface atoms caused by electrode polarization, i.e. oxide ion flux through the membrane are negligible but changes in simultaneously measured electrochemical impedance are significant.

[1] M.L Liu, et al., *Materials Today*, 14 (2011) 534-546.

[2] A. Atkinson, et al., *Nature Materials*, 3 (2004) 17-27.

[3] C.J. Zhang, et al., *Nature Materials*, 9 (2010) 944-949.

Surface defect chemistry and ionic transport in oxides with perovskite related structure

Maxim Ananyev

Institute of High Temperature Electrochemistry of the Ural Branch of the RAS, 20 Akademicheskaya, Yekaterinburg, Russia, 620137

m.ananyev@mail.ru

Mass transfer between the gas phase and oxide materials play an important role in different electrochemical applications (solid oxide and protonic ceramic fuel cells and electrolysis cells, electrochemical exchange reactors etc) and catalytical systems. In this contribution oxygen and hydrogen transfer and surface exchange are considered taking into account defect formation both in the bulk and on the surface of the oxide materials. Parameters of oxygen and hydrogen surface exchange and diffusivities have been determined by means of $^{16}\text{O}/^{18}\text{O}$ and H/D isotope exchange method with gas phase equilibration. It was shown that rate-determining stage of the oxygen surface exchange is caused by the defect chemistry of the outermost layer of the oxides based on cobaltites and nikelites of lanthanides. Protonic defects, local ordering-disordering as well as nano-scale domain structure play an important role in surface exchange and diffusivity of hydrogen in protonic conducting oxides based on lanthanum scandate, Fig. 1.

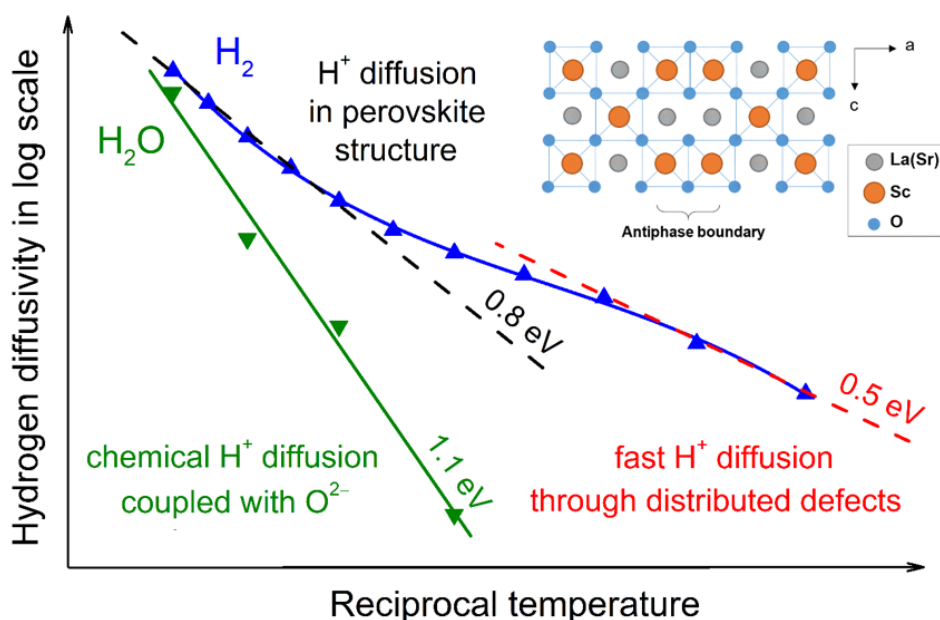


Figure 1 Nanostructured LaScO_3 based oxides demonstrating self-organized defects and related peculiarities in hydrogen diffusivity

- [1] M.I. Vlasov, V.M. Zainullina, M.A. Korotin, A.S. Farlenkov, and M.V. Ananyev. Effect of proton uptake on the structure of energy levels in the band-gap of Sr-doped LaScO_3 : diffuse reflectance spectroscopy and coherent potential approximation calculations. *Physical Chemistry and Chemical Physics*, 21, 7989-7995, (2019).
- [2] E. Tropin, M. Ananyev, N. Porotnikova, A. Khodimchuk, S. Saher, A. Farlenkov, E. Kurumchin, D. Shepel, E. Antipov, S. Istomin, and H. Bouwmeester. Oxygen surface exchange and diffusion in $\text{Pr}_{1.75}\text{Sr}_{0.25}\text{Ni}_{0.75}\text{Co}_{0.25}\text{O}_{4-\delta}$. *Physical Chemistry and Chemical Physics*, 21, 4779-4790, (2019).
- [3] E.S. Tropin, M.V. Ananyev, A.S. Farlenkov, A.V. Khodimchuk, A.V. Berenov, A.V. Fetisov, V.A. Eremin, and A.A. Kolchugin. Surface defect chemistry and oxygen exchange kinetics in $\text{La}_{2-x}\text{Ca}_x\text{NiO}_{4+\delta}$. *Journal of Solid State Chemistry*, 262, 199-213, (2018).
- [4] M.V. Ananyev, A.S. Farlenkov, and E.Kh. Kurumchin. Isotopic exchange between hydrogen from the gas phase and proton-conducting oxides: Theory and experiment. *International Journal of Hydrogen Energy*, 43(29), 13373-13382, (2018).
- [5] M.V. Ananyev, V.A. Eremin, D.S. Tsvetkov, N.M. Porotnikova, A.S. Farlenkov, A.Yu. Zuev, A.V. Fetisov, and E.Kh. Kurumchin. Oxygen isotope exchange and diffusion in $\text{LnBaCo}_2\text{O}_{6-\delta}$ ($\text{Ln}=\text{Pr, Sm, Gd}$) with double perovskite structure. *Solid State Ionics*, 304, 96-106, (2017).
- [6] A.S. Farlenkov, A.G. Smolnikov, M.V. Ananyev, A.V. Khodimchuk, A.L. Buzlukov, A.V. Kuzmin, and N.M. Porotnikova. Local disorder and water uptake in $\text{La}_{1-x}\text{Sr}_x\text{ScO}_{3-\delta}$. *Solid State Ionics*, 306, 82-88, (2017).

Response time as the key functional property of future scintillation materials

G. Tamulaitis¹, E. Auffray², M. Korzhik³, S. Nargelas¹, A. Vaitkevičius¹

1- Institute of Photonics and Nanotechnology, Vilnius University, Saulėtekio al. 3, Vilnius, Lithuania

2- CERN, Switzerland

3- Research Institute for Nuclear Problems, Minsk, Belarus

gintautas.tamulaitis@ff.vu.lt

For decades, the Olympic motto *Citius, Altius, Fortius* might also have been approved as a motto of the development of scintillators, since faster response, higher light yield, and stronger radiation tolerance have been the key properties sought for in the application of scintillating materials in radiation detectors. Currently, the fast luminescence response steps forward as the key challenge in view of the application of scintillator-based radiation detectors in future high-energy physics experiments with high luminosity and in medical imaging with substantially better spatial resolution and full-body scanning capability. The ambitious target of 10 picoseconds for the time resolution of radiation detectors, which has been formulated a few years ago [1] and is being promoted by the Crystal Clear Collaboration at CERN, turns out to be increasingly on demand and more and more realistic. There are two routes to follow the 10 ps challenge. The first one is the development of completely novel detection concepts. The detection based on hot intraband luminescence, cross-luminescence and Cherenkov radiation are fast enough but suffer from basically weak response signal, all-optical detection, e.g., by exploiting free carrier absorption encounter readout difficulties. This presentation focuses on the second route: search for novel scintillating materials or improving the timing properties of the scintillators already in use.

The new benchmark in the luminescence response time of scintillators requires novel techniques for characterization of the new scintillators in picosecond and subpicosecond domains. For decades, the transient absorption (TA) technique is being fruitfully exploited in the study of various semiconductors and semiconductor structures. Recently, we succeeded in productive adoption of this technique in the study of fast processes in scintillators. The measurement of time evolution of differential absorption in pump and probe configuration enables selective excitation of targeted structural elements by using the pump of variable wavelength, whereas the time resolution in these measurements is limited just by the laser pulse duration, thus, might be even in femtosecond domain.

Two types of Ce-doped scintillators have been shown to be prospective for fast scintillation detectors. In garnet type scintillators, $\text{Gd}_3\text{Al}_2\text{Ga}_3\text{O}_{12}:\text{Ce}$ (GAGG:Ce) [2,3] is currently selected as the most prospective candidate for future applications, whereas $\text{Lu}_{2(1-x)}\text{Y}_{2x}\text{SiO}_5:\text{Ce}$ (LYSO:Ce) [4] is currently the first candidate in the family of oxyorthosilicate crystals. Theoretical study of the luminescence response time [3,4] and the comparison of the results obtained by TA and coincidence time resolution techniques [2-4] showed that the key factor limiting the luminescence response time is the excitation transfer to the activator ion, which is strongly affected by electron trapping. It is demonstrated that the TA measurements might be successfully exploited to study the transfer. The study showed that the transfer time might be improved by aliovalent doping even at low concentrations of the aliovalent ions, enabled us to determine certain rate constants characterizing the luminescence response time, and demonstrated the influence of electron trapping at conduction band bottom fluctuations due to random variations in composition in mixed crystals, both garnets and oxyorthosilicates.

[1] P. Lecoq, M. Korzhik, A. Vasiliev, Can Transient Phenomena Help Improving Time Resolution in Scintillators, *IEEE Trans. Nucl. Sci.* 61, 229–234 (2014).

[2] G. Tamulaitis, G. Dosovitskiy, A. Gola, M. Korzhik, A. Mazzi, S. Nargelas, P. Sokolov, and A. Vaitkevičius, Improvement of response time in GAGG:Ce scintillation crystals by magnesium codoping, *Journal of Applied Physics* 124, 215907 (2018).

[3] G. Tamulaitis, A. Vasil'ev, M. Korzhik, A. Mazzi, A. Gola, S. Nargelas, A. Vaitkevičius, A. Fedorov, and D. Kozlov, Improvement of the time resolution of radiation detectors based on $\text{Gd}_3\text{Al}_2\text{Ga}_3\text{O}_{12}$ scintillators with SiPM Readout, *IEEE Trans. Nucl. Sci.* 66, 1879 (2019).

[4] G. Tamulaitis, E. Auffray, A. Gola, M. Korzhik, A. Mazzi, V. Mechinski, S. Nargelas, Y. Talochka, A. Vaitkevičius, A. Vasil'ev, Improvement of the timing properties of Ce-doped oxyorthosilicate LYSO scintillating crystals, *J. Phys. Chem. Solids*, 139, 109356 (2020).

Silicon Carbide Material Development for Semiconductor Power Devices

Anders Hallén

*KTH Royal Institute of Technology, School of EECS
P.O. Box Electrum 229, SE 164 40 Kista-Stockholm, Sweden*

ahallen@kth.se

Silicon carbide has been recognized for many years as an interesting semiconductor material for electronic applications. Improvement of substrate quality and size, in combination with the development of epitaxial growth techniques, eventually made it possible to realize device grade wafers of sufficient diameters to make fabrication of commercial power devices feasible. Today, Schottky diodes and MOSFETs, available from an increasing number of vendors, are taking market shares from silicon power devices, not only in the higher voltage ranges, but also for lower voltages. This presentation will address some of the main road blocks for this journey and how the obstacles could be overcome to make the story of silicon carbide power devices so successful.

The two key material parameters that raised the interest in silicon carbide for power devices are the high thermal conductivity (about 3 times better than silicon) and large dielectric strength (almost 10 times higher than that of silicon). These two parameters are vital for power devices and results in lower switching and on-state losses and much reduced cooling need. The commercial devices now developed are all made from the 4H-SiC polytype, which is the one with the largest bandgap and the highest dielectric strength, although early in the development it was the 6H polytype that was favoured. This was mainly due to difficulties to grow large diameter 4H substrates of high quality, but things improved with the introduction of the seeded sublimation growth introduced in 1978 by Tairov and Tsvetkov [1]. For high voltage devices, a thicker low doped high-quality layer is needed to support the reverse bias. This layer is produced by epitaxial techniques on top of the high-doped substrate. Successive improvements in chemical vapour deposition (CVD) techniques led to significant better doping control, larger wafer diameters, and fewer structural defects, for instance, the hot wall CVD introduced at Linköping University, Sweden [2]. Also, regarding processing of the wafers into devices several improvements and adaption of previous, mainly Si-based, technologies have been needed. This is particularly true for the introduction of dopants by ion implantation, which is the only viable technique to form 3-dimensional regions of n- or p-type, since diffusion of main dopant elements requires extreme temperatures [3,4]. While the quality of material and processes today are sufficient to produce devices that can successfully compete with silicon devices, there are still issues to be improved, for instance the charge carrier lifetimes in the epitaxial layers needed for high voltage bipolar devices, and also the quality of the SiO₂/4H-SiC interface.

- [1] Advanced Silicon Carbide Devices and Processing, Eds. S. Saddow and F. La Via, IntechOpen 2015, ISBN 978-953-51-2168-8
- [2] O. Kordina, C. Hallin, A. HenryP. Bergman, I. Ivanov, A. Ellison, N.T. Son, E. Janzén, Phys. Stat. Sol. B 202 321-334 (1997)
- [3] Advances in Silicon Carbide Processing and Applications, Eds. S. Saddow and A. Agarwal, Artech House 2006, ISBN1-58053-740-5, pp 120-146
- [3] A. Hallén, M.K. Linnarsson, Surface & Coating Technology 306, p.190 (2016)

Field-assisted formed nanostructures of multifunctional 2-D anion exchangers

**A.N. Salak¹, D.E.L. Vieira¹, A.V. Fedorchenko², E.L. Fertman², R.Yu. Babkin³,
Yu.G. Pashkevich³, E. Čížmár⁴, A. Feher⁴, J.M. Vieira¹**

1- Department of Materials and Ceramics Engineering, CICECO – Aveiro Institute of Materials, University of Aveiro, Aveiro 3810-193, Portugal

2- B. Verkin Institute for Low Temperature Physics and Engineering of NASU, Kharkiv 61103, Ukraine

3- O. Galkin Donetsk Institute for Physics and Engineering of NASU, Kyiv 03680, Ukraine

4- Institute of Physics, Faculty of Science, P.J. Šafárik University in Košice, Košice 04154, Slovakia

salak@ua.pt

Owing to unique combinations of functionalities, 2-D nanomaterials find a variety of important applications, such as optoelectronics, catalysis, energy storage and conversion, sensing [1].

Layered double hydroxides (LDHs) also known as anion-exchange clays represent a numerous family of promising 2-D materials. LDHs are composed of parallel layers of the mixed metal M' - M'' hydroxides, in which the oxygen octahedra MO_6 are edge-linked. The thickness of the hydroxide layer does not exceed 0.5 nm, while the interlayer height can be changed from about 0.3 nm to few nanometres depending on size, charge and arrangement of the intercalated anions [2].

Magnetic ordering in the LDHs containing at least one of the cations Co^{2+} , Ni^{2+} , Fe^{3+} , Mn^{3+} as M' and/or M'' was found to occur at very low temperatures that makes unlikely a direct practical exploration of their magnetic properties. However, the dependence of their magnetic behaviour on the cation content and ratio as well as on the interlayer distance can be used in development of hybrid magnets and other functional materials [3,4].

Here we report on a systematic study of magnetic properties Co^{2+} - Al^{3+} LDHs with the cobalt-to-aluminium ratio, $Co/Al=2$, and intercalated with different organic and inorganic anions compositions, which resulted in the layered compositions with the interlayer height values in a range between about 0.3 and 1.2 nm.

Thin transparent films were formed from ordered crystallites of those LDHs precipitated from diluted suspensions on a horizontally oriented substrate in magnetic field directed either perpendicular or parallel to the substrate plane. A mechanism of the field-assisted film formation has been suggested.

Characteristic parameters of magnetic properties and heat capacity of the LDH samples studied between 1.8 and 300 K in a wide range of magnetic fields were analysed and correlated with their interlayer height values.

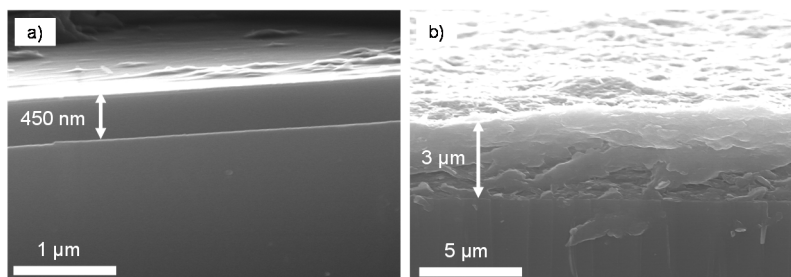


Figure 1 SEM images (cross section views) of layers of the Co_2Al-NO_3 LDH crystallites deposited on glass substrates: (a) with application of an external magnetic field and (b) without magnetic field. The field was perpendicular to the horizontally oriented substrate [5].

This work was supported by the Slovakia-Portugal bilateral project FAST-LDH (2019-2020). The authors also acknowledge the Belarus-Ukraine project "Effect of magnetic field and ultrasound on the anion-exchange properties of iron- and cobalt-containing layered double hydroxides" (2020-2021), grants N0120U000216/T20YKA-020. D.E.L.V. is grateful to the AdvAMtech PhD programme for the support via scholarship PD/BD/143033/2018. A.V.F. acknowledges the support of the European Microkelvin Platform.

[1] C. Tan, X. Cao, X. J. Wu, Q. He, J. Yang, X. Zhang, J. Chen, W. Zhao, S. Han, G. H. Nam, M. Sindoro, and H. Zhang, Recent advances in ultrathin two-dimensional nanomaterials, *Chem. Rev.*, 117, 6225-6331 (2017).

[2] D.E. Evans and R.C.T. Slade, Structural Aspects of Layered Double Hydroxides. In *Structure & Bonding*, Springer-Verlag, Berlin, Germany, 119, 1-87 (2005).

[3] Q. Wang and D. O'Hare, Recent advances in the synthesis and application of layered double hydroxide (LDH) nanosheets, *Chem. Rev.*, 112, 4124-4155 (2012).

[4] G. Ćibellán, C. Martí-Gastaldo, A. Ribera, E. Coronado, Hybrid materials based on magnetic layered double hydroxides: a molecular perspective. *Acc. Chem. Res.*, 48, 1601-1611 (2015).

[5] A.N. Salak, D.E.L. Vieira, I.M. Lukienko, Yu.O. Shapovalov, A.V. Fedorchenko, E.L. Fertman, Yu.G. Pashkevich, R.Yu. Babkin, A.D. Shilin, V.V. Rubanik, M.G.S. Ferreira, J.M. Vieira, High-power ultrasonic synthesis and magnetic-field-assisted arrangement of nanosized crystallites of cobalt-containing layered double hydroxides, *ChemEngineering*, 3, 00062 (2019).

Accumulation and annealing of structural defects in wide-gap metal oxides under intense radiation of different types

Aleksandr Lushchik

Institute of Physics, University of Tartu, W. Ostwald Str. 1, 50411 Tartu, Estonia

Main author email address: aleksandr.lushchik@ut.ee

Insufficient resistance against intense irradiation is considered to be serious limitation for the use of different materials in the harsh environment of future deuterium-tritium reactors. Consequently, the search for materials with optical/diagnostics window capabilities in fusion devices is an urgent task within the programs of the EUROfusion consortium. Several wide-gap metal oxides, in particular MgO, Al₂O₃ and MgAl₂O₄ single crystals and transparent ceramics have been considered as attractive candidates for this purpose. It is generally accepted that just the accumulation of stable (long-lived) structural defects determines the radiation damage and strongly influences the functionality of different optical materials. That is why the investigation and understanding of the mechanisms of Frenkel defect (interstitial-vacancy pairs) creation by different radiation types and doses/fluences; their subsequent thermal annealing as well as the prospects of radiation tolerance enhancement is of a special importance. Note that along with the dominant knock-on mechanism (elastic collisions) of radiation damage under metal oxide irradiation by fast neutrons, additional ionization mechanisms connected with the extremely high density of electronic excitations within cylindrical tracks of swift heavy ions should be also taken into account (see, e.g., [1]).

The processes of radiation damage caused by ~1-MeV fission neutrons, 100-keV protons, and ~GeV heavy ions have been studied in MgO, Al₂O₃ and MgAl₂O₄ single crystals by means of the EPR and optical spectroscopy methods (absorption, photo- and cathodo-luminescence) [2-7]. The accumulation of *F*-type centers (an oxygen vacancy with one to two trapped electrons) under oxide irradiation by ¹³²Xe ions or protons with fluence varying by three orders of magnitude has been investigated [5-7]. The correlation between revealed paramagnetic centers (i.e., *V*-type trapped-hole centers in MgAl₂O₄ [3, 4]) and relevant absorption bands has been elucidated. The annealing of radiation damage was performed in a stepwise regime: the irradiated sample was heated up in a flowing argon atmosphere from room temperature to a certain temperature, kept at this temperature for 5-10 min and then cooled down to RT when all the EPR and optical absorption spectra were measured. Subsequent comparison of the temperature dependences of elementary absorption bands related to different Frenkel defects with the pulse annealing of the EPR signal of different radiation-induced defects has been performed [3, 4].

A tentative scenario of the irreversible annealing of neutron-induced defects (involving both anion and cation sublattice) in MgAl₂O₄ single crystals has been proposed. The features of the ionization mechanisms of structural defect creation manifested via absorption and luminescence spectra have been considered. The experimental annealing data have been also analyzed in terms of the diffusion-controlled bimolecular reactions between *F*-type centers and complementary interstitial oxygen ions [2, 6]. The behavior of the main kinetic parameters – the migration energies and pre-exponential factors – for different irradiation types and fluences has been discussed in terms of Meyer-Neldel rule known in chemical kinetics of condensed matter (see, e.g., [2]).

- [1] A. Lushchik, Ch. Lushchik, A.I. Popov, K. Schwartz, E. Shablonin, E. Vasil'chenko, Influence of complex impurity centres on radiation damage in wide-gap metal oxides, *Nucl. Instrum. Meth. B* 374, 90-96 (2016).
- [2] A.I. Popov, A. Lushchik, E. Shablonin, E. Vasil'chenko, E.A. Kotomin, A.M. Moskina, V.N. Kuzovkov, Comparison of the *F*-type center thermal annealing in heavy-ion and neutron irradiated Al₂O₃ single crystals, *Nucl. Instrum. Meth. B* 433, 93-97 (2018).
- [3] A. Lushchik, S. Dolgov, E. Feldbach, R. Pareja, A.I. Popov, E. Shablonin, V. Seeman, Creation and thermal annealing of structural defects in neutron-irradiated MgAl₂O₄ single crystals, *Nucl. Instrum. Meth. B* 435, 31-37 (2018).
- [4] V. Seeman, E. Feldbach, T. Kärner, A. Maaros, N. Mironova-Ulmane, A.I. Popov, E. Shablonin, E. Vasil'chenko, A. Lushchik, Fast-neutron-induced and as-grown structural defects in magnesium aluminate spinel crystals with different stoichiometry, *Opt. Mater.* 91, 42-49 (2019).
- [5] E. Feldbach, I. Kudryavtseva, K. Mizohata, G. Prieditis, J. Räisänen, E. Shablonin, A. Lushchik, Optical characteristics of virgin and proton-irradiated ceramics of magnesium aluminate spinel, *Opt. Mater.* 96, 109308 (2019).
- [6] G. Baubekova, A. Akilbekov, E.A. Kotomin, V.N. Kuzovkov, A.I. Popov, E. Shablonin, E. Vasil'chenko, M. Zdorovets, A. Lushchik, Thermal annealing of radiation damage caused by swift ¹³²Xe ions in MgO crystals, *Nucl. Instrum. Meth. B* 462, 163-168 (2020).
- [7] G. Baubekova, A. Akilbekov, E. Feldbach, R. Grants, I. Manika, A.I. Popov, K. Schwartz, E. Vasil'chenko, M. Zdorovets, A. Lushchik, Accumulation of radiation defects and modification of micromechanical properties under MgO crystal irradiation with swift ¹³²Xe ions, *Nucl. Instrum. Meth. B* 463, 50-54 (2020).

What is hidden in the background of Bragg diffraction. Diffuse scattering and PDF analysis not only with neutrons

J. Kulda

*Institut Laue-Langevin, BP 156, 380042 Grenoble Cedex, France
kulda@ill.eu*

Many modern materials exhibit a considerable portion of structural disorder, playing a key role in their functionalities. Routine crystallographic structure solutions based on positions and integrated intensities of Bragg peaks only reveal their average structure. In order to access the details of local atomic arrangements and their short-range correlations one has to study the shape of the Bragg lines and the diffuse scattering below and between them.

In the past decade(s) increasing popularity has gained the pair distribution function (PDF) technique. Originally employed to investigation of amorphous structures and liquids, it has been extended to treat also crystalline systems. Its application consists in calculating the Fourier transform of a complete powder diffraction pattern, including the slowly varying part of the signal underneath the Bragg peaks and taking into account instrumental contributions to the line widths [1,2]. The resulting real-space atomic distance distribution by itself often permits qualitative discussions of changes in nearest neighbor distances as a function of chemical composition or of thermodynamic parameter variations (eg. [3]).

More involved and more quantitative interpretations of the PDF necessarily call for (much) more computing effort following one of the two possible approaches. In the first approach, a model-free technique of reverse Monte-Carlo (RMC) is used to build up a model structure providing a diffraction pattern coinciding with the observed one within statistical limits [4]. In an ideal case progress in computing power may permit to treat data obtained by various experimental probes (X-ray, neutron and electron scattering, EXAFS, NMR etc.) simultaneously to remove ambiguities inherent in each single technique [5]. In the second approach molecular dynamics and/or *ab-initio* computational techniques are employed to build up a dynamical model of the studied system, which is then successively refined to match the observed pattern. At the present state of the art DFT molecular dynamics can deal with disorder in quite complicated structures [6].

References

1. Th. Proffen et al., *Z. Kristallogr.* 218 (2003) 132–143
2. S.J.L. Billinge, M.G. Kanatzidis, *Chem. Commun.* (2004) 749–760
3. I.K. Jeong et al., *Phys. Rev. Lett.* 94 (2005) 147602
4. R.L. McGreevy, *J. Phys.: Condens. Matter* 13 (2001) R877–R913
5. I. Levin et al., *Chem. Mater.* 31 (2019) 2450–2458
6. M. Pasciak et al., *Phys. Rev. B* 99 (2019) 104102

Oral Abstracts

Continuous corrosion protection via layered double hydroxide UV-degradation

D. E. L. Vieira^{1*}, A. N. Salak¹, M. G. S. Ferreira¹, J. M. Vieira¹, C. M. A. Brett²

1- Department of Materials and Ceramics Engineering, CICECO – Aveiro Institute of Materials, University of Aveiro, 3810-193 Aveiro, Portugal

2- Department of Chemistry, Faculty of Sciences and Technology, University of Coimbra, 3004-535 Coimbra, Portugal

**danielevieira@ua.pt*

Layered double hydroxides (LDH), of general formula $[M^{II}_{1-x}M^{III}_x(OH)_2]^{x+}(A^{y-})_{x/y} \cdot zH_2O$, are natural 2-D structures. LDH are composed of alternating positively charged mixed metal M^{II} - M^{III} hydroxide layers and interlayers occupied by anions (A^{y-}) and water molecules. [1]. The functionalities of LDH are extended by employing specific cations, for example for corrosion protection. The primary method of synthesis of LDHs is co-precipitation from aqueous solutions followed by anion exchange.

Nowadays, the necessity to exclude chromates from metal surface treatment procedures to protect against corrosion has dramatically affected the industry. To overcome this problem, different solutions have been investigated and developed in recent years and LDH emerge as a possible material to replace Cr(VI), mostly due to LDH's multifunctional capability as a carrier of corrosion inhibiting species.

LDH can be intercalated with many different types of organic anions. Although the mechanisms of protection by LDH are not entirely understood, the basic principle consists in the release of anions from the LDH interlayers. This is followed by the adsorption of the organic molecules on the surface of the metallic substrate with consequent decrease of the corrosion reaction kinetics [2].

Ce(III) is well known for its corrosion protection capabilities [3,4]. However, since cerium is in cationic form, it is often trapped inside bentonite nano-capsules and used alongside LDH for promoting synergetic effects. The efficient inhibition by cerium ions occurs because of the reaction between Ce(III) and hydroxide ions leads to the formation of insoluble hydroxide in the cathodic areas.

In this work, the changes occurring to LDH when exposed for an extended period to UV-radiation and its degradation with release of cerium cations from the hydroxide layers has been examined. This strategy allows continuous corrosion protection after the end of the anion-exchange process. The study was performed using $Mg_3Al_{1-x}Ce_x$ LDH intercalated with nitrate, where x was 7.5 mol%. The UV-induced Ce(III) release promotes the hydroxide layer degradation. UV-visible spectroscopy was used to quantify the amount of Ce(III) released.

The continuous corrosion protection of aluminium alloy 2024 with LDH degradation was assessed using electrochemical impedance spectroscopy (EIS) and optical inspection over a one week period.

[1] D.E. Evans and R.C.T. Slade, Structural Aspects of Layered Double Hydroxides. In Structure & Bonding, Springer-Verlag, Berlin, Germany, 119, 1-87, (2005).

[2] S. Palani, T. Hack, J. Deconinck, H. Lohner, Validation of predictive model for galvanic corrosion under thin electrolyte layers: An application to aluminium 2024-CFRP material combination, Corros. Sci., 78, 89-100, (2014).

[3] D.R. Arnott, N.E. Ryan, B.R.W. Hinton, Auger and XPS studies of cerium corrosion inhibition on 7075 aluminium alloy, App. Surf. Sci., 22/23, 236-251, (1985).

[4] Z. You, L. Jianhua, L. Yingdong, Y. Mei, Y. Xiaolin, L. Songmei, Enhancement of Active Anticorrosion via Ce-doped Zn-Al Layered Double Hydroxides Embedded in Sol-Gel Coatings on Aluminum Alloy, Jour. of Wuhan Uni. of Tech. Mater. Sci. Ed., 32, 1199-1204, (2017).

Influence of In and Ga dopants on structural and scintillating properties of ZnO nanopowders and optical ceramics

**I. Venevtsev¹, P. Rodnyi¹, A. Stulnikov¹, E. Gorokhova², Faina Muktepavela³, Krishjanis Smits³,
A. Chizhov⁴, M. Gaskov⁴,**

1 - Peter the Great St. Petersburg Polytechnic University, 195251, 29 Polytechnicheskaya str., St. Petersburg, Russia

2 - Joint stock company "Research and Production Corporation S.I. Vavilova", 192174, 36 b.1 Babushkina str., St.Petersburg, Russia

3 - Institute of Solid State Physics, University of Latvia, LV-1063, 8 Kengaraga str., Riga, Latvia

4 - Moscow State University, 119991, 1 b.3 Leninskie Gory, Moscow, Russia

Venevtsev.Ivan@gmail.com

ZnO doped with trivalent ions such as Ga or In is a promising material to be used in scintillation detectors. This is due to the presence of fast luminescence band peaking near the absorption edge of ZnO (near-band-edge luminescence or NBL). This band is peaking around 390 nm and has a sub-nanosecond luminescence lifetime. It is known that NBL has an excitonic nature [1]. In and Ga doping is commonly used to suppress another luminescence band with much longer ($\sim 1 \mu\text{s}$) lifetime usually located in the 400-600 nm range (green luminescence or GL) [2]. Obtaining ZnO single crystals is usually long and costly process making it more preferable to manufacture ZnO in a form of optical ceramics. The properties of obtained scintillators can vary depending on the type and the amount of dopant, sintering conditions of both initial powders and ceramics.

In this work the scintillating properties of ZnO:Ga and ZnO:In optical ceramics obtained by uniaxial hot pressing method have been studied. Nanopowders which were used for ceramics preparation were made by precipitation method from commercial ZnO (99%, Sigma Aldrich) powder. The influence of Ga and In dopants on the structural properties of nanopowders and spectral-kinetic characteristics of the resulting ceramics is discussed.



Figure 1 Photograph of ZnO:Ga (1) and ZnO:In (2) ceramic samples.

The stages of the adhesive interaction of ZnO, ZnO:Ga and ZnO:In nanopowders were investigated at the nanostructured level with transmission electron microscopy (TEM). It has been shown that intensive aggregation of nanoparticles occurs already at 300K along prismatic planes, which leads to the formation of nano- and microrods. Donor impurities Ga and In initiate a morphological faceting- rounding transition of particles promoting good sintering with formation of diffusion active high angle grain boundaries. It should be noted that the mechanisms of these processes are different for Ga and In, while In has a greater effect.

Scintillating properties of the ceramics have been studied using X-ray excitation. As an example, the photograph of ceramic samples doped with Ga (1) and In (2) is shown at Fig. 1. It is clearly seen that ZnO:In ceramic is more transparent, i.e. the text underneath is much better visible. This is confirmed by the measurements of full transmittance, which showed that for Ga doped sample maximum transmittance in the range from 350 to 1100 nm is around 20% at 0.5 mm while for In doped sample it reaches 35% at 0.5 mm thickness. Under X-ray excitation in all ceramic samples the NBL was clearly dominant. GL was significantly reduced in In doped and completely suppressed in Ga doped ceramics. Kinetic measurements under pulsed X-ray excitation showed that all samples have fast (~ 0.7 ns) luminescence as a main component.

The present research has been supported by the Project ERANET RUS_ST #18-52-76002 (Russia) and #2017-051 (Latvia).

[1] M.R. Wagner, G. Callsen, J.S. Reparaz, J.-H. Schulze, R. Kirste, M. Cobet, I.A. Ostapenko, S. Rodt, C. Nenstiel, M. Kaiser, A. Hoffmann, A.V. Rodina, M.R. Phillips, S. Lautenschläger, S. Eisermann, B.K. Meyer, Bound excitons in ZnO: Structural defect complexes versus shallow impurity centers, *Phys. Rev. B*, vol. 84, pp. 035313-1-18, (2011).

[2] K.A. Chernenko, E.I. Gorokhova, S.B. Eron'ko, A.V. Sandulenko, I.D. Venevtsev, H. Wiczorek, P.A. Rodnyi, Structural, Optical, and Luminescent Properties of ZnO:Ga and ZnO:In Ceramics, *IEEE Trans. Nucl. Sc.*, vol. 65, pp. 2196-2202, (2018).

Role of interstitial oxygens in Ir-doped ZnO

A. Chesnokov¹, D. Gryaznov¹, J. Purans¹, E. A. Kotomin^{1,2}, N. V. Skorodumova^{3,4}

1- Institute of Solid State Physics, University of Latvia, Riga, Latvia

2- Max Planck Institute for Solid State Research, Stuttgart, Germany

3- Department of Physics and Astronomy, Uppsala University, Uppsala, Sweden

4- Department of Materials Science and Engineering, KTH Royal Institute of Technology, Stockholm, Sweden

Andrejs.Cesnokovs@cfi.lu.lv

Zinc oxide (ZnO) is a well-known, well-researched material. For several decades now, it has been in sight of various industries, most notably semiconductor and optoelectronic industries, whose interests guided many intense studies. ZnO has proved itself to be useful in a diverse assortment of devices. Its utility stems from its properties: it has wide band gap, high electron mobility, high thermal conductivity, strong luminescence, etc. In a relatively easy process, ZnO can be made into a stable n-type conductor. However, despite being thoroughly documented and with a long history as a specimen, research of ZnO still can offer new insights into material science.

Current research around ZnO focuses on synthesizing, stabilizing and describing amorphous phase of the material and on conditions for obtaining stable p-type conductivity. Through measurements of the Seebeck coefficient for Ir-doped ZnO thin films, it has been shown that Ir-doped ZnO can be p-type conducting if concentration of Ir exceeds a certain threshold [1]. In the present study using the density functional calculations we verify whether explanation for this effect can be attributed to oxygen interstitial defects.

To model this system, we have performed spin-polarized, symmetry-omitting density functional calculations within the LCAO approximation and employing hybrid PBE0 functional. We characterize a group of Ir-O complexes embedded in ZnO matrix and discuss their impact on the properties of the material. The characterization involves geometric configuration, chemical environment (oxidation state of the central ion, formation of peroxide fragments), localization of charge carriers and analysis of transport properties, namely, Seebeck coefficient and electronic conductivity.

[1] M. Zubkin, R. Kalendarev, J. Gabrusenoks, A. Plaude, A. Zitolo, A. Anspoks, K. Pudzs, K. Vilnis, A. Azens, J. Purans, Changes in structure and conduction type upon addition of Ir to ZnO thin films, *Thin Solid Films* 636, 694-701 (2017).

Persistent luminescence properties of doped AlN

B. Berzina¹, L. Trinkler¹, R. Ruska¹, G. Kriekē¹, G. Doke¹, A. Antuzevics¹, A. Sarakovskis¹, M. Kemere¹, A. Fedotovs¹, J. Cipa¹, J. Grabis²

*1- Institute of Solid State Physics, University of Latvia, 8 Kengaraga Str., LV-1063, Riga, Latvia
2- Institute of Inorganic Chemistry, Riga Technical University, Str. P. Valdena 3/7-207, Riga, Latvia*

baiba.berzina@cfi.lu.lv

Persistent luminescence (PersL) - a long lasting light emission enduring from minutes to many hours after ceasing of excitation source, is actual for different applications including safety signs, glow-in-the-dark decorations and needs of medicine and biology, where especially red light is determinant due to peculiarities of light spectral transparency of human skin. In the ISSP at LU there is running a new Latvia SC Project with aim to elaborate novel and efficient PersL materials emitting visible light emphasizing red and infrared spectral regions. There are several groups of prospective persistent luminescence materials such as $\text{MgSiO}_3:\text{Mn}^{2+}$, M ($\text{M}=\text{Al}^{3+}$, Ga^{3+} , In^{3+}) and others, included in this investigation and one of them is based on doped AlN. Our long-term spectral investigations of AlN macro- and nano-size materials allow consideration that luminescence of various defects, which is originated by recombination processes, possesses the properties of the PersL.

At present PersL is observed in AlN:Mn (our investigations and [1]). At figure 1 the photoluminescence (PL) and its excitation (PLE) spectra of AlN:Mn nanopowder (NP) are depicted. We have observed that the PL at 600 nm can be excited with light from two wide PLE bands peaking around 250 nm and 480 nm. Two luminescence mechanisms are proposed – the 480 nm excitation results in Mn intra-center excitation, whereas, 250 nm excitation causes recombination processes ending with Mn luminescence. In the last case the PersL is observed being in a good agreement with the results of [1].

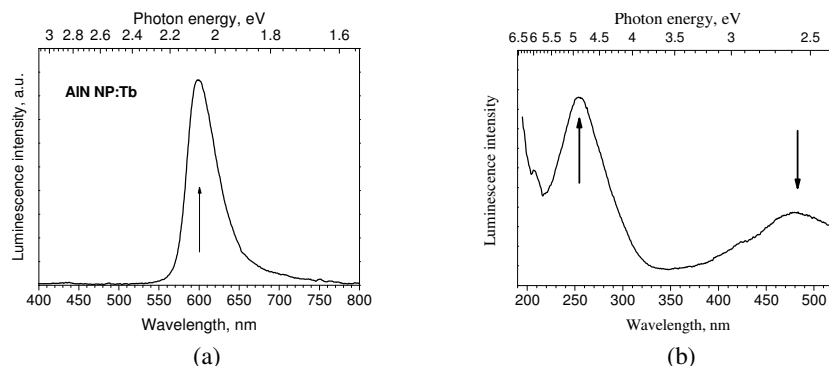


Figure 1. AlN:Mn nanopowder, room temperature. (a) - Photoluminescence spectrum under 250 nm excitation, (b) – excitation spectrum of 600 nm luminescence.

In order to observe PersL we have investigated luminescence properties of different doped AlN materials such as AlN:Eu, AlN:Tb and others using various spectral methods including measurements of PL and PSL spectra within a wide spectral region and temperatures from 10 to 300 K; luminescence kinetics and EPR spectra. Possible luminescence mechanisms including PersL are discussed.

[1] Jian Xu, Nerine J. Cherepy, Jumpei Ueda, Setsuhisa Tanabe, Red persistent luminescence in rare earth-free AlN:Mn phosphor, Materials Letters 206, 175-177, 2017.

The present research is sponsored from the Latvian Sciences Council Grant No lzp-2019/1-0443.

Fano Resonances in Nanostructured Thin Films

L. Grineviciute^{1,2}, J. Nikitina^{1,2}, C. Babayigit³, K. Staliunas^{2,4,5,*}

1-Center for Physical Sciences and Technology, Savanoriu ave. 231, LT-02300 Vilnius, Lithuania
 2-Vilnius University, Faculty of Physics, Laser Research Center, Sauletekio ave. 10, Vilnius, Lithuania
 3-TOBB University of Economics and Technology, Ankara, Turkey
 4-ICREA, Passeig Lluís Companys 23, 08010, Barcelona, Spain
 5-UPC, Rambla Sant Nebridi 22, 08222, Terrassa (Barcelona) Spain

*kestutis.staliunas@icrea.cat

Fano resonances are widespread in nature and technology. After their discovery almost 90 years ago [1], and after their universal mathematical description 60 years ago [2], Fano resonances found numerous applications in different fields, arising from atom and nuclear physics. Especial growth of interest in Fano resonances in last years was boosted by emerging photonics and microphotonics technologies. The essence of Fano resonance can be explained by a simple coupled two-oscillator model: a driven oscillator with a broad resonance coupled to the second oscillator with a narrow resonance. When the frequency of the driving force is tuned around the resonance frequency of the second oscillator, a sharp variation is observed in the response of the first (driven) oscillator. The first oscillator, at a resonance with the second oscillator, shows zero response to the driving force – all the energy of the driving totally reflects. In other words, at certain frequency coupled system becomes out of phase with the driving force, and destructive interference yields a dip in the response of the coupled resonator system. Comparing with the Bragg resonances, the Fano resonances can potentially introduce high frequency sensitivity in the system, thus the absorption and scattering can be efficiently engineered in a narrow frequency ranges.

Conventionally the Fano resonances are considered in coupling of the driven oscillator with compact systems, like dielectric or plasmonic nanospheres, metaatoms. In these systems, the Mie resonances in nanoparticles can play a role of secondary oscillator while non-resonant background forms the driving force. However, nothing is known about the Fano resonances due to the global coupling to the extended modes. Here we propose the Fano coupling to the spatially extended planar waveguiding modes of the thin dielectric films in order to influence the propagation (reflection/transmission) properties of the beam radiation near-to-normally incident to the thin film.

The proposed geometry is shown in Fig.1. A thin film is deposited on a substrate periodically

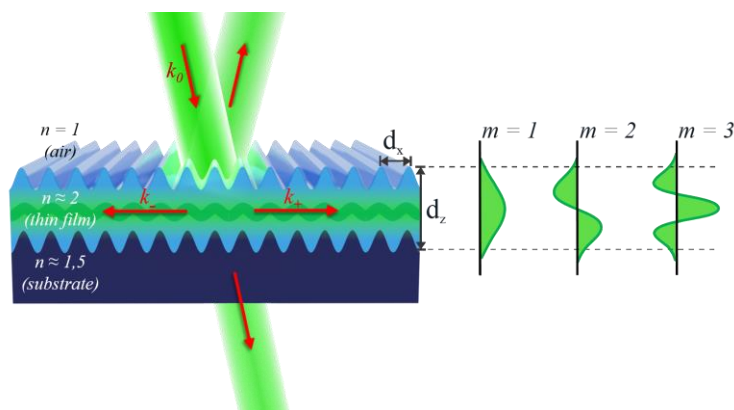


Fig. 1. The schematic representation of excitation of waveguiding modes due to Fano coupling

modulated on a wavelength scale. In our experiments the modulation period was 600 nm., and modulation depth of around 200 nm. Due to the periodic modulation of the substrate, and consequently of the surface of thin film, the Fabry-Perrot modes of the thin film couple with the waveguiding modes of the film. The coupling is highly sensitive to the wavelength and to the incidence angle of the radiation. Consequently, the reflection-transmission characteristics through the film show high sensitivity to the wavelength and the incidence angle as well. The thin film can efficiently work as the filter, both in wavelength domain (frequency filter), and angle domain (spatial filter).

Specifically, we demonstrate frequency filters with the bandwidth of the 10-s of nanometers, and the spatial filters with the angular band-width of several degrees (at normal incidence). The theoretical-numerical analysis shows the potential to scale the frequency band-width down to sub-nanometer regimes.

In the presentation, the physics of Fano resonances will be presented, together with the numerical simulation results, and experimental results achieved to the presentation date.

[1] U. Fano "Sullo spettro di assorbimento dei gas nobili presso il limite dello spettro darco", *Il Nuovo Cimento* **12**, 154 (1935);
 [2] U. Fano "Effects of configuration interaction on intensities and phase shifts. *Phys. Rev.* **124**, 1866 (1961).

Deposition of multilayer optical coatings on corrugated surfaces for 2D photonic crystals formation

L. Grineviciute^{1*}, D. Gailevicius^{2,3}, C. Babayigit⁴, L. Ramalis¹, J. Nikitina¹, K. Staliunas^{5,6}, T. Tolenis¹

1-Center for Physical Sciences and Technology, Savanoriu ave. 231, LT-02300 Vilnius, Lithuania
 2-Vilnius University, Faculty of Physics, Laser Research Center, Sauletekio ave. 10, Vilnius, Lithuania
 3-Femtika LTD, Sauletekio Ave. 15, LT-10224, Vilnius, Lithuania
 4-TOBB University of Economics and Technology, Ankara, Turkey
 5-ICREA, Passeig Lluís Companys 23, 08010, Barcelona, Spain
 6-UPC, Rambla Sant Nebridi 22, 08222, Terrassa (Barcelona) Spain

*lina.grineviciute@ftmc.lt

In micro-lasers, especially in high power emission regimes, the spatial quality of laser light beam deteriorates, i.e. the energy distribution deviates from the Gaussian form. Due to the small laser dimensions, standard multi-lens arrangements cannot be used for beam correction. Recently some of us proposed and provided experimental evidence of the angular filtering in the photonic structures fabricated by physical vapor deposition [1]. The filtering photonic structures must have modulation in both: the longitudinal and transverse directions. The proposed PhCs structure consists of alternating multilayers on a substrate where the interfaces of the layers are modified as a periodic array of sinusoidal wavy curves, see Fig.1. Due to the wavy layers, the modulation of the effective refractive index occurs not only in vertical but also in a horizontal direction. Hence, the proposed structure can be classified as 2D Photonic Crystal structure. However, in order to achieve the required characteristics of such elements, it is necessary to have not only a proper initial structure but also precise control of the growth of the deposited layers, ensuring repeatability or even inducing the necessary divergence of the initial structure geometry.

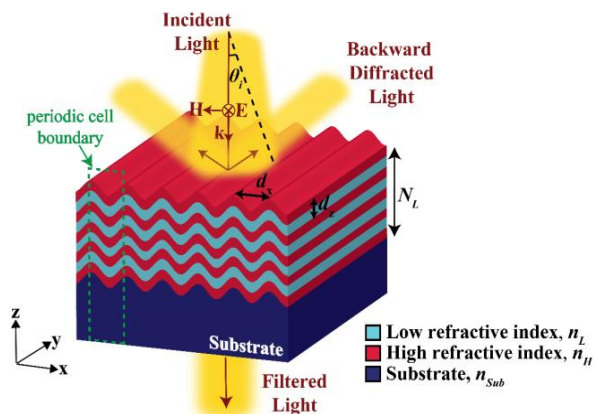


Fig. 1. Three-dimensional representation of designed PhC spatial filter geometry

The present work proposes the deposition of multilayer optical coatings on modulated surfaces employing physical vapor deposition (PVD) technologies together with glancing angle deposition (GLAD) method. GLAD allows forming the so-called sculptured thin films by directing vapor flux towards the substrate at oblique angles. This feature potentially may help to conformally cover non-flat surfaces and maintain initial structure modulation across the film geometry, which is crucial for optical elements with 2D or even 3D periodicity of refractive index. Since several variables appear: substrate orientation and the angle between the substrate normal and the incident vapor flux, it is important to evaluate the growth of the final structure on these values. Primary numerical simulations of layers formation were performed employing NASCAM (NANO SCALE Modeling)

software based on the kinetic Monte Carlo algorithm [2]. This software does not take into account the vibrational movement of atoms or interatomic interactions, hence allows to investigate the time evolution of relatively large systems containing millions of atoms. In practice, multilayer structures on flat surfaces can be easily deposited employing conventional PVD technologies. Unfortunately, layers deposition on corrugated surfaces can face several problems – cracks formation along the film normal or modulation decrease after several layers. Taking these issues into account, the coating evolution depending on deposition parameters for alternating layers of SiO₂ and Al₂O₃ materials were simulated and compared with experimental results.

In the presentation, the PVD technologies together with glancing angle deposition method for the coatings on nanostructured surfaces will be reviewed, paying the main attention to the GLAD method.

[1] L. Grineviciute, C. Babayigit, D. Gailevicius, E. Bor, M. Turdnev, V. Puriys, T. Tolenis, H. Kurt, and K. Staliunas. "Angular filtering by Bragg photonic microstructures fabricated by physical vapor deposition." *Appl Surf Sci.*, 481, 353 (2019);

[2] Moskovkin, P., & Lucas, S. Computer simulations of the early-stage growth of Ge clusters at elevated temperatures on patterned Si substrate using the kinetic Monte Carlo method. *Thin solid films*, 536, 313-317, (2013).

Site-selective laser spectroscopy of Nd³⁺ doped β modification of calcium triphosphate

**E.A. Vagapova^{1,2}, M. Janulevičius³, Evgenii Strugovshchikov¹,
L.D. Iskhakova², A.S. Vanetsev^{1,2}, Aleksandr Pištšev¹, Yu.V. Orlovskii^{1,2}**

1 - Institute of Physics, University of Tartu, W.Ostwald st.1, Tartu 50411, Estonia

2 - A.M. Prokhorov General Physics Institute RAS, Vavilov st. 38, 119991, Moscow, Russia

3 - Institute of Chemistry, Vilnius University, Naugarduko 24, LT-03225 Vilnius, Lithuania

e-mail: ekaterina.vagapova@ut.ee

In recent years, studies of phosphate materials, in particular β modification of calcium triphosphate (β -Ca₂(PO)₄, β -TCP), are becoming more popular due to their compatibility with biological tissues [1]. The β -TCP is mainly used in biomedicine as a bone tissue substitute when such tissue transplantation is impossible [2]. This material is also part of more complex biocompatible materials, for example, BCP (bi-calcium phosphate), which leads to additional interest in the study of its properties [3]. There are various approaches to control changes in the crystal structure of phosphate materials including XRD, FTIR, and solid state NMR. Analysis of impurity fluorescence quenching kinetics (“energy transfer probe”) is another promising method allowing to observe changes in the local crystal structure. For implementation of this method, samples doped with rare-earth (RE) ions, e.g., with Nd³⁺ ions, is necessary [4]. The method is highly sensitive and, when combined with data obtained by other methods, can be used to support interpretation of crystal structure analysis. However, in order to fully use this method, it is necessary to investigate in detail the inhomogeneous splitting of the spectral lines in the material in order to select the kinetics of just one type of optical centers.

The β -TCP samples were prepared by co-precipitation from water-ethanol system followed by annealing step at 800 °C for 2 h. We chose the Nd³⁺ ion as a luminescent probe to track changes in local crystal structure [4] since Nd³⁺ spectral absorption and fluorescence lines are located in the so-called “first” transparency window of biological tissues (700 - 1000 nm), including bone tissue. This enables to detect the fluorescence of the Nd³⁺ ions not only on the surface of sample, but also at a depth of one centimeter allowing to determine local structural changes within crystalline host [5].

Herein, site-selective laser and fluorescence kinetic spectroscopy at low temperature of β -TCP single phase ceramics doped with 0.1 at. % Nd³⁺ was performed to study the optical sites of Nd³⁺. Using the selected method, we studied spectral and kinetic properties of this material at low temperature. The NIR fluorescence excitation spectra detected at the ⁴F_{3/2}(1) → ⁴I_{9/2}(1,2) transitions while tuning pulsed dye laser over the ⁴I_{9/2}(1) → ⁴G_{5/2}(1,2) transitions were recorded with a high spectral resolution (laser line width = 0.065 Å). Site-selective fluorescence spectra and kinetics were recorded exciting into each spectral line of the measured NIR fluorescence excitation spectrum. Thus, it was shown that there are eight spectrally separated optical centers of the Nd³⁺ ion in the studied material.

The fluorescence decay kinetics was used to determine the lifetimes of spontaneous radiative decay for each type of optical centers of the Nd³⁺ ion in β -TCP. The energies of the ⁴G_{5/2}(1), ⁴F_{3/2}(1), ⁴I_{9/2}(1) Stark (crystal-field) levels of Nd³⁺ were determined in Nd³⁺: β -TCP at 4.2K.

Experimental data were compared with calculated ones, which were obtained with DFT method. The theoretical calculations showed that all types of optical centers in this material can be divided into two main groups according to the type of symmetry - C₃ and C_s. A more detailed calculation made it possible to compare the type and mechanism of the formation of experimentally observed optical centers of the Nd³⁺ ion in β -TCP.

[1] Shamsoddin E., Houshmand B., Golabgirani M., Biomaterial selection for bone augmentation in implant dentistry: A systematic review, J Adv Pharm Technol Res., 10(2), 46–50, (2019)

[2] Paderni S, Terzi S, Amendola L, Major bone defect treatment with an osteoconductive bone substitute, Musculoskelet Surg. 93 (2): 89–96, (2009).

[3] G. Daculsi, R. LeGeros, Tricalcium phosphate/hydroxyapatite biphasic ceramics in: T. Kokubo (Ed), Bioceramics and their Clinical Applications 1st Edition, Woodhead Publishing, Chubu, 2008, pp. 395–416

[4] E.V. Samsonova, A.V. Popov, A.S. Vanetsev, K. Keevend, E.O. Orlovskaya, V. Kiisk, S. Lange, U. Joost, K. Kaldvee, U. Maeorg, N.A. Glushkov, A.V. Ryabova, I. Sildos, V.V. Osiko, R. Steiner, V.B. Loschenov, Y.V. Orlovskii, An energy transfer kinetic probe for OH-quenchers in the Nd³⁺:YPO₄ nanocrystals suitable for imaging in the biological tissue transparency window, PCCP, 16, 26806-26815, (2014).

[5] E. Hemmer, A. Benayas, F. Légaré and F. Vetrone, Exploiting the Biological Windows: Current Perspectives on Fluorescent Bioprobes Emitting above 1000 nm, Nanoscale Horiz., 1, 168-184, (2016).

Ultrafast Cross-Luminescence in BaGeF₆ and K₂GeF₆

J. Saaring, E. Feldbach, I. Kudryavtseva, V. Nagirnyi, S. Omelkov, I. Romet, S. Roy, A. Vanetsev, M. Kirm

Institute of Physics, University of Tartu, W. Ostwald Str. 1, 50411 Tartu, Estonia

juhansaaring@gmail.com

Ultrafast scintillators with a superior temporal resolution are needed in different applications: for example, in high-energy physics to prevent pile-up effects at high event rates as well as in medicine in time-of-flight positron emission tomography to improve the resolution in diagnostic images [1]. Cross-luminescence (CL) is an ultrafast intrinsic emission that could be considered to fulfil such needs. CL arises due to the recombination of a relaxed core hole with an electron from the valence band, whereas its decay is governed by the life-time of the core holes. Although the properties of CL have been investigated extensively since its discovery in the 1980's (see review [2]), nowadays cross-luminescence is reconsidered in light of advances in the development of ultrafast silicon photomultipliers sensitive in the UV region [3]. Ternary fluorides, in comparison to binary compounds, can exhibit CL extending into the UV region due to a more complex valence band [2], consisting of multiple sub-bands and thus providing more possibilities for ultrafast radiative transitions between the outermost core band and valence sub-bands. In order to verify this hypothesis, we investigated Ba and K complex fluorides, whose valence are formed by the fluoroanion GeF₆²⁻ terms consisting of the 2p states of F as well as 2p and 2s states of Ge. The Ba 5p and K 3p core excitons are created near 17 and 20 eV in fluorides, respectively. Correspondingly, the excitation onset of CL is found at 18 eV in BaF₂ and 21.8 eV in KMgF₃ [4]. The studied K₂GeF₆ and BaGeF₆ powders were obtained via co-precipitation from concentrated HF solutions and their phase purity was confirmed by X-ray diffraction analysis.

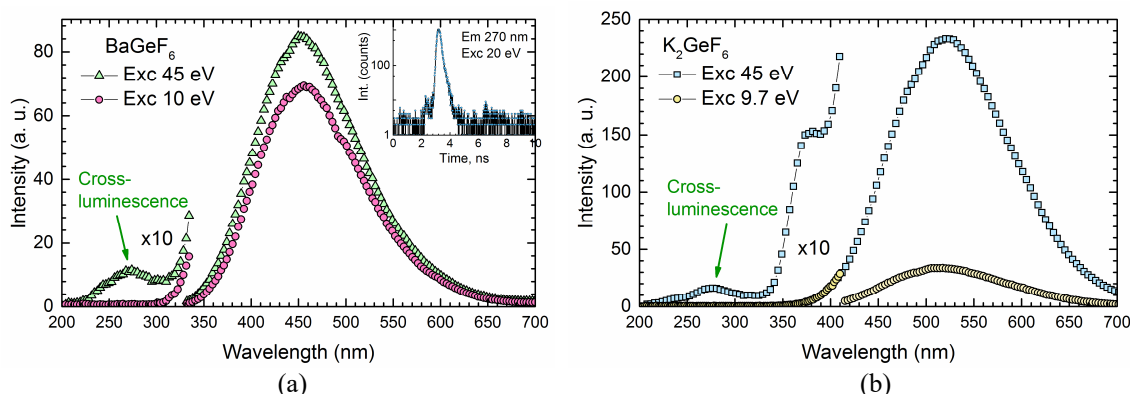


Figure 1 (a) Emission spectra of BaGeF₆ under excitation by 10 eV (red circles) and 45 eV (green triangles) photons. Inset shows the sub-ns decay of cross-luminescence recorded at 270 nm and excited by 20 eV photons. (b) Emission spectra of K₂GeF₆ under excitation by 9.7 eV (yellow circles) and 45 eV (blue squares) photons. The spectra in UV range are multiplied by a factor of 10 on both figures to increase visibility of the cross-luminescence. The emission spectra are presented as recorded without any corrections. T = 7 K

The experimental investigation of samples (T = 5–300 K) was performed by cathodoluminescence under 10 keV electron excitation (emission spectra 1.5–10 eV) and by photoluminescence excited in VUV (4–10 eV) in our home laboratory. Low-temperature time-resolved photoluminescence (200–700 nm) studies were performed under synchrotron radiation excitation by 4.5–45 eV photons in multi-bunch (32 bunches) and single-bunch (320 ns interval between bunches) modes at the [FinEstBeAMS](#) beamline (MAX IV Lab, Lund, Sweden). Our study revealed CL with sub-ns decay in the wavelength range 220–300 nm peaked at 270 nm in both investigated ternary fluorides. Figure 1 shows CL, observable only under 45 eV excitation, i.e. at the energies exceeding the threshold of core hole creation. The broad long-wavelength emission bands in BaGeF₆ (peaked at 450 nm) and in K₂GeF₆ (peaked at 520 nm) are non-elementary and possess much longer decay times. Based on the recorded data, i.e. emission and excitation spectra as well as decay kinetics, the origin of the different types of emissions and the peculiarities of relaxation processes of electronic excitations will be discussed.

[1] C. Dujardin, E. Auffray, E. Bourret-Courchesne, P. Dorenbos, P. Lecoq, M. Nikl, A.N. Vasil'ev, A. Yoshikawa, and R.-Y. Zhu, "Needs, Trends, and Advances in Inorganic Scintillators", IEEE Trans. Nucl. Sci., vol. 65, pp. 1977–1997, (2018).

[2] C.W.E. van Eijk, "Cross-luminescence", J. Luminescence, vol. 60&61, pp. 936–941, (1994).

[3] S. Gundacker, R.M. Turtos, N. Kratochwil, R.H. Pots, M. Paganoni, P. Lecoq, E. Auffray, "Experimental time resolution limits of modern SiPMs and TOF-PET detectors exploring different scintillators and Cherenkov emission", Phys. Med. Biol., in press, (2020).

[4] V.N. Makhov and N.M. Khaidukov, "Cross-luminescence peculiarities of complex KF-based fluorides", Nucl. Instrum. Meth. A, vol 308, pp. 205–207, (1991).

Up-conversion luminescence in Yb doped $\text{Li}_6\text{Y}(\text{BO}_3)_3$ single crystals

V. Nagirnyi¹, K. Lengyel², É. Tichy-Rács², I. Romet¹, K. Timpmann¹, I. Sildos¹, L. Puust¹,
R. Butkus³, M. Vengris³, R. Grigonis³, V. Sirutkaitis³

1- Institute of Physics, University of Tartu, W. Ostwald str. 1, 50411 Tartu, Estonia

2- Wigner Research Centre for Physics, Institute for Solid State Physics and Optics, Konkoly-Thege út 29-33, H-1121 Budapest, Hungary

3- Laser Research Center, Vilnius University, Sauletekio al. 10, LT-10222, Vilnius, Lithuania

vitali.nagirnoi@ut.ee

$\text{Li}_6\text{Y}(\text{BO}_3)_3$ (LYB) may form solid solutions with homologous lithium rare earth (RE) borates, thus allowing single crystals to accommodate large concentrations of RE dopants. Their crystal structure contains edge-sharing REO_8 polyhedra forming chains along the c axis allowing for closely situated RE^{3+} ions at a distance of about 3.85 Å. In case of doping, such geometry, providing very short distances in pairs of RE impurity ions either of the same kind or different, facilitates their interaction leading to various kinds of up-conversion luminescence (UCL). A peculiar case of the UCL is so-called cooperative luminescence (CL) that is the process in which two excited neighbouring RE^{3+} ions relax simultaneously emitting a single photon with the energy twice as high as the energy of a single ion emission.

This report presents the results of spectroscopic study of the UCL in Yb^{3+} doped LYB single crystals under continuous-wave laser excitation at the Institute of Physics, Tartu and pulsed excitation using a tuneable femtosecond laser system Topas at the Laser Research Center of Vilnius University, Lithuania. The studied crystals contained 5 or 20 mol% of Yb, however characteristic emission lines of other RE impurities could also be detected under a powerful laser excitation at 364 nm. The UCL peaking at about 500 nm (20000 cm^{-1}) was successfully generated upon the excitation at the wavelength of 972.3 nm ($\sim 10000\text{ cm}^{-1}$) of the LYB:Yb crystals at temperatures 6-300 K (Fig. 1). The UCL is nearly structureless at room temperature, but demonstrates a pronounced line spectrum at low temperatures (Fig. 1b). The main lines in the UCL spectrum are reliably described to a combination of known radiative transitions in single Yb^{3+} ions (see Fig. 1a), thus representing the cooperative luminescence of the Yb^{3+} - Yb^{3+} pairs. Another part of the spectrum is related to the UCL due to energy transfer from Yb^{3+} to Dy^{3+} ions in the Yb^{3+} - Dy^{3+} pairs. Thus, two types of UCL could be simultaneously studied in LYB crystals. The laser power dependences of intensities were investigated for both kinds of emission at different temperatures and the related saturation processes were described. The temperature dependences of the intensities of both emissions were studied. The decay kinetics of CL was shown to be twice as fast as that of a single ion luminescence as expected, but showed slight shortening with growing Yb concentration. The influence of temperature induced broadening of single centre absorption lines and energy transfer along the Yb chains on the power and temperature dependences of the CL will be discussed.

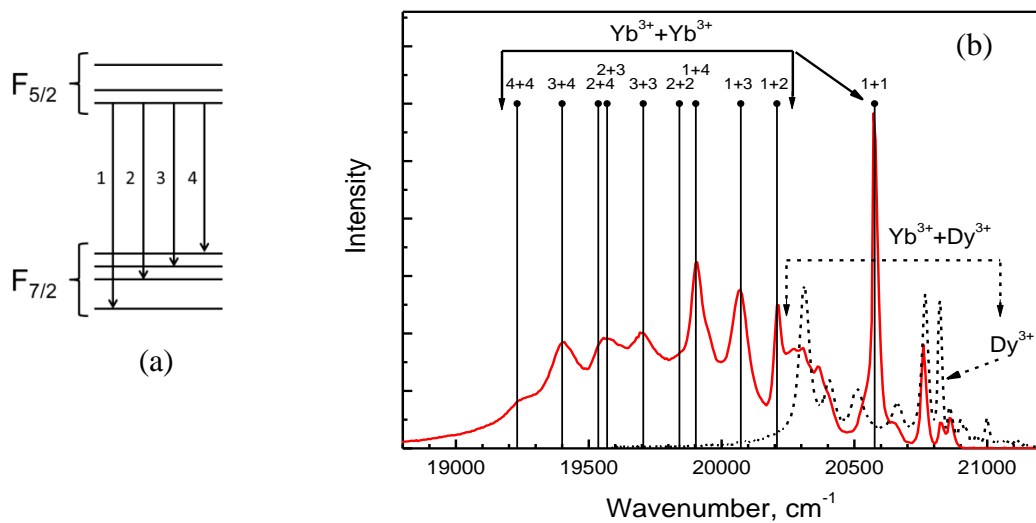


Figure 1. (a) Energy level diagram and radiative transitions 1 – 10288 cm^{-1} , 2 - 9920.6 cm^{-1} , 3 - 9784.7 cm^{-1} , 4 - 9615.4 cm^{-1} of Yb^{3+} ions; (b) UCL spectrum of the 20 mol% Yb doped LYB crystal measured at 6 K under continuous-wave laser excitation at 972 nm (solid line). The line groups related to cooperative luminescence in the Yb^{3+} - Yb^{3+} pairs and up-conversion luminescence in Yb^{3+} - Dy^{3+} pairs are shown by square brackets. Dashed line - a high-energy part of Dy^{3+} emission spectrum under excitation 364 nm in LYB:Dy.

Structural analysis and photoluminescence spectroscopy of rock-salt ZnMgO thin films with high ZnO content

R. Nedzinskas¹, A. Suchodolskis¹, L. Trinkler², L. Chang³, M.M.C. Chou³

1- Center for Physical Sciences and Technology, Saulėtekio ave. 3, LT-10257 Vilnius, Lithuania

2- Institute of Solid-State Physics, University of Latvia, Ķengaraga str. 8, LV-1063 Riga, Latvia

3- Center of Crystal Research, National Sun Yat-sen University, Lienhai Rd. 70, 80424, Kaohsiung, Taiwan, R.O.C.

ramunas.nedzinskas@ftmc.lt

The radiation from the Sun with wavelengths of 200–280 nm is absorbed by the ozone/triatomic oxygen in the atmosphere. Therefore, the light in this *so called* ultraviolet-C (UV-C) region can be detected without the influence of the Sun's radiation. Photodetectors with a cutoff <280 nm thus could be defined as solar-blind. Solar-blind photodetectors are naturally attractive for a many of applications in defense (missile detection), astronomy, flame detection, biomedicine (psoriasis, skin care) chemical sensing (gas analysis, pollution detection, monitoring ozone holes), water purification, UV curing of paints/adhesives, inspection of UV leakage, etc. [1].

Based on recent novel findings [2, 3] of our consortium group from Taiwan, alloying ZnO with MgO in varying amounts allows realization of stabilized ZnO-MgO pseudobinary system with a smooth tuning of the bandgap between 3.37-7.8 eV, previously not accessible. Therefore, ternary alloy of ZnMgO (ZMO) have a great potential application in solar-blind UV detection, significantly enhancing the ability of the devices at different energies simultaneously. Since photodetectors are sensitive to extended defects, the availability of MgO and another lattice-matched melt-grown substrates makes ZMO material very promising for UV sensor applications. In this work novel ZMO thin film structures are studied, as very high concentration of hexagonal-in-nature ZnO (up to 85%) was used to grow rs-ZMO nanolayers. In particular, structural and optical [3, 4] investigation of ~120 nm-thick rock-salt ZMO (rs-ZMO) thin films, grown on lattice-matched MgO (110) substrate is presented. Structural analysis of rs-ZMO thin films we performed using X-ray diffraction (XRD) and scanning electron microscopy (SEM). While optical spectra were recorded using temperature-dependent (down to 3 K) photoluminescence (PL) technique and room temperature absorption spectroscopy.

Structural analysis of the rs-ZMO thin film samples, grown with high (80% and 85%) ZnO content, provided that the morphology of the surface of ZMO thin film is very different, given the concentration of ZnO is similar. In particular, when ZnO content is 80%, the film is very flat and free from cracks and hillocks, and with no wurtzite (wz) phase of ZMO. On the other hand, when ZnO content is 85%, the film shows pilling and has a high in-plane compressive stress. In this latter case, the film mainly consists of a rs-ZMO epitaxial layer and scattered polycrystalline wz-ZMO islands.

The PL features observed are attributed to different processes of carrier dynamics in the rs-ZMO thin film structures studied. It was found that, the sharp high-energy feature is due to interband (band-to-band) optical transitions in ZMO epitaxial layer, while low-energy PL bands are related to the presence of defect states within a bandgap of ZnMgO. Additionally, possible transfer mechanisms of charge carrier are discussed in regard to activation energies calculated.

Room-temperature optical transmittance and reflectance spectroscopy was used to investigate the optical bandgap energies. It was found that, that for the sample with larger amount of ZnO used (85%), absorption onset is significantly shifted to the higher energies as compared to sample with less-rich ZnO, although ZnO content used is only slightly different (by 5%).

The financial support of m-era.net project "ZnMgO materials with tunable band gap for solar-blind UV sensors" (ZMOMUVS) is greatly acknowledged.

- [1] H.Y. Chen, K.W. Liu, L.F. Hu, A.A. Al-Ghamdi, and X.S. Fang, *New concept ultraviolet photodetectors*, *Mater. Today* **18**, 493 (2015).
- [2] C.-Y. James Lu, Y.-T. Tu, T. Yan, A. Trampert, L. Chang, K. H. Ploog, *Growth and stability of rocksalt Zn_{1-x}Mg_xO epilayers and ZnO/MgO superlattice on MgO (100) substrate by molecular beam epitaxy*, *J. Chem. Phys.* **144**, 214704 (2016).
- [3] M.C. Wen, S.A. Lu, L. Chang, M.M.C. Chou, K.H. Ploog, *Epitaxial growth of rocksalt Zn_{1-x}Mg_xO on MgO (100) substrate by molecular beam epitaxy*, *J. Cryst. Growth* **477**, 169 (2017).
- [4] S. Tumėnas, P. Mackonis, R. Nedzinskas, L. Trinkler, B. Berzina, V. Korsaks, L. Chang, M.M.C. Chou, *Optical properties of lithium gallium oxide*, *Appl. Surf. Sci.* **421B**, 837 (2017).
- [5] L. Trinkler, A. Trukhin, B. Berzina, V. Korsaks, P. Ščaev, R. Nedzinskas, S. Tumėnas, M.M.C. Chou, L. Chang, C.-A. Li., *Luminescence properties of LiGaO₂ crystal*, *Opt. Mater.* **69**, 449 (2017).

Photonic solutions for monitoring of pathogen decontamination efficiency

O. Rebane^{1,2}, M. Kirm¹, Larisa Poryvkina², Sergey Babichenko²

1- Institute of Physics, University of Tartu, W.Ostwald str. 1, 50411 Tartu, Estonia

2- LDI Innovation OÜ, Osmussaare str. 8, 13811 Tallinn, Estonia

ott.rebane@ut.ee

Decontamination of publicly usable rooms as well as vehicles of transport helps to prevent the spreading of disease and costs for material damage (e.g., due to mould growth on textiles) introduced by bio-pathogens. One of the most efficient decontamination method is using hydrogen peroxide vapor (HPV) at a few-hundred ppm concentration in the air of the room to be decontaminated since everything in contact with the air is a subject to decontamination process [1]. Typically, the efficiency of such process is evaluated by using hard-to-kill (but harmless to humans) bacterial spore samples located into various places in the room under investigation and afterwards the germination of the decontaminated spore samples is followed during next 2-7 days. This means that there is currently a 2-7 days delay in the detection efficiency of the HPV decontamination procedure, which would greatly benefit in reduction of the feedback loop to real-time monitoring.

The nano-sized functional material applied is the same reliably proven *B. atrophaeus* spore sample that is typically used in classical contamination monitoring by microbiological methods. In this work we studied the change of the fluorescence properties of these spores during decontamination procedure – i.e. the difference of viable dormant spores from the dead ones [2]. The main focus was on the fluorescence intensity decrease [3] under 280nm excitation and monitoring 330nm emission as the on-line indicator of the HPV procedure. Single-photon counting fluorimeters were developed for this task, enabling real-time signal monitoring from the chamber that was decontaminated with HPV. The devices were designed (see main design principle in Fig.1.a) entirely cordless, being battery-powered and transferring data over WiFi.

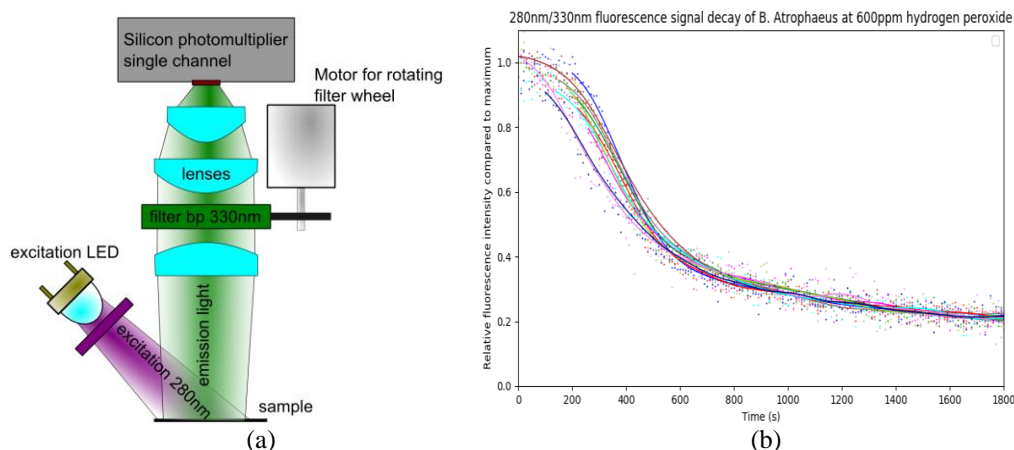


Figure 1 (a) The main design idea of the fluorimeter used to monitor the HPV decontamination procedure. (b) Time dependence of the intensity of Tryptophan-associated main fluorescence peak shown for many decontamination simulation runs.

A reproducible decline (see Fig.1.b) of the Tryptophan fluorescence intensity, which depends on the HPV concentration as well as duration applied, was revealed and it enables estimation of the HPV process efficiency. To enable a more reliable distinction between viable and dead spores, other spectral regions have also been investigated in real-time full-spectrum SFS (Spectral Fluorescence Signature) measurements during the HPV procedure. Using synchrotron radiation in UV (FinEstBeAMS), the ns time dependence of the Tryptophan fluorescence decay of spores were investigated before and after applying the HPV process, which provides additional input to develop more advanced photonic sensor solutions for decontamination monitoring.

[1] T. Holmdahl, P. Lanbeck, M. Wullt and M.H. Walder. A head-to-head comparison of hydrogen peroxide vapor and aerosol room decontamination systems. *Infect Control Hosp Epidemiol.* Vol 32, pp. 831-836, (2011).

[2] R. Li, U. Goswami, M. King, J. Chen, T.C. Cesario and P.M. Rentzepis. *In situ* detection of live-to-dead bacteria ratio after inactivation by means of synchronous fluorescence and PCA. *Proceedings of the National Academy of Sciences of the United States of America*, Vol. 115, 668-673, (2018).

[3] P. Cavatorta, R. Favilla and A. Mazzini. Fluorescence quenching of tryptophan and related compounds by hydrogen peroxide. *Biochim Biophys Acta.* Vol 578, pp. 541-546, (1979).

Metal powder materials with nanomodified oxide coatings and their technical application

A. Vetcher, G. Govor, K. Yanushkevich

Scientific-Practical Materials Research Centre NAS of Belarus, Laboratory of Physics of Magnetic Materials, 220072, Minsk, P.Brovki str., 19, Belarus

E-mail: vetcher@physics.by

In Scientific-Practical Materials Research Centre NAS of Belarus a technology for the manufacture of various composite materials based on metal powders has been developed. Depending on the basis and processing method, it is possible to obtain several classes of material:

- **soft magnetic composites** – for use in electric motors, including linear ones, generators, transformers and other electrical products, for the manufacture of broadband electromagnetic screens;
- **resistive composite materials** – for the production of electric heating elements of various shapes, capacities and configurations;
- **magnetically hard composite materials** – for the production of inexpensive and high-performance magnets;
- **magnetocaloric composite materials** – for the production of working elements of refrigeration machines.

Technical and economic advantages:

- the absence of eddy-current losses at high frequencies due to the electrical insulation of individual iron particles in the soft magnetic composite material;
- great linearity of the magnetic characteristic and thermal stability;
- high specific energy density;
- high manufacturability and simplicity products manufacturing by pressing method;
- non-waste and low price of products;

Field of application:

New composite magnetic materials based on ferritized iron powder with thickness of a ferrite layer - from 1 up to several nanometers can successfully replace laminated electromagnetic steel for many high-frequency applications, such as transformers inductors, modern high-speed valve motors and generators, including electric vehicles and electric buses.

Composite resistive materials allow to create a wide range of electro-ceramic heating devices of any power, shape and configuration.

Hard magnetic materials are used for the manufacture of low-cost and high-performance magnets for various applications.

Magnetocaloric materials allow to make the non-motorized refrigeration devices.



Figure 1 Products based on composite materials

The work is supported by Republic of Uzbekistan and the Academy of Sciences of Republic of Belarus Foundation for Basic Research (bilateral project T19UZBG-004/2019).

[1] G. Govor, A. Vetcher, High-frequency synthesis of magnetic and resistive nanomaterials with special properties, Proceedings of Int. conf. Nanomat_EPC, Minsk, PP. 10-11, (2014).

[2] A.Vetcher, The development of new composite materials, Proceedings of Int. conf. 7 National Conference on Cooperation with the CIS countries, Lin, China, PP.3-6, (2014).

[3] G.A. Govor , V.V. Michnevich, Soft-magnetic composites from insulated iron powder and their potential technological applications, Inorg. Materials, vol.43, PP.711-713, (2007).

Magnetic ordering in multilayered compounds of $M1M2P_2X_6$ (M1, M2 – Mn, Fe, Cr, Cu; X – S, Se) type

K. Glukhov, T. Babuka, Yu. Vysochanskii

*Institute of Physics and Chemistry of Solid State, Uzhgorod National University,
54 Voloshin St., 88000 Uzhgorod, Ukraine,*

E-mail: kglukhov@gmail.com

Recently, the physical properties of layered magnetic atoms containing semiconducting compounds such as $Cu_xFe_{1-x}P_2S_6$, $MnPS_3$ or $CuCrP_2S(Se)_6$ attract the considerable attention of researchers because of its unusual collinear ferro(ferri)magnetic type of spin ordering and perspective of wide device applications of this materials [1,2]. Also, the 2D antiferromagnetic MPX₃ crystals, in which the magnetic interchange and magnon transport [3] have the peculiar character, are of particular interest. Besides, as is shown in [4], antiferromagnetism can be essentially «suppressed» on the transition from bulk to monolayer structure. The main peculiarity of these systems are in the separation of tightly bonded layers containing magnetic atoms by rather broad van der Waals gaps with weak cross interaction. Despite the weakness of interlayered coupling, this interaction can significantly influence the type of spin ordering in whole structure, forming magnetic superstructures including multiple unit cells of initial material.

In the presented study, both ab initio and model approaches involved in the investigation of peculiarities of exchange interaction in these compounds. Density functional methodology implemented in the ABINIT software package [5] had been used for establishing of main structural and energy parameters of $M1M2P_2X_6$ crystals, to use them in the model description of the spin subsystem. Investigation of the nature of spin ordering in $M1M2P_2X_6$ ferroics had been based on evaluating different magnetic configurations within the Monte-Carlo approach and utilizing different models of interactions between local spins. In considered structures, each site in the layer is connected with three nearest neighbors, six next neighbors, and three next-next neighboring sites which can form different in-plane magnetic structures. Hamiltonian of this Ising model written down as follows:

$$H = -\frac{1}{2} \sum_{\langle i,j \rangle} J_{ij}^{(1)} S_i S_j - \frac{1}{2} \sum_{\langle\langle i,j \rangle\rangle} J_{ij}^{(2)} S_i S_j - \frac{1}{2} \sum_{\langle\langle\langle i,j \rangle\rangle\rangle} J_{ij}^{(3)} S_i S_j + \mathbf{H} \sum S_i \quad (1)$$

where $J_{ij}^{(r)}$ corresponds to exchange integral for r^{th} neighbors, and $S_i = \pm 1$, and \mathbf{H} – z-component of external magnetic field.

With a positive exchange interaction J , all spins in the ground state are ordered identically, and with a negative value of J , the spins form two sublattices, the magnetizations of which are antiparallel in the ground state. In this model there is degeneration and frustration is possible. In recent years, low-dimensional structures have been intensively studied using the entropy Monte Carlo methods, one of which is the Wang-Landau algorithm [6]. This algorithm allows finding the density of states function of the system $g(E)$, knowing which, all the other characteristics of the system, such as free energy F , specific heat C , order parameter q and susceptibility χ , and their temperature behavior, can be easily calculated.

Obtained dependencies of magnetization and internal energy on parameters of exchange interaction and magnitude of external magnetic field allowed to built phase diagrams for considered systems and illustrate the general features of cooperative spin effects in layered chalcogen phosphates.

[1] A. Dziaugys, J. Banys, Yu. Vysochanskii, “Dielectric and electric properties of $CuFeP_2S_6$ crystal”, FM&NT-2013, Tartu, Estonia, p. 25, 21–24 April (2013).

[2] De S., Wen X., Bordas S.P.A. et al. “Defect engineering of 2d monatomic-layer materials“, Modern Physics Letters B., V. 27 (23), P. 1330017, (2013).

[3] W. Xing, L. Qiu, X. Wang, Y. Yao, Ya. Ma, R. Cai, S. Jia, X. C. Xie, and W. Han. “Magnon Transport in Quasi-Two-Dimensional van der Waals Antiferromagnets”, Phys. Rev. X, 9, 011026-011029, (2019)

[4] Kim K, Lim S Y, Lee J U, et al. ”Suppression of magnetic ordering in XXZ-type antiferromagnetic monolayer $NiPS_3$ ”, Nat. Commun., 10: 345 (2019)

[5] X. Gonze, B. Amadon, et al., “ABINIT: First-principles approach to material and nanosystem properties”, Comput. Phys. Commun. 180, 2582-2615 (2009)

[6] 9. Landau D.P., Tsai S.-H., Exler M. “A new approach to Monte Carlo simulations in statistical physics: Wang-Landau sampling”, Am. J. Phys., 72 (10), P. 1294–1302, (2004).

Challenges in the development of Commercial Analytical Research Organisations in the Baltic Sea region

M. Kirm¹, O. Rebane¹, U. Sassenberg²

1- Institute of Physics, University of Tartu, W. Ostwald str. 1, 50411 Tartu, Estonia
2- Deutsches Elektronen-Synchrotron, Notkestraße 85, 22607 Hamburg, Germany

marco.kirm@ut.ee

Even in the most developed parts of our World, there is always a challenge for habitants how to keep the competitiveness of region, to achieve its prosperous and sustainable development. An important component to solve this complicated question is always innovation, which strongly depends how various stakeholders in society act together combining resources available and even more important sharing understanding on common goals to be achieved. Thus quite often transnational cross-border cooperation is the most efficient and only the tool to solve this challenge. Innovation activities in the many regions of Europe are coordinated by joint funding and policy programs like the Interreg Baltic Sea Region Programme 2014-2020. Its main goal is integrated territorial development and cooperation for a more innovative, better accessible and sustainable Baltic Sea region. Its priority no 1 in the programme is ‘Capacity for innovation’, which is dedicated to actions strengthening the ability of our region to create and commercialise innovation. The countries around Baltic Sea feature in wide range of research and innovation infrastructures, but their distribution is non-uniform, utilization (incl. access by various actors) and interconnections are very far from optimal.

In order to contribute to the innovation development of the region a number of projects like Science Link [1], Baltic Tram [2] and now their successor CAROTS [3] “*Commercial Analytical Research Organisations Transnational Strategy*” have been funded by the Interreg BSR programme. The two successful former projects were focused on the building links between entrepreneurs and large scale facilities as well as with university labs and other research service providers, respectively. However, the CAROTS project aims to analyse the

current situation in Europe, world-wide best practices and conditions (incl. socio-economical polices) needed to establish a new type of private or public-private companies in the Baltic Sea region - a Commercial Analytical Research Organisation (CARO). CAROs act as intermediary bodies between industry and academia, can provide enterprises with much quicker yet complete assistance in analytical research in the fields of e.g. new materials, nanotechnology and life sciences.

The research and analysis performed by project partners will allow us to discuss the following aspects: Business models and financing of CAROs; networking and visibility of CAROs; cooperation with public sector and between CARO’s; public and private support programs (incl. funding); developing policy recommendations in transnational level, activities and impact of CAROs associated with the project, bottlenecks related to developing analytical research services, etc. Analysis of various innovation related challenges and possible solutions will be presented from a viewpoint of different stakeholders obtained through Interreg BSR programme supported collaborations with our direct participation.

The CAROTS project is part financed by the Interreg Baltic Sea Region Programme and by contribution of the BSR member states.

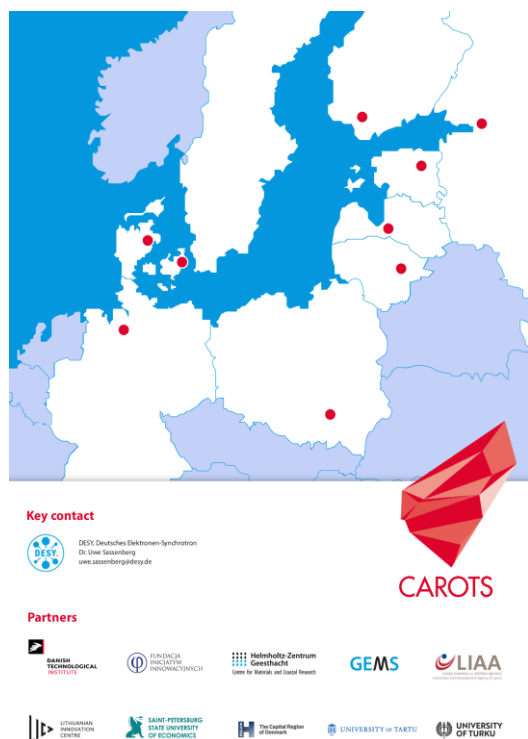


Figure 1 Baltic Sea region map showing the locations of the CAROTS project partners and geographical coverage. The project activities are funded by the Interreg Baltic Sea Region Programme 2014-2020 and its member states.

[1] <https://www.science-link.eu/>

[2] <https://www.baltic-tram.eu/>

[3] <https://www.carots.eu/>

Ab initio calculations of ReO_3 (001) as well as ABO_3 perovskite (001), (011) and (111) nano-surfaces, interfaces and defects therein

R.I. Eglitis¹, J. Purans¹

1- Institute of Solid State Physics, University of Latvia, 8 Kengaraga Str., Riga LV1063, Latvia

e-mail: rieglitis@gmail.com

By means of the hybrid exchange-correlation functionals, *ab initio* calculations for ReO_3 as well as main ABO_3 perovskite surfaces, namely SrTiO_3 , BaTiO_3 , PbTiO_3 , CaTiO_3 , SrZrO_3 , BaZrO_3 , PbZrO_3 and CaZrO_3 , were performed [1-7]. For ABO_3 perovskite (001) surfaces, with a few exceptions, all atoms of the upper surface layer relax inwards, all atoms of the second surface layer relax outwards, and all third layer atoms, again, inwards. The relaxation of (001) surface metal atoms for ABO_3 perovskite upper two surface layers for both AO and BO_2 -terminations, in most cases, are considerably larger than that of oxygen atoms, what leads to a considerable rumpling of the outermost plane. The ABO_3 perovskite (001) surface energies always are smaller than the (011) and especially (111) surface energies. The ABO_3 perovskite AO and BO_2 -terminated (001) surface band gaps always are reduced with respect to the bulk values. The B-O chemical bond population in ABO_3 perovskite bulk always are smaller than near the (001) and especially (011) surfaces. Electronic and atomic structure of $\text{BaTiO}_3/\text{SrTiO}_3$ and $\text{SrZrO}_3/\text{PbZrO}_3$ (001) interfaces are analyzed [8,9]. Systematic trends of *F*-center calculations in ABO_3 perovskite bulk and on their (001) surfaces are analyzed.

- [1] R.I. Eglitis, J. Kleperis, J. Purans, A.I. Popov and Ran Jia, Ab initio calculations of CaZrO_3 (0110 surfaces: systematic trends in polar (011) surface calculations of ABO_3 perovskites, *J. Mater. Sci.*, **55**, 203-217, (2020).
- [2] R.I. Eglitis, J. Purans, J. Gabrusenoks, A.I. Popov and Ran Jia, Comparative ab initio calculations of ReO_3 , SrZrO_3 , BaZrO_3 , PbZrO_3 and CaZrO_3 (001) surfaces, *Crystals* **10**, 745 (2020).
- [3] R.I. Eglitis and A.I. Popov, Systematic trends in (001) surface ab initio calculations of ABO_3 perovskites, *J. Saudi Chem. Soc.* **22**, 459-468 (2018).
- [4] R. I. Eglitis, *Ab initio* hybrid DFT calculations of BaTiO_3 , PbTiO_3 , SrZrO_3 and PbZrO_3 (111) surfaces, *Applied Surface Science* **358**, 556-562 (2015).
- [5] R.I. Eglitis, and David Vanderbilt, *Ab initio* calculations of BaTiO_3 and PbTiO_3 (001) and (011) surface structures, *Phys. Rev. B* **76**, 155439 (2007).
- [6] R.I. Eglitis, and D. Vanderbilt, First-principles, calculations of SrTiO_3 (001) and (011) surfaces, *Phys. Rev. B* **77**, 195408 (2008).
- [7] R.I. Eglitis, and D. Vanderbilt, *Ab initio* calculations of CaTiO_3 (001) and (011) surfaces, *Phys. Rev. B* **78**, 155420 (2008).
- [8] S. Piskunov and R. I. Eglitis, Comparative *ab initio* calculations of $\text{SrTiO}_3/\text{BaTiO}_3$ and $\text{SrZrO}_3/\text{PbZrO}_3$ (001) heterostructures, *Nuclear Instruments and Methods in Physics Research B* **374**, 20-23 (2016).
- [9] S. Piskunov and R. I. Eglitis, First principles hybrid DFT calculations of $\text{BaTiO}_3/\text{SrTiO}_3$ (001) interface, *Solid State Ionics* **274**, 29-33 (2015).

Modelling of oxygen reduction reaction at solid oxide fuel cell cathode

Yu. A. Mastrikov¹, E. A. Kotomin^{1,2}

1- Institute of solid State Physics, University of Latvia, Ķengaraga 8, Rīga, LV1029, Latvia
2- Max Planck Institute for Solid State Research, Heisenbergstraße 1, D70569 Stuttgart, Germany

Main author email address: yuri.mastrikov@cfi.lu.lv

ABO_3 perovskites is a typical material for Solid Oxide Fuel Cells (SOFC). Performance of the latter strongly depends on the efficiency of Oxygen Reduction Reaction (ORR) on the SOFC cathode. AO - and BO_2 -terminated (001) surfaces are the most stable ones. Five times higher oxygen vacancy concentration on MnO_2 termination make this termination much more favourable for ORR on the $(La,Sr)MnO_3$ (001) surface. In agreement with experimental data, the ORR kinetics is mostly determined by the BO_2 termination, which in a long-term, however, gets degraded by segregated Sr. An extensive first-principles study gives a broad and detailed overview of the ORR on SOFC prototype material $(La,Sr)MnO_3$.

[1] E. Kotomin, Y. Mastrikov, R. Merkle and J. Maier, "First principles calculations of oxygen reduction reaction at fuel cell cathodes," *Current Opinion in Electrochemistry*, vol. 19, pp. 122-128, (2020).

Slater Insulator Phase of $A_2(A=Li, Na)IrO_3$: first principal calculations

Husnu Koc¹, Amirullah M. Mamedov^{2,3}, Ekmel Ozbay²

1- Department of Physics, Faculty of Sciences, Siirt University, Siirt, Turkey

2- Nanotechnology Research Center (NANOTAM), Bilkent University, 06800 Bilkent, Ankara, Turkey

3- International Scientific Center, Baku State University, Baku, Azerbaijan

mamedov@bilkent.edu.tr

Recently, there have been intensive studies concerning the interplay between the spin-orbit coupling, the Coulomb repulsion and the bandwidth in the perovskite antiferromagnetic insulators - A_2IrO_3 . The spin-orbit coupling driven $J_{\text{eff}}=(1/2)$ Mott mechanism remains as the most successful model to explain the antiferromagnetic insulating ground state of iridates [1]. In this model, the crystal field split t_{2g} states of Ir(Ru) 5d manifold are further split by spin-orbit coupling leading to fourfold degenerate $J_{\text{eff}}=(3/2)$ quartet and a twofold $J_{\text{eff}}=(1/2)$ doublet states. For iridates with a formal valence of + 4, which implies to an electronic configuration of $5d^5$, the low energy $J_{\text{eff}}=(3/2)$ states are fully occupied with two electrons each and, the $J_{\text{eff}}=(1/2)$ doublet remain singly occupied. However, since the bandwidth of the $J_{\text{eff}}=(1/2)$ doublets are narrow, Coulomb correlations set in splitting the doublets into an upper and lower Hubbard band, thereby opening an electronic gap. Although the correctness of the model is debated on the role of Coulomb correlations [2], the J_{eff} model not only accounts for the electron localization and insulating state of iridates, but also predict several physical properties which are consistent with the experiments [3].

Our study based on density functional theoretical methods find that local approximations to the exchange-correlation potential correctly predicts A_2IrO_3 as an antiferromagnetic insulator. Unlike that for Ir+4 iridates, the Coulomb correlation effects are found to be of little relevance in rendering the system its insulating ground state. In the present study, the first principle calculations have been used also to evaluate the structural, electronic, magnetic and elastic properties of A_2IrO_3 . The computed equilibrium properties are in good agreement with reported experimental and theoretical results. The electronic structure were calculated for all antiferromagnetic structures considered. The calculated band gap values for A_2IrO_3 are found to be larger with GGA method as compared to the results obtained using the GGA + U approximation. The calculation showed the dependence of the magnetic properties on the d element in the investigated systems. It is found that the antiferromagnetic state is more stable than the nonmagnetic and ferromagnetic configurations in the P4/mmm structure. Furthermore, the studied compounds have demonstrated a certain mechanical stability performance against compression. Overall, our calculations revealed novel properties of the A_2IrO_3 . Since, there are no experimental studies on elastic properties of such compounds in the P4/mmm structure available in the literature to compare with, future experimental may be realized using appropriate synthesis conditions. These compounds can be considered as an ideal electrode material for magnetic tunnel junctions, giant magnetoresistance devices, and for injecting spin polarized currents into semiconductors.

[1] B.J. Kim, H. Jin, S.J. Moon, J.-Y. Kim, B.-G. Park, C.S. Leem, J. Yu, T.W. Noh, C. Kim, S.-J. Oh, J.-H. Park, V. Durairaj, G. Cao, E. Rotenberg, Novel $J_{\text{eff}}=1/2$ Mott State Induced by Relativistic Spin-Orbit Coupling in Sr_2IrO_4 Phys. Rev. Lett. 101, 076402 (2008).

[2] R. Arita, J. Kune, A.V. Kozhevnikov, A.G. Eguiluz, M. Imada, Ab initio Studies on the Interplay between Spin-Orbit Interaction and Coulomb Correlation in Sr_2IrO_4 and Ba_2IrO_4 , Phys. Rev. Lett. 108, 086403 (2012)

[3] A. Author G. Cao, P. Schlottmann, The challenge of spin-orbit-tuned ground states in iridates: a key issues review, Rep. Prog.Phys. 81 042502 (2018)

Revealing polymer contact electrification mechanisms and designing triboelectric nanogenerators

A. Šutka¹, K. Mālnieks¹, L. Lapčinskis²

1- Research Laboratory of Functional Materials Technologies, Faculty of Materials Science and Applied Chemistry, Riga Technical University, Paula Valdena 3/7, LV-1048, Riga, Latvia.

2- Institute of Technical Physics, Faculty of Materials Science and Applied Chemistry, Riga Technical University, Paula Valdena 3/7, LV-1048, Riga, Latvia

andris.sutka@rtu.lv

The triboelectric nanogenerators are becoming more and more popular because they provide mechanical energy harvesting and conversion in to the electricity by using cheap and simple polymer materials. The source of mechanical energy that can be converted in electricity by triboelectric nanogenerator can be human motion, ambient vibrations and even noise. This energy can be further used to charge capacitor or battery and supply energy for portable electronic device.

The surface charge formation on polymers upon contacting-separating is the key factor to ensure the energy harvesting function for triboelectric nanogenerator devices. The three main mechanisms considered for polymer electrification are: (i) electron transfer [1], (ii) heterolytic covalent bond break and material transfer [2], and (iii) ion transfer [3]. The ion transfer, where ions are separated between water adsorbate layers on contacted polymers, seems not the dominating mechanism as proven by several studies from independent groups [4]. The polymer contact electrification has been observed in the complete absence of water and between identical materials which should exhibit the same affinity between cationic and ionic species in water. Thus, in the past few years, the debate has concentrated on electron transfer and covalent bond breaking as possible dominating polymer triboelectrification mechanisms. In recent years we have investigated the surface charge formation (triboelectrification) mechanisms on large variety of polymer materials with difference in cohesion energy, surface adhesion and structural state. The experimental results indicate that the triboelectrification mechanism for polymer insulators is heterolytic covalent bond cleavage (heterolysis or heterolytic fission) alongside with material transfer [4-6]. The surface charge increases with decreasing cohesion energy [4] or increasing surface adhesion [5]. We observed also a dramatic three orders of magnitude increase in surface charge when passing the transition temperature from glassy to a rubbery state [6]. When crossing the glass transition temperature, the adhesion, softness and deformation increases, thus enhance the covalent bond cleavage, material transfer, and surface charge formation. We also show the pathways to enhance the triboelectrification avoiding expensive and complicated nanostructuring approaches.

[1] J. Chen and Z. L. Wang, Reviving vibration energy harvesting and self-powered sensing by a triboelectric nanogenerator, *Joule*, 1, 480-521, (2017).

[2] H. T. Baytekin, A. Z. Patashinski, M. Branicki, B. Baytekin, S. Soh and B. A. Grzybowski, The mosaic of surface charge in contact electrification, *Science*, 333, 308, (2011).

[3] L. S. McCarty and G. M. Whitesides, Electrostatic charging due to separation of ions at interfaces: contact electrification of ionic electrets, *Angew. Chem., Int. Ed.*, 47, 2188-2207, (2008).

[4] A. Šutka, K. Mālnieks, L. Lapčinskis, P. Kaufelde, A. Linarts, A. Bērziņa, R. Zābels, V. Jurkāns, I. Gorņevs, J. Blūms and M. Knite, The role of intermolecular forces in contact electrification on polymer surfaces and triboelectric nanogenerators *Energy Environ. Sci.*, 12, 2417-2421, (2019).

[5] L. Lapčinskis, K. Mālnieks, J. Blūms, M. Knite, S. Oras, T. Käämbre, S. Vlassov, M. Antsov, M. Timusk and A. Šutka, The Adhesion-Enhanced Contact Electrification and Efficiency of Triboelectric Nanogenerators, *Macromol. Mater. Eng.*, 305, 1900638, (2020).

[6] A. Šutka, A. Linarts, K. Mālnieks, K. Stiprais and L. Lapčinskis, Dramatic increase in polymer triboelectrification by transition from a glassy to rubbery state, *Mater. Horiz.*, 7, 520-523, (2020).

Reduction of impurity sources in Si crystal growth system with electron gun beam heating

A. Kravtsov¹, J. Virbulis², A. Krauze²

1- KEPP EU, Carnikavas str. 5, Riga, Latvia

2- Institute of Numerical Modeling, University of Latvia, Jelgavas str. 3, Riga, Latvia

Main author email address: armands.krauze@lu.lv

Many variations of Chochralski method are used for growing monocrystalline materials. For silicon (Si), the most widely used method is pulling monocrystals from melt heated in a crucible by resistance heating. The key problem of this method is introduction of impurities due to a contact between the melt and the crucible. In this article we describe results of development of an alternative crystal growth method which uses electron gun beams for Si heating. 300 mm diameter crystals of up to 80 kg mass were grown from a quartz crucible by this method [1].

Some of the results were already published [1,2]. The Si material in a cold crucible with heat insulation was heated by two electron gun heaters with cold cathodes and a hydrogen-oxygen mixture as a working gas (the oxygen content less than 1%). The purity of the obtained crystals was comparable to that of the float zone Si samples, but the Si material remaining after the growth showed the presence of metallic impurities that were introduced during the growth process.

A new series of experiments was conducted to determine the source of the impurities. A copper crucible was used, and the system was simplified by discarding the heat insulation and some other parts. It was assumed that the gas flow from the gun and the interaction between the electron beam or reflected electrons and the crucible and growth chamber vessel must be reduced. For this purpose, a gas-dynamic window was placed between the electron gun and the growth chamber. Also positively-charged charge traps were placed along the crucible to reduce the number electrons hitting the vessel and crucible.

Five experiments were conducted; two with the window only, two with the charge traps only, and one with both the window and the charge traps. The generated power was close to that in the original growth processes, and the melt was saturated with impurities for six hours.

The analysis of obtained samples showed that:

- The Na and Ca impurities, discovered in [9], disappeared in the experiments. This suggests that their source was the discarded heat insulation. The disappeared Sb impurities were generated by the inner growth chamber surface which was contaminated with Sb during growth processes conducted before the experiments;
- It seems that Fe and Cr impurity sources are the growth chamber walls. The window has no influence on them, but the charge traps significantly reduced them.
- It seems that there are two Cu impurity sources: the gun and the irradiated crucible. Both the window and the charge traps significantly reduce the Cu concentration;
- Al impurities come only from the gun, but the window cannot eliminate them completely;
- The window reduces the oxygen flow from the gun 25 times.

The Fe, Cr, and Cu impurities could be generated by electron irradiation of the chamber walls and crucible. Numerical modeling of the electron beam, [3], showed that it is very unlikely that this irradiation came directly from the beam. Our suggested explanation is that backscattered electrons from the beam have energy high enough to cause ion emission from the chamber walls and crucible. This would explain the reduction of the Fe and Cr impurities by the charge traps.

It seems that Al impurities come either as neutral atoms carried by the gas or as positively charged ions. To reduce these impurities, a separation of the Al flow from the beam by the magnetic field is proposed. The magnetic field is to be generated by a special system for electron beam deflection. A numerical model was developed for optimization of the parameters of this beam deflection system.

Considering all the above, the obtained results can be considered good for all impurities except Al.

[1] A. Kravtsov, Developing of silicon growth techniques from melt with surface heating, IOP Conf. Series Materials Science and Engineering, vol. 355, p. 012007, (2018)

[2] A. Kravtsov, Novel metod for feedstock production for high efficiency FZ c-Si PV, IOP Conf. Series Materials Science and Engineering, vol. 77, p. 012037, (2015)

[3] A. Kravtsov, Al. Kravtsov, R. Fuksis and M. Pudzs, Ingot pulling with electron beam heating: Process enhancements, 2015 IEEE 42nd Photovoltaic Specialist Conference (PVSC 2015), New Orleans, LA, 2015, pp. 686-689

[4] A. Krauze, J. Virbulis, A. Kravtsov, Modeling electron beam parameters and plasma interface position in an anode plasma electron gun with hydrogen atmosphere, IOP Conf. Series Materials Science and Engineering, vol. 355, p. 012008, (2018)

Characterization of ZnMgO Based Solar-blind Photodetector with Supercritical Fluid Treatment

Tsung-Ming Tsai^{1,*}, Liuwen Chang¹, Chih-Cheng Yang¹, Li-Chuan Sun¹, M. C. Mitch Chou¹

1-Department of Materials and Optoelectronic Science, National Sun Yat-Sen University, No.70, Line-hai Rd., Kaohsiung 80424, Taiwan

**email address: tmsai@faculty.nsysu.edu.tw*

Deep UV photon sensors based on wide or ultra-wide bandgap semiconductors, such as II-oxides, III-nitrides, diamond, and SiC can be used extensively in applications such as biological and chemical sensors for ozone detection, detectors for water purification, determination of pollution levels in air or any biological agent, etc [1-4]. However, more and more applications require the photosensing device/system enabling discrimination between emitting or polluting species. For example, current aerosol ultraviolet laser-induced fluorescence (UV-LIF) detection systems measure fluorescence intensity using bulky spectral filters and multi-anode photomultiplier for acquiring multiple-point spectra. The identification and quantification of SO₂, NO_x, H₂S and O₃ emission based on photo-absorption/fluorescence techniques can also be benefited by the solid state detectors with multiple-bandwidth capability of detection. However, the bandgaps of diamond and SiC are not tunable, whereas those of AlGa_n (composite III-nitrides) can only be varied from 3.4 eV to less than 4.5 eV through bandgap engineering [5-7].

The radically novel concept of this study is to use the ZnO-MgO pseudobinary system, which has the merit of providing materials with tunable bandgap from 3.3~7.8 eV as shown in Fig. 1, thus significantly enhancing the ability of the devices at different energies simultaneously. Our recent results indicated that the limitation of ZnO and MgO mutual solubilities can be broken by stabilizing the high MgO-content wurtzite Zn_{1-x}Mg_xO and high

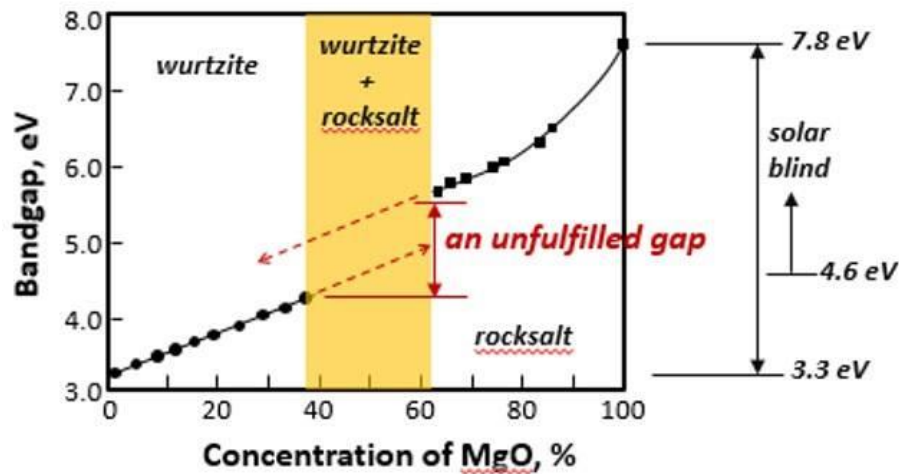


Figure 1 Energy bandgap of Zn_{1-x}Mg_xO vs the doping concentration of MgO.

ZnO-content rocksalt Zn_{1-x}Mg_xO by using low lattice mismatch substrates such as ScAlMgO₄, MgO and Cu₂O. Various Zn_{1-x}Mg_xO MSM-type devices with different low lattice mismatch substrates will be fabricated for deep UV photosensing. Such devices for deep UV solar-blind detection will have advantages of easy fabrication and low cost. However, the success of the devices relies on a thorough understanding of the basic microstructural, optical and electrical properties of the materials and the devices. We will explore the physics operation mechanism of Zn_{1-x}Mg_xO devices through electrical and material analysis. Finally, the effect of the supercritical fluid technology to improve the optoelectronic properties of Zn_{1-x}Mg_xO MSM-type devices for solar-blind photodetector application will be discussed in this work.

[1] X. C. Guo et al, beta-Ga₂O₃/p-Si heterojunction solar-blind ultraviolet photodetector with enhanced photoelectric responsivity, J. Alloys Comp., vol. 660, pp. 136-140 (2016).

[2] P. Wu, M. Funato & Y. Kawakami, Environmentally friendly method to grow wide-bandgap semiconductor aluminum nitride crystals: Elementary source vapor phase epitaxy, Sci. Rep., vol. 5, pp. 17405 (2015).

[3] Y. Koide et al., Schottky photodiode using submicron thick diamond epilayer for flame sensing, Nano-Micro Lett., vol. 1, pp. 30-33 (2009).

- [4] M. Liao et al., Comprehensive Investigation of Single Crystal Diamond Deep-Ultraviolet Detectors, *Jpn. J. Appl. Phys.*, vol. 51, pp. 090115 (2012).
- [5] C. Coughlan et al., Band gap bowing and optical polarization switching in $\text{Al}_{1-x}\text{Ga}_x\text{N}$ alloys, *Stat. Soild. B*, vol. 252, pp. 879-884 (2015).
- [6] P. Vennegues et al., Relaxation mechanisms in metal-organic vapor phase epitaxy grown Al-rich (Al,Ga)N/GaN heterostructures, *J. Appl. Phys.*, vol. 97, pp. 024912 (2005).
- [7] B. Neuschl et al., Composition dependent valence band order in c-oriented wurtzite AlGaIn layers, *J. Appl. Phys.*, vol. 116, pp. 113506 (2014).

Organic solar cells: from light absorption to electric power

Rokas Jasiūnas¹, Huotian Zhang³, Armantas Milianas³, Andrius Devižis¹, Juozas Šulskus², Feng Gao³ and Vidmantas Gulbinas^{1,2}

1 Center for Physical Sciences and Technology, Sauletekio av.3, Vilnius, 10257 (Lithuania)

2 Institute of Chemical Physics, Faculty of Physics, Vilnius University, Sauletekio av. 9-III, 10222 Vilnius (Lithuania)

3 Department of Physics Chemistry and Biology (IFM), Linköping University, Linköping SE-58183, Sweden

vidmantas.gulbinas@ftmc.lt

Organic photovoltaics (OPV) has been persistently developing for over three decades as one of the alternative solar energy-harvesting technology. Advantages of being light-weight, flexible, transparent and low-cost stimulated the research in materials design, morphology optimization, device engineering and mechanism study in order to increase solar-to-electrical power conversion efficiency (PCE). Even though it has remarkably increased since their appearance, and now record values exceed 16% for single junction OPV devices [5], yet it is still insufficient to compete with state-of-the-art inorganic semiconductor photovoltaic technologies. During the last few years a rapid PCE increase was achieved by employing small low-bandgap molecules as an alternative to well established fullerene type acceptors.

Among different organic solar cell technologies, all-organic bulk heterojunction devices currently demonstrate the best PCE. However, major photo physical processes in these devices still lack in-depth understanding. We used several advanced investigation techniques covering exceptionally wide temporal window to address all sequence of processes starting from photon absorption and photogeneration of Frenkel exciton to carrier extraction. We address several non-fullerene organic solar cells and compare them with cell with conventional PCBM acceptor. To better reproduce the cell operation conditions we apply simulated solar light during some measurements.

Solar cells, based on non-fullerene acceptors, benefit from a longer wavelength absorption, however possess additional loss channels. Small HOMO level offset of electron donating and accepting materials in all-organic solar cells causes inefficient hole transfer under excitation of acceptor material and also enhanced geminate recombination of interfacial charge transfer state during initial several picoseconds, which is almost absent in cells with PCBM acceptor. Depending on the HOMO level offset, the geminate recombination causes up to 20-50% losses. The CT state splitting takes place during tens of ps allowing negligible additional geminate carrier recombination during this time. Subsequent carrier extraction is very similar between all investigated non-fullerene solar cells and is slightly faster than in cell with PCBM acceptor. Non-geminate carrier recombination, competing with the carrier extraction, correlates with the power conversion efficiency. In the best performing non-fullerene devices, it is slightly slower than in cells with PCBM, however, in the worse performing non-fullerene cells it is up to two times faster.

The investigation revealed major loss channels in the state-of-the-art organic solar cells giving directions to further optimisation of solar cell materials and device fabrication technologies.

[1] . Hou, O. Inganäs, R. H. Friend, and F. Gao, "Organic solar cells based on non-fullerene acceptors," Nature Materials, vol. 17, no. 2, pp. 119–128, Jan. 2018.

Towards the Understanding of NASICON Structured Systems for the Na-ion Energy Storage

D. Gryaznov¹, G. Snarskis¹, J. Pilipavičius¹, J. Juodkazytė¹, L. Vilčiauskas¹

¹Center for Physical Sciences and Technology, Saulėtekio al. 3, LT-10257 Vilnius, Lithuania

Linias.Vilciauskas@ftmc.lt

NASICON (Na SuperIonic Conductor) structured phosphate framework compounds are attracting a lot of attention from the battery research community as potential Na-ion battery electrodes. They offer high Na-ion mobility, structural stability, electrochemical durability and widely tunable redox potentials via selection of different metals [1]. We focus on a special class of NASICON-structured $\text{Na}_x\text{Mn}_y\text{Ti}_{2-y}(\text{PO}_4)_3$ ($x = 1.0 - 4.0$; $y = 0.0 - 1.5$) solid solutions which could be applied both as positive and negative Na-ion electrode materials [2]. In this work a wide range of theoretical and experimental methods were applied in order to gain a deep understanding of electronic, structural and electrochemical properties of $\text{Na}_x\text{Mn}_y\text{Ti}_{2-y}(\text{PO}_4)_3$ ($x = 1.0 - 4.0$; $y = 0.0 - 1.5$) systems.

A series of $\text{Na}_x\text{Mn}_y\text{Ti}_{2-y}(\text{PO}_4)_3$ ($x = 1.0 - 4.0$; $y = 0.0 - 1.5$) compounds were studied by high level Density Functional Theory (DFT) calculations using hybrid and DFT+U methodologies. The systems were analyzed in detail in terms of the necessary symmetry changes involving Na^+ -vacancy and mixed titanium valence charge ordering at $x = 1.0 - 4.0$ and $y = 0.0$. A number of interesting correlations between the latter and the electronic properties such as the origin and size of band gaps were discovered. The overall stability of this series at $x = 1.0 - 4.0$; $y = 0.0 - 1.5$ was investigated in detail by calculating the phase diagram from the first principles using the SCAN+U and cluster expansion formalisms. The results indicate a non-uniform thermodynamic stability of these solid solutions over the full $y = 0.0 - 1.5$ range.

The structural properties of $\text{Na}_x\text{Mn}_y\text{Ti}_{2-y}(\text{PO}_4)_3$ ($x = 1.0 - 3.0$; $y = 0.0 - 1.0$) were investigated by first preparing these materials using various soft-chemistry and solid-state methods and then analyzing them using X-Ray powder diffraction, X-Ray photoelectron spectroscopy, Scanning/Transmission Electron Microscopies and elemental analysis. The electrochemical properties of these materials were investigated using Cyclic Voltammetry and galvanostatic charge/discharge cycling in a three-electrode setup. The results indicate a number of interesting properties dependent on the Mn content in $\text{Na}_x\text{Mn}_y\text{Ti}_{2-y}(\text{PO}_4)_3$, such as the changing behaviour from the typical solid-state diffusion to pseudo-capacitance for the $\text{Ti}^{4+}/\text{Ti}^{3+}$ redox couple as y changes from 0.0 to 1.0.

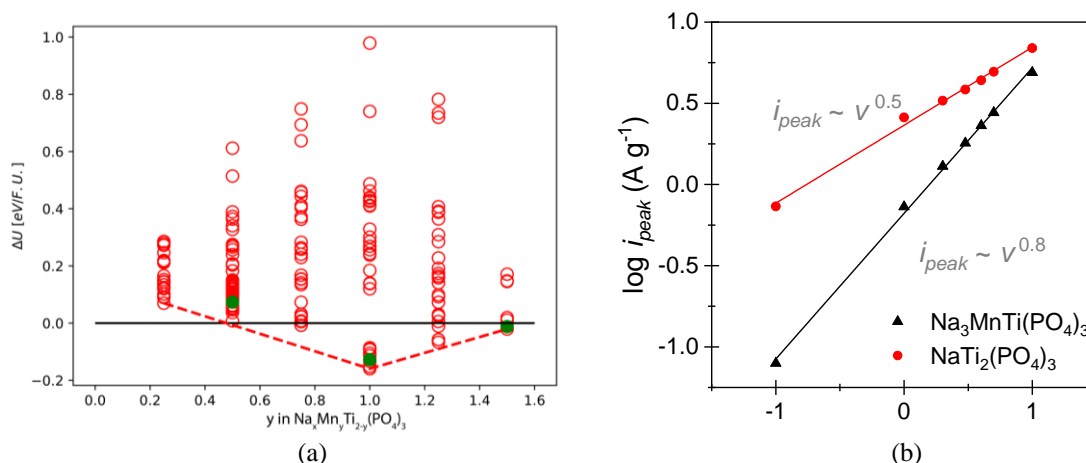


Figure 1 a) Convex hull of $\text{Na}_x\text{Mn}_y\text{Ti}_{2-y}(\text{PO}_4)_3$: red circles - GGA-PBE formation energies, green dots - B1WC formation energies; b) Cyclic voltammetry peak current dependence on the voltage scan rate and the resulting exponents distinguishing between the solid-state diffusive and pseudo-capacitive behavior.

Acknowledgements:

This project has received funding from the European Regional Development Fund (Project No. 01.2.2-LMT-K-718-02-0005) under grant agreement with the Research Council of Lithuania (LMTLT).

[1] S. Chen, C. Wu, L. Shen, C. Zhu, Y. Huang, K. Xi, J. Maier, Y. Yu, Challenges and Perspectives for NASICON-Type Electrode Materials for Advanced Sodium-Ion Batteries, *Adv. Mater.*, 29 1700431 (2017).

[2] H. Gao, Y. Li, K. Park, J. B. Goodenough, Sodium Extraction from NASICON-Structured $\text{Na}_3\text{MnTi}(\text{PO}_4)_3$ through Mn(III)/Mn(II) and Mn(IV)/Mn(III) Redox Couples, *Chem. Mater.*, 28, 6553-6559 (2016).

Electro-optical characteristics of NIR light emitting sources

S. Pūkienė, A. Jasinskas, V. Bukauskas, V. Agafonov, M. Kamarauskas, A. Lukša, A. Bičiūnas, B. Čechavičius, A. Šetkus, R. Butkutė

Center for Physical Sciences and Technology, Saulėtekio av. 3, LT-10257, Vilnius, Lithuania

simona.pukiene@ftmc.lt

Recently, the infrared (IR) spectral region has attracted huge attention. Due to a number of vibrational absorption lines of organic molecules, IR becomes very important for applications in various areas, such as biomedicine, life and environmental sciences. For example, Light identification and ranging (LiDAR) called Frequency-Modulated Continuous-Wave LiDAR require narrow linewidth laser of the sub-MHz range and high power (up to 200 mW at 1550 nm). New emerging field of quantum cryptography requires single-frequency lasers at 785 nm for sending encoded information over the fiber networks and from nano-satellites down to Earth. High power, high brightness and narrow-line 785 nm lasers are on demand in Raman Spectroscopy for industrial setups and remote environmental contamination measurements. However, most of these applications are limited by the lack of efficient semiconductor IR sources and detectors. High temperature operation of semiconducting lasers is limited by losses due to non-radiative Auger recombination. Thus, the engineering and study of new materials functioning at room temperature in IR is still important and challenging. The research focuses on two objectives: first, low power, small size and weight NIR sources for applications in wireless sensing systems and, secondly, narrow linewidth and high power NIR lasers for remote applications. In this work, A3B5 compounds were used into the active area of NIR emitters operating up to 860 nm, while bismide-based A3B5 MQW structures, exhibiting strong energy bandgap reduction (70 to 90 meV/%Bi) and increased spin-orbit splitting energy ΔSO [1, 2] as well as lower temperature sensitivity [3, 4], have been employed in sources covering the 1.0 μm -1.55 μm wavelength region.

The diode structures were grown by molecular beam epitaxy (MBE) under optimized growth condition onto n-GaAs(100) substrate. Both the n-type and p-type AlGaAs waveguide layers were of 1.5 μm thickness and doped of $1 \times 10^{18} \text{ cm}^{-3}$ by silicon and beryllium, respectively. The surface morphology of the structures examined by atomic force microscopy (AFM), optical properties evaluation by measuring room-temperature photoluminescence. Grown structures were processed using UV photolithography. As-cleaved electrical properties of LDs and LEDs were investigated using Keithley 4200 semiconductor characterisation system and Cascade Microtech Summit probe station. DC, pulsed current-voltage (I-V, pulsed I-V, see Fig. 1) and capacitance-voltage (C-V) dependences were measured in air at room temperature. Closed chamber was used to avoid illumination of the samples.

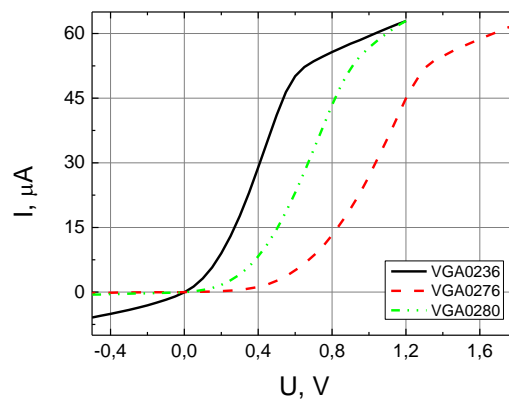


Fig. 1. DC I-V characteristics of several laser structures in the dark.

- [1] K. Oe et al., New Semiconductor Alloy $\text{GaAs}_{1-x}\text{Bi}_x$ Grown by Metal Organic Vapor Phase Epitaxy, Jpn. J. Appl. Phys., 37, L1283 (1998).
- [2] S. Tixier et al., Molecular beam epitaxy growth of $\text{GaAs}_{1-x}\text{Bi}_x$, Appl. Phys. Lett., 82, 2245 (2003).
- [3] K. Oe et al., Proposal on a temperature-insensitive wavelength semiconductor lasers. IEICE Transactions on Electronics, E79-C:1751_9 (1993).
- [4] W. M. Linhart et al., Temperature dependence of band gaps in dilute bismides. Semicond. Sci. Technol., 33(7), 073001 (2018).

Radiation-Induced Point Defects and Processes in Ionic Oxides – where we are standing now and what we understand better

A. I. Popov, E.A. Kotomin

Institute of Solid State Physics, University of Latvia, 8 Kengaraga, LV-1063, Riga, Latvia

popov@latnet.lv, popov@cfi.lu.lv

Already about 60 years ago, Levi and Dienes performed first studies of radiation damage in Al_2O_3 crystals caused by fast neutrons, and almost fifty years ago, Compton and Arnold measured the threshold energy to displace atoms by incident energetic electrons. At the Second International Conference on Radiation Effects in Insulators (Albuquerque, 1983), J.H. Crawford summarized in his report the work done by that time and discussed what we still did not know at all or not enough [1]. In particular, he highlighted how scanty was our knowledge of interstitial defects.

Since then, many attractive ideas have been suggested, and many precise experiments have been carried out. It is impossible to list all or even the most interesting and important of them in a single presentation (see, e.g., [2, 3]). Therefore, in the present talk we will try to summarize only key results related to simple electron centers (F, F^+ and their dimers, colloids) with a special attention to interstitial defects: their electronic structure, role and manifestations in the processes of thermal annealing of the F-type centers in Al_2O_3 [4] and several other ionic oxides, such as MgO, MgAl_2O_4 , ZnO, BeO and $\text{Y}_3\text{Al}_5\text{O}_{12}$.

We will also discuss the possible solution of the second puzzle, mentioned by Crawford, namely why and how the so-called hole V-type centers could be formed under optical transformation of the electron centers $\text{F}^+ \rightarrow \text{F}$ in $\alpha\text{-Al}_2\text{O}_3$ and MgO single crystals. Finally, we will discuss the process of the intrinsic high-temperature migration/transformation of F centers in ionic oxides and demonstrate how F-type dimer centers and metallic colloids could be formed as a part of the process [5, 6].

[1] J.H. Crawford, Nucl. Instrum. Meth. B 1 (1984) 159-165.

[2] E.A. Kotomin and A.I. Popov, Nucl. Instrum. Meth. B 141 (1998) 1-15.

[3] S.J. Zinkle and C. Kinoshita, J. Nucl. Mat. 251 (1997) 200-217.

[4] A.I. Popov, A. Lushchik, et al. Nucl. Instrum. Meth. B 433 (2018) 93-97.

[5] V.N. Kuzovkov, E.A. Kotomin, and A.I. Popov, J. Nucl. Mater., 502 (2018) 295-300.

[6] E.A. Kotomin, V.N. Kuzovkov, A.I. Popov, R. Vila, Nucl. Instrum. Meth. B 374 (2016) 107-110

Synthesis of AlON powders and ceramics and their optical and luminescent properties

Anna P. Kozlova^{1,2}, Sergey I. Rupasov¹, Tigran G. Akopdzhanyan³, Vladimir Pankratov²

1- National University of Science and Technology "MISIS", 4 Leninsky prospekt, Moscow, 119049, Russia

2- Institute of Solid State Physics, University of Latvia, 8 Kengaraga, LV-1063, Riga, Latvia

3- Merzhanov Institute of Structural Macrokinetics and Materials Science Russian Academy of Sciences, 8 Academician Osipyan str., Chernogolovka, Moscow Region, 142432, Russia

kozlova.ap@misis.ru

Aluminum oxynitride (AlON) ceramics is well known due to combination of its thermomechanical [1] properties and transparency in UV, VIS, and IR wavelength range [0, 3]. In this regard, AlON can be an alternative to tempered glass and sapphire single crystals and is also promissory for high-temperature applications in aerospace engineering and power industry [4].

The main methods of AlON powder synthesis are solid state reaction of AlN and Al₂O₃ [5, **Error! Reference source not found.**] and carbothermal reduction of Al₂O₃ [7] at temperatures higher than 1700 °C for a few hours. Self-propagating High-temperature Synthesis (SHS) is a highly efficient method to produce powders and ceramics, especially nitride ceramics [8]. However at the same time there are no reports about production of transparent AlON ceramics from SHS powders as pure single-phase AlON powder has not been synthesized yet. The reason is synthesis of pure single-phase AlON powder by combustion is still difficult. We studied combustion of Al/Al₂O₃ mixture in high-pressure nitrogen in order to produce pure single-phase AlON powder. Addition of Mg(ClO₄)₂ or KClO₄ and extra Al were proposed to increase combustion temperature.

Different methods to produce transparent ceramics from AlON powder are known such as pressureless sintering, hot isostatic pressing, microwave sintering. All these methods require high sintering temperatures, about 1800–2000 °C. We utilized pressureless sintering of SHS-AlON powder with 0.5 wt. % Y₂O₃ as sintering additive at 1930 °C for 2-6 h to show the possibility of transparent ceramics formation from SHS AlON powder.

The optical transmission and reflection characteristics of the ceramic samples were measured using the UV-Vis-NIR spectrophotometer Cary-5000 (Agilent Technologies). The ceramic samples in the form of polished plates with ~1.5 mm thickness were measured. Using reflection spectra by the Kubelka-Munk formula, the band gap values of raw powder samples were estimated. Luminescence properties of both ceramic and powder AlON samples have been studied under vacuum ultraviolet (VUV) excitations of 1.5 GeV storage ring of MAX IV synchrotron. The photoluminescence setup [9] of the FinEstBeAMS beamline [10] of MAX IV was exploited for the luminescence experiments.

It will be demonstrated that both optical and luminescence properties of the final ceramic samples strongly depend on the ceramics' sintering time as well as on the preparation technology of raw AlON powders. Two main emission bands at 280 nm and 350 nm were observed under 45 eV excitation at low temperature in all ceramic samples studied. The 350 nm emission reveals a well pronounced excitonic peak at 5.6 eV in the excitation spectra, while the 280 nm emission can be excited under deep VUV excitations only. It is remarkable that the intensity of 280 nm emission is sample dependent and the correlation between synthesis parameters and the intensity of the high-energy emission band is established. The luminescence centers responsible for both emission bands as well as the energy transfer processes from host lattice to the emission centers will be discussed.

The reported study was funded by RFBR according to the research project № 19-08-00655.

- [1] T. M. Hartnett, C. T. Warner, D. Fisher, W. Sunne, *Ceramic Transactions* 178 (2006) 19–35
- [2] N. D. Corbin, *Journal of the European Ceramic Society* 5 (1989) 143–154
- [3] F. Y. C. Boey, X. L. Song, Z. Y. Gu, A. Tok, *Journal of Materials Processing Technology* 89–90 (1999) 478–480
- [4] J. W. McCauley et al., *Journal of the European Ceramic Society* 29 (2009) 223–236
- [5] S. Bandyopadhyay et al., *Journal of the American Ceramic Society* 85 (2002) 1010–1012
- [6] Y. Wang, T. Lu, L. Gong, J. Qi, J. Wen, J. Yu, L. Pan, Y. Yu, N. Wei., *Journal of Physics D: Applied Physics*, 43 (2010) 275403,
- [7] J. Zheng, B. Forslund, *Journal of the European Ceramic Society* 15 (1995) 1087–1100
- [8] Borovinskaya, I.P., Loryan, V.E., and Zakorzhevsky, V.V., *Nitride Ceramics: Combustion Synthesis, Properties and Applications* (Weinheim: Wiley–VCH), Combustion synthesis of nitrides for development of ceramic materials of new generation, pp. 1–47, (2014).
- [9] V. Pankratov, R. Pärna, M. Kirm, et al., *Radiation Measurements* 121 (2019) 91-98
- [10] R. Pärna, R. Sankari, E. Kukk, et al., *Nuclear Inst. and Methods in Physics Research A* 859 (2017) 83-89

Synthesis and Photophysical Features of Several (2,4-dinitrophenyl)hydrazones from Various Alicyclic Mono- and Diketones

J. Anulytė¹, G. Juška¹, S. Višniakova², K. Arlauskas¹, A. Žilinskas²

1- Institute of Chemical Physics, Vilnius University, Saulėtekio av. 3, Vilnius, Lithuania

2- Institute of Chemistry, Department of Organic Chemistry, Vilnius University, Naugarduko 24, Vilnius, Lithuania

kestutis.arlauskas@ff.vu.lt

We have synthesized (Fig. 1) several (2,4-dinitrophenyl)hydrazones from various alicyclic mono- and diketones including 5,5-dimethylcyclohexane-1,3-dione, 1,7,7-trimethylbicyclo[2.2.1]heptane-2-one, bicyclo[3.3.0]octane-3,7-dione, bicyclo[3.3.1]nonane-2,6-dione and 2-adamantanone. All of these hydrazones are non-planar in contrast to ordinary polycyclic aromatic systems. Such a geometry of compounds often changes their photophysical properties because it depends on possibilities to compose amorphous photoactive layers.

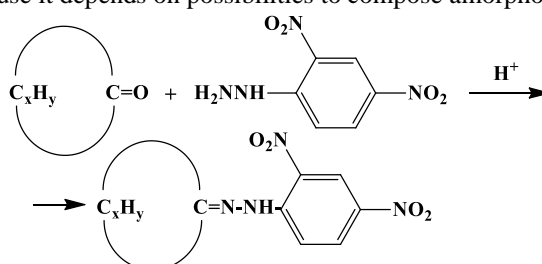


Fig. 1. General route of synthesis

In progress synthesized (2,4-dinitrophenyl)hydrazones will be converted by reaction with benzoyl isothiocyanate into next series conjugated heterocycles thiadiazoles and investigated their photophysical properties.

The spectra of absorption of light, photoluminescence of the solutions as well as of the layers, deposited using spin-coating, solution cast and thermal deposition in vacuum techniques, have been measured. From the spectral dependencies of absorption of light and of ionization potential the energy of the HOMO and LUMO states have been evaluated. An influence onto energy of HOMO and LUMO states of geometry of compounds of these newly synthesized hydrazones together with deposition conditions of layers is discussed. The possibilities to apply these materials to create optoelectronic devices are also discussed.

Extension of Spectral Sensitivity of GeSn IR Photodiode after Laser Annealing

P. Ščajev¹, P. Onufrijevs², A. Mekys¹, L. Subačius³, A. Medvids², H. H. Cheng⁴

¹ Institute of Photonics and Nanotechnology, Vilnius University, Sauletekio av. 3, Vilnius 10257, Lithuania

² Institute of Technical Physics, Faculty of Materials Science and Applied Chemistry, Riga Technical University, P. Valdena 3/7, Riga, LV-1048, Latvia

³ Center for Physical Sciences and Technology, Sauletekio av. 3, Vilnius 10257, Lithuania

⁴ Center for Condensed Matter Sciences and Graduate Institute of Electronic Engineering, National Taiwan University, Roosevelt Road No 1, Section 4, Taipei 10617, Taiwan

e-mail: patrik.scajev@ff.vu.lt

Photo-detection in the near-infrared is commonly performed by Ge or InGaAs-based photodetectors. Further extension of the detection range to the mid-infrared region can be performed by germanium-tin (GeSn) material which shows promising characteristics [1].

In this study, we focused on the optoelectronic properties of the photodiodes prepared by using 200 nm thick Ge_{0.95}Sn_{0.05} epitaxial layers on Ge/n-Si substrate with aluminium contacts. Photodiodes were formed on non-irradiated and Nd:YAG laser irradiated Ge_{0.95}Sn_{0.05} layers. The samples were irradiated by pulsed Nd:YAG laser with the following parameters: $\lambda = 1064$ nm, $\tau = 6$ ns, $I = 107.8$ -463.5 MW/cm²; 10 Hz repetition rate and 1.0 mm beam diameter. Scanning of the laser beam was performed normally to the GeSn surface with a speed of 1.0 mm/s. The irradiation of the samples was carried out at room temperature in Ar chamber.

The photodiodes were characterized by using pulsed 200 fs 10 kHz laser in 2.0-2.6 μ m wavelength range. Photocurrents at a different wavelength and applied bias were recorded by using Keithley 2400 source meter (Figure 1a). Temporal response of the detectors was investigated by 6 GHz oscilloscope (Figure 1b). The response of the diodes was found rather fast, indicating their suitability for image sensors. The laser-irradiated diode was found more sensitive in the long wavelength due to laser induced Sn atoms redistribution providing formation of graded bandgap structure [2]; its comparison to the non-irradiated structure is provided in Figure 1c. This opens the perspective for improving the sensitivity of GeSn alloys in the mid-infrared by pulsed laser processing.

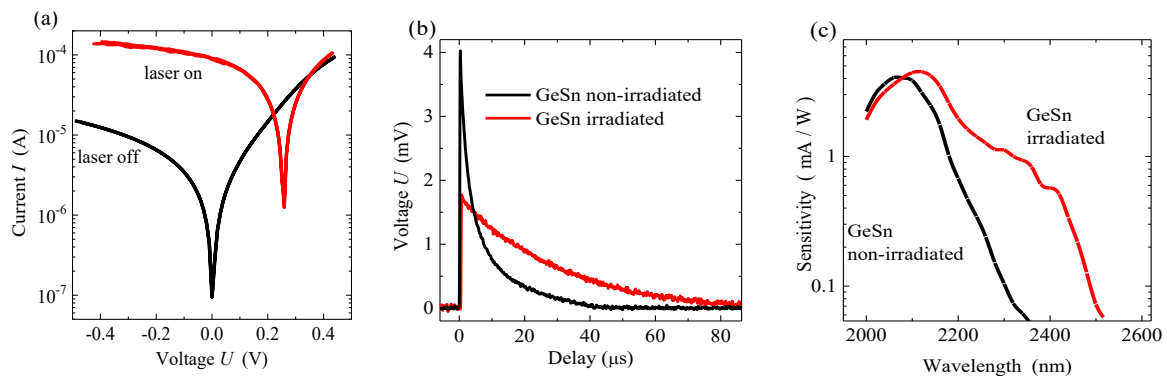


Figure 1. IV curves (a) temporal photoresponse (b) and spectral sensitivity (c) of the GeSn photodiodes.

Acknowledgment

The work was supported as part of the Program on Mutual Funds for Scientific Cooperation of Lithuania and Latvia with Taiwan project: GeSn-based photo sensor - from basic research to applications. Pavels Onufrijevs has been supported by the European Regional Development Fund within the Activity 1.1.1.2 “Post-doctoral Research Aid” of the Specific Aid Objective 1.1.1 “To increase the research and innovative capacity of scientific institutions of Latvia and the ability to attract external financing, investing in human resources and infrastructure” of the Operational Programme “Growth and Employment” (No. 1.1.1.2/VIAA/3/19/409).

[1] E. Kasper, *J. Mater. Res.* **31**, 3639-3648 (2016).

[2] P. Onufrijevs et al., *Opt. Laser Technol.* **128**, 106200 (2020).

Thermomechanical response of main-chain liquid crystal elastomers with different degrees of crosslinking

N.K. Derets^{1,2,3}, A. Rešetič¹, J. Milavec¹, P. Umek¹, M. Sluban¹, B. Zalar^{1,2}, V. Domenici⁴, V. Cresta⁴

1- Department of Solid State Physics, Jožef Stefan Institute, Jamova 39, 1000 Ljubljana, Slovenia

2- Jožef Stefan International Postgraduate School, Jamova 39, 1000 Ljubljana, Slovenia

3- On leave from: Ioffe Institute, Politekhnicheskaya 26, 194021 St. Petersburg, Russia

4- Dipartimento di Chimica e Chimica Industriale, Università degli studi di Pisa, via Moruzzi 3, 56124 Pisa, Italy

email: Nikita.Derets@ijs.si

Liquid crystal elastomers (LCEs) are composed of mesogens attached to crosslinked polymer chains. Materials with such structure combine entropic elasticity of elastomers and orientational order of liquid crystals [1]. They typically exhibit a phase transition from the nematic phase into the isotropic phase, associated with macroscopic changes of their physical properties, e.g., of the length and elastic modulus. In main-chain LCEs (MC-LCEs), mesogens themselves form the polymer network. Used as filler material for polymer-dispersed LCEs (PDLCEs), they are expected to exhibit larger elastic modulus and thermomechanical response as compared to side-chain LCEs [2].

Eleven MC-LCE samples were prepared according to Finkelmann's two-stage procedure [3], with crosslinker-to-mesogen relative concentrations ranging from 5% to 10% in steps of 0.5%. Measurements of temperature dependence of thermomechanical (TM) response were carried out in the range of 300 K – 430 K, using a homemade extensometer. Mechanical stress was applied along the direction of the orientation of the mesogens in the elastomer. TM response was determined during both heating and cooling.

Gradual loss of TM response was observed in the repetitive measurements, and the goal of this work was to investigate the origin of such behavior and to minimize the degradation of the MC-LCEs.

Preliminary results show that the concentration of crosslinker only slightly affects the amplitude of TM response, whereas it impacts the stability of the system in repetitive measurement cycles. The degradation is reduced with lowering the concentration and is found to be negligible in the 5% sample.

[1] T.J. White and D.J. Broer. Programmable and adaptive mechanics with liquid crystal polymer networks and elastomers. *Nature Materials* **14**, 1087-1098 (2015).

[2] A. Rešetič, J. Milavec, B. Zupančič, V. Domenici, B. Zalar. Polymer-dispersed liquid crystal elastomers. *Nature Comm.* **7**, 13140 (2016).

[3] J. Küpfer and H. Finkelmann. Nematic liquid single crystal elastomers. *Makromol. Chem., Rapid Commun.* **12**, 717-726 (1991).

Enhanced Photocatalytic Activity of ZnO Nanorods by Surface Treatment with H₂AuCl₄: Synergic Effects Through an Electron Scavenging, Plasmon Resonance and Surface Hydroxylation

T. Dedova¹, I. Oja Acik¹, Z. Chen¹, A. Katerski¹, T. Nagyné-Kovács², I. M. Szilágyi², M. Krunks¹.

1. Department of Materials and Environmental Technology, Tallinn University of Technology, Ehitajate tee 5, 19086 Tallinn, Estonia

2. Department of Inorganic and Analytical Chemistry, Budapest University of Technology and Economics, H-1111 Budapest, Muegyetem rakpart 3., Hungary

Currently, environmental investigations around the world have gained increasing attention in environmental problems related to the removal of toxic organic substances (dyes, antibiotics, e.t.c.) from wastewater. Ultimately, research activities on wastewater treatment methods have focused on advanced oxidation processes (AOP), mainly due to the complete degradation of a wide range of organic contaminants that are resistant to conventional purification methods of water, absence of waste disposal problems and low cost. Among the AOPs, a heterogeneous photocatalysis, a new wastewater treatment technique, is a rapidly growing research area in recent decades.

In this research, we demonstrate an enhanced photocatalytic activity (PA) of ZnO_R/Au composites compared to PA of plain ZnO_R structures. The ZnO_R were produced by a hydrothermal growth method and the surface treatment of the ZnO_R crystals was carried out with H₂AuCl₄ using a spin coating technique. In this study, methyl orange was chosen to evaluate the photocatalytic activity of the ZnO_R and ZnO_R/Au. The highest degradation efficiency of MO was achieved with ZnO_R/Au layers. The XPS and wettability measurements have confirmed the increase in the amount of hydroxyl groups on the surface of the ZnO_R/Au. Taking into account the physical and chemical characterizations of the samples, the enhanced photocatalytic activity of the ZnO_R/Au composites has been attributed to the surface plasmon resonance from Au nanoparticles and increase of the hydroxylation of the ZnO_R crystals surface after H₂AuCl₄ interaction with ZnO_R surface.

Structure, ferroelectric and local piezoelectric properties of lead-free KNN- based perovskite ceramics

E.D. Politova¹, G.M. Kaleva¹, A.V. Mosunov², S. Yu. Stefanovich², N.V. Sadovskaya³, D.A. Kiselev⁴, T.S. Ilina⁴

1- Semenov Institute of Chemical Physics, Russian Academy of Sciences, Kosygina, 4, Moscow 119991 Russia

2- Lomonosov Moscow State University, Leninskie gory 1, Moscow 119992 Russia,

3 - FSRC «Crystallography and Photonics» RAS, Leninskii pr. 59, Moscow 119333 Russia

4 - National University of Science and Technology "MISIS", Leninskii pr. 4, Moscow 119991 Russia

Presenting author email address: politova@nifhi.ru

Lead-free ferroelectric oxide materials based on the $(\text{K}_{0.5}\text{Na}_{0.5})\text{O}_3$ (KNN) perovskite are among the most intensively studied for replacement of toxic lead-based ones [1-3]. We studied influence of preparation conditions on structure parameters, microstructure, ferroelectric, and local piezoelectric properties of KNN-based solid solutions. Dense ceramic samples substituted with Li^+ , Ca^+ and Ba^{2+} in A- and with Sb^{5+} , W^{6+} , Cu^{2+} , Ni^{2+} cations in B-sites of perovskite lattice were prepared by the two-step solid-state reaction method at temperatures of 800 – 1400 K. In order to improve density of ceramics overstoichiometric additives KCl and LiF were used [4].

The samples were studied using complex of physico-chemical methods: X-ray Diffraction, Scanning Electron Microscopy, Second Harmonic Generation (SHG), Dielectric Spectroscopy (DS), and Atomic Force Microscopy in Piezoresponse Force Mode (PFM).

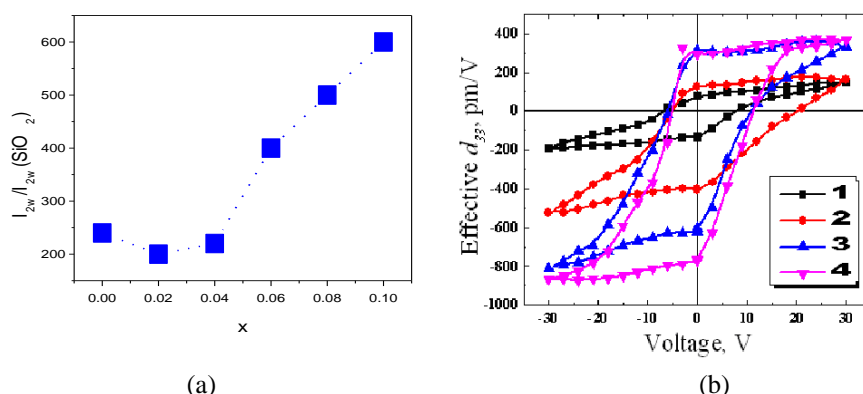


Figure 1. (a) Concentration dependence of the SHG signal for samples $(1-x)(\text{K}_{0.5}\text{Na}_{0.5})\text{NbO}_3 - x\text{LiSbO}_3$ modified by LiF (b) Effective d_{33} values of the samples with $x=0$ (1), 0.06 (2), 0.08 (3) and 0.10 (4) calculated from PFM hysteresis loops for locations with large domain contrast.

In modified ceramics the unit cell volume changes were observed depending on ionic radii of substituting cations. Mean size of grains slightly decreased from initial $\sim 5 \mu$ with x increasing. The SHG measurements confirmed polar nature and ferroelectric properties of the samples. With increasing LiSbO_3 content, increase in intensity of the SHG signal was observed at the room temperature (Figure 1a). Ferroelectric phase transitions at ~ 400 and near 700 K were confirmed using both the DS and SHG methods. Ferroelectric polarization switching at nanoscale was observed using PFM method, with high values of effective d_{33} piezoelectric coefficient ~ 300 pm/V reached (Figure 1b). The results obtained confirm prospects of creating new lead-free materials on the base of modified KNN- based compositions.

Acknowledgment. The work was supported by the Russian Foundation for Basic Research (Project 18-03-00372).

[1] Coondoo, N. Panwar, A. Kholkin, Lead-free piezoelectrics: Current status and perspectives, *J. Adv. Dielectr.* **3**, 1330002 (2013).

[2] P. K. Panda and B. Sahoo, PZT to Lead-Free Piezo Ceramics, *Ferroelectrics* **474**, 128-143 (2015).

[3] J. Rödel and J. Li, Lead-free piezoceramics: Status and perspectives. *MRS Bulletin*, **43**, 576-580 (2018).

[4] E.D. Politova, N.V. Golubko, G.M. Kaleva, A.V. Mosunov, N.V. Sadovskaya, S.Yu. Stefanovich, D.A. Kiselev, A.M. Kislyuk, P.K. Panda, Processing and characterization of lead-free ceramics on the base of sodium-potassium niobate, *J. Adv. Diel.* **8** (2018) 1850004. (2018).

Phase transitions in the $\text{BiFe}_{1-x}\text{Cr}_x\text{O}_3$ multiferroics

J. P. Cardoso¹, Y. V. Radyush², A. V. Pushkarev², N. M. Olekhovich², O. Opuchovič³,
E. L. Fertman⁴, A. V. Fedorchenko⁴, V. Gribauskaitė⁵, E. Palaimienė⁵, R. Grigalaitis⁵, J. Banys⁵,
V. V. Shvartsman⁶, D.D. Khalyavin⁷, J. M. Vieira¹, A. N. Salak¹

1- Department of Materials and Ceramics Engineering and CICECO – Aveiro Institute of Materials,
University of Aveiro, 3810-193, Aveiro, Portugal

2- Scientific-Practical Materials Research Centre of NASB, 220072, Minsk, Belarus

3- Faculty of Chemistry and Geosciences, Vilnius University, LT-03225 Vilnius, Lithuania

4- B. Verkin Institute for Low Temperature Physics and Engineering of NAS, 61103, Kharkov, Ukraine

5- Faculty of Physics, Vilnius University, LT-10222, Vilnius, Lithuania

6- Institute for Materials Science and CENIDE – Center for Nanointegration Duisburg-Essen,
University of Duisburg-Essen, 45141, Essen, Germany

7- ISIS Facility, Rutherford Appleton Laboratory, Chilton, Didcot, OX11 0QX, UK

joapcardoso@ua.pt

New single-phase type I multiferroics are actively pursued since the 60's, and the wide range of compositions has been possible by high pressure synthesis (HPS) [1]. To this day, BiFeO_3 and its derivatives remain among the few materials to simultaneously present antiferromagnetic and ferroelectric orders at room temperature. HPS enables to introduce considerable chemical modifications to the parent bismuth ferrite, which result in significant changes in structure and physical properties observed thus far. In a recently published paper, the authors presented a phase diagram of the reversible and irreversible phase transformations of the metastable phases of the $\text{BiFe}_{1-y}\text{Sc}_y\text{O}_3$ solid solution system obtained via HPS [2]. The irreversible annealing-stimulated phase transitions of the metastable polymorphs were reported for the first time, and the phenomenon of *conversion polymorphism* has been introduced [3].

BiScO_3 requires HPS and stabilizes at room temperature as a monoclinic $C2/c$ phase. BiCrO_3 is a multiferroic metastable perovskite, with the monoclinic $C2/c$ symmetry as well, stable up to ~410 K, with a reversible phase transition to the non-polar orthorhombic $Pnma$ structure. In 2007, Suchomel *et al.* [4] reported a HPS prepared $\text{BiFe}_{0.5}\text{Cr}_{0.5}\text{O}_3$ composition with the same rhombohedral $R3c$ symmetry as that of the parent bismuth ferrite. Then the samples of the entire $\text{BiFe}_{1-x}\text{Cr}_x\text{O}_3$ system have been prepared [5]. However, no phase transitions (reversible or irreversible) have been reported to date.

Here we report on the phase diagram of the system

$\text{BiFe}_{1-x}\text{Cr}_x\text{O}_3$ and physical properties of the metastable phases produced *via* HPS. The as-prepared and the annealed $\text{BiFe}_{1-x}\text{Cr}_x\text{O}_3$ ceramics were characterized using *in-situ* x-ray diffraction (XRD), scanning electron microscopy, dielectric spectroscopy, and SQUID magnetometry. Among the compositions studied, that with $x=0.55$ is of particular interest. The microstructure of the $\text{BiFe}_{0.45}\text{Cr}_{0.55}\text{O}_3$ ceramics shows no regions of chemical inhomogeneity and a bimodal grain size distribution. The as-prepared antipolar $Pnma$ polymorph of $\text{BiFe}_{0.45}\text{Cr}_{0.55}\text{O}_3$ transforms to the non-polar $Pnma$ phase between 523 and 543 K upon heating followed by a transformation to the two-phase ($R3c$ + antipolar $Pnma$) mixture at ~543 K upon cooling (Figure 1). Subsequent *in-situ* XRD experiments revealed that the temperature-induced transitions between this phase mixture and the non-polar $Pnma$ phase are reversible. The annealing stimulated transformation observed in $\text{BiFe}_{0.45}\text{Cr}_{0.55}\text{O}_3$ is an example of the conversion polymorphism, although incomplete.

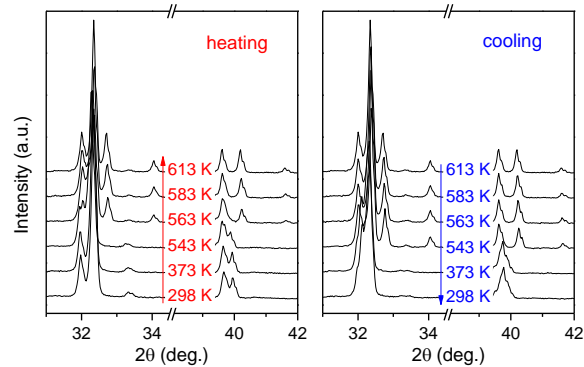


Figure 1. The most representative regions of *in situ* XRD patterns of $\text{BiFe}_{0.45}\text{Cr}_{0.55}\text{O}_3$ upon heating up to 613 K followed by cooling to room temperature.

J. P. Cardoso acknowledges FCT – Fundação para a Ciência e Tecnologia, Portugal, for the Ph.D. grant SFRH/BD/145281/2019.

[1] E. Gilioli and L. Ehm, High pressure and multiferroics materials: A happy marriage, *IUCrJ*, 1, 590–603, (2014).

[2] A. Salak, D. Khalyavin, E. Eardley, N. Olekhovich, A. Pushkarev, Y. Radyush, A. Shilin, V. Rubanik, Temperature-induced reversible and irreversible transitions between metastable perovskite phases in the $\text{BiFe}_{1-y}\text{Sc}_y\text{O}_3$ solid solutions, *Crystals*, 8, 91–101, (2018).

[3] D.D. Khalyavin, A.N. Salak, E.L. Fertman, O.V. Kotlyar, E. Eardley, N.M. Olekhovich, A.V. Pushkarev, Yu.V. Radyush, A.V. Fedorchenko, V.A. Desnenko, P. Manuel, L. Ding, E. Čizmar, A. Feher, The phenomenon of conversion polymorphism in Bi-containing metastable perovskites, *Chem. Commun.*, 55, 4683–4686, (2019).

[4] M. R. Suchomel, C. Thomas, M. Allix, M. Rosseinsky, A. Fogg, and M. Thomas, High pressure bulk synthesis and characterization of the predicted multiferroic $\text{Bi}(\text{Fe}_{1/2}\text{Cr}_{1/2})\text{O}_3$, *Appl. Phys. Lett.*, 90, 2–5, (2007).

[5] I. P. Raevski, S. Kubrin, A. Pushkarev, N. Olekhovich, Y. Radyush, V. Titov, M. Malitskaya, S. Raevskaya, H. Chen, The effect of Cr substitution for Fe on the structure and magnetic properties of BiFeO_3 multiferroic, *Ferroelectrics*, 525, 1–10, (2018).

Ferroelectricity induced by germanium dopants in quantum paraelectrics in $\text{Pb}_2\text{P}_2(\text{S},\text{Se})_6$

I. Zamaraitė¹, V. Liubachko^{2,3}, A. Oleaga³, A. Salazar³, A. Dziaugys¹,
J. Banys¹, Yu. Vysochanskii²

¹ - Faculty of Physics, Vilnius University, Sauletekio 9, 10222 Vilnius, Lithuania

² - Institute for Solid State Physics and Chemistry, Uzhgorod University, Pidgirna Str. 46, Uzhgorod 88000, Ukraine

³ - Departamento de Física Aplicada I, Escuela Técnica Superior de Ingeniería, Universidad del País Vasco, Alameda Urquijo s/n, 48013 Bilbao, Spain

vysochanskii@gmail.com

Earlier was found [1] that Ge doping shifts the ferroelectric second order phase transition in $\text{Sn}_2\text{P}_2\text{S}_6$ crystals toward higher temperatures. Increase of the phase transition temperature under the influence of Ge impurities also is known for $\text{Pb}_{1-x}\text{Ge}_x\text{Te}$ and $\text{Sn}_{1-x}\text{Ge}_x\text{Te}$ ferroelectrics, what demonstrates universal property of Ge impurities in tin or lead containing hosts is to elevate the ferroelectric phase transition temperature. By X-ray photoelectron spectroscopy together with first-principles calculation of electronic spectra was found [2] that the germanium impurity in $\text{Sn}_2\text{P}_2\text{S}_6$ improves stereoactivity of the cation sublattice that is related to the nature of ferroelectricity. While germanium can only be introduced up to a certain quantity, the lead can completely substitute tin in $(\text{Pb}_y\text{Sn}_{1-y})_2\text{P}_2\text{S}_6$ and $(\text{Pb}_y\text{Sn}_{1-y})_2\text{P}_2\text{Se}_6$ continuous solid solution. The addition of Pb has the effect of diluting the stereoactivity as it weakens the bonding hybridization responsible for ferroelectricity. Formally, introducing of lead atom creates a “chemical pressure” with similar effects to the mechanical pressure. The properties of the $(\text{Pb}_y\text{Sn}_{1-y})_2\text{P}_2\text{S}_6$ mixed crystals have been described [3] within the framework of Blume-Emery-Griffith model taking into account the presence of random fields created at tin by lead substitution.

In mixed crystals $(\text{Pb}_y\text{Sn}_{1-y})_2\text{P}_2\text{S}_6$ and $(\text{Pb}_y\text{Sn}_{1-y})_2\text{P}_2\text{Se}_6$ at $y > 0.61$ and $y > 0.65$, sequentially, the paraelectric phase is stable in ground state, and pure compounds $\text{Pb}_2\text{P}_2\text{S}_6$ and $\text{Pb}_2\text{P}_2\text{Se}_6$ obviously are quantum paraelectrics. By dielectric investigations we have shown that for $\text{Pb}_2\text{P}_2\text{S}_6$ crystal the real part of dielectric susceptibility increases monotonously with decreasing temperature in range from 300 K till 20 K. It was found that in the quantum critical regime the usual Curie-Weiss law of the inverse of dielectric susceptibility $1/\epsilon(T) \sim T$ changes into $1/\epsilon(T) \sim T^2$ what is the prominent criterion of quantum critical behavior. The temperature dependences of dielectric permittivity were analysed in terms of the Barrett model. This detailed analysis has provided the indications that $\text{Pb}_2\text{P}_2\text{S}_6$ type crystals exhibit a quantum paraelectric state. For $(\text{Pb}_y\text{Sn}_{1-y})_2\text{P}_2\text{S}_6$ and $(\text{Pb}_y\text{Sn}_{1-y})_2\text{P}_2\text{Se}_6$ mixed crystals at 0 K a quantum critical point can be attained by changing of chemical composition, where the quantum fluctuations drive a phase transition. The influence of this critical point extends over a wide range at $T > 0$ determining the regime of quantum criticality.

We have carried out a dielectric study for single crystals $(\text{Pb}_{0.98}\text{Ge}_{0.02})_2\text{P}_2\text{S}_6$, $(\text{Pb}_{0.7}\text{Sn}_{0.3})_2\text{P}_2\text{S}_6 + 5\% \text{Ge}$ and $(\text{Pb}_{0.7}\text{Sn}_{0.3})_2\text{P}_2\text{Se}_6 + 5\% \text{Ge}$ with special emphasis on low temperatures. By introducing small amounts of germanium dopants in $(\text{Pb}_{0.98}\text{Ge}_{0.02})_2\text{P}_2\text{S}_6$ crystal, the ferroelectric phase appears. The long-range ferroelectric order manifested by a broad peak at 40 K for the temperature dependence of the real part of dielectric susceptibility. But doping with germanium decreases the value of dielectric permittivity below 75 K deviating from the Barrett's fit. It suggests that the possible phase transition might occur in this region. Also, there are two peaks of the imaginary part of dielectric susceptibility with a frequency dispersive behavior, and the temperatures of the loss peaks are around 50 K and 100 K at 100 kHz. Evidently the phase transition might occur in this region.

Real part of dielectric permittivity for $(\text{Pb}_{0.7}\text{Sn}_{0.3})_2\text{P}_2\text{S}_6 + 5\% \text{Ge}$ sample at cooling from room temperature to 20 K increases continuously. However, there is the dielectric loss peak with frequency dispersive behavior, and the temperature of the loss peak is around 50 K at 100 kHz. By fitting with the Barrett's equation a good agreement with the experimental data was found. The obtained dielectric susceptibility behavior demonstrate that $(\text{Pb}_{0.7}\text{Sn}_{0.3})_2\text{P}_2\text{S}_6 + 5\% \text{Ge}$ crystal does not undergo a ferroelectric phase transition with polar ordering at macroscopic scale at any finite temperature, obviously a dipole glass state appears below 50 K. Temperature dependence of the dielectric susceptibility at different frequencies for $(\text{Pb}_{0.7}\text{Sn}_{0.3})_2\text{P}_2\text{S}_6 + 5\% \text{Ge}$ sample is similar to just described one for sulfide mixed crystal and here the dipole glass state at low temperatures can also be supposed.

The thermal properties of $\text{Pb}_2\text{P}_2\text{S}_6$, $(\text{Pb}_{0.98}\text{Ge}_{0.02})_2\text{P}_2\text{S}_6$, $(\text{Pb}_{0.7}\text{Sn}_{0.3})_2\text{P}_2\text{S}_6 + 5\% \text{Ge}$ and $(\text{Pb}_{0.7}\text{Sn}_{0.3})_2\text{P}_2\text{Se}_6 + 5\% \text{Ge}$ single crystals have been studied by means of ac photopyroelectric calorimetry, measuring thermal diffusivity, as earlier was performed for $\text{Sn}_2\text{P}_2\text{S}_6$ crystal doped by germanium, where named impurity sharpens Ising like critical anomaly at continuous ferroelectric transition [4]. With using of data about the temperature dependence of the heat capacity for these materials, their thermal conductivity was determined. For $(\text{Pb}_{0.98}\text{Ge}_{0.02})_2\text{P}_2\text{S}_6$ crystal the thermal conductivity at low temperature (near 50 K) is bigger than in the case of pure $\text{Pb}_2\text{P}_2\text{S}_6$ crystal. Obviously it is related to the Ge impurity inducing polar clusters of the ferroelectric phase. Dielectric susceptibility of such clusters is smaller than susceptibility of the paraelectric phase and the frequency of the lowest energy soft optical mode near Brillouin zone (BZ) center is obviously elevated. Growth of the soft optical mode frequency diminishes the probability of the optic phonons resonance scattering by acoustic phonons. At low temperatures heat is transferred by the acoustic and the lowest frequency optical phonons. Acoustic phonons with the small wave numbers are involved mostly in normal scattering processes that don't contribute into a thermal resistivity. The phonons from optical branch near BZ center also participate in unklap scattering by lattice imperfection which provide effective thermal resistivity. So, hardening of the optical branch lowers the population of the optical phonons and increases thermal conductivity of $(\text{Pb}_{0.98}\text{Ge}_{0.02})_2\text{P}_2\text{S}_6$ crystal. In the case of $(\text{Pb}_{0.7}\text{Sn}_{0.3})_2\text{P}_2\text{S}_6 + 5\% \text{Ge}$ mixed crystals thermal conductivity monotonically decreases at cooling, like in glassy materials, what demonstrates an effective phonon scattering in solid solutions with sublattice of mixed tin and lead cations. Here germanium impurity obviously induces the dipole glass state, what appeared in complex dielectric susceptibility frequency dependence below 70 K.

[1] M. M. Maior, M. I. Gurzan, Sh. B. Molnar, I.P. Prits, Yu. M. Vysochanskii, IEEE Trans. of Ultrasonics, Ferroelectrics and Frequency Control, vol. 47, pp. 877-880, (2000).

[2] J. Grigas, E. Talik, K. Glukhov, K. Fedyo, I. Stoika, M. Gurzan, I. Prits, A. Grabar, Yu. Vysochanskii, Ferroelectrics, vol. 418, pp. 134 – 142, (2001).

[3] R. Yevych, V. Haborets, M. Medulych, A. Molnar, A. Kohutych, A. Dziaugys, Ju. Banys, Yu. Vysochanskii, Low Temperature Physics, vol. 42, pp. 1155 – 1162, (2016).

[4] V. Shvalya, A. Oleaga, A. Salazar, I. Stoika, Yu. M. Vysochanskii, J. Mater. Sci., vol. 51, pp. 8156 – 8167, (2016).

DNP enhanced solid-state NMR and its application to investigate novel catalyst

V. Klimavičius¹

1- TU Darmstadt, Eduard-Zintl-Institute for Inorganic and Physical Chemistry, Alarich-Weiss-Straße 8, 64287 Darmstadt, Germany

vytautas.klimavicius@chemie.tu-darmstadt.de

Solid-state Nuclear Magnetic Resonance spectroscopy (NMR) within last decades has developed into powerful tool to investigate technologically important innovative materials, as well as bio-solids. These include the investigation of intermolecular interactions at the interfaces of nanomaterials, as for example nano-particles, zeolites, metal-organic-frameworks (MOFs) or supported catalysts on carrier materials such as mesoporous silicates or other oxides.[1] Nevertheless, a major drawback in the application of solid-state NMR techniques is the inherent low sensitivity. The reasoning is the small energy differences of the nuclear spin-levels, which result in small population differences in thermal equilibrium, in other words, polarization. This could be overcome by employing hyperpolarization techniques, and namely, Dynamic Nuclear Polarization (DNP). DNP fundamentally is based on the transfer of strong electron spins polarization from stable radicals to the NMR nuclei of interest. In the last decade, due to the pioneering work of Griffin group and development of commercial gyrotron systems as microwave (μw) source DNP become feasible in strong magnetic fields.[2] Basic principles of DNP enhanced solid-state NMR are presented during the talk. After brief theoretical introductory part successful applications of DNP solid-state NMR on catalytically active and functional materials are shown. These include supported noble metal metallic nanoparticles, organotin catalysts, impregnated mesoporous materials, etc.

[1] T. Gutmann, G. Buntkowsky, Solid-state NMR Studies of Supported Transition Metal Catalysts and Nanoparticles, *Modern Magnetic Resonance*, 1-21, (2017).

[2] T. Maly, G. T. Debelouchina, V. S. Bajaj, K. Hu, C. Joo, M. L. Mak-Jurkauskas, J. R. Sirigiri, P. C. A. Wel, J. Herzfeld, R. J. Temkin, R. G. Griffin, Dynamic nuclear polarization at high magnetic fields, *Journal of Chemical Physics*, 128, 052211, (2008)

Estimation of the degree of antsite disordering of magnetoactive ions in $\text{Sr}_2\text{FeMoO}_{6-\delta}$ by means of the intensity of the X-ray peak (101)

E. Artsiukh¹, G. Suchaneck²

1- SSPA Scientific and Practical Materials Research Center of NAS of Belarus, Cryogenic Research Division, Minsk 220072, Belarus
2- TU Dresden, Solid State Electronics Laboratory, Dresden 01062, Germany

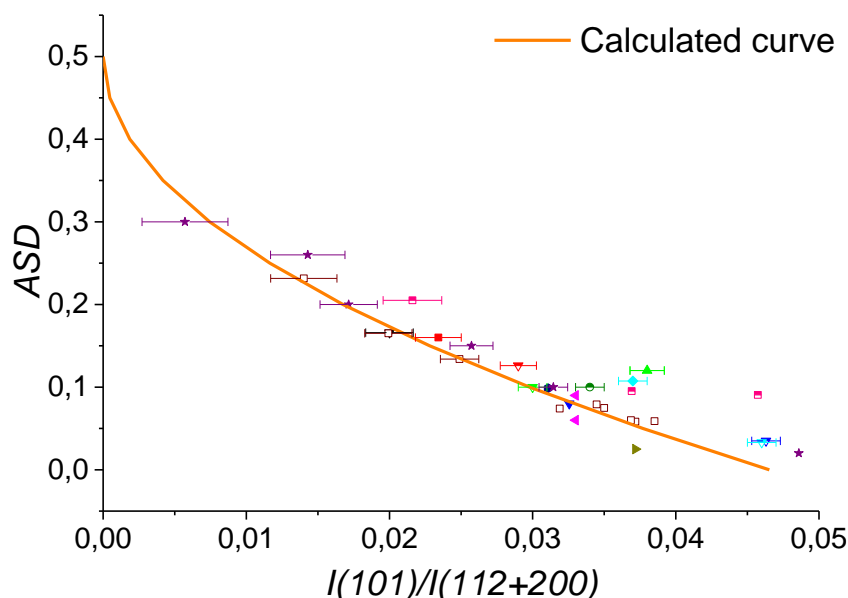
sirfranzferdinand@yandex.ru

$\text{Sr}_2\text{FeMoO}_{6-\delta}$ (SFMO) double perovskite is a promising candidate for room-temperature spintronic applications since it possesses a half-metallic character (with theoretically 100% spin polarization), a high Curie temperature of about 415 K, and a low-field magnetoresistance. However, the saturation magnetization of SFMO deteriorates with increasing B-site disorder, e.g. the formation of Fe_{Mo} and Mo_{Fe} antsite defects.

Usually, antsite disorder (ASD) in SFMO is determined by Rietveld refinement using a least square approach to fit theoretical X-ray diffraction pattern to experimental data. Thus, a reliable analysis requires very long exposition times or high X-ray intensity. Also, the analysis itself is very time-consuming. On the other hand, the intensity of the (101) superstructure reflection is indicative of Fe/Mo rocksalt ordering. Divided by aggregated intensity of most intensive reflections (112)+(200), it provides an estimation of ASD [1]. But, regardless of a large number of experimental data, there is still no analytical description of the relation between ASD and the X-ray intensity ratio $I(101)/[I(112)+I(200)]$. In this work, we fill this gap.

The dependence of ASD on the ratio $I(101)/[I(112)+I(200)]$ was calculated by means of VESTA [2] and RIETAN-FP·VENUS [3] software packages. Obtained curve is in a good agreement with literature data taken from various literature sources. The analytical expression describing the curve is then given by:

$$\text{ASD} = 0.5 - 2.318 \cdot \sqrt{\frac{I(101)}{[I(112) + I(200)]}} \quad (1)$$



This work was supported by the European project H2020-MSCA-RISE-2017-778308–SPINMULTIFILM.

[1] Balcells L., Navarro J., Bibes M., Roig A., Martínez B., Fontcuberta J. Cationic ordering control of magnetization in $\text{Sr}_2\text{FeMoO}_6$ double perovskite, *Applied Physics Letters*, vol. 78, pp. 781-783, (2001)

[2] Momma K. and Izumi F., VESTA 3 for three-dimensional visualization of crystal, volumetric and morphology data, *Journal of Applied Crystallography*, vol. 44, pp. 1272-1276, (2011).

[3] Izumi F. and Momma K., Three-dimensional visualization in powder diffraction, *Solid State Phenomena*, vol. 130, pp. 15-20, (2007).

100 years with ferroelectricity

J.Dec

Institute of Materials Science, University of Silesia, Katowice, Poland

jan.dec@us.edu.pl

Today it is difficult to imagine medical diagnostic without ultrasound scanner or mid-range car lacking parking sensors. Piezo lighters and motion sensors are commonly used. A new generation of radar was constructed, which is used in the rocket PATRIOT system. All it began 100 years ago thanks to Joseph Valasek [1] – an American physicist of Czech origin, who first observed the ferroelectric hysteresis loop.

From an engineering point of view, ferroelectrics as materials possess macroscopic spontaneous polarization, the direction of which can be changed by means of external electric field (so called switching). It is therefore an electric analogue of ferromagnetics. Ferroelectrics are usually considered as multifunctional materials. Hence their various applications, which vary from their generic property, emerge. During this lecture difficult entry, current state and perspectives for further development of this class of materials will be presented in a popular way.

[1] J.Valasek, Phys. Rev., **15.**, 537 - 538., (1920).

Growth of dendrite domains and superfast domain shape transformation in ferroelectrics

V. Ya. Shur¹, A. R. Akhmatkhanov¹, A. A. Esin¹, M. A. Chuvakova¹

1 - School of Natural Sciences and Mathematics, Ural Federal University, 51 Lenin Ave., 620000 Ekaterinburg, Russia

vladimir.shur@urfu.ru

The experimental study of the shape transformation after merging of the polygonal domains by superfast wall motion and growth of the dendrite domains will be presented and discussed. The obtained results will be considered in terms of the unified kinetic approach. The analogy between kinetics of ferroelectric domains and crystal growth will be demonstrated.

The shape evolution of the isolated domains during polarization reversal in uniform electric field has been studied in lithium niobate LiNbO_3 (CLN) and potassium titanyl phosphate KTiPO_4 (KTP) single crystals by *in situ* optical visualization with high temporal resolution. The static domain patterns at the surface have been imaged by optical, piezoresponse force and scanning electron microscopy, and in the bulk – by confocal Raman microscopy and Cherenkov-type second harmonic generation.

The first experimental study of the fast transformation of the concave polygonal domain appeared after merging to the convex one (shape stability effect) [51] has been realized. It was shown that the convex growth of isolated domains was governed by motion of the slowest domain walls, while the domain merging leads to formation of the superfast short-lived domain walls with several orders of magnitude higher motion velocity. The angular dependencies (kinetic Wulff plots) for sideways domain wall motion has been reconstructed experimentally by analysis of convex and concave domain growth in CLN and KTP crystals [6, 7 2,3]. It was demonstrated that switching at the elevated temperatures in the plates of CLN covered by artificial dielectric layer leads to instability of the domain wall shape and dendrite domain growth [1,2 4,5]. The field dependence of the dendrite domain shape (snowflakes) has been revealed [3 6].

For explanation of the observed domain shape evolution the domain growth has been considered as a result of step (pairs of kinks) generation and kink motion along the domain wall [4 7]. It was supposed that the step generation probability and kink motion velocity depend linearly on the excess of the local sum of external and residual depolarization fields over the appropriate threshold values. The domain shape change caused by formation of the trail of residual charges for ineffective screening was demonstrated by computer simulation. It was shown that the determined step nucleation at the vertices and anisotropic kink motion dominated at weak fields, whereas the stochastic nucleation with equiprobable positions of the step nucleation sites is observed at the strong fields. The convex hexagon domain shapes determined by CLN symmetry have been observed for effective screening of depolarization field only. The screening retardation results in growth of the irregular polygons, stars and dodecagons.

Acknowledgements: The research was made possible by Russian Science Foundation (Project № 19-12-00210). The equipment of the Ural Center for Shared Use “Modern nanotechnology” Ural Federal University was used.

- [1] V.Ya. Shur, A.I. Lobov, A.G. Shur, E.L. Romyantsev, K. Gallo, Shape evolution of isolated micro-domains in lithium niobate, *Ferroelectrics*, vol.360, pp.111-119 (2007).
- [2] A.A. Esin, A.R. Akhmatkhanov, V.Ya. Shur, Superfast domain wall motion in lithium niobate single crystals. Analogy with crystal growth, *Appl. Phys. Lett.*, vol.114, pp.192902 (2019).
- [3] V.Ya. Shur, A.A. Esin, M.A. Alam, A.R. Akhmatkhanov, Superfast domain walls in KTP single crystals, *Appl. Phys. Lett.*, vol.111, pp.152907 (2017).
- [4] V.Ya. Shur, D.S. Chezganov, M.S. Nebogatikov, I.S. Baturin, M.M. Neradovskiy, Formation of dendrite domain structures in stoichiometric lithium niobate at elevated temperatures, *J. Appl. Phys.*, vol.112, pp. 104113 (2012).
- [5] V.Ya. Shur, M.S. Kosobokov, E.A. Mingaliev, D.K. Kuznetsov, P.S. Zelenovskiy, Formation of snowflake domains during fast cooling of lithium tantalate crystals, *J. Appl. Phys.*, vol.119, pp.144101 (2016).
- [6] V.Ya. Shur and A.R. Akhmatkhanov, Domain shape instabilities and dendrite domain growth in uniaxial ferroelectrics, *Phil. Trans. R. Soc. A.*, vol.376, p.20170204 (2018).
- [7] V.Ya. Shur, Kinetics of ferroelectric domains: Application of general approach to LiNbO_3 and LiTaO_3 , *J. Mater. Sci.*, vol.41, pp.199-210 (2006).

Triggered incommensurate transitions

**Roman G. Burkovsky¹, Iurii Bronwald², Daria Andronikova², Georgiy Lityagin¹, Julita Piecha³,
Sofia-Michaela Souliou⁴, Andrzej Majchrowski⁶, Alexey Filimonov¹, Andrey Rudskoy¹,
Krystian Roleder³, Alexei Bosak⁴ and Alexander Tagantsev^{2,7}**

1 - Peter the Great Saint-Petersburg Polytechnic University, 29 Politekhnicheskaya, 195251 St. Petersburg, Russia

2 - Ioffe Institute, 26 Politekhnicheskaya, 194021 St. Petersburg, Russia

3 - Institute of Physics, University of Silesia, ulica 75 Puuku Piechoty 1, 41-500 Chorzów, Poland

4 - European Synchrotron Radiation Facility, BP 220, F-38043 Grenoble Cedex, France

5 - Karlsruher Institut für Technologie, Institut für Festkörperphysik, 76021 Karlsruhe, Germany

6 - Institute of Applied Physics, Military University of Technology, ulica Gen. W. Urbanowicza 2, 00-908 Warszawa, Poland

7 - Swiss Federal Institute of Technology (EPFL), School of Engineering, Institute of Materials Science, CH-1015 Lausanne, Switzerland

roman.burkovsky@gmail.com

Perovskite materials have wide range of important applications, ranging from sensing and actuating, to energy harvesting and non-volatile memory technologies [1]. Highly diverse are various structures and phase transitions in these crystals, posing numerous technological, as well as purely scientific questions. In particular, a challenging question is on the incommensurate phases of perovskites – why and how are they formed [2,3]. We report an unusual link between these phases and another highly unusual phenomenon – triggered transitions, where the formation of one order parameter attracts the formation of the other order parameter. Such transitions were thoroughly analyzed in theory, but their observations in real crystals are rare, because order parameters usually tend to be repulsive with each other.

We report [4] on the triggered incommensurate transition in perovskite PbHfO_3 , in which the initiating agent of the transition is antiferrodistortive soft mode associated with the oxygen octahedral tilts. This highly surprising, because incommensurate transitions in dielectrics have not been previously observed in the other way but due to the condensation of incommensurate soft mode. Here it is other way around – in the absence of incommensurate soft mode, the incommensurate transition is triggered by the antiferrodistortive instability, similarly to triggered ferroelectricity in the Holakovskiy scenario [5].

Our findings are obtained by a combination of synchrotron diffraction, diffuse and inelastic scattering experiments, performed at ID28 of ESRF, using single crystal samples. The results are analyzed in the framework of Landau-Ginzburg-like model for first order transition with two order parameters. Interesting aspect is the emerging character of interaction between the waves in Pb sublattice and oxygen tilts: these distortions are repulsive for very long waves, but become attractive at shorter wavelengths, which makes it possible for the free energy minimum to correspond to incommensurate wave vector.

The results give important technological insights on the possibilities of manipulating the ordering of cations by externally controlling the state of oxygen tilt subsystem *via* pressure or epitaxial strain, which can be useful in tuning perovskite materials for energy storage and non-volatile memory applications.

[1] J. F. Scott, Application of modern ferroelectrics, *Science* 315, 954 (2007).

[2] A. K. Tagantsev, K. Vaideeswaran, S. B. Vakhrushev, A. V. Filimonov, R. G. Burkovsky, A. Shaganov, D. Andronikova, A. I. Rudskoy, A. Q. R. Baron, H. Uchiyama, D. Chernyshov, A. Bosak, Z. Ujma, K. Roleder, A. Majchrowski, J.-H. Ko, N. Setter. The origin of antiferroelectricity in PbZrO_3 / *Nature Communications* 4, 2229 (2013).

[3] Burkovsky R.G., Bronwald Yu., Andronikova D., Wehinger B., Krisch M., Jacobs J., Gambetti D., Roleder K., Majchrowski A., Filimonov A.V., Rudskoy A.I., Vakhrushev S.B., Tagantsev A.K. Critical scattering and incommensurate phase transition in antiferroelectric PbZrO_3 under pressure. *Scientific Reports*. 7, 41512 (2017).

[4] Burkovsky, R. G., Bronwald, I., Andronikova, D., Lityagin, G., Piecha, J., Souliou, S., Filimonov, A., Rudskoy, A., Tagantsev, A. Triggered incommensurate transition in PbHfO_3 . *Physical Review B*, 100, 014107 (2019).

[5] J. Holakovskiy, A new type of the ferroelectric phase transition, *Phys. Status Solidi B* 56, 615 (1973).

Poster Abstracts

Corrosion resistance of V4A stainless steel in different seawaters conditions

O. Demidenko¹, A. Zhyvulka¹, K. Yanushkevich¹, V. Constantin², E.I. Neacsu², C. Donath² and A.M. Popescu²

1- Scientific-Practical Materials Research Centre NAS of Belarus, Laboratory of Physics of Magnetic Materials, 220072, Minsk, P.Brovki str., 19, Belarus

2- "Ilie Murgulescu" Institute of Physical Chemistry, Laboratory of Electrochemistry and Corrosion, Splaiul Independentei 202, Bucharest-Sector 6-PO Box 12-194, Romania

E-mail: demiden@physics.by, orion_minsk@tut.by

Number of industries has no alternative to use a corrosion-resistant steels and alloys based on iron. Most of metal ware is operating in natural environments. Application field of stainless steels and alloys based on iron is very wide: from the heavy engineering industry and power engineering to mechanics and electronics. A problem of corrosion resistance of such materials is still actual [1-4]. Therefore, a clear data of marine corrosion resistance, mechanical and physical properties of stainless steels, stability properties, the temperature ranges of usage and knowledge of their processing and exploitation is a key to significant economy. In this work we report a study of corrosion resistance of V4A stainless steels under corrosion action of Mediterranean, Black and Aegean sea waters.

X-ray analysis of the studied samples was carried out on the modified and automatized apparatus "DRON-2" in $CuK\alpha$ – radiation in the $20^\circ \leq 2\theta \leq 100^\circ$ angle range at room temperature. Corrosion tests were carried out through potentiodynamic polarization method in a standard three electrode cell. The polarization tests were conducted using a Princeton Applied Research-PAR, model PARSTAT 2273 potentiostat/galvanostat, with "Power Corr" software. A thermostatic electric furnace was used. A specific area (1cm^2) of the alloy sample was used as the working electrode (WE); a platinum sheet and glassy carbon were employed as reference (RE) and respectively counter electrode (CE).

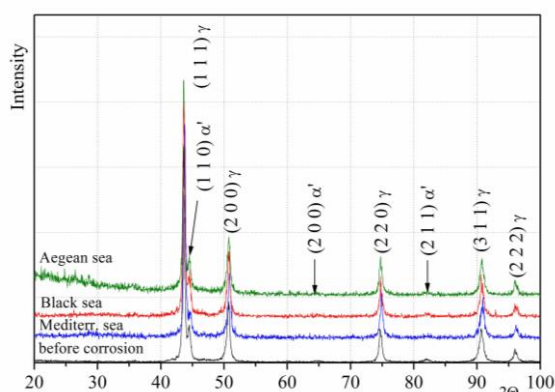


Figure 1 The comparison of XRD patterns for V4A stainless steel before and after corrosion action of sea waters

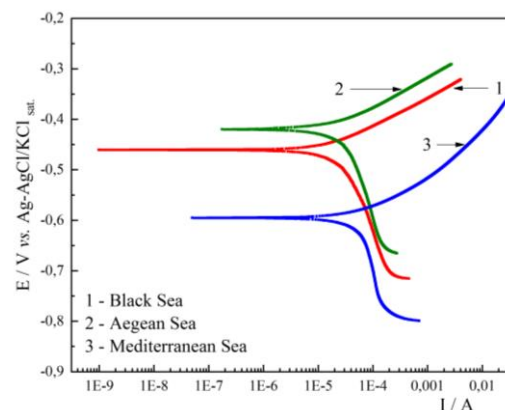


Figure 2 The comparative Tafel polarization curves of V4A stainless steel in different seawaters

It was found that V4A alloy has two crystalline phases – austenic $FeNi$ $Fm\bar{3}m$ sp. gr. and ferritic $FeCr$ $Im\bar{3}m$ sp. gr. The cell parameter a before corrosion action is 0.3595 nm for the $FeNi$ phase and 0.2877 nm for the $FeCr$ phase with a phase ratio of 6/1. X-ray patterns analysis after different seawaters electrochemical action showed that in all cases V4A alloy structure was preserved. The formation of iron oxides and hydroxides on the surface of the samples is not observed. Analysis of the corrosion parameters showed that the greatest corrosive effect on studied alloy has a Mediterranean Sea water, which is confirmed by the results of a study of surface morphology. In this case corrosion rate is 0.1290 mm/year .

The work was supported by the Romanian Academy and the Academy of Sciences of the Republic of Belarus Foundation for Basic Research (project F18RA-002/2018).

- [1] J. Alcántara, D. Fuente, B. Chico, J. Simancas, I. Díaz, M. Morcillo, Marine Atmospheric Corrosion of Carbon Steel: A Review. Materials, vol.10, PP.406(1-67), (2017).
- [2] R. Jeffrey, L. Boulton, Corrosion of stainless steel in aggressive water environments, Waste + Water Management Australia, vol. 45, No. 6, PP.45-48, (2019).
- [3] R.E. Melchers, Principles of Marine Corrosion. In: Dhanak M.R., Xiros N.I. (eds) Springer Handbook of Ocean Engineering. Springer Handbooks. Springer, Cham (2016).
- [4] M. Wu, Z. Zhao, X. Wang, C. Wang, P. Liang, Corrosion behavior of 17-4 PH stainless steel in simulated marine environment, Materials and Corrosion, PP. 1-9, August 2018.

Study of alkaline earth metal substitution effects in sol-gel derived mixed-metal oxides and $Mg_{2-x}M_x/Al_1$ (M = Ca, Sr, Ba) layered double hydroxides

L. Valeikiene¹, I. Grigoraviciute-Puroniene², A. Kareiva³

*Institute of Chemistry, Faculty of Chemistry and Geosciences, Vilnius University,
Naugarduko 24, LT-03225 Vilnius, Lithuania
ligita.valeikiene@chgf.vu.lt*

Layered double hydroxides (LDH) have two-dimensional structure which consists of positively charged layers and interlayer anions [1]. LDHs have a large surface area, good thermal stability and high anion exchange capacity comparable to those of anion exchange resins [2]. Layered double hydroxides (LDHs) are anionic clays with unique physical and chemical properties. In this study an indirect sol-gel synthesis method was applied to prepare alkaline earth metal substituted layered double hydroxides of $Mg_{2-x}M_x/Al_1$ (M = Ca, Sr, Ba). In the sol-gel processing metal nitrates $Mg(NO_3)_2 \cdot 6H_2O$, $Al(NO_3)_3 \cdot 9H_2O$, $Ca(NO_3)_2 \cdot 4H_2O$, $Sr(NO_3)_2$, and $Ba(NO_3)_2$ dissolved in deionized water were used as starting materials and citric acid monohydrate and 1,2-ethanediol were used as complexing agents. The mixed metal oxides (MMO) were obtained after thermal treatment of precursor gels at 650 °C and subsequently reconstructed in water to the LDHs. The synthesis products were characterized using X-ray powder diffraction (XRD) analysis and scanning electron microscopy (SEM). Nitrogen adsorption by the Brunauer, Emmet and Teller (BET) and Barret method was used to determine the surface area and pore diameter of the synthesized alkaline earth metal substituted MMO materials. It was demonstrated for the first time that the formation of $Mg_{2-x}M_x/Al_1$ (M = Ca, Sr, Ba) LDH from the sol-gel derived powders depends significantly on the nature and concentration on the alkaline earth metal.

[1] D.G. Evans, Slade RCT Structural aspects of layered double hydroxides, *Structure and Bonding*, 119., pp. 1–87, (2006)

[2] F. Cavani, F. Trifiro, A. Vaccari, Hydrotalcite-type anionic clays: Preparation, properties and applications, *Catalysis Today*, 11., pp. 173-301 (1991)

Synthesis and characteristic of ZnSe₂O₅ nanocrystals

A. Akylbekova¹, Sh. Giniyatova¹, A. Usseinov¹, Z. Baimukhanov¹,
A. Kozlovskiy², A. Dauletbekova¹

1- Eurasian National University. L.N. Gumilyov, Nur-Sultan, Kazakhstan
2- Astana Branch of the INP, Nur-Sultan, Kazakhstan

Aiman88_88@mail.ru, Giniyat_shol@mail.ru

In this work, we present the results of template synthesis (chemical deposition) of ZnSe₂O₅ nanocrystals into a track template a-SiO₂/Si-n.

SiO₂/Si structures were irradiated with Xe 200 MeV ions to a fluence of 10⁸ ions/cm² followed by chemical etching in a 4% aqueous HF solution; the etchant included m(Pd) = 0.025 g, etching time 20 minutes, etching temperature T = 25°C. For chemical deposition, the following composition was used: ZnCl₂ – 3.4 g/l, SeO₂ – 0.2 g/l, and deposition time – 60 min.

After chemical deposition, the morphology of the surface and transverse cleavage was studied using a Hitachi S-4800 scanning electron microscope. SEM studies showed that most of the pores of the template are filled and the chemical precipitation method is excellent for growing with a controlled morphology and a high degree of orderliness. It was found that the filling of nanopores depends on the temperature and deposition time.

An X-ray structural study of the samples revealed the creation of single-phase ZnSe₂O₅ nanocrystals with an orthorhombic crystal structure and the Pbcn space group (60). The unit cell parameters we obtained coincide with published data [1].

We also performed non-empirical LCAO calculations, which confirmed our experimental studies of basic properties of ZnSe₂O₅ nanocrystals. As a result of calculations, it was shown that the ZnSe₂O₅ nanocrystal has direct bandgap 3.86 eV at the Γ -point that has good agreement with other theoretical studies of ZnSe₂O₅ bandgap. For example, I. Castelli et. al. [2] reported 3.6 eV (Kohn-Sham) and 4.85 eV (quasi-particle) computed bandgaps that obtained using GLLB-SC potential by Gritsenko et. al. [3] and Kuisma et. al. [4]. The charge distribution analysis showed significant covalent contribution to chemical bounds of crystal.

Thus, in this work, we studied and characterized the structural, morphological, and electronic properties of ZnSe₂O₅ zinc diselenide nanocrystals, first obtained by chemical deposition into a-SiO₂/Si-n track templates.

[1] G. Meunier, M. Bertaud, *Cristallochimie du Sélénium(+IV)*. II. Structure cristallinede ZnSe₂O₅. *Acta crystallographica. Section B, Structural science* 30, pp. 2840-2843 (1974)

[2] I.E. Castelli, F. Hüser, M. Pandey, H. Li, K.S. Thygesen, B. Seger, A. Jain, Kristin A. Persson, G. Ceder, and K.W. Jacobsen, *New Light-Harvesting Materials Using Accurate and Efficient Bandgap Calculations*. *Adv. Energy Matter.*, Vol. 1400915, pp. 1-7 (2014)

[3] O. Gritsenko, R. van Leeuwen, E. van Lenthe, and E. Jan Baerends, *Self-consistent approximation to the Kohn-Sham exchange potential*. *Phys. Rev. A*, Vol. 51, pp. 1944-1954 (1995)

[4] M. Kuisma, J. Ojanen, J. Enkovaara, and T.T. Rantala, *Kohn-Sham potential with discontinuity for band gap materials*, *Phys. Rev. B*, Vol. 82, 115106, pp. 1-7 (2010)

Magnetic properties of materials based on FeNi-50, FeSi and ASC100.29 iron powders with nanomodified coatings

A. Vetcher¹, G. Govor¹, A. Larin¹, K. Yanushkevich¹, Yu. Timoshkov²

1- Scientific-Practical Materials Research Centre NAS of Belarus, Laboratory of Physics of Magnetic Materials, 220072, Minsk, P.Brovki str., 19, Belarus

2- Belarusian State University of Informatics and Radioelectronics, 220072, Minsk, P.Brovki str., 6, Belarus

E-mail: vetcher@physics.by

The widespread use of valve electric motors with an inverter drive, for which the working magnetization reversal frequency significantly exceeds the industrial frequency, required the development of new soft magnetic materials [1-4]. However, the results of these studies do not allow us to unequivocally talk about the successful solution of the developing composite magnetic soft material problem.

For uniform applying protective and insulating coatings, a special technique has been developed in order to obtain isolated powders of magnetically soft materials. Using this technique, each individual particle of powder material is coated with a layer of a given thickness in the range from one nanometer to several micrometers. To study the magnetic properties were prepared composite magnetic material samples with dimensions of $24 \times 13 \times 8$ mm by compacting the treated powder with an insulating coating by pressure of 7-8 t/cm², followed by annealing in vacuum at 400°C during 1 hour. Magnetic properties were measured by an express magnetometer at a magnetic field frequency of 1 kHz: the magnetization reversal curves of the samples were recorded, and the area of the hysteresis loop in pixels was determined. The pixel dimension was determined by measuring the magnetic flux on a graduated fluxmeter F5050.

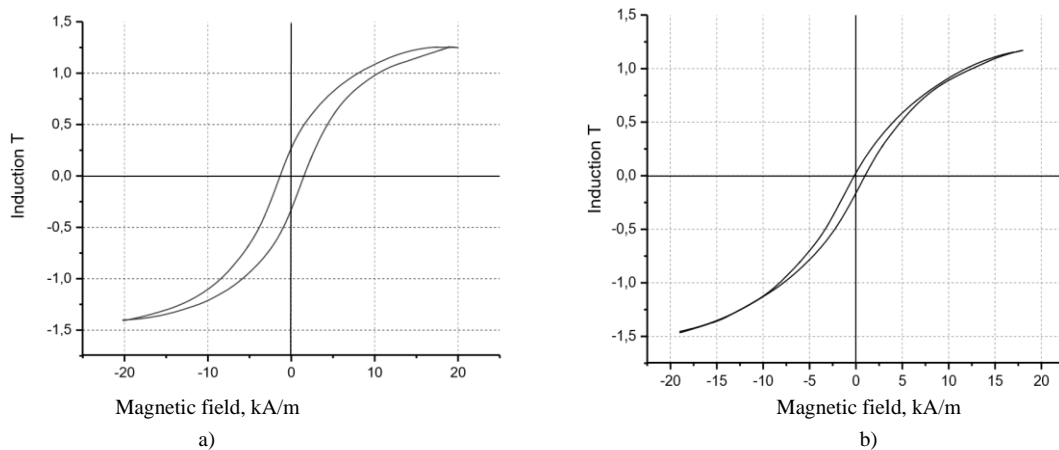


Figure 1 Hysteresis loop of 1 kHz for powder based on FeNi-50 sample:
a) without an insulating particles coating at sintering to a metallic state at a temperature 700°C;
b) coated with an insulating phosphorus oxide coating.

Performed in this work preliminary studies showed that higher values of magnetic parameters - magnetic induction and magnetic permeability - are characteristic for composite materials based on pure water-sprayed iron powders ASC100.29 with a particle size less than 100 microns and an amount of impurities not more than 1%, compared with materials based on powders of iron alloys FeNi and FeSi, while maintaining relatively low magnetization reversal losses.

The proposed method for composite magnetic materials producing allows a wide range to change both the thickness of the coatings and directly its chemical composition. All this opens up great opportunities in terms of creating new magnetic materials with desired properties.

The work is supported by Republic of Uzbekistan and the Academy of Sciences of Republic of Belarus Foundation for Basic Research (bilateral project T19UZBG-004/2019).

[1] Production of iron powder having high electrical resistivity: pat. US 3245841 / F.A. Jack, G.C. Sydney. – Publ. date 12.04.1966.

[2] Magnetic powder compacts: pat. US 4602957 / H.C. Pollock, A.L. Smith. – Publ. date 29.07.1986

[3] Stator assembly for an alternating current generator: pat. US 4947065 / R.W. Ward, R.E. Campbell, W.E. Boys. – Publ. date 07.08.1990.

[4] Jack A.G. Exploitation of Soft Magnetic Composites for Electrical Machines. 1998 PM World Congress Special Interest Seminar.

Nanostructured porous hybrid network of nitrogen-doped carbon as an anode for Li-ion batteries

Kaspars Kaprāns¹, Aleksandrs Volperts², Gunars Bajars¹, Gints Kucinskis¹, Galina Dobele², Janis Kleperis¹

¹*Institute of Solid State Physics, University of Latvia, Latvia, e-mail: kasparsk@cfi.lu.lv*

²*Latvian State Institute of Wood Chemistry*

Lithium-ion batteries (LIBs) open up huge potential markets for rechargeable batteries in powering vehicles and storing electric power for the grid [1]. Carbon nanomaterials have been widely explored for use as electrode materials for the fabrication of LIB. Nitrogen doping represents a general and effective method in further improving the physical and chemical properties of carbon nanomaterials to enhance the energy storage capabilities and cyclability of the resulting batteries [2].

Firstly, nitrogen doping provides higher electrochemical activity, due to two lone pair electrons, nitrogen atom is more electronegative than carbon atom. Thus, the electron density of nitrogen becomes higher (leading to stronger interactions with positive particles), while the electron density of adjacent carbon becomes lower for stronger interactions with negative particles. Secondly, nitrogen doping can increase the electrical conductivity of carbon nanomaterials. For instance, the electrical conductivity of the N-Carbon film reached 410 S cm^{-1} compared with 200 S cm^{-1} in the bare carbon film. The lone pair electrons in nitrogen and π electrons in carbon and graphene form p- π conjugations to increase the density of charge carriers. Generally, the conductivity of N-doped carbon nanomaterials verified from several to hundreds of S cm^{-1} according to the different carbon materials and preparation methods. For example, N-doped carbon nanofibers showed a conductivity of 4.9 S cm^{-1} , while N-doped graphene demonstrated a conductivity as high as 270 S cm^{-1} [4]. Thirdly, a lot of defects are produced after nitrogen doping, and the resulting defects can provide channels for ion and electrolyte diffusions, which are important in batteries [5].

We report a facile and scalable process to prepare nanostructured N-doped porous carbon network as a promising anode material for (LIBs).

The formed electrically conducting porous network containing carbon structures maintain stable crystal structure during lithiation-delithiation process and porous architecture provides a fast electrolyte penetration/diffusion. Therefore, the designed material presents a reversible capacity of 247 mAhg^{-1} at a current density of 0.3 mA g^{-1} (C/3) based on the total mass loading of the composite, suggesting a good potential for application as an anode material for lithium-ion batteries.

Acknowledgements The financial support of Nanostructured Nitrogenated Carbon Materials as Promoters in Energy Harvesting and Storage Technologies (NN-CARMA) and CO₂EXIDE – CO₂-based electrosynthesis of ethylene oxide projects are greatly acknowledged

[1] XiaoyanLi, KyusungPark Nitrogen-Doped Carbon for Sodium-Ion Battery Anode by Self-Etching and Graphitization of Bimetallic MOF-Based Composite, Volume 3, Issue 1, 13 July 2017, Pages 152-163

[2] Wu, Jingxia & Pan, Zhiyong & Zhang, Ye & Wang, Bingjie & Peng, Huisheng. (2018). The recent progress of nitrogen-doped carbon nanomaterials for electrochemical batteries. *Journal of Materials Chemistry A*. 6. 10.1039/C8TA03968B.

[3] Wu, Jingxia & Pan, Zhiyong & Zhang, Ye & Wang, Bingjie & Peng, Huisheng. (2018). The recent progress of nitrogen-doped carbon nanomaterials for electrochemical batteries. *Journal of Materials Chemistry A*. 6. 10.1039/C8TA03968B.

[4] Y. Qiu, W. Li, W. Zhao, G. Li, Y. Hou, M. Liu, L. Zhou, F. Ye, H. Li, Z. Wei, S. Yang, W. Duan, Y. Ye, J. Guo and Y. Zhang, *Nano Lett.*, 2014, 14, 4821-4827.

[5] W. H. Shin, H. M. Jeong, B. G. Kim, J. K. Kang and J. W. Choi, *Nano Lett.*, 2012, 12, 2283-2288.

Hydro(solvo)thermal synthesis of NASICON-type materials for Na-ion batteries

G. Plečkaitytė¹, J. Pilipavičius¹, M. Petrulevičienė¹, J. Juodkazytė¹, L. Vilčiauskas¹

¹Center for Physical Sciences and Technology, Saulėtekio al. 3, LT-10257 Vilnius, Lithuania

gintare.pleckaityte@fmnt.lt

Electrochemical batteries are recently sought as of the most attractive technologies for storing electrical storage, having superior round-trip energy efficiencies, low environmental footprint easy scalability and most importantly the widest available power and energy range. Li-ion batteries have become the technology of choice due to their exceptional energy and power densities. However, the highly volatile cost and supply of lithium and some necessary transition metals (e.g. cobalt, nickel) as well as safety issues related to the use of highly flammable organic electrolytes is calling for the search of alternatives. Na-ion batteries, especially those employing aqueous electrolytes, are attracting increasing attention as potential candidates for large-scale energy. The aqueous aspect makes them significantly safer, non-flammable, low cost and environmentally friendlier with respect to the comparable Li-ion technologies in addition to the accessible and unlimited sodium resources and elimination of cobalt and other rare metals [1-3]. NASICON (Na SuperIonic Conductor) structured compounds have been recently attracting increasing attention not as original solid electrolytes but as promising electrode materials for Na-ion batteries. The open phosphate framework enables fast Na ionic conduction, superior electrochemical durability and wide selection of metals with variable redox potentials [4].

The aim of this work is to search for novel phosphate frameworks materials such as NASICONs and optimize their performance for the application in Na-ion batteries. In this study, we present the results of hydro(solvo)thermal synthesis of NASICON-type $\text{NaTi}_2(\text{PO}_4)_3$ and the characterization of its structural, morphological and electrochemical properties. Single phase $\text{NaTi}_2(\text{PO}_4)_3$ is synthesized by hydro(solvo)thermal synthesis method by varying a number of parameters such as solvent (ethylene glycol, ethanol, water), temperature (140-200°C) and synthesis time (2-24h). The structure and morphology of all prepared materials are characterized by X-Ray Diffraction, Scanning Electron Microscopy and Thermal Analysis. The electrochemical properties of prepared electrodes utilizing $\text{NaTi}_2(\text{PO}_4)_3$ as an active negative material ($\sim 2.1\text{V}$ vs. Na^+/Na) is investigated by Cyclic voltammetry and Charge/Discharge galvanostatic cycling in the three-electrode bottom mount flat sample beaker cells with aqueous and non-aqueous electrolytes. The results (Figure 1) show that nanostructured pure $\text{NaTi}_2(\text{PO}_4)_3$ and as composites with carbon are obtained using the hydro(solvo)thermal methods which show superior electrochemical response as aqueous Na-ion electrode active materials.

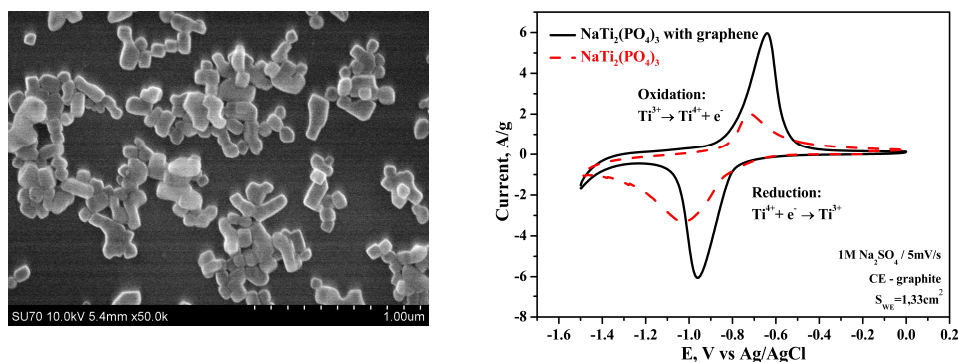


Figure 1. SEM image (left) and cyclic voltammogram (right) of $\text{NaTi}_2(\text{PO}_4)_3$.

Acknowledgements:

This project has received funding from the European Regional Development Fund (Project No. 01.2.2-LMT-K-718-02-0005) under grant agreement with the Research Council of Lithuania (LMTLT).

- [1] X. Pu, H. Wang, D. Zhao, H. Yang, X. Ai, S. Cao, Z. Chen, Y. Cao, Recent Progress in Rechargeable Sodium-Ion Batteries: toward High-Power Applications, *Small* 15, 1805427 (2019).
- [2] P. K. Nayak, L. Yang, W. Brehm, P. Adelhelm, From Lithium-Ion to Sodium-Ion Batteries: Advantages, Challenges and Surprises, *Angew. Chem. Int. Ed.* 57, 102–120 (2018).
- [3] H. Kim, H. Kim, Z. Ding, M. Hwan Lee, K. Lim, G. Yoon, K. Kang, Recent Progress in Electrode Materials for Sodium-Ion Batteries, *Adv. Energy Mater.*, 1600943 (2016).
- [4] C. Masquelier, L. Croguennec, Poly-anionic (Phosphates, Silicates, Sulfates) Frameworks as Electrode Materials for Rechargeable Li (or Na) Batteries, *Chem. Rev.* 113, 8, 6552-6591 (2013).

Research toward development of reiterated third generation biosensors using thermally reduced graphene oxide fractions

G. Rimkutė^{1,2}, V. Gurevičienė², J. Gaidukevič¹, I. Šakinytė², J. Razumienė²

1- Vilnius University, Faculty of Chemistry and Geosciences, Institute of Chemistry, Naugarduko str. 24, LT- 03225, Vilnius, Lithuania

2- Vilnius University, Life Sciences Center, Institute of Biochemistry, Saulėtekio av. 7, LT-10257, Vilnius, Lithuania

gintare.rimkute@chgf.stud.vu.lt

The biosensor market is steadily rising and is expected to be worth \$31.5 billion by 2024. This growth is influenced by progressing technological advancements and increasing demand for inexpensive and portable analytical devices [1]. Researchers are especially focusing on new materials that could also improve reiteration of the mentioned technologies [2]. This could be achieved by integrating carbon materials, which are characterized by unique mechanical, thermal, electric properties and can also be favourable for immobilization of the enzymes. One of these materials is graphene, which after special modification can be promising for creation of third-generation biosensors that use direct electron transfer (DET) between the enzyme and the electrode and therefore do not require any intermediate mediating materials [3].

The aim of this study is to investigate synthesized thermally reduced graphene oxide (TRGO) fractions and use them in the development of third-generation biosensors based on pyrroloquinoline quinone-dependent glucose dehydrogenase (PQQ-GDH). While PQQ-GDH possesses substrate specificity to wide range of carbohydrates, the enzyme could be very promising for creation of new technologies that further can be used both in medicinal and industrial devices.

During this study we used thermal reduction and fractionation equipment to reduce graphite oxide, which was initially synthesized by modified Hummers' method. Three fractions of TRGO were obtained and characterised by x-ray diffraction, Brunauer–Emmett–Teller and thermogravimetric analysis. Afterwards biosensors were constructed using membranes, made from PQQ-GDH immobilised into layer of TRGO. The main characteristics of proposed biosensors and especially stability, were investigated. Results will be introduced in more detail during the poster presentation.

ACKNOWLEDGEMENTS:

This project has received funding from European Social Fund (project No [09.3.3-LMT-K-712-16-0125]) under grant agreement with the Research Council of Lithuania (LMTLT).

[1] <https://www.marketsandmarkets.com/Market-Reports/biosensors-market-798.html>. Accessed 21 Jan 2020.

[2] da Silva Neves MMP, González-García MB, Hernández-Santos D, Fanjul-Bolado P. Future trends in the market for electrochemical biosensing. *Current Opinion in Electrochemistry* 2018;10:107-11.

[3] Sakinyte I, Barkauskas J, Gaidukevic J, Razumiene J. Thermally reduced graphene oxide: The study and use for reagentless amperometric D-fructose biosensors. *Talanta* 2015;144:1096-103.

CO₂ Adsorption on Copper Catalyst as Enhanced by Ion Liquid

G. Chikvaidze¹, J. Kleperis¹, G. Vaivars^{1,2}

1- Institute of Solid State Physics, University of Latvia, Kengaraga 8, Riga, Latvia

2- University of Latvia, Faculty of Chemistry, Jelgavas 1, Riga, Latvia

Main author email address: Guntars.Vaivars@cfi.lu.lv

Electroreduction of CO₂ represents a promising solution toward addressing global challenges in energy and sustainability [1-3]. The technology success depends on developing efficient electrocatalysts capable of selectively reducing CO₂ to valuable hydrocarbon products at low overpotentials (ethylene, methanol, CO etc.). So far, the best candidate is nanostructured copper and for efficient catalyst reaction, the CO₂ should adsorb from gaseous phase on the catalyst surface. CO₂ capture with ionic liquids is well known. The distinct properties of ionic liquids such as negligible vapor pressure and their affinity to capture the CO₂ molecules make them a feasible alternative for currently available solvents including, different amines. [4]. In this work, we investigated the adsorption process stimulated by ionic liquid. CO₂ adsorption on Cu surface was studied by ATR-FTIR spectroscopy and electrochemical processes by voltammetry.

Spectra measured using FTIR spectrometer Vertex 80v (Bruker, Germany) together with ATR accessory: VeeMAX III (PIKE Technology Inc., USA). The surface of the ATR crystal from germanium was coated with 20 nm thick copper. This surface was blown by a stream of CO₂. In situ measurements showed a significant increase in the adsorption of CO₂ on the surface of copper in the presence of an ionic liquid.

Electrochemical measurements were performed using Autolab potentiostat/ galvanostat in electrochemical cell with KHCO₃ electrolyte (1M and 2.5M) at a room temperature. Three-electrode configuration was applied with a copper on ATR crystal as a working electrode and black platinum as a counter electrode.

The financial support of European Union`s Horizon 2020 Research and Innovation Program project under grant agreement No 768789 is greatly acknowledged.

[1] Zhouyang Yin, G. Tayhas R. Palmore, Shouheng Sun, Electrochemical Reduction of CO₂ Catalyzed by Metal Nanocatalysts, Trends in Chemistry, vol. 1(8), pp. 739-750 (2019).

[2] E.E. Benson, C. P. Kubiak, A. J. Sathrum, J. M. Smieja, Electrocatalytic and homogeneous approaches to conversion of CO₂ to liquid fuels, Chem. Soc. Rev., vol. 38, pp. 89-99 (2009).

[3] H.-R. Jhong, S. Ma, P.J.A. Kenis, Electrochemical conversion of CO₂ to useful chemicals: current status, remaining challenges, and future opportunities, Curr. Opin. Chem. Eng., vol. 2, pp. 191-199 (2013).

[4] M. Aghaie, N. Rezaei, S. Zandehboudi, A systematic review on CO₂ capture with ionic liquids: Current status and future prospects, Renewable and Sustainable Energy Reviews, vol. 96, pp. 502-525 (2018).

Cross-linkable fluorene-based enamines as hole transporting materials for perovskite solar cells

D. Vaitukaityte¹, G. Bubniene¹, A. Magomedov¹, E. Kamarauskas², V. Jankauskas², M. Daskeviciene¹, A. Al-Ashouri³, B. Barvainiene⁴, S. Albrecht³, V. Getautis¹

1- Department of Organic Chemistry, Kaunas University of Technology, Radvilenu pl. 19, Kaunas, 50254, Lithuania

2- Department of Solid State Electronics, Vilnius University, Sauletekio 9, Vilnius 10222, Lithuania

3- Young Investigator Group Perovskite Tandem Solar Cells, Helmholtz-Zentrum Berlin, Kekuléstraße 5, 12489 Berlin, Germany

4- Department of Media Technologies, Kaunas University of Applied Sciences, Pramonės pr. 20, LT-50468 Kaunas, Lithuania

deimante.vaitukaityte@ktu.lt

Perovskite solar cells (PSCs) at the moment are demonstrating efficiencies comparable to that of the best Si-based devices, and their further progress is strongly dependent on the available organic hole transporting materials (HTMs). Currently, the highest published certified efficiency of 25.2% was achieved [1]. Among other things, further advancement of PSCs depends on the development of novel materials that can serve as efficient hole transporters. It is thus necessary to use simple and short synthesis pathways since it was recently shown that multi-step schemes lead to extremely high materials costs [2]. In addition, it is better to avoid the use of metal-catalyzed reactions, as metal traces are known to have detrimental effects on the performance of optoelectronic devices [3], and therefore additional purification processes are required, which further increases the price of the final material.

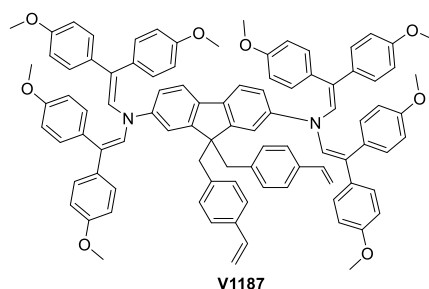


Figure 1. Cross-linkable fluorene-based enamine **V1187**.

In this work, enamine-based cross-linkable HTM **V1187**, containing two vinyl groups, was synthesized and investigated. In order to study the electrical properties of the synthesized HTMs, hole drift mobility was measured with the xerographic time-of-flight (XTOF) technique. **V1187** showed very good charge transporting properties, reaching 10^{-2} cm²/Vs at strong electrical fields. As the cross-linking process is not affecting the chromophoric system of the HTMs, it had only a minor influence on the hole drift mobility. In addition to charge transporting properties, ionization potentials were measured through photoelectron spectroscopy in air (PESA). The value was 5.11 eV. It is consistent with the values reported for other HTMs used in PSCs. To evaluate the performance of the materials acting as hole-selective layers in PSCs, devices with the p-i-n architecture were fabricated and characterized. To check the influence of the cross-linking on the performance of the devices, we have compared thermally cross-linked HTM films with that of the pristine films. The device with the **V1187** monomer film showed low open-circuit voltage (Voc) (0.89V). This can be attributed to the formation of direct contact between perovskite and ITO, due to the damage of the HTM film during solution-processing of the perovskite film. In contrast, after thermal polymerization, Voc was significantly improved up to the 1.04V on average. This result states that after cross-linking the HTM films have improved resistance against solvents. The device with **V1187** showed the highest PCE of 16.8%. As the films are used without oxidizing dopants, such improvement can be attributed to the higher values of the hole drift mobilities, and as a result better transport of the charges through the film. To further optimize the HTM film, the concentration of the **V1187** starting solution was varied from 2mg/ml down to 0.5mg/ml. As expected, the lower concentration led to the improved FF, however at the cost of reduced Voc. Overall, an optimized PCE of 18.1% for the cross-linked films prepared from the 1.5 mg/ml solutions were achieved.

[1] <https://www.nrel.gov/pv/assets/pdfs/cell-pv-eff-emergingpv.20200803.pdf>.

[2] A. K. Jena, A. Kulkarni, T. Miyasaka, Halide Perovskite Photovoltaics: Background, Status, and Future Prospects, *Chemical Reviews*, 119, 3036-3103, (2019).

[3] T. P. Osedach, T. L. Andrew, V. Bulović, Effect of synthetic accessibility on the commercial viability of organic photovoltaics, *Energy & Environmental Science*, 6, 711-718, (2013).

Synthesis and characteristics of organic semiconductors with one, two, three and four carbazolyl chromophores

P. Luizys¹, M. Daskeviciene¹, V. Jankauskas², E. Kamarauskas²

1- Department of Organic Chemistry Kaunas University of Technology, Radvilenu pl. 19, Kaunas LT-50254, Lithuania

2- Institute of Chemical Physics Vilnius University, Sauletekio al. 3, Vilnius LT-10257, Lithuania

povilas.luizys@ktu.lt

There is a global growing focus on renewable energy sources and solar energy being the most promising. Solar energy could theoretically satisfy the energy needs of mankind. Therefore, in many countries, development of technologies utilizing solar energy is stimulated in various ways. Perovskite solar cells, which just in a last decade have become a subject of great interest in the development of next generation solar cells that have already exceeded 25,2% power conversion efficiency [1]. Perovskite solar cells hold promise for low consumption of material and reduced processing costs. Commercialization of the perovskite solar cells is hindered by drawbacks which need to be resolved. One of them is that hole transporting organic semiconductor spiro-OMeTAD crystallizes in the device over the time, thus reducing its efficiency [2], furthermore additives are needed to increase the conductivity, which may cause the device degradation. Therefore, the search for alternative organic materials for perovskite solar cells remains highly relevant.

In this work, new hole transporting organic semiconductors with one, two, three and four carbazolyl chromophores were synthesized for the use in fabrication of perovskite solar cells.

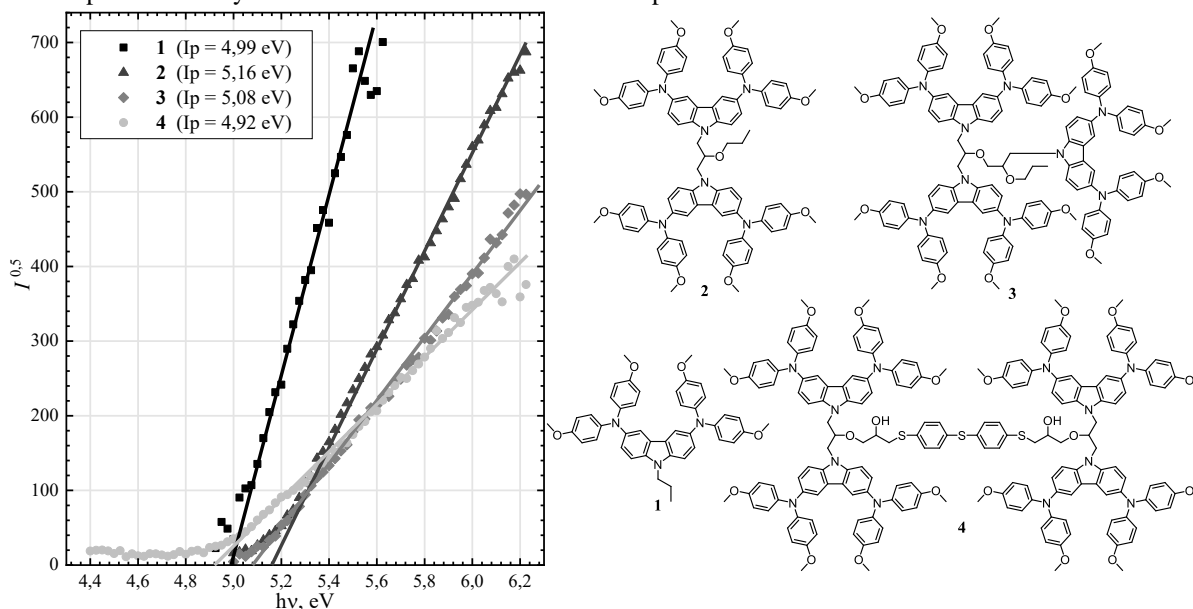


Figure 1 Ionization potential measurement results of synthesized organic semiconductors with carbazolyl chromophores.

New organic compounds were obtained via multi-step synthesis. Molecular structure of the newly synthesized semiconductors was confirmed by ¹H NMR, ¹³C NMR and IR spectroscopy. Differential scanning calorimetry analysis results of target compounds proved that they are molecular glasses and demonstrate stable amorphous state. Glass transition temperatures vary between 80-139 °C. Thermogravimetric measurements show that organic semiconductors are thermally stable at relatively high temperatures with a thermal decomposition starting at 350 °C. Photoelectron spectroscopy in air method was used to measure ionization potentials of the investigated molecules. Obtained *I_p* values (4,92 - 5,16 eV) indicate that the HOMO energy level of the synthesized products is compatible with the valence band of the photoactive perovskite layer. Charge transport properties were measured using xerographic time-of-flight technique. At high electric fields, compounds reach the hole drift mobility up to $\mu = 1,7 \cdot 10^{-4}$ cm²/V·s. Therefore, new organic semiconductors **2**, **3**, and **4** could potentially be used in construction of solar cells.

[1] Best Research-Cell Efficiencies, <https://www.nrel.gov/pv/assets/pdfs/best-research-cell-efficiencies.20190802.pdf> (accessed 2020-01-26), (2019).

[2] Tobat P. I. Saragi, T. Spehr, A. Siebert et al., Spiro compounds for organic optoelectronics, Chemical Reviews, 107, 1011-1065, (2007).

Carbazole-terminated isomeric hole transporting materials for perovskite solar cells

**S. Daskeviciute¹, K. Rakstys¹, P. Sanghyun², A. Drevilkauskaitė¹, H. Kanda², N. Shibayama³,
M. Daskeviciene¹, A. Gruodis⁴, E. Kamarauskas⁴, V. Jankauskas⁴, V. Getautis¹,
M. K. Nazeeruddin²**

1- Department of Organic Chemistry, Kaunas University of Technology, Lithuania

2- Group for Molecular Engineering of Functional Material, Institute of Chemical Sciences and Engineering, École Polytechnique Fédérale de Lausanne, Switzerland

3- Department of General Systems Studies, Graduate School of Arts and Sciences, the University of Tokyo, Japan

4- Institute of Chemical Physics Vilnius University, Lithuania

sarune.daskeviciute@ktu.lt

In the last decade, perovskite solar cells (PSCs) have attracted vast attention in the photovoltaic community leading to the enormous improvement in the power conversion efficiency (PCE), currently exceeding 25% [1]. Solid-state organic hole transporting materials (HTMs) are one of the important components of the perovskite solar cells (PSCs), ensuring stability of the perovskite absorber layer, good charge separation, and as a consequence high performance of the devices. Currently, Spiro-OMeTAD is the most popular choice for the HTM layer, and is used for the majority of the state-of-the-art PSC devices. However, due to the complicated multi-step synthetic procedure, price of the Spiro-OMeTAD remains at a very high level [2]. Therefore, huge research interest directed into new HTM candidates has been raised to find an ideal HTM.

It is known that various carbazole-structured small organic HTMs have been widely applied in PSCs and showed comparable photovoltaic performance [3]. In this work, three carbazole-based twin molecules termed **V1209**, **V1221**, **V1225** and “half” molecule **V1207** were designed based on π -extension through additional carbazole unit and successfully synthesized (Fig. 1).

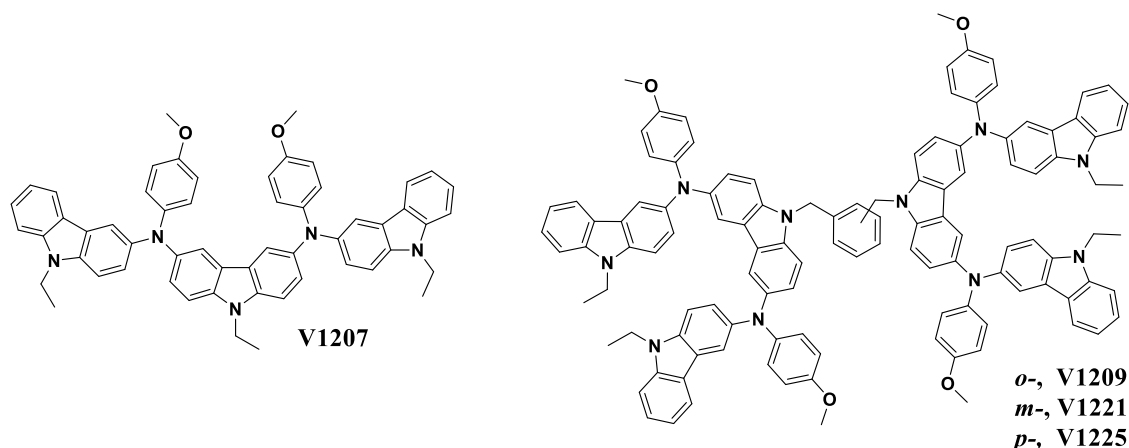


Figure 1. Structures of HTMs **V1207**, **V1209**, **V1221**, **V1225**

Twin molecules **V1209**, **V1221**, and **V1225** exhibit excellent thermal stability up to 440°C combined with suitable ionisation energies that properly align with the valence band of the perovskite. In addition, hole drift mobility values of isomers reached the 10^{-5} cm²/Vs order of magnitude, while **V1207** has the highest hole mobility of 6×10^{-4} cm²/Vs outperforming that of spiro-OMeTAD. The most efficient perovskite devices contained double-armed HTMs **V1221** and **V1225** reaching the PCE of 17.81%, however, based on the stability results, we conclude that *p*-isomer **V1225** is the most successful across the series and holds a great promise for practical wide-scale application in commercial perovskite solar cells.

[1] A. Kojima, K. Teshima, Y. Shirai, T. Miyasaka, Organometal Halide Perovskites as Visible-Light Sensitizers for Photovoltaic Cells, *J. Am. Chem. Soc.*, 131 (17), 6050-6051, (2009).

[2] U. Bach, D. Lupo, P. Comte, et al., Solid-State Dye-Sensitized Mesoporous TiO₂ Solar Cells with High Photon-to-Electron Conversion Efficiencies, *Nature*, 395 (6702), 583-585, (1998).

[3] H. Jiang, J. Sun, J. Zhang, A Review on Synthesis of Carbazole-based Chromophores as Organic Light-Emitting Materials, *Curr. Org. Chem.* 16 (17), 2014-2025, (2012).

NEW FLUORENE DERIVATIVES AS HOLE TRANSPORTING MATERIALS FOR EFFICIENT PEROVSKITE SOLAR CELLS

Aistė Ilčiukaitė¹, Marytė Daškevičienė¹, Egidijus Kamarauskas², Vygintas Jankauskas², Vytautas Getautis¹

¹ Department of Organic Chemistry, Kaunas University of Technology, Lithuania

² Institute of Chemical Physics, Vilnius University, Lithuania

aiste.ilciukaite@ktu.edu

Solar energy is the most powerful source of renewable energy. Properly refined solar cell technology can fully meet society's energy needs. Currently, silicon solar elements are mainly used, but they are expensive and complicated to manufacture. However, in the last decade organic and hybrid solar cells are gaining ground. Among them are the perovskite solar cells (PSCs), which have already reached 24% efficient [1]. The benefits of these elements are cheap starting materials and a variety of different fabrication methods that could simplify industrial applications. However, there are still several drawbacks of PSCs. In particular the rather expensive p-type organic semiconductor spiro-OMeTAD used for hole transport is synthesized by a five step reaction, and also the unresolved stability problem of these devices [2]. Currently, there is an intense search for more simple synthesis methods to produce cheaper and efficient organic semiconductors. The aim of this work was to synthesize fluorene-based semiconductors, that could be used as a hole transporting material in PSCs, and estimate the influence of the length of alkylchains on the properties of new compounds.

Table 1. Hole mobility of new compounds.

Comp.	$\mu(E = 0)$, $\text{cm}^2/\text{V}\cdot\text{s}$	$\mu(E = 1 \cdot 10^6)$ V/cm , $\text{cm}^2/\text{V}\cdot\text{s}$
1	$1,5 \cdot 10^{-4}$	$4 \cdot 10^{-4}$
2	$2,7 \cdot 10^{-3}$	$8 \cdot 10^{-3}$
3	$2 \cdot 10^{-5}$	$3 \cdot 10^{-3}$
4	$2,3 \cdot 10^{-5}$	$1,9 \cdot 10^{-4}$
5	$4,9 \cdot 10^{-5}$	$3,2 \cdot 10^{-5}$

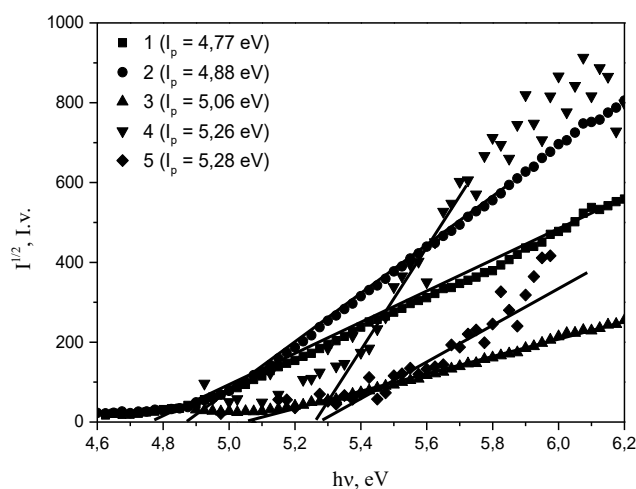


Figure 1. Ionization potential of fluorene-based derivatives.

During this work, new fluorene class compounds (1-5) were obtained in three-step reaction. All target substances have two maximum absorption peaks between 303 and 377 nm. From investigated thermal properties, it is evident that all compounds are amorphous and have thermal stability greater than 400 °C. It has been observed that longer alkyl chains reduce the thermal stability and glass transition temperature. Hole drift mobility ($3,25 \cdot 10^{-5} - 3 \cdot 10^{-3} \text{ cm}^2/\text{V}\cdot\text{s}$) and ionization potential (3,77-5,28 eV) of new fluorene-based derivatives are favorable for the use in PSCs as positive charge carrier. However, the obtained data show that the increase in the length of alkyl chains tend to decrease the charge carrier mobility and rise the numeric value of ionization potential.

[1] Q. Jiang, Y. Zhao et al. Surface passivation of perovskite film for efficient solar cells, *Nat. Photonics* **13**, 460–466 (2019).

[2] T. P. I. Saragi, T. Spehr et al. Spiro Compounds for Organic Optoelectronics, *Chem. Rev.* **107**, 1011-1065 (2007).

Method of laser structuring of multiwall nanotube arrays for terahertz applications

**G. Gorokhov^{1,2}, D. Bychanok^{1,3}, P. Kuzhir^{1,4}, J. Macutkevici², J. Banys², D. Gorodetskiy⁵,
A. Kurennya⁵, O. Sedelnikova⁵, L. Bulusheva⁵, A. Okotrub⁵**

1- Institute for Nuclear Problems Belarusian State University, 11 Bobruiskaya str., 220030, Minsk, Belarus

2- Physics Faculty, Vilnius University, Sauletekio 9, Vilnius LT-10222, Lithuania

3- Tomsk State University, 36 Lenin Ave, Tomsk 634050, Russia

4- Institute of Photonics, University of Eastern Finland, Yliopistokatu 7, FI-80101 Joensuu, Finland

5- Nikolaev Institute of Inorganic Chemistry, SB RAS, 3 Acad. Lavrentiev Ave., 630090, Novosibirsk, Russia

glebgorokhov@yandex.ru

Here the simple and adaptable method of terahertz metasurfaces creation is introduced. Aligned layers of multiwall carbon nanotubes (MWCNT) grown by APCVD method [1] were structured by means of industrial CO₂ laser engraver. 2D-pyramidal structures with 250 μm period were created (Figure 1(a)). Engraved structures were impregnated with viscous epoxy resin under vacuum in order to ensure their mechanical stability.

The reflection spectra of obtained structures were investigated in 0.1 – 1 THz range by means of EXPLA T-spec time domain terahertz spectrometer. The model of pyramid-based surface [2] reflection was modified in order to take into account the contribution of epoxy resin layer. Figure 1(b) depicts the good agreement between the experiment and applied model.

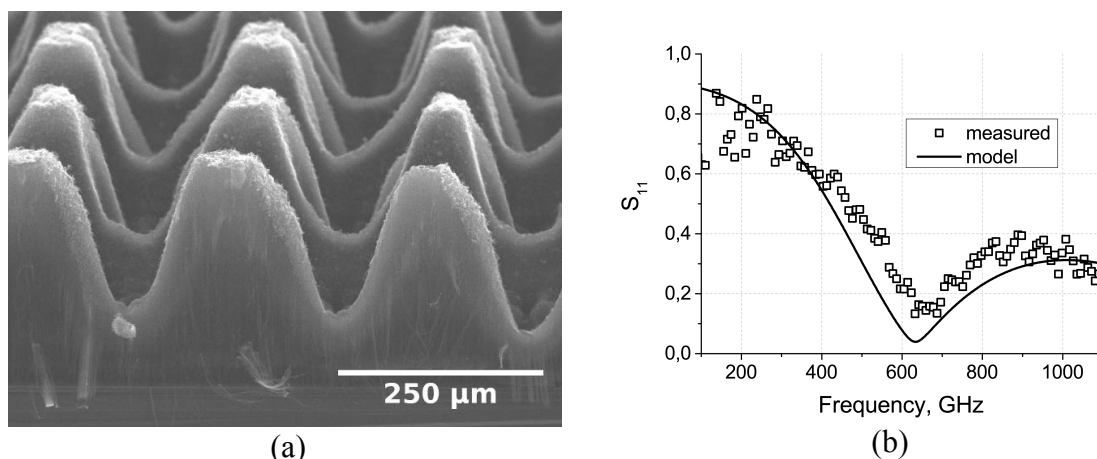


Figure 1 (a) SEM image of pyramidal structure engraved on aligned MWCNT array (b) measured amplitude of back-reflected signal S_{11} for pyramidal structure with ~ 250 μm (dots) and its model fitting (line).

Structures under the investigation are applicable as phase gratings in THz frequency region, and may be considered as a proof of concept for the method used. Method itself is suitable for manufacturing of ultralightweight terahertz components with complex surface geometry including frequency-selective surfaces, reflective filters, polarizers [3] and attenuators.

Acknowledgements: this work is supported by supported by the World Federation of Scientists project «Science and Technologies», RFBR Grant number 19-33-50048

- [1] A. V. Okotrub, L. G. Bulusheva, A. G. Kudashov, V. V. Belavin, and S. V. Komogortsev, “Arrays of carbon nanotubes aligned perpendicular to the substrate surface: Anisotropy of structure and properties,” *Nanotechnologies Russ.*, vol. 3, no. 3–4, pp. 191–200, Apr. 2008, doi: 10.1134/S1995078008030051.
- [2] D. S. Bychanok, A. O. Plyushch, G. V. Gorokhov, U. S. Bychanok, P. P. Kuzhir, and S. A. Maksimenko, “Microwave radiation absorbers based on corrugated composites with carbon fibers,” *Tech. Phys.*, vol. 61, no. 12, pp. 1880–1884, Dec. 2016, doi: 10.1134/S1063784216120094.
- [3] D. S. Bychanok *et al.*, “Anisotropic electromagnetic properties of polymer composites containing oriented multiwall carbon nanotubes in respect to terahertz polarizer applications,” *J. Appl. Phys.*, vol. 114, no. 11, p. 114304, Sep. 2013, doi: 10.1063/1.4821773.

Electrochemical exfoliation – streamline method for synthesis of nitrogen doped graphene

R. Olins^{1,2}, P. Lesnicenoks^{1,2}, J. Kleperis¹, A. Knoks¹, I. Lukosevics¹

¹*Institute of Solid State Physics, University of Latvia*

²*FMSAC, Riga Technical University*

roberts.olins@cfi.lu.lv

Graphene was discovered in the early 21st century, but has already proven itself in many applications - energy, medicine, electronics, food and sports, and more. Functionalization of nanostructured carbon materials with both non-metallic and metallic atoms is possible in various ways, imparting enhanced or new properties to the starting material, even catalytic activity. Graphene was discovered in the early 21st century, but has already proven itself in many applications - energy, medicine, electronics, food and sports, and more. Functionalization of nanostructured carbon materials with both non-metallic and metallic atoms is possible in various ways, imparting enhanced or new properties to the starting material, even catalytic activity. A method of electrochemical exfoliation was used to obtain the graphene sheets.[1] To ensure N-doping the process is done in a NaN_3 electrolyte solution which provides less quantity of oxygen groups that tend to strongly bond at defect sites on the graphene, comparing with such solvents as NH_4OH . Two graphite electrodes are inserted into the electrolyte and a pulse power of 0-10V is applied. [2] The solution containing the obtained material is filtered through a $0,2\mu\text{m}$ filter, dried and then reduced in a tube furnace with a constant flow of Ar/H_2 (95/5%) gas. The material is characterized using SEM, AFM, XPS and other methods.

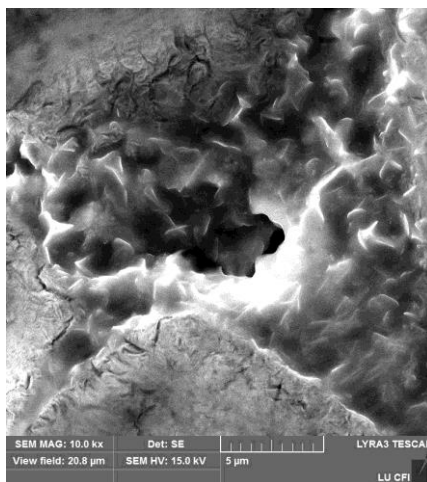


Figure 1. SEM image of agglomerated GSS particles on silicon.

Authors acknowledge financial support from Latvian Science Council project LZP FLPP No. LZP-2018/1-0194.

[1] G. Wang, B. Wang, J. Park, Y. Wang, B. Sun, J. Yao, Highly efficient and large-scale synthesis of graphene by electrolytic exfoliation, Elsevier, CARBON 47, 3242–3246.(2009)

[2] O. Ustavytska, Y. Kurys, V. Koshechko, V. Pokhodenko, One-Step Electrochemical Preparation of Multilayer Graphene Functionalized with Nitrogen, Nanoscale Research Letters, Ustavytska et al. Nanoscale Research Letters 12:175, 1-7 page.(2017)

Scalable Solar Simulators Based on Arrays of Light-Emitting Diodes

Ž. Vosylius¹, A. Novičkovas¹, K. Laurinavičius^{1,2}, V. Kavaliauskas¹ and V. Tamošiūnas¹

1- Institute of Photonics and Nanotechnology, Vilnius University, Saulėtekio Ave. 3, LT 10257 Vilnius, Lithuania

2- Center for Physical Sciences and Technology, Saulėtekio Ave. 3, LT 10257 Vilnius, Lithuania

zygimantas.vosylius@ff.vu.lt

Rapid production growth of solar cell and modules also increases a need of novel device characterization equipment. One of quality control stages in solar cell production is device testing under standardized irradiation conditions, provided by solar simulators. Solar simulator is an artificial device that closely resembles the Solar irradiance for the purpose of testing photovoltaic devices in a controlled environment. The most commonly used irradiance and spectral distributions of such simulators aim to match so-called AM1.5G conditions [1]. IEC 60904-9 Ed.2.0[2] standard defines criteria of how A, B or C class can be assigned to solar simulator in three categories: spectral distribution match, temporal stability, irradiance distribution uniformity. Traditionally, Xenon arc lamps were the mostly used light source of solar simulators. However, they suffer from issues related to a relatively short lamp life and stability. Therefore, development of simulators based on light emitting diodes, such as ones reported in [3, 4], are getting more and more attention due stability and long-time performance of light sources.

The purpose of this work is to reveal the rational design sequence of solar simulators based on compact and efficient high-power light emitting diode (LED) arrays. Blend of ray-tracing simulation results, experimentally measured irradiance distributions and obtained from manufacturers angular flux distributions was employed to predict the properties of prototype solar simulators while adjusting their designs. While [3] design was the starting point for rational selection of LED power levels and their approximate numbers, LED positioning flexibility and dual reflector systems of individual and common reflectors were fully employed to increase the illuminated area towards typical industrial solar cell sizes.

Two designs were selected for implementation and more detailed experimental verification after numerical design procedures revealed that sufficient irradiance uniformity might be expected for solar cells of 4 inch and 5 inch size, respectively. Our investigations of the first prototype revealed that illuminated according to AAA class area reached 93.5 cm² in case of the first prototype with 19 – 25 LEDs (Fig. 1). Design enhancements and improvements to mirror system increased this area to more than 14×15 cm² rectangular area, fitting standard 5 inch industrial solar cells with considerable margin.

Finally, discrepancies between previously calculated and experimental data were addressed by additional comprehensive ray-tracing simulation series using POV-Ray software. These simulations revealed additional peculiarities related to edge effects, gaps between the mirror system and sample plane, and other inevitable features of real devices which have to be accounted when designing simulators with even lower numbers of LEDs per unit area.

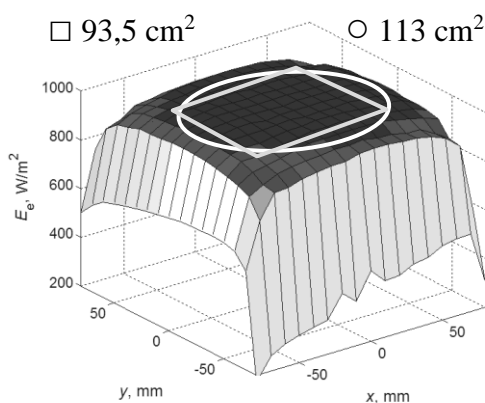


Figure 1 Irradiance distribution obtained for 25 LED solar simulator with system of double reflectors.

[1] Photovoltaic Devices – Part 3: Measurement Principles for Terrestrial Photovoltaic (PV) Solar Devices With Reference Spectral Irradiance Data, IEC 60904-3 Ed.2.0 (2006).

[2] Photovoltaic Devices – Part 9: Solar Simulator Performance Requirements, IEC 60904-9 Ed.2.0 (2007).

[3] A. Novičkovas, A. Baguckis, A. Mekys, and V. Tamošiūnas, “Compact Light-Emitting Diode-Based AAA Class Solar Simulator: Design and Application Peculiarities”, IEEE Journal of Photovoltaics, vol. 5, no. 4 (2015).

[4] A. Y. Al-Ahmad, J. Holdsworth, B. Vaughan, G. Sharafutdinova, X. Zhou, W. J. Belcher, P. C. Dastoor, „Modular LED arrays for large area solar simulation“. Prog. Photovolt. Res. Appl., vol. 27, pp. 179 – 189 (2019).

Swelling of composite sulfonated polyetheretherketone (SPEEK)/ ZrO₂ membranes in electrolytes

R. Kaparkalējs¹, E. Sprūģis¹, G. Vaivars^{1,2}

1- Institute of Solid State Physics, University of Latvia, Kengaraga 8, Riga, Latvia

2- University of Latvia, Faculty of Chemistry, Jelgavas 1, Riga, Latvia

Main author email address: Guntars.Vaivars@cfi.lu.lv

The interest of the research, during the last 20 years, was addressed to the improvement of existing polymer electrolyte membranes for fuel cells and the development of new ones [1] due to the need to develop alternative energy systems. Problems related to CO₂ emissions and climate changes are accelerating the new technology development. For this reason, the focus of research is changing to direct methods reversing CO₂ emissions. Availability of local alternative energy sources (wind, solar) makes it possible to discuss the electrochemical CO₂ transformation to useful chemicals – methanol, acetic acid, carbohydrates, etc.

Sulfonated polyetheretherketone (SPEEK) was synthesized from polyetheretherketone (PEEK, obtained from *Sigma Aldrich*) [2-3]. Degree of sulfonation = 0.70. Polymer membranes prepared by using a solvent cast method. Polymer solutions were poured into Petri dishes and dried for 48 h at 80 °C.

Water uptake and swelling degree were determined for each of the prepared membranes. Dry membranes weighted and measured length and thickness. After that, membranes immersed in deionised water for 24 h, weighted and measured again. Alternatively, membranes immersed in a 1M KHCO₃ solution. Metrohm Autolab potentiostat/galvanostat PGSTAT204 was used for impedance/ conductivity measurements, and measuring parameters were as follows: frequency range was 50 kHz to 100 Hz; 10 frequencies per decade; signal amplitude 10 mV. Potassium content after ion-exchange obtained using XRF element analysis (Bruker S8 Tiger).

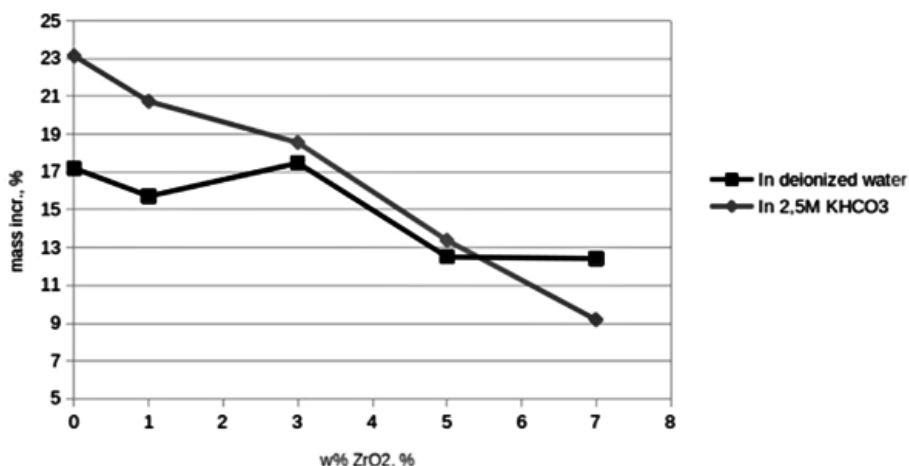


Figure 1 Thickness and mass changes for ZrO₂/ SPEEK composite membranes with a different ZrO₂ content in deionized water and 2.5M KHCO₃

The financial support of European Union's Horizon 2020 Research and Innovation Program project under grant agreement No 768789 is greatly acknowledged.

[1] A. Carbone, R. Pedicini, G. Portale, A. Longo, L. D' Ilario, E. Passalacqua, Sulphonated poly(ether ether ketone) membranes for fuel cell application: Thermal and structural characterisation, *J Power Sources*, vol. 163, pp. 18–26 (2006).

[2] H. Hou, B. Maranesi, J.-F. Chailan, M. Khadhraoui, R. Polini, M.L. Di Vona, P. Knauth, Crosslinked SPEEK membranes: Mechanical, thermal, and hydrothermal properties, *J Mater Res*, vol. 27, pp.1950–1957 (2012).

[3] D. Fedorenko and G. Vaivars Different approaches in sulfonated poly (ether ether ketone) conductivity measurements, *IOP Conf. Ser.: Mater. Sci. Eng.*, vol. 503, 012030 (2019).

Colloidal noble metal nanoparticles deposited on ZnO nanowires

D. Kulmatova, M. Baitimirova, U. Malinovskis, D. Erts, J. Prikulis

Institute of Chemical Physics, University of Latvia, 19 Raina Blvd., LV-1586, Riga, Latvia

juris.prikulis@lu.lv

Isolated noble metal nanoparticles are known for their applications for refractometric localized surface plasmon resonance (LSPR) sensor applications [1]. Ag and Au nanoparticles with diameters in tenths of nanometers range can be synthesized using many established protocols and obtained commercially in form of colloidal solutions and have the LSPR resonance in the visible to near infrared spectral range, which is convenient for optical detection. For improved signal to background ratio in LSPR sensing it is desirable to produce high surface coverage with isolated, non-touching nanoparticle arrays. However, dense colloidal nanoparticle deposition on surface without aggregation is complicated, and aggregates lose the required properties for LSPR detection.

Recently, dense non-touching Au nanoparticle arrays were produced by capillary force assisted colloid deposition on nanoporous anodic alumina templates [2]. In this study a similar approach was employed for the decoration of ZnO nanorod arrays with Au and Ag nanoparticles. ZnO – Au nanoparticle hybrids are of interest for biosensor applications (for example, as glucose sensor) [3].

ZnO nanorod arrays were grown by hydrothermal method on ZnO-seed substrates. For dip-coating 60 nm in diameter Au and Ag nanoparticle colloidal solution was used. The different withdrawal speeds and repeating times were applied for the optimization of Au nanoparticle coverage on ZnO nanorods. The influence of Au nanoparticle density and coverage area on transmittance and fluorescence of ZnO nanorod arrays were studied.

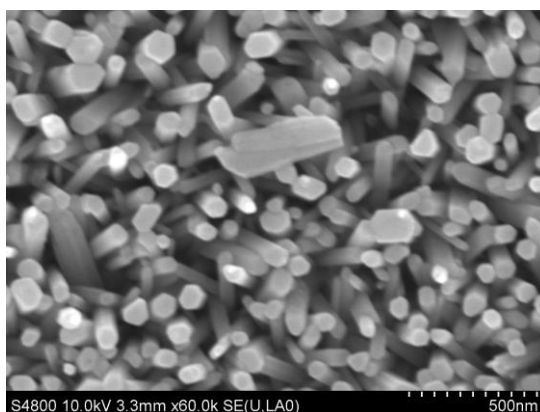


Figure 1 SEM image of ZnO nanorods with Au nanoparticles

Individual Au nanoparticles can be observed in SEM images (fig.1) only on the top surface of ZnO Nanowire network, therefore it is difficult to determine the exact coverage. The nanoparticle density can be tuned by modification of dip-coating withdrawal speed and surface modification with poly-L-lysine. The approximate density 1-5 particles per μm^2 , which is sufficient for optical detection.

Preliminary transmission measurements indicate that the nanoparticles on ZnO preserve their single-particle optical properties although diffuse scattering by ZnO prevents accurate measurements of elastic scattering spectra. Comparative photoluminescence spectra before and after nanoparticle deposition show more distinct differences that may be better resolved in comparison to relatively flat transmission spectra.

[1] K. Willets, and R. P. Van Duyne. "Localized Surface Plasmon Resonance Spectroscopy and Sensing." *Annu. Rev. Phys. Chem.* 58, no. 1 267–97. (2007)

[2] U. Malinovskis, R. Poplauskis, D. Erts, K. Ramser, S. Tamulevičius, A. Tamulevičienė, Y. Gu, and J. Prikulis. "High-Density Plasmonic Nanoparticle Arrays Deposited on Nanoporous Anodic Alumina Templates for Optical Sensor Applications." *Nanomaterials* 9, no. 4: 531. (2019)

[3] Wei, Yinyin, Ying Li, Xiaoqian Liu, Yuezhong Xian, Guoyue Shi, and Litong Jin. "ZnO Nanorods/Au Hybrid Nanocomposites for Glucose Biosensor." *Biosensors and Bioelectronics* 26, no. 1 (September 15, 2010): 275–78. <https://doi.org/10.1016/j.bios.2010.06.006>.

Ferroelectric based multi-type energy-harvesting device to power a mobile medical telemetry system

A. Molnar¹, V. Gerasimov², D. Gal¹

1- Uzhhorod National University, Department of the Physics of Semiconductors, Voloshina Str. 54, Uzhhorod, Ukraine, 88000

2- Mukachevo State University, Department of Light Industry, Mukachevo, Ukraine

alex.molnar@uzhnu.edu.ua

We have developed a multilayer converter of heating-deformation-lighting and motion/vibration into electricity for mobile medical telemetry system. The design of the generator is shown in Fig. 1. A composite or ceramic material (2) based on $\text{Sn}_2\text{P}_2\text{S}_6$ powder is applied to the base, for which a thin aluminum plate is used (3). It simultaneously serves as a mechanical base, one of the electrodes of the multi-type transducer and another one of the plates of the triboelectric nanogenerator (TENG) transducer.

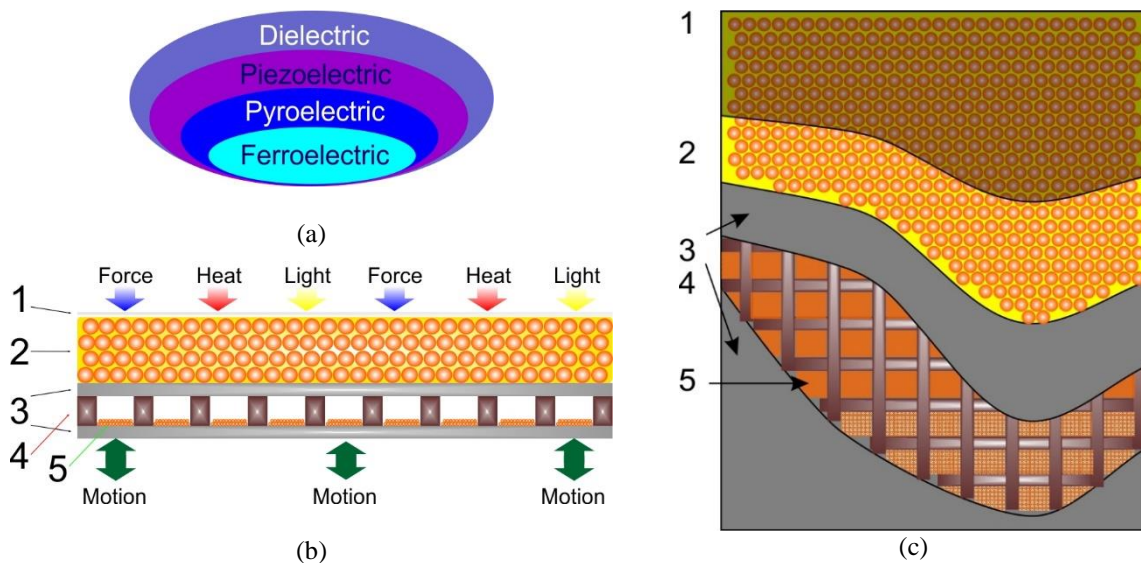


Figure 1 Piezoelectric, pyroelectric and ferroelectric material relationships (a). Sectional drawing (b,c) of a multilayer transformer of deformation-motion-lighting and heating into electric current. 1 - translucent electrode, 2 - composite based on $\text{Sn}_2\text{P}_2\text{S}_6$ powder, 3 - aluminum electrodes, 4 - rubber insulators, 5 - $\text{Sn}_2\text{P}_2\text{S}_6$ powder.

A thin translucent SnO electrode (1) was deposited on top of the composite layer by vacuum deposition. A grid of rubber insulators (4) is glued to the underside of the aluminum base electrode, which forms the elementary cells of TENG. The obtained cells of the triboelectric nanogenerator are 20% filled with $\text{Sn}_2\text{P}_2\text{S}_6$ powder (5), with a particle size of 50-100 micrometers.

During vibrations or movement, these particles rub against each other, forming a charge on the surface of the particles due to the piezoelectric effect as well as to the electrodes, accumulating and transferring the charge due to the triboelectric effect. This combination creates an 180V potential between the electrodes.

A grid of rubber partitions insulates one cell from another, which creates the effect of parallel connection of a large number of elementary generator cells (to increase the output current) and preventing the flowing of active substance from the cell to the cell.

Aluminum was not chosen as an electrode by chance, but based on its position in the triboelectric table [1]. To increase the efficiency of the triboelectric nanogenerator and improve adhesion when applying the composite layer, the aluminum plate is microstructured by etching.

The upper composite layer based on $\text{Sn}_2\text{P}_2\text{S}_6$ microcrystals provides the transformation of deformation/compression (due to the piezoelectric effect), lighting (due to the photovoltaic effect) and temperature change (due to the pyroelectric effect) to electricity. This ferroelectric semiconductor has a number of unique characteristics. As shown earlier, in order to increase the operating temperature range $\text{Sn}_2\text{P}_2\text{S}_6$ single crystals must be doped with germanium which increases the phase transition temperature by 20 degrees without affecting its electrophysical parameters.

[1] O. Molnar, V. Gerasimov, I.P. Kurytnik, Triboelectricity and construction of power generators based on it, *Przegląd Elektrotechniczny*, No. 1, pp. 167-171, 2018.

Electrochemical CO₂ conversion: a method of electrode formation and its composition impact on products

P.Lesnicenoks^{1,2}, **A.Knoks**¹, **I.Lukosevics**¹, **R.Olins**^{1,2}, **K.E. Krikis**², **A. Berzina**², **L.Grinberga**¹, **J.Kleperis**¹

1- Institute of Solid State Physics, University of Latvia

2- Faculty of Materials Science and Applied chemistry, Riga technical University

Main author email address: peteris.lesnicenoks@cfi.lu.lv

Electrochemical deposition is used to fabricate electro-catalytic coatings for CO₂ conversion - Cu-GSS (Cu coated graphene sheet stack material) and Cu/Cu₂O nanostructures [1]. Their structural characterisation by XRD, Raman, SEM methods has been realised. Data from gas product analysis using quadrupole MS (RGA100) and liquid products in used electrolyte are discussed here. The CO₂ electrochemical reduction takes place in well

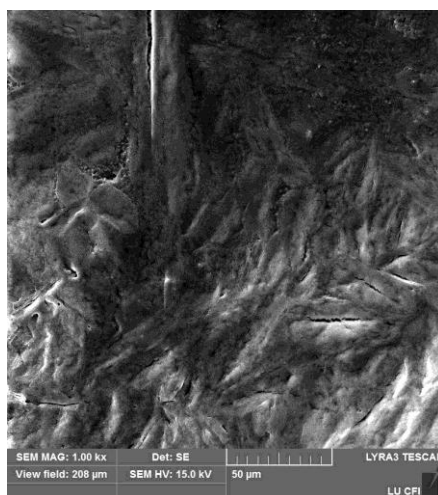


Figure 1 SEM image of GSS coated electrode.

carbonated electrolyte to ensure the presence of OH and CO groups and good contact between them and the catalyst. The gas flow was normalised to fit the samples and faradaic efficiency (FE) of required product. The presence of Cu₂O content on electrode surface and relationship towards H₂ production was observed. Samples with high Cu₂O content is present in electrochemically produced electrodes, develops larger amount of hydrocarbons molecules and up to 3% of ethyl based compounds can be detected in gas phase. During electrocatalysis the electrolyte exhibits fast pH change in both anolyte and catholyte compartments, but can sustain continuous 150mA current flow through SPEEK membrane for at least 1 hour. The Autolab PGSTAT302N Potentiostat is used to perform electrolysis and information about charge used, current and voltage are collected in 2 electrode setup.

- [1] Qiao J, Jiang P, Liu J, Zhang J. Formation of Cu nanostructured electrode surfaces by an annealing-electroreduction procedure to achieve high-efficiency CO₂ electroreduction. *Electrochem Commun* 2014;38:8–11. doi:10.1016/j.elecom.2013.10.023.

Acknowledgement: Funding from European Union's Horizon 2020 Research and Innovation Program project under grant agreement No 768789 is greatly acknowledged.

Preparation of Titanium Nickelide Coatings by Hypersonic Metallization

V. Rubanik¹, M. Belotserkovskiy², V. Rubanik jr¹, A. Shilin¹, M. Lomach¹

¹The Institute of Technical Acoustics of the NAS of Belarus, 210009, Ave. Generala Lyudnikova, 13, Vitebsk, Belarus

²The Joint Institute of Mechanical Engineering of the NAS of Belarus, 220072, Akademicheskaya str.12, Minsk, Belarus

ita@vitebsk.by

Currently, several methods have been developed for applying protective coatings to steel products and structures. All these methods differ in the coating technology and are united by the goal of creating a protective layer that is well connected to the base and is continuous, non-porous, and stable in this environment. The highest properties are provided by the method of hypersonic metallization (GM) [1]. One of the promising areas of application of this method is the production of corrosion-resistant coatings with adaptive properties to the environment. These include coatings based on the TiNi alloy, which has a shape memory [2]. The thickness of the resulting coating is 500 to 900 μm (Figure 1). The particle size of the spray coating, in the case of TiNi, is from 5 to 25 microns. The coating was formed by spraying the material melted in the electric arc of the wires, the formation of particles under conditions of their intense interaction with the spray torch, as well as the subsequent laying of the molten droplets in a layer. Since processes of rapid crystallization, deformation, and tempering occur in the layer, the structural state and properties of the coating depend on a combination of the parameters of the GM process.

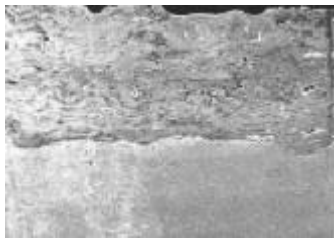


Figure 1 – Microstructure of $\text{Ti}_{49.6}\text{Ni}_{50.4}$ Alloy Coating

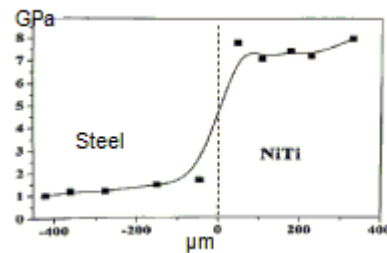


Figure 2 – Microhardness near the base/coating interface after annealing 500 °C for two hours

The microhardness measurements of coatings showed that the microhardness of the substrate increases near the interface from 0.50 to 2.5 GPa in comparison with the base. The microhardness of the coatings increases with distance from the interface from 4.5 to 6.0 GPa. This is due to the fact that the spraying process involved three stages. At the first stage, the coating temperature was 150 °C, which led to the release of the first layer of material. The hardness of the sprayed layer after annealing at 500 °C is 7.0-8.0 GPa (Figure 2) [3].

It was experimentally established that coatings with a thickness of the order of 500 μm formed by the GM method from a $\text{Ti}_{49.6}\text{Ni}_{50.4}$ alloy wire have a predominantly B19 structure that is characteristic of the martensitic state of titanium nickelide. It was found that heat treatment at 500 °C for two hours changes the phase composition of the coatings and provides an increase in their hardness to 8 GPa. High microhardness values obtained from $\text{Ti}_{49.6}\text{Ni}_{50.4}$ wire coatings make it possible to use them not only as bio- and corrosion-resistant, but also hardening [4].

[1] M. Belotserkovsky, Technological features and areas of use of hypersonic metallization, Engineering Innovation, P.479-484, (2018).

[2] J.M. Guilemany, Corrosion behavior of thermal sprayed nitinol coatings, Corrosion Science, P.171-180, 2009).

[3] V.V. Rubanik, M.A. Belotserkovsky, V.V. Rubanik Jr, Microstructure and microhardness of wire flame spraying nitinol coating, Shape memory and superelastic technologies, P.364-365, (2013).

[4] V.V. Rubanik, Theoretical and technological foundations of high-energy processing of materials with shape memory, P.420, (2017).

Na₂FeP₂O₇/C cathode for sodium-ion batteries: preparation and electrochemical properties

G. Kucinskis, I. Nesterova, G. Bajars

Institute of Solid State Physics, University of Latvia, Kengaraga Street 8, Riga, LV-1063, Latvia

gints.kucinskis@cfi.lu.lv

As growing price and demand for lithium motivates a search for alternatives to lithium-ion batteries, sodium-ion batteries emerge as a good candidate for stationary energy storage [1]. Although many of the materials used in Na-ion batteries are analogous to materials used in lithium-ion batteries, because of higher Na ion size and different chemical properties, further materials' optimization is needed.

During the work, we synthesized Na₂FeP₂O₇ and characterized its electrochemical properties as a function of synthesis route and carbon content. We added different carbon sources to the synthesis: citric acid, glucose and graphene, the mass content of carbon was up to 10 wt.%, as it has been shown previously that carbon additives can increase both capacity and rate capability of battery electrodes [2].

By analyzing the phase purity and electrochemical properties of Na₂FeP₂O₇, we find that the two-step solid-phase synthesis yields the most promising results. After adding carbon, charge capacity and purity of end-product is significantly improved. We obtained charge capacity of up to 80 mAh/g (82% of theoretical charge capacity 97 mAh/g) for carbon-containing Na₂FeP₂O₇, see figure 1 for details on electrochemical properties. The sample not containing carbon displayed significantly smaller capacity of 49 mAh/g. We suggest the improvement is due to improved electron conduction as a consequence of carbon additive. Additionally, carbon might play a significant role during synthesis by reacting and therefore eliminating residual oxygen and limiting grain growth.

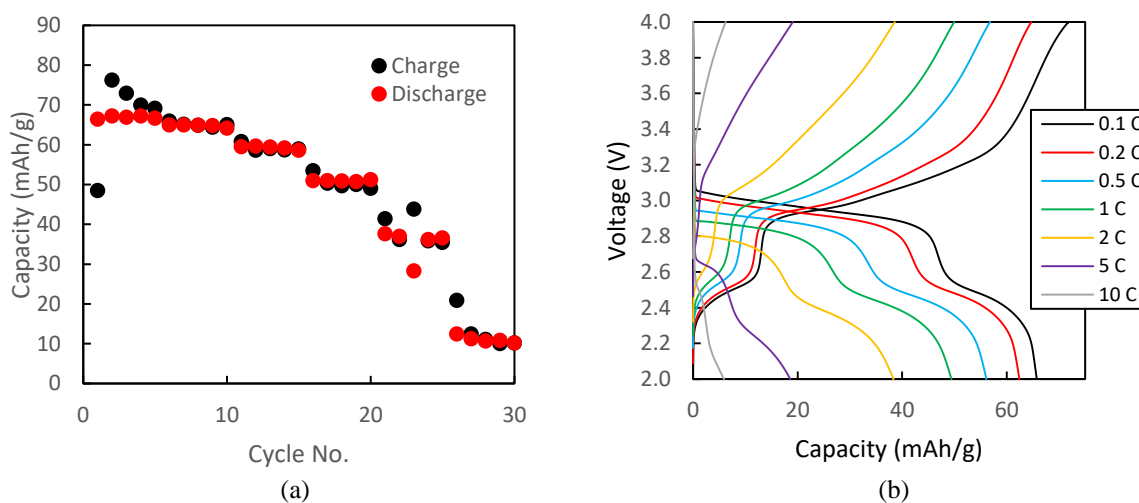


Figure 1. (a) Charge capacities and (b) charge-discharge curves of Na₂FeP₂O₇/C composite cathode

Authors acknowledge project Advanced Materials for Sodium Ion Batteries, project No. 1.1.1.2/VIAA/1/16/166.

- [1] A. Ponrouch, M.R. Palacín, Post-Li batteries: promises and challenges, *Philos. Trans. R. Soc. A Math. Phys. Eng. Sci.* 377 (2019) 20180297. <https://doi.org/10.1098/rsta.2018.0297>.
- [2] M. Park, X. Zhang, M. Chung, G.B. Less, A.M. Sastry, A review of conduction phenomena in Li-ion batteries, *J. Power Sources.* 195 (2010) 7904–7929. <https://doi.org/10.1016/j.jpowsour.2010.06.060>.

Prediction of triboelectric series based on polymer physico-chemical properties

L. Gērmans¹, L. Lapčinskis¹, M. Knite¹, A. Šutka²

1- Institute of Technical Physics, Faculty of Materials Science and Applied Chemistry, Riga Technical University, Paula Valdena 3/7, Riga LV1048, Latvia

2- Research Laboratory of Functional Materials Technology, Faculty of Materials Science and Applied Chemistry, Riga Technical University, Paula Valdena 3/7, Riga LV1048, Latvia

Andris.Sutka@rtu.lv

As mankind faces the depletion of fossil energy, it is vital to explore all aspects of green energy. Contact electrification, also known as triboelectrification, is a natural phenomenon when static charge is created on the surface by contacting and separating two materials. Although this effect has been known for a long time, the mechanism is still under discussion. Three various mechanisms were previously proposed for contact electrification of polymers: electron transfer, ion transfer, and heterolytic covalent bond scission mechanism [1]. As mechanisms of contact electrification were made clearer, devices for generating electricity based on this phenomenon were also developed [2]. Triboelectric nanogenerators (TENGs) are devices in which the contact electrification effect is combined with electrostatic induction to generate electrical power (schematically shown in Figure 1 a).

Traditionally, empirically compiled triboelectric series are used to determine suitable materials for TENG construction. It is a sequence in which materials are arranged according to tendency charge positively or negatively. However, occasionally series differ among the authors and can be seen only as vague guides. Recent papers show that charge formed in triboelectrification strongly correlates with physico-chemical properties and morphology of polymer used as foreseen by covalent bond scission mechanism [3-5].

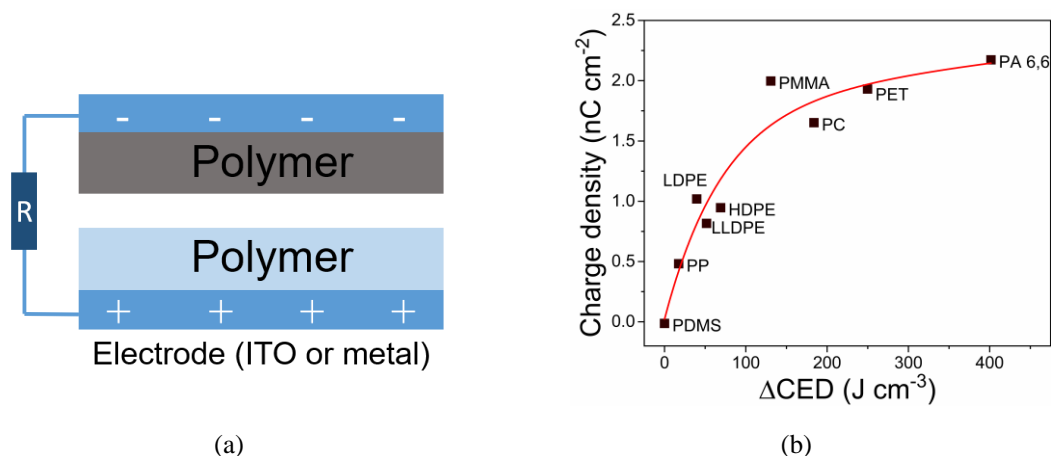


Figure 1 (a) Schematic showing triboelectric nanogenerator comprised of conductive electrodes covered by polymer layers. (b) Charge density in contact electrification as a function of CED discrepancy between PDMS and the opposite polymer.

This work shows that knowledge of polymer's properties allows to predict charge formed when various polymers are contact-separated in triboelectric measurements. It is achieved by establishing a correlation between charge density and difference of cohesive energy densities (CED) of both involved polymers (Figure 1 b for PDMS tested against other polymers). One of the polymer samples was connected in Faraday cup mode and current was measured (Keithley 6514 electrometer connected to a Picoscope 5444B PC oscilloscope) while it was contact-separated against the opposite sample using INSTRON E1000 All-Electric Dynamic Test Instrument. Charge was calculated as integral of current peak.

- [1] D. J. Lacks, T. Shinbrot, Long-standing and unresolved issues in triboelectric charging, *Nat. Rev. Chem.*, 3, pp. 465 – 476, (2019).
- [2] G. Zhu, B. Peng, J. Chen, Q. Jing, Z.L. Wang, Triboelectric nanogenerators as a new energy technology: from fundamentals, devices, to applications, *Nano Energy*, 14., pp. 126 – 138, (2015).
- [3] L. Lapčinskis, K. Mālnieks, J. Blūms, M. Knite, S. Oras, T. Käämbre, S. Vlassov, M. Antsov, M. Timusk, A. Šutka, The adhesion-enhanced contact electrification and efficiency of triboelectric nanogenerators, *Macromol. Mater. Eng.*, 305, 1900638, (2019).
- [4] A. Šutka, K. Mālnieks, L. Lapčinskis, P. Kaufelde, A. Linarts, A. Bērziņa, R. Zābels, V. Jurkāns, I. Gorņevs, J. Blūms, M. Knite, The role of intermolecular forces in contact electrification on polymer surfaces and triboelectric nanogenerators, *Energy Environ. Sci.* 12, pp. 2417 – 2421, (2019).
- [5] A. Šutka, A. Linarts, K. Mālnieks, K. Stiprais, L. Lapčinskis, Dramatic increase in polymer triboelectrification by transition from a glassy to rubbery state, *Mater. Horiz.*, 7, pp. 520 – 523, (2020).

Microstructure properties of formed doped barium cerate thin film formed on different alloy substrates.

Monica Susana Campos Covarrubias¹, Mantas Sriubas¹, Kristina Bockute¹, Piotr Winiarz², Maria Gazda², Giedrius Laukaitis¹

(1) Kaunas University of Technology, Physics Department, Studentu str. 50, LT-51368, Kaunas, Lithuania

(2) Gdansk University of Technology, Faculty of Applied Physics and Mathematics, Narutowicza 11/12, 80-233 Gdansk, Poland

e-mail: monica.campos@ktu.lt

Proton conductive ceramics are highly studied due to their main applications to electrochemical devices as fuel cells, sensors, batteries, hydrogen separators[1–6], hydrogenation/dehydrogenation reactions as ammonia formation[7], and ethylene production[8]. BaCeO₃ is a perovskite oxide ABO₃. The B side can be doped with lower oxidation state metals (e.g. Y⁺³, Yb⁺³, Gd⁺³, Sm⁺³, Nd⁺³ and La⁺³)[9] to create oxygen vacancies to promote proton conduction. BaCeO₃ doped materials are stable at intermediate temperatures above 600°C¹⁰ and present high proton conductivity in comparison to oxide ion conductors (metal oxides[11]). However, their sintering requires high temperatures to achieve high density to reach higher proton conductivities[12]. Then, it is a problem to obtain high-density materials at a reasonable temperature[13]. E-beam vapor deposition allows the evaporation of high melting point materials due high beam power to improve the density of the films at low substrate temperatures[14].

Barium cerates formed films were obtained by e-beam vapor deposition at substrate temperatures between 150 °C to 560°C and deposition rates 2-12Å/s. This works shows the effect in morphology, crystallinity and orientation in barium cerate films formed on different alloy substrates composition (Invar, Stainless steel, Glass sealing alloy and Inconel 600) . The films were characterized by X-ray diffraction (XRD) and Scanning electron microscopy (SEM).

The research was financially supported by project no. 2017/27/L/ST5/03185 founded by the National Science Centre, Poland, and Research Council of Lithuania (LMTLT), agreement No S-LL-18-3.

- [1]. Mazzei, L. *et al.* Local structure and vibrational dynamics in indium-doped barium zirconate. *J. Mater. Chem. A* (2018) doi:10.1039/C8TA06202A.
- [2]. Sažinas, R. *et al.* Surface reactivity and cation non-stoichiometry in BaZr_{1-x}Y_xO_{3-δ} (x = 0–0.2) exposed to CO₂ at elevated temperature. *J. Mater. Chem. A* (2019) doi:10.1039/C8TA11021B.
- [3]. Morejudo, S. H. *et al.* Direct conversion of methane to aromatics in a catalytic co-ionic membrane reactor. *Science* **353**, 563–566 (2016).
- [4]. Duan, C. *et al.* Readily processed protonic ceramic fuel cells with high performance at low temperatures. *Science* **349**, 1321–1326 (2015).
- [5]. Kilner, J. A. & Burriel, M. Materials for Intermediate-Temperature Solid-Oxide Fuel Cells. *Annual Review of Materials Research* **44**, 365–393 (2014).
- [6]. Malavasi, L., Fisher, C. A. J. & Islam, M. S. Oxide-ion and proton conducting electrolyte materials for clean energy applications: structural and mechanistic features. *Chem. Soc. Rev.* **39**, 4370–4387 (2010).
- [7]. Kim, J. *et al.* Proton conducting oxides: A review of materials and applications for renewable energy conversion and storage. *Renewable and Sustainable Energy Reviews* **109**, 606–618 (2019).
- [8]. Wang, S., Luo, J.-L., Sanger, A. R. & Chuang, K. T. Performance of Ethane/Oxygen Fuel Cells Using Yttrium-Doped Barium Cerate as Electrolyte at Intermediate Temperatures. *J. Phys. Chem. C* **111**, 5069–5074 (2007).
- [9]. Fu, Y.-P. & Weng, C.-S. Effect of rare-earth ions doped in BaCeO₃ on chemical stability, mechanical properties, and conductivity properties. *Ceramics International* **40**, 10793–10802 (2014).
- [10]. Bae, K. *et al.* Micro ceramic fuel cells with multilayered yttrium-doped barium cerate and zirconate thin film electrolytes. *Journal of Power Sources* **248**, 1163–1169 (2014).
- [11]. Bae, J., Samek, I. A., Stair, P. C. & Snurr, R. Q. Investigation of the Hydrophobic Nature of Metal Oxide Surfaces Created by Atomic Layer Deposition. *Langmuir* **35**, 5762–5769 (2019).
- [12]. Lacz, A. Effect of microstructure on chemical stability and electrical properties of BaCe_{0.9}Y_{0.1}O_{3-δ}. *Ionics* **22**, 1405–1414 (2016).
- [13]. Muccillo, R., Muccillo, E. N. S. & Kleitz, M. Densification and enhancement of the grain boundary conductivity of gadolinium-doped barium cerate by ultra fast flash grain welding. *Journal of the European Ceramic Society* **32**, 2311–2316 (2012).
- [14]. Laukaitis, G., Dudonis, J. & Milcius, D. YSZ thin films deposited by e-beam technique. *Thin Solid Films* **515**, 678–682 (2006).

1,8-Naphthalimide-based derivatives for potential optoelectronic devices

D. Gudeika^{1,2}, D. Volyniuk², J. V. Grazulevicius²

1- Institute of Solid State Physics, University of Latvia, 8 Kengaraga St., Riga LV-1063, Latvia.

2- Department of Polymer Chemistry and Technology, Kaunas University of Technology, Radvilėnų pl. 19, LT-50254 Kaunas, Lithuania.

gudeika.dalius@gmail.com

Organic materials possessing extended π -conjugation have received immense attention in recent years owing to their unique photophysical and charge transport properties, which make them potential materials for application in electronic devices such as organic light-emitting diodes [1], organic photovoltaics [2], organic thin film transistors [3] and *etc.*

In this study, we reported on new solution-processable donor-acceptor organic molecules with triphenylamino moiety as a donor and 1,8-naphthalimide fragment as an electron acceptor which were synthesized by palladium-catalyzed Sonogashira, reactions. The optical, thermal, and photoelectrical properties of the synthesized compounds have been investigated. The optical properties of the materials are highly dependent on the number of acceptor substituents present on the triphenylamino core. The synthesized molecules exhibit high thermal stability with the thermal degradation onset temperatures ranging from 451 to 452 °C. The compounds form glasses with glass-transition temperatures of 76-93 °C. The solid state ionization potential values range from 6.07 to 6.24 eV.

Acknowledgements

DG acknowledges to the ERDF PostDoc project No. 1.1.1.2/VIAA/1/16/177.

[1] S. Tao, Y. Zhou, C. S. Lee, X. Zhang and S. T. Lee, High-efficiency nondoped deep-blue-emitting organic electroluminescent device, *Chem. Mat.*, 22, 2138-2141 (2010).

[2] J. N. Clifford, E. Martínez-Ferrero, A. Viterisia and E. Palomares, Sensitizer molecular structure-device efficiency relationship in dye sensitized solar cells, *Chem. Soc. Rev.*, 40, 1635-1646 (2011).

[3] S. Paek, N. Cho, S. Cho, J. K. Lee and J. Ko, Planar star-shaped organic semiconductor with fused triphenylamine core for solution-processed small-molecule organic solar cells and field-effect transistors, *Org. Lett.*, 14, 6326-6329 (2012).

Magnetolectric effect in a planar composite ferromagnet-piezoelectric-meander structure

L. Fetisov, D. Saveliev, D. Chashin, Y. Fetisov

MIREA –Russian Technological University, Pr. Vernadskogo, 78, 119454 Moscow, Russia

E-mail: fetisovl@yandex.ru

The magnetolectric (ME) effect in composite ferromagnet-piezoelectric (FM-PE) structures occurs due to combination of magnetostriction of the FM layer and piezoelectric effect in the PE layer because of mechanical coupling between the layers. The effect manifests itself in the generation of an alternating voltage between electrodes of the PE layer when a structure is undergoing an excitation alternating magnetic field h and a constant magnetic field H [1]. An excitation field $h(f)$ with a frequency of $f = 1\text{-}10^6$ Hz is usually generated using an electromagnetic coil with a current enclosing the structure. However, this design is not technological, takes up a large volume and consumes a lot of energy. In [2], the excitation of the ME effect in the FM-PE structure was demonstrated by a single strip with a current located near the surface of the FM layer. In this work, for the first time, the excitation of the ME effect in a planar FM-PE structure using a planar meander line with an alternating current is studied.

The structure is shown schematically in Fig. 1. It contains a layer of piezoelectric lead zirconate titanate (PZT) with electrodes of dimensions $20\text{ mm} \times 10\text{ mm}$ and a thickness $a_p = 200\text{ }\mu\text{m}$ and a layer of amorphous ferromagnet FeBSiC (Metglas) of dimensions of $9\text{ mm} \times 20\text{ mm}$ and a thickness of $a_m = 20\text{ }\mu\text{m}$, connected with epoxy glue. The PZT piezomodule was $d_{31} \approx 175\text{ pC/N}$, and the saturation magnetostriction of Metglas was $\lambda_s \approx 25 \cdot 10^{-6}$. A magnetic field H was applied in a plane along the long axis of the structure. The structure was placed on the Cu-meander-line, $20\text{ mm} \times 10\text{ mm}$ in dimensions, with a strip width $w = 50\text{ }\mu\text{m}$ and a period of $70\text{ }\mu\text{m}$, fabricated on a dielectric substrate. An alternating current with an amplitude $I = 0\text{-}500\text{ mA}$ and a frequency $f = 0\text{-}300\text{ kHz}$ was passed through the meander. The current created an alternating field $h(f)$ directed parallel to H , causing local deformation of the sections of the FM layer. Alternating fields near adjacent meander stripes were directed in opposite directions. The deformation of the sections of the FM layer was transferred to the PE layer and it generates an alternating voltage $u(f)$ due to ME effect.

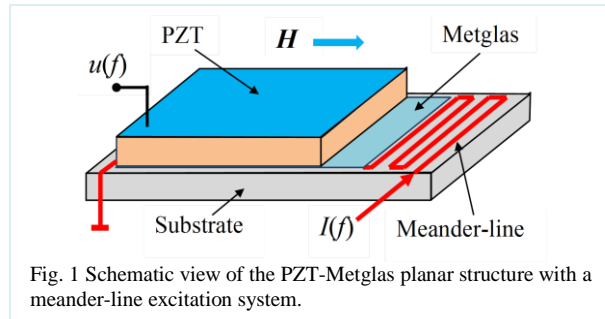


Fig. 1 Schematic view of the PZT-Metglas planar structure with a meander-line excitation system.

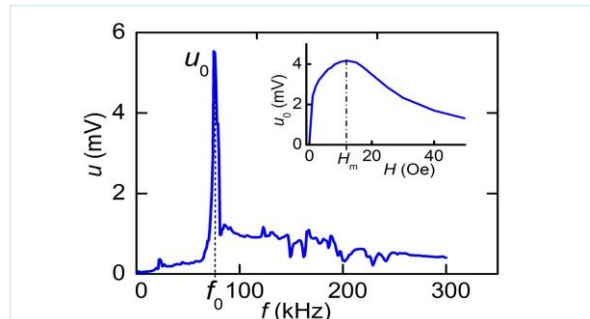


Fig. 2 Dependence of the ME voltage u on the excitation current frequency f . The inset shows the dependence of u_0 on the bias permanent magnetic field H .

Figure 2 shows the dependence of the ME voltage u on the current frequency f , measured for the current amplitude $I = 0.25\text{ A}$ and the field $H = 12\text{ Oe}$. The pick near the frequency $f_0 \approx 74.5\text{ kHz}$ with amplitude $u_0 \approx 5.5\text{ mV}$ and quality factor $Q \approx 28$ corresponds to the resonance of planar acoustic vibrations in the structure. The inset shows the dependence of the resonant voltage u_0 on the permanent field H for $I = 0.25\text{ A}$. The maximum of the voltage at the field $H_m \approx 12\text{ Oe}$ corresponds to the maximum of the piezomagnetic coefficient of the FM layer, $\lambda^{(1)} = \partial\lambda / \partial H$, where $\lambda(H)$ is the magnetostriction of the FM layer. The amplitude of the excitation field created by a single strip of the meander near its surface is $h \approx I / (2w) \approx 3\text{ Oe}$. Then, one can estimate the ME coefficient of the structure at a resonance frequency as $\alpha_E = u / (a_p h) \approx 90\text{ mV} / (\text{Oe} \cdot \text{cm})$. It is shown, that amplitude of the ME voltage u_0 grows linearly with an increase in the excitation current up to 500 mA . With increasing current, a nonlinear ME effect, the generation of a voltage with a doubled frequency, was also observed. A theory is constructed that describes characteristics of the ME effect in planar FM-PE structures upon excitation using a meander-line with alternating current. The research was supported by the Russian Science Foundation, project No 19-79-10128.

- [1] J.-M. Hu and C.-W. Nan, Opportunities and challenges for magnetolectric devices, APL Advances, vol. 7, p. 080905 (2019).
 [2] D.V. Chashin, L.Y. Fetisov, D.V. Saveliev, and Y.K. Fetisov, Magnetolectric monolithic resonator based on the ferromagnetic-piezoelectric structure excited with a linear current, Sensors Letters, vol. 3, p. 2500804 (2019).

Novel Hydrophobic Deep Eutectic Solvents Based on Fluorinated Hydrogen Bond Donors

V. Kavaliauskas, V. Olšauskaitė, A. Padarauskas

Faculty of Chemistry and Geosciences, Vilnius University, Naugarduko 24, 03225 Vilnius, Lithuania

e-mail: vytautas.kavaliauskas@chf.vu.lt

Deep eutectic solvents (DESs) are a new class of ionic liquid-like solvents formed by combining hydrogen-bond acceptor (HBA) with hydrogen-bond donor (HBD) which result in the depression of the melting point of the solvent [1]. One of the major advantages of DESs lies in simplicity of their preparation, requiring only mixing components and heating for a short time. Despite the numerous publications about DESs since their first introduction in 2001 [2], most of the research work has concentrated mainly on hydrophilic DESs. However, the hydrophilicity of DESs limits their practical application to only polar compounds, which is a major drawback of the solvent. The first hydrophobic DESs (HDESs) were introduced by van Osch and co-workers [3] in 2015 when they combined diverse quaternary ammonium salts with decanoic acid. HDESs are generally immiscible with water and have high extraction efficiency for nonpolar compounds. Thus, they have been suggested as potential extraction media to replace toxic organic solvents or expensive hydrophobic ionic liquids.

In this study, six hydrophobic deep eutectic solvents were synthesized using menthol, tetrabutylammonium and tetrahexylammonium chlorides as hydrogen-bond acceptors and trifluoroacetic acid and hexafluoro-2-propanol as hydrogen-bond donors (Table 1). All six tested compositions formed homogeneous colorless liquids at room temperature. Initial experiments suggested that five of them are hydrophobic, forming two stable phases when mixed with water. TBACl:TFA solvent precipitated after mixing with water.

Table 1. Composition and abbreviations of the HDESs studied

HBA	HBD	Abbreviation	Molar ratio (HBA:HBD)
Tetrabutylammonium chloride	Hexafluoroisopropanol	TBACl:HFIP	1:2
Tetrahexylammonium chloride	Hexafluoroisopropanol	THACl:HFIP	1:2
Menthol	Hexafluoroisopropanol	Men:HFIP	1:2
Tetrabutylammonium chloride	Trifluoroacetic acid	TBACl:TFA	1:2
Tetrahexylammonium chloride	Trifluoroacetic acid	THACl:TFA	1:2
Menthol	Trifluoroacetic acid	Men:TFA	1:2

The densities measured at 25 °C are within range of 1.061 to 1.255 g/mL, which is considerably higher than found for most HDESs and water. Densities higher than water are preferred for microextraction techniques. The high densities of the solvents can be explained by the high densities of both fluorinated hydrogen-bond donors used to prepare the HDESs. As expected, density is correlated with the density of hydrogen-bond donor: higher density values were observed for HDESs contained heavier HFIP. Moreover, both TBACl-based liquids have higher densities than corresponding those containing THACl.

Viscosity is another important parameter that strongly affects extraction performance. Low viscosity liquids are generally preferred for the higher mass transfer rate resulting in improved extraction efficiency. Developed HDESs exhibit relatively high viscosities (>100 mPa·s) at room temperature as a result of the extended hydrogen-bonding network. In contrast to the density, higher viscosities are obtained for liquids containing quaternary ammonium salt with longer alkyl chain. The viscosities of both menthol-based liquids are considerably lower than those containing quaternary ammonium salts.

Finally, the extraction properties of the solvents and their compatibility with high performance liquid chromatography (HPLC) were evaluated employing phthalates, parabens and natural dyes as model analytes. In general, all five developed HDESs showed good extractability of the analytes. However, the solvents based on HFIP caused significant peak broadening or even peak distortion for some compounds. Thus, these HDESs are not compatible with HPLC. In contrast, the TFA-based HDESs exhibited good performance for microextraction of hydrophobic compounds and excellent compatibility with HPLC analysis.

[1] E.L. Smith, A.P. Abbott, K.S. Ryder, Deep eutectic solvents (DESs) and their applications, *Chemical Reviews*, vol. 114, pp. 11060-11082, (2014).

[2] A.P. Abbott, G. Capper, D.L. Davies, H.L. Munro, R.K. Rasheed, V. Tambyrajah, Preparation of novel, moisture-stable, Lewis-acidic ionic liquids containing quaternary ammonium salts with functional side chains, *Chemical Communications*, vol. 19, pp. 2010-2011, (2001).

[3] D.J.G.P. van Osch, L.Z. Zubeir, A. van den Bruinhorst, M.A.A. Rocha, M.C. Kroon, Hydrophobic deep eutectic solvents as water-immiscible extractants, *Green Chemistry*, vol. 17, pp. 4518-4521, (2015).

One-Step Phosphor in Glass Synthesis and Characterization

M. Norkus¹, G. Niaura^{2,3}, R. Skaudžius¹

1- Faculty of Chemistry and Geosciences Institute of Chemistry, Naugarduko st. 24, LT-03225 Vilnius, Lithuania
2- Department of Organic Chemistry, Center for Physical Sciences and Technology (FTMC), Saulėtekio Ave. 3, LT-10257, Vilnius, Lithuania
3- Institute of Chemical Physics, Faculty of Physics, Vilnius University, Saulėtekio Ave. 3, LT-10257, Vilnius, Lithuania

mantas.norkus@chgf.vu.lt

As a solid-state lighting source, LEDs have been phasing-out incandescent and fluorescent lamps since the improvement of blue LEDs and white LED commercialization in 1996 [1]. Currently to produce white light, blue LEDs are combined with a yellow YAG:Ce³⁺ phosphor which is dispersed in silicone or other organic resin. However, to use them in high brightness applications, high current densities are needed to generate high intensity emission in LEDs. Past a certain point, the amount of generated light drops due to so called efficiency droop phenomena [2]. To circumvent the need for increased current densities, a larger number of LEDs are used instead. As the junction temperature increases, currently used silicone suffers from color shifting, and luminous efficiency degradation with prolonged use [3]. One of the means to improve thermal conductivity of phosphor plates, allowing higher LED operating temperature range, is to disperse phosphors in glass, ceramic or glass-ceramic matrices [4].

In this work phosphate glasses with different compositions were synthesized. The glass precursors and luminescent materials were ground and mixed together, melted in muffle furnace: molten liquid was poured into premade molds and heated again at lower temperatures to relieve internal stress. As obtained samples were polished and characterized by x-ray diffractometry, scanning electron microscopy, Raman spectroscopy, photoluminescence measurements and inductively coupled plasma optical emission spectrometry.

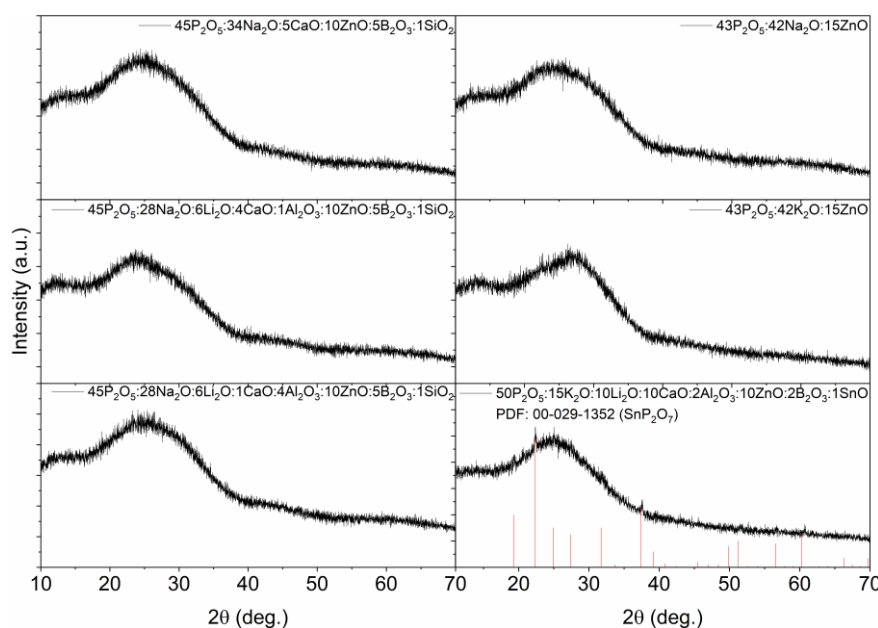


Figure 1 XRD patterns representing samples with different glass compositions

- [1] S. Nakamura, M. Senoh, S.I. Nagahama, N. Iwasa, T. Yamada, T. Matsushita, H. Kiyoku, Y. Sugimoto, InGaN-Based Multi-Quantum-Well-Structure Laser Diodes, Japanese Journal of Applied Physics, 35, L74-L76, (1996).
- [2] J. J. Wierer, J. Y. Tsao, D. S. Sizov, Comparison between blue lasers and light-emitting diodes for future solid-state lighting, Laser & Photonics Reviews, 7, 963-993, (2013).
- [3] M.H. Chang, D. Das, P. V. Varde, M. Pecht, Light emitting diodes reliability review, Microelectronics Reliability, 52, 762-782, (2012).
- [4] H. Lin, T. Hu, Y. Cheng, M. Chen, Y. Wang, Glass Ceramic Phosphors: Towards Long-Lifetime High-Power White Light-Emitting-Diode Applications–A Review, Laser & Photonics Reviews, 12, 1700344 (2018).

Low temperature sol-gel synthesis of transparent nanoporous silicon dioxide glass

M. Leimane¹, I. Bite¹, L. Skuja¹

1- Institute of Solid State Physics, University of Latvia, Latvia

madaral@cfi.lu.lv

High purity synthetic SiO₂ glass is widely used in deep ultraviolet, radiation-resistant optics, high-power lasers, and optical fibres due to its excellent transparency, radiation toughness, and large bandgap [1]. While gas-phase synthesis by oxidation of SiCl₄ or Si-organic compounds (T≈2000 °C) dominates the industrial production, the wet-chemistry (sol-gel) synthesis route is interesting by requiring lower temperatures (T≈600 °C), offering versatile ways of introducing dopants, and modifying the stoichiometry and morphology of the glass. Naturally, using relatively low-temperature processes is advantageous for preventing devitrification during the glass formation and obtaining high purity homogeneous samples. Sol-gel synthesized pure SiO₂ glasses and the evolution of their properties in the synthesis process have been addressed in a number of papers (e.g. [2-7]). In the sol-gel formation of SiO₂ glass, its structure, morphology, and other properties are influenced by multiple parameters. Here, the major problem to overcome is the cracking, which occurs during drying and sintering process. It is caused by inhomogeneous shrinkage due to the large capillary pressure in pores during the evaporation of the solvent. Using HNO₃ as a catalyst helps to obtain homogeneous crack-free glassy SiO₂ samples. To avoid cracking of gels, careful control of drying and sintering conditions must be used [3].

In this work transparent SiO₂ glasses were obtained by the sol-gel method [3]. Transparent glass or white ceramics were obtained dependent on the heating mode in the 200-1200°C region with a retention time of 2h at air atmosphere. The vibrational spectra of obtained samples were characterized by Raman spectroscopy. X-ray diffractometry and electron microscopy were used to characterize SiO₂ glass structure and morphology. Differential scanning calorimetry combined with a thermogravimetry was used to monitor the mass change during the glass formation and Archimed's method (using toluene) was used to determine the apparent density of synthesized samples.

The results show that **it is possible to obtain glassy SiO₂ samples even at a relatively low temperature of 600 °C**. Compared to standard gas-phase synthetic silica, these glasses have a significant amount of **nanopores in their structure**, as evidenced by the evolution of the sharp, surface-type vibration band at 3748 cm⁻¹ of the non-hydrogen-bonded ("free") silanol ≡Si-O-H groups in Raman spectra of samples treated between 600°C and 1000°C. The 606 cm⁻¹ vibrational mode due to planar 3-fold rings of Si-O bonds emerge in the same T range, while bands due to interstitial H₂O decrease and those due to C-H vibrations disappear. In addition, synthesized glass samples have a lower density (1,6 g/cm³) as compared to conventional SiO₂ glass (2.20 g/cm³) providing further evidence of the nanoporous glass structure. Increasing the temperature to 1200 C° results in glass-ceramics with features of both cristobalite and glass present in Raman and XRD spectra.

This work was supported by project No. LZP-2018/1-0289 "Optical properties of advanced silicon dioxide-based materials for ultraviolet and high-power photonics".

- [1] S. Girard, A. Alessi, N. Richard, L. Martin-Samos, V. De Michele, L. Giacomazzi, S. Agnello, D. Di Francesca, A. Morana, B. Winkler, I. Reghioua, P. Paillet, M. Cannas, T. Robin, A. Boukenter, Y. Ouerdane, Overview of radiation induced point defects in silica-based optical fibers, *Rev. Phys.* 4 (2019) 100032. doi:10.1016/j.revip.2019.100032.
- [2] K. Kajihara, Recent advances in sol-gel synthesis of monolithic silica and silica-based glasses, *J. Asian Ceram. Soc.* (2013). doi:10.1016/j.jascer.2013.04.002.
- [3] K. Kajihara, M. Hirano, H. Hosono, Sol-gel synthesis of monolithic silica gels and glasses from phase-separating tetraethoxysilane-water binary system, *Chem. Commun.* (2009) 2580–2582. doi:10.1039/b900887j.
- [4] D.L. Wood, E.M. Rabinovich, Study of alkoxide silica gels by infrared spectroscopy, *Appl. Spectrosc.* 43 (1989) 263–267. doi:10.1366/0003702894203282.
- [5] A. Duran, C. Serna, V. Fornes, J.M. Fernandez Navarro, Structural considerations about SiO₂ glasses prepared by sol-gel, *J. Non. Cryst. Solids.* 82 (1986) 69–77. doi:10.1016/0022-3093(86)90112-2.
- [6] H. Yoshino, K. Kamiya, H. Nasu, IR study on the structural evolution of sol-gel derived SiO₂ gels in the early stage of conversion to glasses, *J. Non. Cryst. Solids.* 126 (1990) 68–78. doi:10.1016/0022-3093(90)91024-L.
- [7] A. Bertoluzza, C. Fagnano, M. Antonietta Morelli, V. Gottardi, M. Guglielmi, Raman and infrared spectra on silica gel evolving toward glass, *J. Non. Cryst. Solids.* 48 (1982) 117–128. doi:10.1016/0022-3093(82)90250-2.

Increase in Polymer Triboelectrification by Transition from a Glassy to Rubbery State

A. Linarts¹, L. Lapcinskis², K. Malnieks², A. Sutka²

1- Institute of Technical Physics, Riga Technical University, Paula Valdena 3/7, Riga, Latvia, LV-1048

2- Research Laboratory of Functional Materials Technologies, Riga Technical University, Paula Valdena 3/7, Riga, Latvia, LV-1048

artis.linarts@rtu.lv

Triboelectric nanogenerators (TENG) are intriguing energy harvesting devices that convert mechanical energy into electricity and could power small portable devices or charge batteries [1]. Here we report contact electrification of glassy polymers at different temperatures and observing a dramatic three orders of magnitude increase in surface charge when passing the transition temperature to a rubbery state. Transition is accompanied by a larger force required for separation due to material softening and increased stickiness. This enhances material transfer during contact/separation cycles and indicates covalent bond breaking as the mechanism for increased polymer triboelectrification. Undeniably, surface roughness plays a great role in contact electrification, however in our study its impact is overrated when compared to the influence of physical properties.

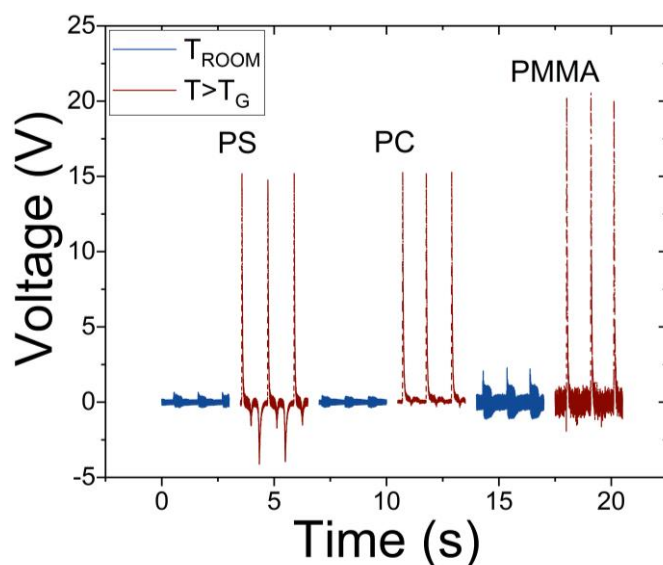


Figure 1 Open circuit voltage of Polystyrene, Polycarbonate and Poly(methy methacrylate) at room temperature and at temperature above glass transition temperature.

[1] Z.L. Wang "Triboelectric Nanogenerators as New Energy Technology for Self-Powered Systems and as Active Mechanical and Chemical Sensors", ACS Nano 7 (2013) 9533-9557

Nanocellulose filled acrylated epoxidized soybean oil inks for UV-assisted 3D printing

M. Jurinovs¹, A. Barkane¹, Z. Zelca², Y. Habbibi³, S. Gaidukovs¹

1- Institute of Polymer Materials, Faculty of Materials Science and Applied Chemistry, Riga Technical University, P. Valdena 3/7, LV-1048 Riga, Latvia

2- Institute of Design Technologies, Faculty of Materials Science and Applied Chemistry, Kipsalas street 6, LV-10-48 Riga Technical University, Latvia

3- Luxembourg Institute of Science and Technology, Department of Materials Research and Technology (MRT), Esch-sur-Alzette, Luxembourg

e-mail: anda.barkane@rtu.lv

In recent years bio-based materials from renewable sources are tending to replace the petroleum-derived plastics. Bio-materials offer easy processing and the same or even better technological, functional and mechanical properties, while ensuring recycling, lower cost and reduced environmental impact. At the same time 3D printing is an additive manufacturing technology developed as a way for efficient, affordable and low waste production method. The combination of bio-material and UV 3D printing technology can help to reduce and avoid the dependence on petroleum-derived plastics.

Wood pulp nanomaterials are new materials with many promising uses [1]. One of the following aims is to improve the mechanical properties of polymeric materials, while maintaining its bio-basic content [2]. The purpose of this work was to get such improvements in UV-assisted 3D printing of bio-based resin blended with nanofibrillated cellulose (NFC).

In this study stereolithography (SLA) 3D printing technology was used to initiate free-radical polymerization of acrylated epoxidized soybean oil (EASO) systems with addition of several reactive monomers and NFC. 4 types of such system were prepared: neat system without NFC addition and 3 systems with NFC content of 0.1, 0.5 and 1 wt.%

Viscosity measurements were performed to control the 3D printing technological properties of the prepared resin blends; while maximal viscosity value of 5 Pa/s is reported for 3D printing inks [3]. The optical properties were measured by UV-VIS transmittance spectroscopy. Tensile, bending and impact resistance tests were performed to investigate the mechanical properties of prepared resins. It is concluded that NFC loading into the AESO resin significantly enhance the elastic modulus and strength of the materials. While the elongation at the breaks also shows the drastic increasement.

Acknowledgement

This research is funded by the M-era.net 2017 project "3D Printable Innovative Biobased Materials for Wood Mimics", 3DPrintInn; Nr.1.1.1.5/ERANET/18/05

Refences

- [1] D. Trache *et al.*, "Nanocellulose: From Fundamentals to Advanced Applications," *Front Chem*, vol. 8, p. 392, 2020.
- [2] K.-Y. Lee, Y. Aitomäki, L. A. Berglund, K. Oksman, and A. Bismarck, "On the use of nanocellulose as reinforcement in polymer matrix composites," *Composites Science and Technology*, vol. 105, pp. 15-27, 2014.
- [3] G. Taormina, C. Sciancalepore, M. Messori, and F. Bondioli, "3D printing processes for photocurable polymeric materials: technologies, materials, and future trends," *J Appl Biomater Funct Mater*, vol. 16, no. 3, pp. 151-160, Jul 2018.

Biobased low density and high porosity lignocellulose composite materials from wood and hemp waste

S. Beluns¹, S. Gaidukovs¹

¹- Institute of Polymer Materials, Faculty of Materials Science and Applied Chemistry, Riga Technical University, P. Valdena 3/7, LV-1048 Riga, Latvia

e-mail:sergejs.beluns@rtu.lv

Nature is a source of inspiration for many materials scientists to design materials and composites of high performance and functionality. Lignocellulose is one of the most common and abundant materials, which attracts scientists due to its properties and availability. Lignocellulose derived materials have substantial advantages, such as renewability, biodegradability, excellent toughness, and the possibility for novel functionalities [1]. Wood-like and wood mimic material preparation based on lignocellulose attracts much interest in the scientific research field for the past decade [2]. One of possible routes is to prepare wood-like lignocellulose composite films or functional materials like aerogels. Aerogels are low density and highly porous solid-state structure, consisting of nano-dimensional materials. Highly porous and exclusive structure of aerogel has various properties such as low thermal conductivity, high sound absorption capacity, low dielectric constant, super absorption activity and, they are super lightweight. Thermal and acoustic insulators, flexible energy storage devices, drugs, and catalyst carrier as well as template for other functional materials are a few possible application areas where the unique combination of aerogel properties can come handy [3].

Current work involves cellulose film and aerogel preparation approaches and research routes. Herein, we report the manufacturing, characterization, and comparison of nanofibrillated lignocellulose composite materials obtained from different lignocellulose sources. Nanofibrils were obtained from several lignocellulose waste sources – wood flour and hemp fibers via microfluidization process. 3 weight % lignocellulose concentrations dispersions have been processed to prepare composite samples. Size of the particles was evaluated by TEM and DLS measurements. Composite films were obtained by simple casting and evaporation in petri dish; while the aerogels were prepared by freeze drying technology. The structure and properties of the received composite materials were investigated by FTIR, XRD, SEM and TGA analysis.

Received results are very promising that contributes for the simple manufacturing method of the novel composite with the controlled structure hierarchy.

- [1] Z.-L. Yu *et al.*, "Bioinspired polymeric woods," *Science Advances*, vol. 4, no. 8, 2018.
- [2] A. Zaman, F. Huang, M. Jiang, W. Wei, and Z. Zhou, "Preparation, Properties, and Applications of Natural Cellulosic Aerogels: A Review," *Energy and Built Environment*, vol. 1, no. 1, pp. 60-76, 2020.
- [3] P. Gupta, B. Singh, A. K. Agrawal, and P. K. Maji, "Low density and high strength nanofibrillated cellulose aerogel for thermal insulation application," *Materials & Design*, vol. 158, pp. 224-236, 2018.

Electromagnetic shielding material based on porous alumina membranes filled with nickel and carbon-containing needle-punched textile

H. Abdulhadi¹, E. Belousova¹, O. Boiprav¹, A. Prudnik¹, N. Mukhurov²

1- Belarusian State University of Informatics and Radioelectronics

6 P. Brouka, 220013, Minsk, Belarus

2- State Scientific and Production Association "Optics, Optoelectronics and Laser Technology"

68 Nezavisimosti avenue, 220072, Minsk, Belarus

aleksander.prudnik@bsuir.by

One of the ways to ensure the safety of information system resources and activities is to reduce the electromagnetic radiation emanating from them [1]. For these purposes, we can use shields of the electromagnetic radiation. To obtain better properties, as a rule, multilayer composite materials are used. For further increasing the value of the reflection coefficient, non-flat elements can be formed on the surface of materials to ensure the scattering of electromagnetic waves.

The proposed composite materials are flexible and consist of two layers. The outer layer (relatively to the direction of propagation of electromagnetic waves) is an anodized aluminium oxide film with thickness of 50 μm . The inner layer is a carbon-containing needle-punched textile [2].

The aluminium film was anodized in the galvanostatic mode in a solution of oxalic acid with a constant current density. The thickness of the layer of anodized alumina formed on the surface of the film was 5...25 μm . The layers of anodized alumina film completely repeat the surface of the aluminium film with protrusions from 0.5 up to 2.0 mm. The periodicity of the porous system varies from 50 up to 70 nm. Then, nickel was electrochemically deposited into pores of the alumina. The elemental analysis of the obtained structures was carried out by energy dispersive X-ray spectroscopy. The SEM image of the porous alumina (Fig. 1,a) filled with nickel and the elemental composition of the sample were used to analyze the distribution of nickel in the porous alumina.

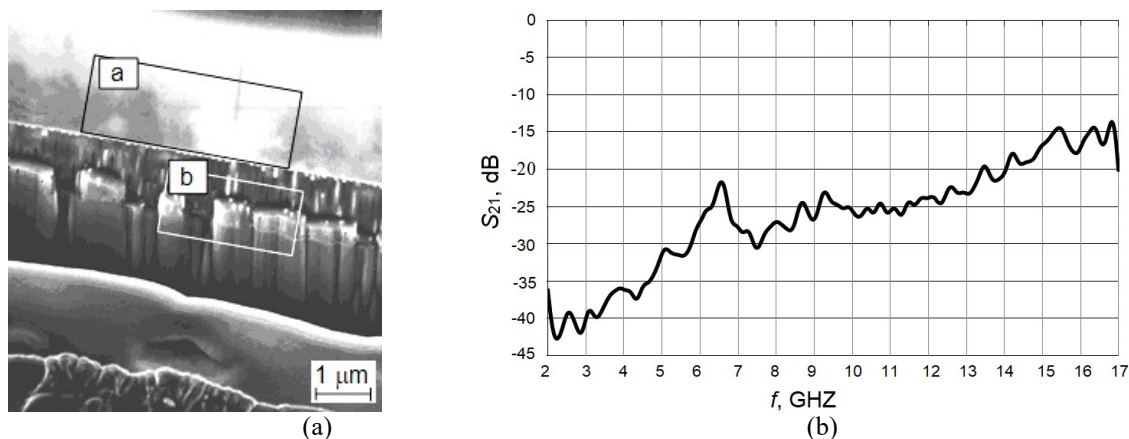


Figure 1 SEM image of the porous alumina membranes filled with nickel (a). Transmission coefficients properties of the material based on porous alumina membranes filled with nickel and carbon-containing needle-punched textile in the range 2–17 GHz (b).

The effectiveness of the electromagnetic radiation shielding by the material based on porous alumina membranes filled with nickel and carbon-containing needle-punched textile was measured by the ratio of the electric field strength at the point of space in the absence of this material to the electric field strength at the same point in the presence of the material and was characterized by the transmission and reflection coefficients. The values of the electromagnetic radiation transmission coefficient in the frequency range 2...17 GHz of the studied sample ranged from -20 up to -37 dB (Fig. 1,b).

[1] R.J. Anderson, Security Engineering: A Guide to Building Dependable Distributed Systems (Wiley), Chapter 17: Emission Security, (2010).

[2] A. Prudnik, A. Beloglazov, T. Kudryavtseva, L. Lynkou, Production technology and shielding properties of the needle-punched non-woven fabrics with carbon additives, Proc. of the 24th International conference EMD 2017. Białystok, Poland. P. 108–111.

Preparation and investigation of bulk $\text{Bi}_3\text{Fe}_5\text{O}_{12}$

A. Pakalniškis, R. Skaudžius, I. Grigoraviciute-Puroniene, A. Zarkov, A. Kareiva

Institute of Chemistry, Vilnius University, Naugarduko 24, LT-03225 Vilnius, Lithuania

andrius.pakalniskis@chgf.vu.lt

The ability to control magnetic properties of materials via electric field has attracted a lot of attention over the last few decades. Especially the usage of this phenomenon at room temperature could be exceptionally important. Very few materials, such as BaTiO_3 , BiFeO_3 , LuFe_2O_4 , have large magnetoelectric coupling at room temperature [1, 2]. While most of these materials have perovskite crystal structure, the garnets also have been reported to show magnetoelectric effect, but with a smaller magnetoelectric coefficient [3]. One such garnet could be $\text{Bi}_3\text{Fe}_5\text{O}_{12}$ (BIG), in which Fe^{3+} ions occupy tetrahedra and octahedral sites and Bi^{3+} ions occupy the dodecahedral sites. BIG could be used as a magnetoelectric material for magneto-optical devices [4]. However, the biggest problem is that the synthesis of bismuth iron garnet is very problematic. Since the bismuth ion has a large radius, its incorporation into the garnet structure leads to an expansion of the lattice, and the material also becomes thermodynamically unstable at high bismuth concentrations. It is therefore very difficult to increase the bismuth concentration in bismuth-doped iron garnets up to the maximum value of 3 bismuth atoms per chemical formula because it forms in a non-thermodynamic way. Thus only thin films of BIG on garnet substrate have been prepared [5]. However, materials that are prepared by thin film deposition are usually not ideal because their properties depend on a lot of factors such as the orientation of the film, as well as thickness and the reproducibility as rather complex. Based on this preparation of powder BIG would be beneficial. Bulk $\text{Bi}_3\text{Fe}_5\text{O}_{12}$ has not been prepared yet, only other garnets such as $\text{Y}_3\text{Fe}_5\text{O}_{12}$ doped with bismuth were obtained [6]. Preparation of single-phase bulk BIG could lead to new applications and potentially different properties than the conventional thin films.

In this work the attempts to prepare BIG samples at different temperatures using aqueous sol-gel method were made. The overall phase transitions in this system were evaluated happening from 400 to 700 °C. X-ray diffraction was used to determine the structure and purity of formed crystalline phases. The SEM analysis was also performed to determine the particle size and morphology of the samples.

Acknowledgements

This work was supported by a Research grant NEGEMAT (No. S-MIP-19-59) from the Research Council of Lithuania.

References

- [1] A. Sundararaj, G. Chandrasekaran, et al, Room temperature magnetoelectric coupling in $\text{BaTi}_{1-x}\text{Cr}_x\text{O}_3$ multiferroic thin films, *Journal of Applied Physics*, 119 024107A (2016).
- [2] Guo, Z., et al., Structural, magnetic and dielectric properties of Fe-doped BaTiO_3 solids. *Modern Physics Letters B*, 26.,1 250056 (2012)
- [3] Chen, F., et al., Ferromagnetic resonance induced large microwave magnetodielectric effect in cerium doped $\text{Y}_3\text{Fe}_5\text{O}_{12}$ ferrites. *Scientific reports*, 6, 28206-28206, (2016).
- [4] Khartsev, S. and A. Grishin, High performance $[\text{Bi}_3\text{Fe}_5\text{O}_{12}/\text{Sm}_3\text{Ga}_5\text{O}_{12}]_m$ magneto-optical photonic crystals. *Journal of Applied Physics*, 101, 053906-053906, (2007).
- [5] Heinrich, A., et al., Pulsed Laser Deposition and Growth Studies of $\text{Bi}_3\text{Fe}_5\text{O}_{12}$ on $\text{Gd}_3\text{Ga}_5\text{O}_{12}$ and SiO_2 . *Journal of the Magnetism Society of Japan*, 30, 584-587, (2006).
- [6] Matsumoto, K., et al., Preparation of bismuth-substituted yttrium iron garnet powders by the citrate gel process. *Journal of Applied Physics*, 69, 5918-5920, (1991).

Barkhausen type Pulses during Generation the High Voltage Pulse by PZT Igniters

O. Kiprijanovič, L. Ardaravičius, S. Ašmontas

Center for Physical Sciences and Technology, Vilnius, Saulėtekio al. 3, LT-10257, Lithuania

oleg.kiprijanovič@ftmc.lt

In 2019, it was celebrated the 100-th anniversary of Barkhausen paper publication, where he presented registration of noises during a magnetization reversal of ferromagnetic samples [1]. Thus, the investigations of domain structure dynamics on micro- and nanoscale level were initiated. Repolarization processes in plumbum-zirconate-titanate (PZT) ceramics are also accompanied by Barkhausen pulses because it has granular and domain structure. The modified Barkhausen method was applied for investigation of high voltage pulses produced by PZT igniters [2]. The super wideband arrangement allows registration of not only the high voltage pulses, the main part of which has duration about 10 μs , but also of the shorter and relatively high voltage spikes of 10-15 ns at the base. Simultaneously it was registered electromagnetic pulses, which were generated during the formation of the spikes. We assign the term Barkhausen type pulses to the spikes, because observation of real Barkhausen pulses and noises is hardly expected at a strong attenuation. During the investigations it was found that the aging process of the PZT ceramics imparts a new, yet potentially useful quality.

We used commercially available igniters. They have two PZT cylinders, which are 4 mm in height and 2 mm in diameter with metalized bases, connected in parallel. A hammer having weight of 0.3 g induces piezoelectric forces by shock. The igniters were loaded by a 0.5-1 M Ω resistor as an upper divider shoulder. A lower shoulder of the divider is a 50 Ω oscilloscope input and, therefore, the division coefficients are in the range of (1-2)·10⁴. The registered amplitudes of the high voltage pulses are about 12-15 kV for the “fresh” igniters and they decrease with the growth of ignitions number.

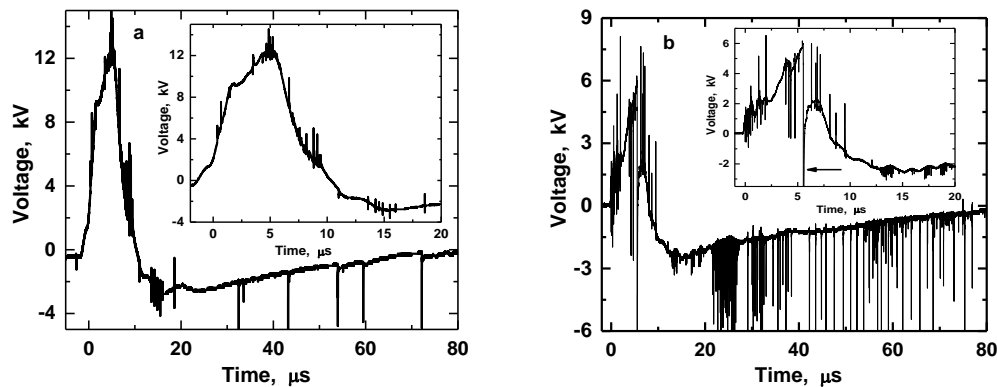


Figure 1(a,b). Complex electric signal generated by the “fresh” igniter - (a) and by the aged igniter, that had above $5 \cdot 10^3$ ignitions - (b). The inserts show the high voltage pulses without relaxation part. Arrow in insert in Fig.1 (b) indicates moment of parasitic partial discharge.

As one can see in Fig.1, increasing the number of ignitions causes decreasing of the pulse amplitude but the number of the spikes and the amplitudes are increased. Considering that the every spike radiates 3-5 ns long electromagnetic pulses (EM), we can conclude that the aged igniter effectively transforms mechanical energy of the shock into the EM one. Thus, a complex stochastic signal having large bandwidth and long duration is radiated [3]. Such igniters, still having several thousands of operations in stock, can find applications in modern facilities. Internal processes in the ceramics during repolarization at ns time scale and the high voltage generation are barely investigated. We suppose that the electron emission from the surface, which is confirmed by burnout of the metallization, and the formation of micro-cracks are responsible for the increase in the number of spikes and their amplitudes.

[1] H. Barkhausen, Zwei mit Hilfe der neuen Verstärker entdeckte Erscheinungen, Physische Zeitschrift vol. 20, pp. 401–403, (1919).

[2] L. Ardaravičius, S. Keršulis, O. Kiprijanovič, Č. Šimkevičius, S. Ašmontas, The Barkhausen Method to Investigate Powerful Processes during Action of Piezoelectric Igniters, Materials Science (Medžiagotyra), vol.26 (3), (2020), to be published.

[3] F. Anisimovas, S. Ašmontas, O. Kiprijanovič, J. Matuzas, Radiation of Large Bandwidth and Long Durations Signals by Pulsed Excitation of Monopole Antennas, Proc. 4-rd Intern. Conference “Radiation interaction with materials and its use in technologies” Kaunas, Lithuania, May 14-17, pp. 574-577, (2012).

Large barocaloric effect at ferroelectric phase transitions in ammonium hydrogen sulfate

E.A. Mikhaleva¹, I.N. Flerov^{1,2}, M.V. Gorev^{1,2}, E.V. Bogdanov^{1,3}

1- Kirensky Institute of Physics, Federal Research Center KSC SB RAS, 660036 Krasnoyarsk, Russia

2- Institute of Engineering Physics and Radioelectronics, Siberian Federal University, 660074 Krasnoyarsk, Russia

3- Institute of Engineering Systems and Energy, Krasnoyarsk State Agrarian University, 660049 Krasnoyarsk, Russia

katerina@iph.krasn.ru

For at least the last two decades, considerable attention has been paid to calorific effects (CE) in solids, particularly in ferroics. The barocaloric effect (BCE) has a significant advantage in comparison with CE of a different nature (electrocaloric - ECE, magnetocaloric - MCE), due to its universality. Indeed, both extensive, ΔS_{BCE} , and intensive, ΔT_{AD} , barocaloric parameters strongly depend on the volume thermal expansion $(\partial V/\partial T)_p$, which very often shows large change near the temperature of any phase transitions: ferroelectric, ferroelastic, ferromagnetic

$$\Delta S_{BCE} = - \int (\partial V/\partial T)_p dp; \quad \Delta T_{AD} = - (T/C_p) \Delta S_{BCE}, \quad (1)$$

where C_p is the heat capacity.

This report is devoted to the study of extensive and intensive barocaloric efficiency of NH_4HSO_4 undergoing two successive ferroelectric phase transitions: $P2_1/c$ ($T_1=271$ K) \leftrightarrow Pc ($T_2=159$ K) \leftrightarrow $P1$ and its dependence on the thermal expansion of the crystal lattice. For this aim, the dependencies of $\Delta S_{BCE}(T, p)$ and $\Delta T_{AD}(T, p)$ were determined using data on total and anomalous heat capacity, the $T - p$ phase diagram and the dependencies of entropy and thermal expansion of the phase transitions on temperature.

At the first stage, the influence of pressure on the entropy of the crystal lattice, ΔS_{LAT} , was not taken into account. The values and behavior of extensive BCE at different pressure were determined from temperature dependencies of the total entropy as a difference $\Delta S_{BCE} = S(T, p) - S(T, p=0)$ at constant temperature (Figure 1a).

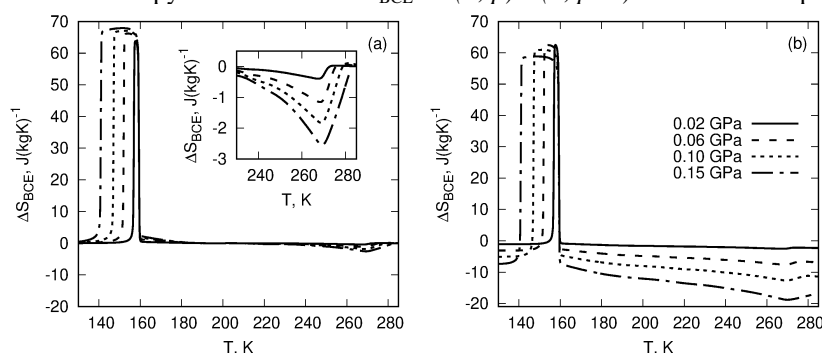


Figure 1 (a) Barocaloric entropy at different hydrostatic pressure in a wide temperature range determined without taking into account the effect of thermal expansion of the crystal lattice. (b) Effect of thermal expansion of the crystal lattice on ΔS_{BCE} .

In accordance with (1), the conventional, $(\Delta S_{BCE})_{conv} < 0$, and inverse, $(\Delta S_{BCE})_{inv} > 0$, BCE are due to the different signs of the $(\partial V/\partial T)_p$ derivatives at T_1 and T_2 . The very different degree of proximity of both phase transitions to the tricritical point and significant difference in entropies ($\Delta S_1 = 10.5$ J/kg·K; $\Delta S_2 = 66$ J/kg·K) are the reasons of a very strong increase in $(\Delta S_{BCE})_{inv}$ in comparison with $(\Delta S_{BCE})_{conv}$ at the same pressure.

At the second stage, we studied the effect of the lattice entropy change under pressure on BCE. Figure 1(b) demonstrates that due to the same sign of both derivatives, $(\partial V/\partial T)_{T_1}$ and $(\partial V_{LAT}/\partial T)_p$, there is a strong increase in BCE_{conv} . At $p=0.15$ GPa, the value $(\Delta S_{BCE})_{T_1} = -19$ J/kg·K is almost twice the entropy of the phase transition ΔS_1 . Thus, contribution of $(\Delta S_{BCE}^{LAT})_{T_1}$ to the full BCE at T_1 is predominant. On the other hand, at the same pressure, BCE_{inv} at T_2 , is reduced to $(\Delta S_{BCE})_{T_2} = 59$ J/kg·K due to occurrence of the conventional lattice effect BCE_{LAT}^{conv} : $(\Delta S_{BCE}^{LAT})_{T_2} = -9.0$ J/kg·K.

Comparison of BCE in NH_4HSO_4 with ECE and MCE in other ferroics showed that ferroelectric under study can be considered as a competitive solid-state refrigerant.

Acknowledgments:

The study was carried out with a grant from the Russian Science Foundation (RSF) grant (No. 19-72-00023).

Influence of the Ni-PZT composite structure dimensions on characteristics of the magnetoelectric effect

F. Fedulov, D. Chashin, L. Fetisov, Y. Fetisov

MIREA –Russian Technological University, Pr. Vernadskogo, 78, 119454 Moscow, Russia

E-mail: ostsilograf@ya.ru

Magnetoelectric (ME) effect in layered composite ferromagnetic– piezoelectric (FM - PE) structures is used to create highly sensitive magnetic field sensors, magnetic storage elements, energy harvesting devices, etc. [1]. The effect arises due to the combination of magnetostriction of the FM layer and the piezoelectric effect in the PE layer and manifests itself in the generation of an alternating voltage between the electrodes of the PE layer when the structure is excited by an alternating magnetic field h and is placed under the bias magnetic field H . Until now, ME effects have been studied mainly for structures with layer dimensions of the order of several cm in plane, with this layers made of different materials connected to each other with a glue. It is necessary to reduce the size of ME composite structures in order to create commercially competitive devices. Previously it was shown [2] that a decrease in the size of structures, made of layers of an amorphous alloy and a PVDF piezopolymer, from 3 cm to 0.5 cm leads to an increase in the resonance frequency and optimal field H_m . The effect of layer sizes on the characteristics of the ME effect in monolithic structures fabricated by the electrolytic deposition of Ni onto a $\text{Pb}_{0.48}\text{Sr}_{0.52}\text{TiO}_3$ (PZT) piezoceramic layer is studied in this paper for the first time.

Commercially available PZT plates with a thickness of 200 μm , 1 mm in width, and with different length from 1 mm to 10 mm were used to manufacture composite structures. Ag electrodes were deposited on both surfaces of the plate, and then a ~ 10 μm thick Ni layer was electrolytically deposited on the one side of the PZT plate. The structure was placed into a constant magnetic field H directed lengthwise and an exciting alternating magnetic field $h\cos(2\pi ft)$ with the amplitude h up to 1.5 Oe and frequency f range 100 – 500 kHz. The ME voltage $u(f)$ was recorded using a digital oscilloscope.

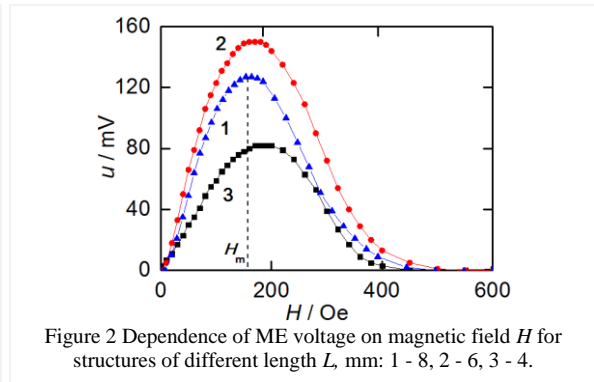
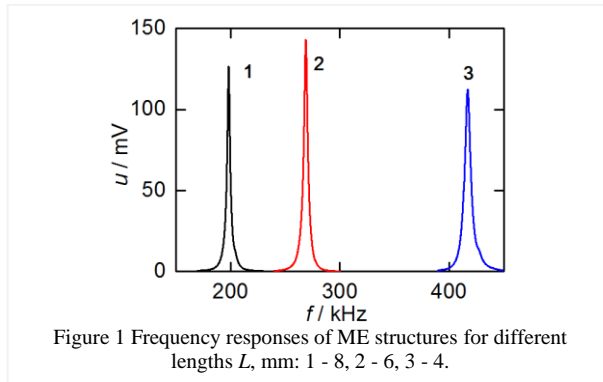


Figure 1 shows the measured dependencies of ME voltage u on the frequency of the excitation field f for structures with length $L = 4$ mm, 6 mm, and 8 mm. The peaks correspond to the excitation of the longitudinal acoustic resonance of the structure. The resonance frequency can be found by the expression $f_0 = (1/L)\sqrt{Y/\rho}$, where Y and ρ - the effective Young's modulus and density of the structure, respectively. The resonance frequency f_0 increases with decreasing of the length L , according to the theory. The maximum value of the ME coefficient was $\alpha_{me} = 5.5$ V/(Oe·cm). Figure 2 shows the ME voltage dependencies on the field H at resonance frequency for each of the structure. The maximum voltage at the field H_m corresponds to the maximum of the piezomagnetic coefficient $\lambda^{(1)} = \partial\lambda/\partial H$, where $\lambda(H)$ - the field dependence of the magnetostriction λ of FM layer. The optimal field H_m increases with decreasing of the L due to the growing role of demagnetization effects, which is in agreement with [2]. The decrease in $u(H_m)$ in this case is mainly due to the decrease in the piezomagnetic coefficient $\lambda^{(1)}$. The effective excitation of the ME effect in monolithic Ni-PZT structures with a length of up to 1 mm at frequencies up to ~ 1.5 MHz was experimentally demonstrated. In the same Ni-PZT structures with a size of ~ 1 mm, the ME effect was observed at lower frequencies, up to 50 kHz, using low-frequency bending vibrations.

The research was supported by the Russian Science Foundation, project No 19-79-10128.

[1] J.-M. Hu, C.-W. Nan, Opportunities and challenges for magnetoelectric devices, APL Advances, vol. 7, p. 080905 (2019).

[2] A. Lasheras, J.Gutiérrez, J.M. Barandiaran, Quantification of size effects in the magnetoelectric response of metallic glass/PVDF laminates, Appl. Phys. Lett., vol. 108, p. 222902 (2016).

The effect of changes in chemical composition and uniaxial compression on the phase transition of CuInP_2S_6 crystals

A. Molnar, K. Glukhov, M. Medulych, D. Gal, H. Ban, Yu. Vysochanskii

Institute of Physics and Chemistry of Solid States, Uzhhorod National University, Voloshina Str. 54, Uzhhorod, 88000

alex.molnar@uzhnu.edu.ua

Recently interest in layered 2D crystals of the $\text{Me}_1\text{Me}_2\text{P}_2\text{S}(\text{Se})_6$ family has significantly increased due to their unique physical properties [1] and the possibility of creating active components based on them for promising electronics products [2]. One of the most interesting of these is CuInP_2S_6 ferroelectric at room temperature, in which the polar state is maintained at a thickness of several structural layers [3]. However due to the fact that its phase transition temperature is 315K, the search for ways to increase this parameter is relevant. In this work we studied the effect of changes in the chemical composition and uniaxial compression on the phase transition temperature of CuInP_2S_6 crystals.

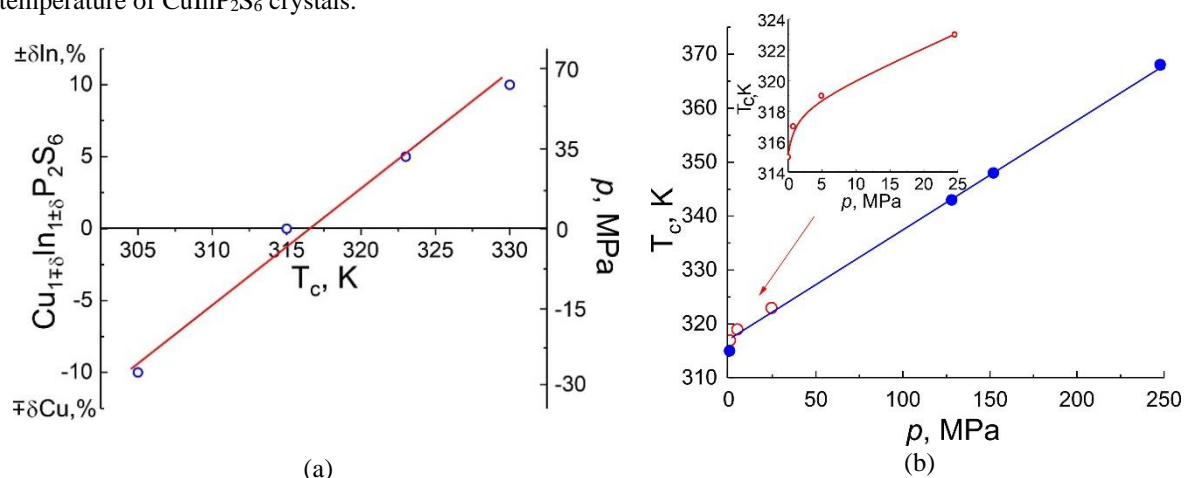


Figure 1 Dependence of the phase transition temperature of $\text{Cu}_{1\pm\delta}\text{In}_{1\pm\delta}\text{P}_2\text{S}_6$ crystals upon deviation ($\delta=\pm 10\%$) according to Cu and In stoichiometry (a) and also under uniaxial (○) and hydrostatic (●) [4] compression (b).

We found that the substitution of copper for indium shifts the temperature of the phase transition in CuInP_2S_6 crystals toward high temperatures. The stoichiometric deviation by 10% towards indium increases the temperature of the phase transition by 15 degrees (up to 330K). Uniaxial or hydrostatic compression of CuInP_2S_6 crystals by 70 MPa leads to a similar shift. In the case of enrichment of samples with copper, a reverse shift of the phase transition temperature to lower temperatures to 305 K is observed. Such a shift is equivalent to stretching the sample by 30 MPa. This behavior is most likely can be explained by the larger size of indium (220 pm) in comparison with copper (128 pm) atoms, which leads to a decrease the interlayer distance in the CuInP_2S_6 crystal when samples are enriched in indium, which is equivalent to uniaxial or hydrostatic compression. In the case of a decrease in the amount of indium, there will be an increase in the distance between the layers of the crystal, which is equivalent to uniaxial stretching.

A similar conclusion is confirmed by the fact that an additional peak appears in the Raman spectra in crystals enriched in copper in the 520 cm^{-1} region, which is not present in the samples enriched by indium. According to first-principle calculations, the appearance of this peak is associated with a change in the interlayer distance of CuInP_2S_6 crystals.

Based on the experimental data we can conclude that samples with an excess of indium are most suitable for practical applications, or more preferable the use of the technology of “strained” CuInP_2S_6 .

- [1] M. A. Susner, M. Chyasnachyus, M. A. McGuire, P. Ganesh, P. Maksymovyc, Metal Thio- and Selenophosphates as Multifunctional van der Waals Layered Materials, *Advanced Materials*, vol. 29, pp.1602852(39), 2017.
- [2] S. Mengwei, P.Y. Liao, G. Qiu, Yu. Duan, P.D. Ye, Ferroelectric Field-Effect Transistors Based on MoS_2 and CuInP_2S_6 Two-Dimensional Van der Waals Heterostructure, *ACS Nano*, vol. 12, pp. 6700-6705, 2018.
- [3] L. Fucai, Yo.Lu, K.L. Seyler, L. Xiaobao, Yu Peng, L. Junhao, W. Xuwen, Z. Jiadong, W. Hong, He Haiyong, S.T. Pantelides, Z. Wu, S. Pradeep, Xu Xiaodong, P.M. Ajayan, W. Junling, L. Zheng, Room-temperature ferroelectricity in CuInP_2S_6 ultrathin flakes, *Nature Communications*, vol. 7, pp.12357(6), 2016.
- [4] V.S. Shusta, I.P. Prits, P.P. Guranich, E.I. Gerzanich, A.G. Slivka, Dielectric properties of CuInP_2S_6 crystals under high pressure, *Condensed Matter Physics*, vol. 10, pp. 91–94, 2007.

Structural instability and electron-phonon interaction in the $\text{CuInS}(\text{Se})_2$ semiconductor-ferroelectrics

K.E.Glukhov, T.Ya.Babuka, L.Yu.Kharkhalis

*Institute of Physics and Chemistry of Solid State, Uzhhorod National University,
54 Voloshin St., 88000 Uzhhorod, Ukraine*

E-mail: lkharkhalis@gmail.com

Electron-phonon interaction is strongly dependent on the chemical bonding between atoms and significantly affects the physical properties and characteristics of the phase transformations occurring in chalcogenides of $\text{M1M2P}_2\text{S}(\text{Se})_6$ type. As it is known the transition from paraelectric to ferroelectric phase is taken place in the $\text{CuInP}_2\text{S}(\text{Se})_6$ crystals, and it is caused by electron-phonon interaction and the second order Jan-Teller (SOJT) cooperative effect. In the work [1,2], it was demonstrated that the SOJT instability is associated with the d^{10} copper electronic configuration in octahedral symmetry. Recently [3], basing on the investigations of the structural and electronic properties in the different phases we established that the strong recharging of Cu and In cations at the phase transition and on switching from selenide to sulfide structure have been observed. The driving force of the ferroelectric structural phase transition has been linked to the peculiarity of the Cu atomic orbitals placement on the energy scale. The indium ion was also found to be an important counterpart for the ferroelectric phase transition realization. From the Mulliken charge calculations one can conclude that the CuInP_2S_6 crystal is more ionic than the $\text{CuInP}_2\text{Se}_6$ crystal. Substitution of S by Se atom (with a larger radius of ions) leads to a decrease in the potential relief for copper ions in $\text{CuInP}_2\text{Se}_6$ relative to CuInP_2S_6 . The difference associated with the change of the anionic complex (P_2S_6 to P_2Se_6) has been explained in terms of the change in the covalent bond ionicity and has been shown to be an important factor for realizing the second-order Jan-Teller effect, which is the main mechanism of ferroelectric phase transition in these compounds. With the purpose of the explanation of the structural instability at the phase transition and elucidation of possible preconditions for the second-order Jahn-Teller effect realization in the considered crystals, we also study the vibration properties and calculate the strength of the electron-phonon coupling.

In our work, we present the *ab initio* investigation of the evolution of lattice dynamics and the density of phonon states at the disorder-order transition in $\text{CuInP}_2\text{S}(\text{Se})_6$. Imaginary frequencies were found in the phonon spectra of the paraelectric phase of $\text{CuInP}_2\text{S}(\text{Se})_6$ crystals, confirming the structural instability of these materials, and the nature of this instability, which connected with the oscillations of Cu and In atoms, was established. Comparing these two structures was found that unstable oscillations involving only copper ions but not indium ones in the selenide compounds were observed. This peculiarity can be explained by the fact that the covalence of the In–Se bonds increases compared with the nature of the In–S bonds. More covalent In–Se chemical bonds cause more rigid pinning of indium ions in their metastable positions than that observed in the sulfide compound.

For the first time, we investigated the electron-phonon interaction in $\text{CuInP}_2\text{S}(\text{Se})_6$ utilizing the first-principles approach. In the framework of the program packet ABINIT [4] with the application of the updated methodology of the density functional perturbation theory (DFPT) we calculated the Eliashberg spectral function $\alpha^2F(\omega)$ and electron-phonon coupling strength λ . The phonon spectra with the phonon linewidths $\Gamma_{\text{el-ph}}$ have been obtained. Our analysis of the parameters of electron-phonon interaction supports that the main contribution in these characteristics is due to vibrations that are connected with the Jan-Teller instability in the materials with the phase transitions. Calculated considerable values of the electron-phonon interaction parameter ($\lambda \sim 0.6$) demonstrate the strong interaction between the electron and phonon subsystems that agrees with the appearance of the structural instability in these crystals.

[1] J. K. Burdett and O. Eisenstein, From three- to four-coordination in copper(I) and silver(I), *Inorg. Chem.*, vol. 31, no. 10, pp. 1758-1763 (1992).

[2] D. Bercha, S. Bercha, K. Glukhov and M. Sznajder, Electron-Phonon Interaction as a Mechanism of Phase Transition in the CuInP_2S_6 Crystal, *Acta Physica Polonica A*, vol. 126, pp. 1143-1145 (2014).

[3] T. Babuka, K. Glukhov, Yu.M.Vysochanskii, M. Makowska-Janusik. Layered ferroelectric crystals $\text{CuInP}_2\text{S}(\text{Se})_6$: a study from the first principles, *Phase Transitions*, 2019, V.92, №5, P 440-450 (2019)

[3]. X. Gonze, J. Beuken, R. Caracas, F. Detraux, M. Fuchs, G. Rignanese, L. Sindic, G. Verstraete, G. Zerah, F. Jollet, M. Torrent, A. Roy, M. Mikami, P. Ghosez, J.-Y. Raty and D. Allan. First-principles computation of material properties: the ABINIT software project, *Comput. Mater. Sci.*, vol. 25, p. 478 (2002).

Photorefractive parameters of $\text{Sn}_2\text{P}_2\text{S}_6$ crystals modified by doping, co-doping, and indiffusion

A. Grabar¹, A. Molnar¹, A. Kohutych¹, K. Glukhov¹, M. Tsyhyka¹,
S. Hasynets¹, Yu. Vysochanskii¹, and D. R. Evans²

1 - Institute for Solid State Physics and Chemistry of Uzhhorod National University, Uzhhorod, 88000, Ukraine
2 - US Air Force Research Laboratory, Materials and Manufacturing Directorate, Wright-Patterson AFB, OH 45433, USA

alexander.grabar@uzhnu.edu.ua

The $\text{Sn}_2\text{P}_2\text{S}_6$ ferroelectrics crystals are studied as efficient photorefractive, pyro- and piezoelectric materials. The optical, dielectric and photorefractive parameters of these crystals can be efficiently modified by doping. Partially, the growth of these crystals by vapor-transport technique with addition of Sb, Te, Bi [1, 2] allows to vary their properties, partially to enhance the photorefractive parameters. Our further technological works are directed to search of the new efficient dopants, as well as to elaboration other ways of the after-growth sample modification, particularly using thermo-induced indiffusion of dopant atoms. In the communication, we present the results of the complex investigations of the optical, photorefractive and dielectric parameters of $\text{Sn}_2\text{P}_2\text{S}_6$ crystals modified by the doping in process of vapor-transport crystal growth, co-doping with two different dopants, and by thermally-induced indiffusion of the Cu atoms from the surfaces.

In our experiments, the $\text{Sn}_2\text{P}_2\text{S}_6$ specimens with gradients of the indiffused Cu atoms along different crystallographic directions were obtained and studied. We measured the variation of the dielectric constant, optical transmission and photorefractive two-wave mixing gain at 633 nm along the direction of diffusion. We also studied these Sb- and Te-doped crystals, modified by Cu indiffusion after growth. It was found that an impact of both doping at growth and post-growth indiffusion on the photorefractive parameters leads to an increasing of the compensative component of the photoinduced space-charge grating, i. e. screening effects due to increased electric conductivity. In addition, the $\text{Sn}_2\text{P}_2\text{S}_6$ co-doped with Cu1% and Sb1% crystals were grown. We found that the optical transmission spectra of these materials are similar to the case of the Sb-doped sample, but the photorefractive parameters show a substantial difference: the formation of the space-charge grating is single-exponential, and practically without the compensation processes. This is a substantial advantage for use this photorefractive material in holographic schemes, that is illustrated by high stability of the dynamical interferometers and other photorefractive schemes exploiting the double-doped $\text{Sn}_2\text{P}_2\text{S}_6:(\text{Sb}, \text{Cu})$ crystals.

The obtained experimental results well correlate with *ab initio* calculations of the electron spectra in the $\text{Sn}_2\text{P}_2\text{S}_6$ lattice with various defects. The calculated potential barriers between probable positions of the indiffused atoms in the $\text{Sn}_2\text{P}_2\text{S}_6$ lattice correlate with the experimental results on the thermo-induced diffusion in different crystallographic directions. Besides, the model calculation of the electron spectra in the $\text{Sn}_2\text{P}_2\text{S}_6$ lattice with two defects (Cu and Sb) in the same unit cell give an explanation of the absence of the compensations processes in the double-doped crystal. As it was shown in [3], the Sb^{3+} impurity replaces the Sn^{2+} cations, charge-compensated by appearance the Sn vacancies. This leads to formation the defects of two types, including tin vacancies, that can be a reason of the electron-hole compensation at the formation of the photorefractive holograms. As it follows from the calculations of the electron spectra, the Cu^{1+} impurity, located near Sb^{3+} , form the additional electron states that correspond to the same energy, and so are forming single electron level in the gap. This well correlates with the exponential dynamics of the space-charge grating formation, that is predicted by a single-level model of the photorefractive effect.

The financial support of the European Office of Aerospace Research and Development via Project P438b of Science and Technology Center Ukraine is gratefully acknowledged.

[1] A. A. Grabar, M. Jazbinšek, A. N. Shumelyuk, Yu. M. Vysochanskii, G. Montemezzani and P. Günter. Photorefractive effects in $\text{Sn}_2\text{P}_2\text{S}_6$. In: "Photorefractive Materials and Their Applications II. Springer, New York 327 (2007).

[2] I. V. Kedyk, P. Mathey, G. Gadret, O. Bidault, A. A. Grabar, I. M. Stoika, Yu. M. Vysochanskii, J. Opt. Soc. Am. **B 25(2)**, 180, (2008).

[3] B. E. Kananen, E. M. Golden, S. A. Basun, D. R. Evans, A. A. Grabar, I. M. Stoika, W. McClory, N. C. Giles, L. E. Halliburton, Optical Materials Express **6(12)**, 3992, (2016).

Stability and nanocrystalline structure investigation of Se-based chalcogenide glasses

A. Horvat¹, N. Mehta², V. Mikla¹, V. Minkovich¹, A. Molnar¹, A. Solomon²,

1- *Uzhgorod National University, Uzhgorod, 88000, Ukraine*

2- *Institute of Science, Banaras Hindu University, Varanasi, 221 005, India*

3- *Institute of Electron Physics, National Academy of Science, Uzhgorod, 88000, Ukraine*

victormkl836@gmail.com

The fundamental scientific problem of amorphous materials based on chalcogenide systems consists in establishing the causes leading to devitrification and oxidation of fusible chalcogenide glasses, and the identification of factors affecting the nature of the instability of amorphous condition. Chalcogenide glassy semiconductors (ChGs) belong to the non-crystalline materials with sophisticated structure which is not structurally in equilibrium state [1, 2]. The processes of structural relaxation lead to a change (sometimes significant) in physical properties, including mechanical and dielectric. Selenium, the simplest representative of amorphous chalcogenides is known to consist of a chain and ring fragments [3].

Selenium is a nutritiously essential element. People used selenium for healthy joints, heart and eyes [4]. It plays a crucial role in DNA system, the immune system and the reproductive system [1]. It also helps fight cancer and other diseases [4]. Over than internal human uses selenium it also used in manufacturing. It is known as a color and decolorized glasses. Thanks to these structural peculiarities, Se has a very broad spectrum of applications in chemical, electrical and electronic industries, as it is characterized by a high photo- and thermal-conductivity, as well as electrocatalytic and photovoltaic activities [5]. Therefore glassy selenium is one of the potential productive materials of the materials science.

It is known that the introduction of elements such as As, Sb, Bi (pnictogens) with similar structure but different radius in varying degrees stabilizes the amorphous structure. It is also known that an increase in the degree of metallization of the bond makes the structural framework more rigid and reduces its flexibility, which affects the area of possible glasses in systems with different types of pnictogen. In this sense, the most convenient from the point of view of obtaining glasses for practical application is Arsenic.

In all glasses with small concentration of As upon time relaxation at room temperature in differential thermal analysis at low scan rates glass transition width becomes narrow and the non-reversing enthalpy at T_g increases. In Raman scattering, such structural relaxation leads decreasing of width and scattering strength of the modes which corresponding to Se_n-chains near 250 cm⁻¹ and 235 cm⁻¹, while the modes near 264 cm⁻¹ associated with Se₈ rings systematically grows. These calorimetric and Raman scattering results are consistent with the “molecular” chains of Se_n, predominant in the fresh glass, reconstructing with each other to compact and partially order the network. Consequences of the aging induced reconstruction of the long super-flexible and uncorrelated Se_n-chains are also manifested upon alloying up to 4 mol. % of As as revealed by a qualitative narrowing of the Raman vibrational mode of the corner-sharing AsSe₃ pyramids. Thus the reason for the instability of Se-based glasses is the presence in the structure of polymer chains Se_n and monomer rings Se₈, inside of which there are strong covalent bonds, and between them weak intermolecular bonds with a tendency to radicalization. Last are centers of crystallization with a small energy exposure. The introduction of low concentrations of As into the Se glassy system should increase the stability of glasses and lead to the formation of pyramids in places dangling S_n chains, while maintaining a low temperature plasticity.

The effect of structural relaxation (physical ageing) indicate that the different behavior of aged and as-quenched samples of glassy selenium properties is observed due to the presence of crystalline phase nuclei (nanocrystals) in aged samples. At room temperature, the whole relaxation normally occurs over a time scale of approximately 1000 hours (42 days).

The processes of structural relaxation lead to a change (sometimes significant) in physical properties, including X-ray diffraction, electric, thermomechanical, and kinetic characteristics of Se-based glass in depending of As atoms concentration make it possible to determine changes in the structure of amorphous material, define more precisely the stable glasses regions, explain the structural changes, get compositions which is useful for application.

- [1] L. Tichy and H. Ticha, “On the Chemical Threshold in Chalcogenide Glasses,” *Materials Letters*, vol. 21, No. 3-4, pp. 313-319, (1994).
- [2] L. Tichy and H. Ticha, Covalent bond approach to the glass-transition temperature of chalcogenide glasses, *J. Non-Cryst. Solids*, vol. 189, pp.141-146, (1995).
- [3] V. I. Mikla, J. M. Turovci, V. V. Mikla and N. Mehta, Molecular structure of Se-rich amorphous films, *Prog. Sol. Stat. Chem.*, vol. 49, pp. 1-15, (2018).
- [4] *Handbook of Chalcogen Chemistry (New Perspectives in Sulfur, Selenium and Tellurium)*, 2nd Edition, Edited by: F. A. Devillanova and W.-W. du Mont, The Royal Society of Chemistry (RSC) Publishing, Volume 1, (2013).
- [5] S. Choudhary, A. Umar, S. K. Mehta, Selenium nanomaterials: an overview of recent developments in synthesis, properties and potential applications. *Prog. Mater. Sci.*, vol. 83, pp. 270–329, (2016).

DIELECTRIC PROPERTIES OF THE RELAXOR FERROELECTRIC $(1-x)\text{Pb}(\text{Zn}_{1/3}\text{Nb}_{2/3})\text{O}_3-x\text{PbTiO}_3$

Arnoldas Solovjovas¹, Šarūnas Svirskas¹, Džiugas Jablonskas¹, Shinya Tsukada², Seiji Kojima³, Jūras Banys¹

1- Faculty of Physics, Vilnius University, Sauletekio 9/3, LT10222 Vilnius, Lithuania

2- Faculty of Education, Shimane University, Matsue 690-8504, Japan

3- Graduate School of Pure and Applied Sciences, University of Tsukuba, Tsukuba, Ibaraki 305-8573, Japan

Arnoldas.solovjovas@ff.vu.lt

The history of ferroelectrics starts back in 1940s. Ferroelectric materials are known for having a high dielectric permittivity value. Usually in ferroelectrics temperature of second-order phase transition is related with maximum value of real dielectric permittivity temperature. Also, there is a related group of ferroelectrics that received special attention for the past decades due to extraordinary dielectric properties – relaxor ferroelectrics (relaxors) [1].

Compared to ‘normal’ ferroelectrics, relaxors have several distinctive features, which does not correspond to structural phase transition. Relaxors have a diffuse peak of dielectric permittivity. the maximum value of real (ϵ') and imaginary (ϵ'') components of the dielectric permittivity are observed at different temperature values for the different probing frequency [1],[2].

$\text{Pb}(\text{Zn}_{1/3}\text{Nb}_{2/3})\text{O}_3$ (PZN) together with $\text{Pb}(\text{Mg}_{1/3}\text{Nb}_{2/3})\text{O}_3$ (PMN) are so called canonical relaxors and play a crucial role in the field of piezoelectrics and are highly suitable for ultrasonic transducers, electromechanical actuators [3]. The main goal of our work is to investigate dielectric properties of $\text{PZN}-x\text{PbTiO}_3$ (PT) single crystal along morphotropic phase boundary (MPB). In this paper four samples with different x concentrations (4.5PT, 6PT, 7PT and 12PT) were investigated.

The dielectric spectroscopy experiments were carried in two different experimental setups. The first one was done using impedance analyzer HP Agilent 4284A in the frequency range of 20 Hz to 1000 Hz. The second setup was done by measuring complex reflection coefficient using network analyzer Agilent 8714ET/ES in 1 MHz-300 MHz frequency range, while the sample is placed at the end of coaxial line.

Below in Fig. 1 you can see temperature dependence of real (ϵ') and imaginary (ϵ'') components of dielectric permittivity. The sample with 4.5PT concentration has a usual single broad peak. In 6PT and 7PT concentrations we can observe two phase transitions, because we are approaching morphotropic phase boundary. In 12PT concentration we observe a single sharp peak and a phase transformation from cubic to tetragonal phase.

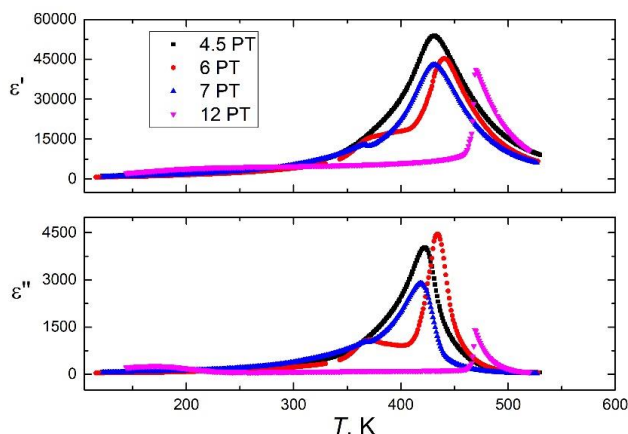


Figure 1 Real and imaginary components of dielectric permittivity dependence to temperature

[1] A. Peliz-Barranco, F. Calderin-Piar, O. Garca-Zaldvar, and Y. Gonzalez-Abreu, “Relaxor Behaviour in Ferroelectric Ceramics,” in *Advances in Ferroelectrics*, A. Peliz-Barranco, Ed. InTech, 2012.

[2] C. W. Ahn *et al.*, “A brief review on relaxor ferroelectrics and selected issues in lead-free relaxors,” *J. Korean Phys. Soc.*, vol. 68, no. 12, pp. 1481–1494, Jun. 2016, doi: 10.3938/jkps.68.1481.

[3] K. Uchino, “The Development of Piezoelectric Materials and the New Perspective,” in *Advanced Piezoelectric Materials*, Elsevier, 2017, pp. 1–92.

ELECTROMECHANICAL PROPERTIES IN (0.8Na_{0.5}Bi_{0.5}TiO₃-0.2BaTiO₃)-CaTiO₃ SOLID SOLUTIONS

Miks Jurjans, Maris Kundzins, Eriks Birks, Andris Sternberg

Institute of Solid State Physics, University of Latvia

Miks.Jurjans@cfi.lu.lv

Na_{0.5}Bi_{0.5}TiO₃ (NBT) - based compositions are widely studied due to environmental requirements to replace lead-containing ferroelectrics in a large variety of devices, where piezoelectric effect is applied. Usually, the large values of piezoelectric coefficients are found in the region of a morphotropic phase boundary (MPB). Unlike lead-containing perovskites, one of the drawbacks of NBT-based compositions is reducing of the phase transition temperature upon approaching the MPB. Such a trend inspires an idea to shift the phase transition temperature to the room temperature region by using appropriate additives, thus achieving large strains at the electric field-induced phase transition. Still, in the framework of such a concept, the restriction regarding the solid solution concentration range to the MPB compositions does not look convincing. The aim of the present work is to study electromechanical properties of (1-x)(0.8NBT-0.2BaTiO₃)-xCaTiO₃ solid solutions, searching compositions with high values of electric field induced strains at the room temperature. The choice of 0.8NBT-0.2BaTiO₃ (which is located far away from the MPB in the region of the tetragonal ferroelectric phase) as a starting composition is motivated by large tetragonality in this concentration range of (1-y)NBT-yBaTiO₃ solid solutions [1]. Whereas, CaTiO₃ is added to reduce the phase transition temperature, which is an important condition to achieve large strains at room temperature. It was found that, in (1-x)(0.8NBT-0.2BaTiO₃)-xCaTiO₃ composition with x = 0.10, the phase transition is shifted below room temperature, allowing to obtain strains above 0.2% at E = 70 kV/cm in the temperature range from room temperature up to 90°C (Fig.1a) with small hysteresis (Fig.1b), which is preferable for practical use. In the composition with lower CaTiO₃ content (x=0.075), strain at the electric field-induced phase transition was studied, focusing on strain dependence on polarisation.

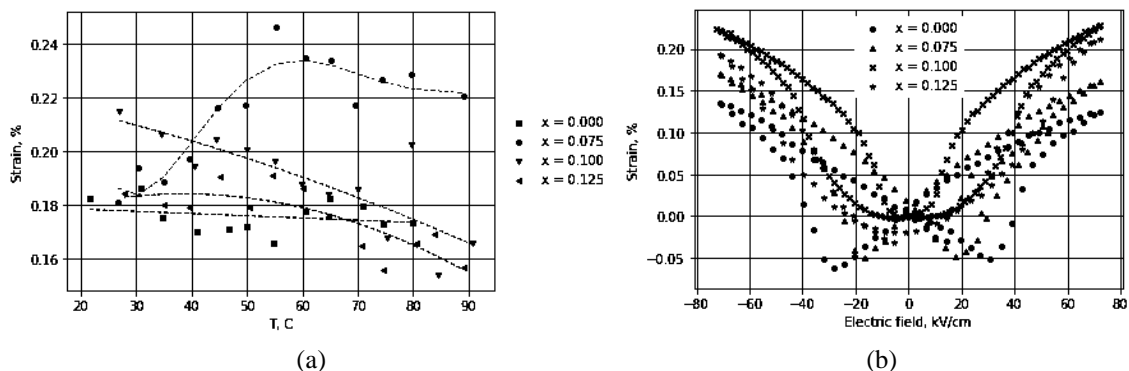


Figure 1 (a) Temperature-dependence of strain at E = 70 kV/cm for (1-x)(0.8NBT-0.2BaTiO₃)-xCaTiO₃ compositions with various CaTiO₃ concentrations x; (b) Electric field-dependence of strain for the compositions with various CaTiO₃ concentrations measured at 35°C.

[1] M.Dunce, E.Birks, M.Antonova, A.Plaude, R.Ignatans, A.Sternberg. Structure and Dielectric Properties of Na_{1/2}Bi_{1/2}TiO₃-BaTiO₃ Solid Solutions. *Ferroelectrics*, vol. 447, pp.1-8 (2013).

Dielectric Investigations of Ba_{0.17}Ca_{0.83}TiO₃ Ceramic

E. Palaimiene¹, J. Macutkevicius¹, A. Molak², I. Gruszka², J. Banys¹

1- Institute of Applied Electrodynamics and Telecommunications, Vilnius University, Vilnius, Lithuania

2- Institute of Physics, University of Silesia, Chorzow, Poland

edita.palaimiene@ff.vu.lt

Perovskite barium titanate BaTiO₃ (BTO) possesses the high dielectric permittivity value, the large spontaneous polarization, good piezoelectric, and nonlinear optical properties at room temperature. It is ferroelectric at room temperature and it is paraelectric beyond the Curie temperature T_C close to 403 K [1]. BaTiO₃ ceramics doped with Ca (BCTO) exhibit improved piezoelectric properties in comparison with pure BaTiO₃. Moreover, the stabilization of BCTO is considered to result from the slight modification of Ba site with small Ca addition [2]. Barium calcium titanate is a very useful compound in the creation of electro-optical materials for holographic and photo-refractive applications [3] and show promising applications in advanced laser systems, optical interconnects and electronic or optical storage devices [4].

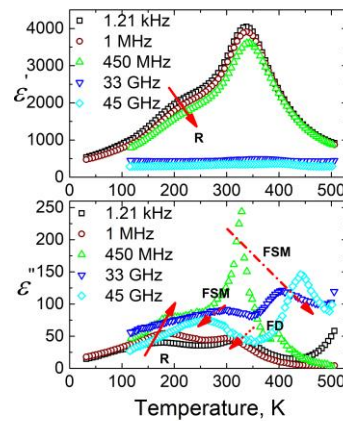


Figure 1 Temperature dependence of the real and the imaginary parts of complex dielectric permittivity $\epsilon^* = \epsilon' - i\epsilon''$ for Ba_{0.17}Ca_{0.83}TiO₃ ceramics measured at several frequencies (R—relaxor, FSM—ferroelectric relaxational soft mode, FD—ferroelectric domains related dielectric dispersions).

In this work we present broad band dielectric spectroscopy results of barium calcium titanate ceramic, Ba_{0.17}Ca_{0.83}TiO₃. Dielectric measurements were performed in wide temperature region (30 K – 500 K) at 20 Hz - 50 GHz frequencies. The temperature dependences of complex dielectric permittivity for Ba_{0.17}Ca_{0.83}TiO₃ ceramics are presented in Fig. 1. Two dielectric anomalies can be clearly separated. The most pronounced dielectric anomaly is observed close to 340 K. At low frequencies (below 1 MHz) the position of complex dielectric permittivity maximum is frequency independent and only at higher frequencies (above 1 MHz) the maximum shifts to the higher temperatures with frequency. Such dielectric anomaly is typical for ferroelectric phase transition. Moreover, the significant dielectric dispersion occurs for this material in microwaves. The dielectric anomaly at lower temperatures is strongly frequency dependent. Such anomaly can be typical for relaxor or dipolar glass behaviour or ferroelectric domains. The dielectric relaxation in the investigated ceramics will be discussed in the presentation.

[1] M.H. Khedhri, N. Abdelmoula, H. Khemakhem, R. Douali, F. Dubois, Structural, spectroscopic and dielectric properties of Ca-doped BaTiO₃, Applied Physics A, 125:193, (2019).

[2] D. Fu, M. Itoh, S. Koshihara, Crystal growth and piezoelectricity of BaTiO₃-CaTiO₃ solid solution, Applied Physics Letters 93, 012904 (2008).

[3] F.V. Motta A.P.A. Marques, J.W.M. Espinosa, P.S. Pizani, E. Longo, J.A. Varela, Room temperature photoluminescence of BCT prepared by Complex Polymerization Method, Current Applied Physics 10, 16–20, (2010).

[4] H. Veenhuis, T. Börger, K. Peithmann, M. Flaspöhler, K. Buse, R. Pankrath, H. Hesse, E. Krätzig, Light-induced charge-transport properties of photorefractive barium-calcium-titanate crystals doped with rhodium, Applied Physics B 70, 797–801 (2000).

TAPE CASTING AND DIELECTRIC CHARACTERISTICS OF NBYT THICK FILMS

T. Kudrevičius¹, A. Plyushch¹, Š. Svirskas¹, A. Selskis¹, M. Duncce², E. Birks², J. Banys¹

1- Faculty of Physics, Vilnius University, Sauletekio 9/3, LT10222 Vilnius, Lithuania
2- Institute of Solid State Physics, University of Latvia, Kengaraga str. 8, 1063, Riga, Latvia

tomas.kudrevicius@ff.stud.vu.lt

Due to environmental regulations against high amounts of lead used in ferroelectric materials (RoHS directive in EU), a lot of studies have been done in order to find the best lead-free alternatives. $\text{Na}_{0.5}\text{Bi}_{0.5}\text{TiO}_3$ (NBT) -based compositions possess quite large dielectric permittivity values and high electromechanical strain [1]. One of the most prominent techniques to create multi-layered ceramic structures is tape casting. This technology can provide high-quality, large-area and thin functional materials, such as ferroelectrics, piezoelectrics for multilayered capacitors [2]. Tape casting is mostly based on non-aqueous solvent, but aqueous-based tape casting is also used as a simple and eco-friendly method.

In this work, thick films of Bi-stoichiometric NBT doped with 1at% Yb ($(\text{Na}_{0.5}\text{Bi}_{0.49}\text{Yb}_{0.01})\text{TiO}_3$) and Bi-overstoichiometric $(\text{Na}_{0.5}\text{Bi}_{0.51}\text{Yb}_{0.01})\text{TiO}_3$ were prepared by tape casting. The films were produced via an aqueous tape casting method. Dispex AA4040 was used as a surfactant and PVP solution (Luvitec K 90 Pulver) – as a binder. Both chemicals were provided by BASF. Two-step thermal treatment (at 500 °C and at 1200 °C (2 h)) on platinum substrate, was followed by the casting and drying. The obtained films were of 170 μm thickness. Dielectric properties were measured at a temperature range 30 K - 750 K upon cooling with a rate of 1 K/min. Also, electromechanical properties were investigated using commercial aixACCT TF 2000 analyzer.

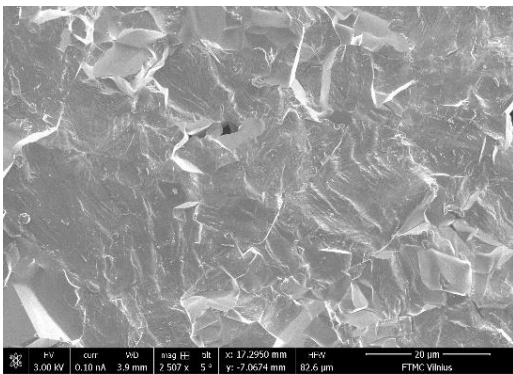


Figure 1 Scanning electron micrograph of $\text{Na}_{0.5}\text{Bi}_{0.49}\text{Yb}_{0.01}\text{TiO}_3$.

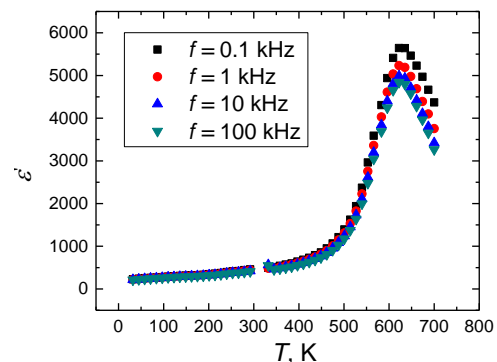


Figure 2 Temperature dependence of dielectric permittivity of $\text{Na}_{0.5}\text{Bi}_{0.49}\text{Yb}_{0.01}\text{TiO}_3$.

Figure 1 shows SEM image of $(\text{Na}_{0.5}\text{Bi}_{0.49}\text{Yb}_{0.01})\text{TiO}_3$ thick film. This image shows that the film is quite dense, as there are just a few pores on the surface. Figure 2 shows temperature dependence of dielectric permittivity $\epsilon'(T)$ of NBT. There are no signs of shoulder in the low-temperature direction from the maximum of $\epsilon'(T)$, usually observed in bulk NBT, and the maximum is shifted in the direction higher temperatures ($T_m=630$ K).

ACKNOWLEDGEMENTS

This work was supported by the Research Council of Lithuania (Project P-LLT-20-9).

- [1] V. V. Shvartsman and D. C. Lupascu, "Lead-Free Relaxor Ferroelectrics," *Journal of the American Ceramic Society*, vol. 95, no. 1, pp. 1–26, Jan. 2012.
- [2] M. Jabbari, R. Bulatova, A. I. Y. Tok, E. Mitsoulis, and J. H. Hattel, "Ceramic tape casting: A review of current methods and trends with emphasis on rheological behaviour and flow analysis," *Materials Science and Engineering: B*, vol. 212, pp. 39–61, Oct. 2016.

ROLE OF THERMAL TREATMENT IN SURFACE MORPHOLOGY OF NBT-BASED CERAMICS

L.Bikshe, K.Kundzins, M.Dunce, E.Birks, A.Sternbergs

Institute of Solid State Physics, University of Latvia

lbikshe@gmail.com

Thermal etching is a fruitful tool in study of microstructure of NBT-based compositions. It is based on the fact that sublimation rate from a surface is different, comparing grains and grain boundaries. Still published articles, devoted to studies of NBT-based compositions, reveal more a complex process characteristic to this high-temperature treatment [1, 2]. Various kinds of microstructure can be divided into three groups. One group represents “plain” patterns where grain boundaries appear as thin lines separating grains (Fig.1a). In the second group, pattern is characterised by well-expressed relief, where grains are not plain objects anymore (Fig.1b). The third group represents microstructure, where grains appear as regular parallelepipeds with very well expressed faces and edges (Fig.1c). The aim of this study is to determine the role of heat treatment parameters in appearance of microstructure, containing grains in the form of parallelepipeds. Structure and chemical composition of such a surface is characterised by x-ray diffraction, EDS and micro-Raman spectroscopy study. The obtained results also contain recommendations for optimal thermal etching parameters to obtain the most qualitative etched surface for grain characterisation of NBT-based compositions.

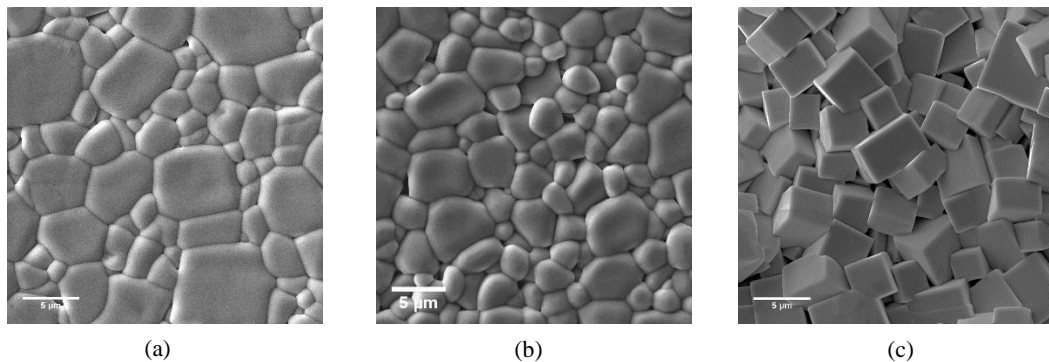


Figure 1 Three types of surface patterns obtained by thermal etching: “plain” (a), with relief (b) and parallelepipeds (c)

[1] Ko S.-Y., Kang S.-J., L. J. Eur. Ceram. Soc. vol.36, p.1159 (2016)

[2] Li A., Wu J., Qiao S., et al. Phys. Stat. Sol. (a) vol.209, p1213 (2012)

Microstructural properties and free-volume defects in the doped BaTiO₃ ceramics

H. Klym¹, I. Karbovnyk², Yu. Kostiv¹, A.I. Popov³

1-Lviv Polytechnic National University, 12 Bandera St., Lviv 79013, Ukraine

2-Ivan Franko National University of Lviv, 107 Tarnavskogo St., Lviv 79017, Ukraine

3-Institute of Solid State Physics, University of Latvia, 8 Kengaraga St., Riga, LV-1063, Latvia

klymija@yahoo.com; halyna.i.klym@lpnu.ua

Barium titanate (BaTiO₃) is a displacement-type ferroelectric perovskite, widely studied for its basic properties and extensive applications [1]. In this materials defects originated by the preparation method. The aim of this work is study of free-volume defects in undoped and Ca-doped BaTiO₃ ceramics using positron annihilation lifetime (PAL) spectroscopy in comparison with scanning electron microscopy (SEM) method.

Undoped BaTiO₃ ceramics and doped with 5, 10 and 15 mol% of Ca were sintered at 1250 °C. The PAL measurements were performed with an ORTEC spectrometer using ²²Na source placed between two sandwiched ceramic samples. The obtained data were treated with LT computer program, the best results corresponding to two-component fitting procedures. The numerical values of trapping parameters (positron lifetime in defect-free bulk τ_b , average positron lifetime τ_{av} , and positron trapping rate of defect κ_d) were calculated using short and long positron-trapping lifetimes τ_1 and τ_2 , as well as component intensities I_1 and I_2 ($I_1 + I_2 = 1$). The difference ($\tau_2 - \tau_b$) can be accepted as a size measure of extended defects where positrons are trapped, the τ_2/τ_b ratio represents the nature of these defects.

In respect to SEM investigations, typical ceramic samples show grain-porous microstructure and assemblies of fractional grains (Fig. 1). By accepting two-state positron trapping model, for polycrystalline ceramic materials the short lifetime of $\tau_1 \sim 0.15$ ns is generally attributed to the free annihilation of positrons. This value also correlated with theoretically calculated free positron lifetime in BaTiO₃ [2]. The obtained value is closed to BaTiO₃ single crystal. The second lifetime τ_2 arises from annihilation of positrons at defect sites. The presently observed values of $\tau_2 \sim 0.32$ ns which is believed to come from the annihilation of positrons at vacancy complexes formed between the oxygen vacancies and the metal ion vacancies. It is obvious from Fig. 2 that τ_2 increases with rise of Ca amount in BaTiO₃ ceramics from 5 to 10 mol% and decreases in samples with 15 mol% of Ca. the intensity I_2 decreases from 22 to 16 % and increases to 25 % in samples with 15 mol% of Ca.

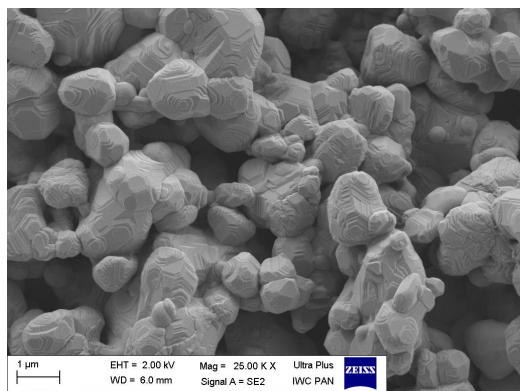


Figure 1 Microstructure of the BaTiO₃ ceramics

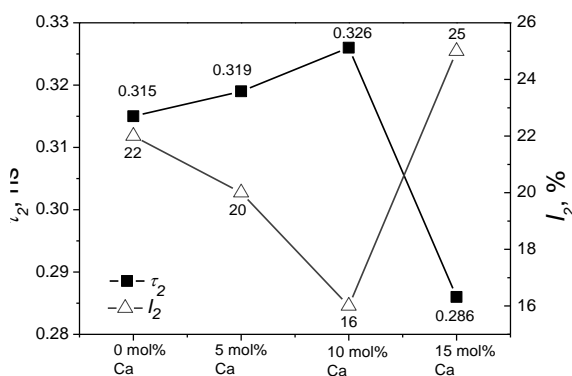


Figure 2 Dependences of the lifetime τ_2 and the intensity I_2 on Ca content in the BaTiO₃ ceramics

This indicates that doping of Ca results in increasing of the size of free-volume defects in ceramics and decreasing of their amount. So, process of agglomeration of defects is take place at posing of BaTiO₃ ceramics By Ca in amount of 5 and 10 mol%, while future increasing the Ca content to 15 mol% leads to fragmentation of free-volume defects.

This work was supported by the Ministry of Education and Science of Ukraine

- [1] C. Macchi, C. Somo Macchi, A. Somoza A., A. Dupasquier, A.L. García, and M. Castro, Positron trapping in BaTiO₃ perovskite, Journal of Physics: Condensed Matter, vol. 13(24), 5717 (2001).
- [2] R.V.K. Mangalam, M. Chakrabarti, D. Sanyal, A. Chakrabati and A. Sundaresan, Identifying defects in multiferroic nanocrystalline BaTiO₃ by positron annihilation techniques, Journal of Physics: Condensed Matter, vol. 21(44), 445902 (2009).

Dielectric and pyroelectric properties of $\text{Sn}_2\text{P}_2\text{S}_6$ ferroelectrics with double – loop switching

I. Zamaraitė¹, A. Dziaugys¹, R. Yevych², S. Svirskas¹, J. Banys¹, Yu. Vysochanskii²

1- Faculty of Physics, Vilnius University, Sauletekio 9, 10222 Vilnius, Lithuania

2- Institute for Solid State Physics and Chemistry, Uzhgorod University, Pidgirna Str. 46, Uzhgorod 88000, Ukraine

vysochanskii@gmail.com

For proper uniaxial ferroelectrics $\text{Sn}_2\text{P}_2\text{S}_6$ below temperature of continuous phase transition $T_0 \approx 337$ K, the spontaneous polarization switching in the form of double hysteresis loops is observed [1]. For these crystals the maximum on pyroelectric current temperature dependence is observed near 280 K where the double hysteresis loop transforms into usual ferroelectric loop. In the case of $(\text{Pb}_y\text{Sn}_{1-y})_2\text{P}_2\text{S}_6$ and $\text{Sn}_2\text{P}_2(\text{Se}_x\text{S}_{1-x})_6$ mixed crystals, usual ferroelectric loops are observed only. In these mixed crystals the maxima on pyroelectric current and dielectric susceptibility temperature dependencies are placed near ferroelectric phase transition temperature.

Earlier, for explanation of peculiar switching processes in $\text{Sn}_2\text{P}_2\text{S}_6$ ferroelectrics, the quantum anharmonic oscillator model was proposed, which considers two structural sublattices and negative ratio of interactions inside and between the sublattices [1]. This discrete model accounts only short range interactions and can explain the coexistence of ferroelectric and antiferroelectric states in mean field approximation. The spontaneous polarization fluctuates in three – well local potential and its origin is determined by changes in the chemical bonding that can be presented as a second order Jahn-Teller effect based on the electron lone-pair stereoactivity of the Sn^{2+} cations and the $\text{P}^{4+} + \text{P}^{4+} \longleftrightarrow \text{P}^{3+} + \text{P}^{5+}$ valence fluctuations of the phosphorous cations [2-4].

The three-well shape of the local potential for spontaneous polarization fluctuations naturally determines possibility of metastable nonpolar regions existence below the second order phase transition temperature T_0 . In addition to the frustration of polar fluctuations near the center of the Brillouin zone, the antipolar fluctuations also strongly develop in the paraelectric phase of $\text{Sn}_2\text{P}_2\text{S}_6$ crystal on cooling to the continuous phase transition temperature. This is confirmed by observation in neutron scattering experiments of flat polar soft optical phonon branch [5] and by development of diffuse X-ray scattering along q_y direction in the Brillouin zone of the paraelectric phase near temperature T_0 [6]. Such experimental data confirm important role of nonlinear coupling between two order parameters, related to polar fluctuation near the Brillouin zone center and to antipolar fluctuations near its edge.

The frequency dependence of dielectric susceptibility temperature anomaly together with aging effects around T_0 and transformation of double hysteresis loops into usual ferroelectric like loops confirm the possibility of simultaneous development of polar and antipolar fluctuations at cooling in paraelectric phase of $\text{Sn}_2\text{P}_2\text{S}_6$ and the coexistence of antipolar and polar clusters below T_0 . In the elementary cell of $\text{Sn}_2\text{P}_2\text{S}_6$ crystals all atoms are placed in general positions. As follows, the atomic substitution increases of the crystal lattice defectives and avoid possibility of the double loops observation in solid solutions.

[1] I. Zamaraitė, R. Yevych, A. Dziaugys, A. Molnar, J. Banys, S. Svirskas, Yu. Vysochanskii, *Phys. Rev. Appl.*, vol. 10, pp. 034017-1 – 034017-6, (2018).

[2] K. Z. Rushchanskii, Yu. M. Vysochanskii, D. Strauch, *Phys. Rev. Lett.*, vol. 99, pp. 207601-1 – 207601-4, (2007).

[3] K. Glukhov, K. Fedyo, J. Banys, Yu. Vysochanskii, *Int. J. Mol. Sci.*, vol. 13, pp. 14356 – 14384, (2012).

[4] R. Yevych, V. Haborets, M. Medulych, A. Molnar, A. Kohutych, A. Dziaugys, Ju. Banys, Yu. Vysochanskii. *Low Temperature Physics*, vol. 42, pp. 1155 – 1162, (2016).

[5] S. W.H. Eijt, R. Currat, J. E. Lorenzo, P. Saint-Groire, B. Hennion, Yu. M. Vysochanskii, *Eur. Phys. J. B*, v. 5, pp. 169 – 178, (1998).

[6] J. Hlinka, R. Currat, M. de Boissieu, F. Livet, Yu. M. Vysochanskii, *Phys. Rev. B*, v. 71, pp. 052102 – 052105, (2005).

Layered GeP_2S_6 , GeP_2Se_6 , GeP_2Te_6 , SnP_2S_6 , SnP_2Se_6 polar crystals with by pressure or chemical composition induced semiconductor – metal transition

V. Haborets¹, K. Glukhov¹, J. Banys², Yu. Vysochanskii¹

1 - Institute for Solid State Physics and Chemistry, Uzhgorod University, Pidgirma Str. 46, Uzhgorod 88000, Ukraine

2 - Faculty of Physics, Vilnius University, Sauletekio 9, 10222 Vilnius, Lithuania

vysochanskii@gmail.com

Earlier was found [1] that Ge doping shifts the ferroelectric second order phase transition in $\text{Sn}_2\text{P}_2\text{S}_6$ crystals toward higher temperatures. The germanium impurity in $\text{Sn}_2\text{P}_2\text{S}_6$ improves stereoactivity of the 2+ charged cation sublattice that is related to the nature of ferroelectricity [2]. The tin hexathiophosphate SnP_2S_6 crystal has layered rhombohedral structure that is composed by nonstereoactive Sn^{+4} cations and $(\text{P}_2\text{S}_6)^{4-}$ anions [3]. In this crystal structure one-half the metal ions are absent with respect to the parent $\text{Sn}_2\text{P}_2\text{S}_6$ structure. According investigations [4] within frame of the density functional theory in LDA approximation of the pressure dependence of the structural, dynamical, and electronic properties in the range up to 35 GPa the SnP_2S_6 crystal is semiconductor with acentric layered structure.

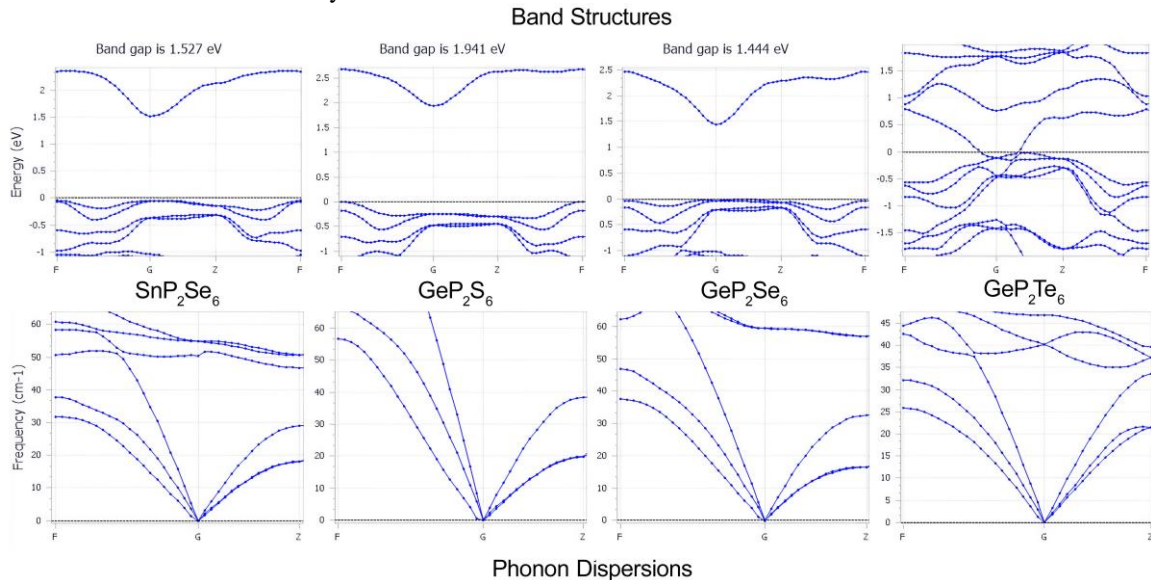


Figure 1. Calculated electron band structures and phonon spectra for SnP_2Se_6 , GeP_2S_6 , GeP_2Se_6 and GeP_2Te_6 crystals.

We have studied possibility of metal and chalcogen atoms substitution in SnP_2S_6 crystal lattice. The structure optimization, the electron band structure and phonon spectra calculations for SnP_2S_6 , SnP_2Se_6 , GeP_2S_6 , GeP_2Se_6 and GeP_2Te_6 crystals have been performed within GGA approximation using the norm - conserving pseudopotentials for R3 phase in pressure range 0 - 80 GPa. For SnP_2S_6 crystal at ambient pressure calculated band gap equals 2.15 eV, with compression it decreases and disappears near 65 GPa. At transition from semiconductor to metal state the calculated phonon spectra becomes unstable what gives us the evidence of structural transformation accompanying metallization in SnP_2S_6 compound. Predicted compounds SnP_2Se_6 , GeP_2S_6 , GeP_2Se_6 , GeP_2Te_6 have rhombohedral R3 crystal lattice and calculated phonon spectra demonstrate their dynamic stability. For SnP_2Se_6 and GeP_2Se_6 direct band gap around 1.53 eV and 1.44 eV is expected, the GeP_2S_6 compound is predicted to be indirect band gap (≈ 1.94 eV) semiconductor. Telluride compound GeP_2Te_6 already is in metal state (Figure 1) with polar structure of R3 symmetry group. At normal pressure the phonon spectra for all newly predicted isostructural compounds are qualitatively similar to early observed [4] for SnP_2S_6 crystal. Spectral range of the lattice vibrations decreases from 590 cm^{-1} in SnP_2S_6 till 390 cm^{-1} in case of GeP_2Te_6 .

[1] M. M Maior, M. I. Gurzan, Sh. B Molnar, I.P. Prits, Yu. M. Vysochanskii, IEEE Trans. of Ultrasonics, Ferroelectrics and Frequency Control, vol. 47, pp. 877-880, (2000).

[2] K. Z. Rushchanskii, Yu. M. Vysochanskii, D. Strauch, Phys. Rev. Lett., vol. 99, pp. 207601-1 – 207601-4, (2007).

[3] Z. Wang, R. D. Willett, R. A. Laitinen, D. A. Cleary. Chem. Mater., 1995, vol. 7, pp. 856 – 858, (1995).

[4] K.Z. Rushchanskii, Yu.M. Vysochanskii, V.B. Cajipe, X. Bourdon. Phys. Rev. B, vol. 73, pp. 115115-1 – 115115-12, (2006).

Influence of Compacting Pressure on the Dielectric Properties of Bismuth Iron Oxide Multiferroic

A.V. Pashchenko^{1,2,3,4}, N.A. Liedienov^{1,2}, Ziyu Wei¹, Mung Yun¹, Qianjun Li¹, I.I. Makoed⁵, D.D. Tatarchuk⁶, Y.V. Didenko⁶, O.A. Gorban², I.A. Danilenko², V.G. Pogrebnyak⁴, G.G. Levchenko^{1,2}

¹ State Key Laboratory of Superhard Materials, International Center of Future Science, Jilin University, 130012 Changchun, China

² Donetsk Institute for Physics and Engineering named after O.O. Galkin, NASU, 03028 Kyiv, Ukraine

³ Institute of Magnetism NASU and MESU, 03142 Kyiv, Ukraine

⁴ Ivano-Frankivsk National Technical University of Oil and Gas, MESU, 76019 Ivano-Frankivsk, Ukraine

⁵ A. S. Pushkin Brest State University, 224016 Brest, Belarus

⁶ National Technical University of Ukraine "Igor Sikorsky KPI", 03056 Kyiv, Ukraine

Main author email address: alpash@ukr.net

The phase composition, crystal structure, microstructure, chemical composition, and dielectric properties of bismuth ferrite multiferroic modified lanthanum have been investigated using XRD, SEM, and dielectric spectroscopy methods. Single phase $\text{Bi}_{0.9}\text{La}_{0.1}\text{FeO}_3$ ceramics was obtained by rapid liquid-phase sintering (RLS) method in a record short time of 8 min at various compacting pressures of the initial precursors P from 90 to 1080 MPa. It has been established that the $R3c$ symmetry of the crystal lattice and the unit cell parameters are independent of pressure. Despite the short sintering time, the microstructure is well formed with clear boundaries of the intergranular zones. An average crystallite size is in the range 200–300 nm and is independent of pressure. The compacting pressure affects the dielectric constant in both the low-frequency range up to 1 MHz and microwave range over 8 GHz (see Figure 1). It has been established that the influence of P on the dielectric properties of the multiferroic is caused by decreasing the porosity of grains during RLS and, as a result, decrease in a charge accumulation on the boundaries. The promising RLS method and the established regularities of the compacting pressure effect P on the dielectric constant can be used for controlling magnetoelectric coupling in bismuth ferrite multiferroics.

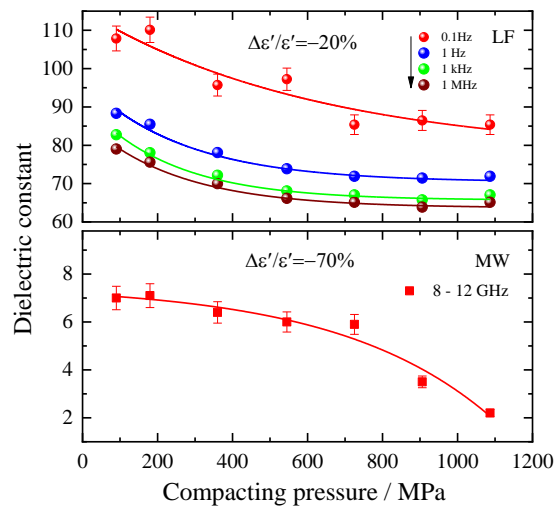


Figure 1. Influence of the compacting pressure on the dielectric constant of the $\text{Bi}_{0.9}\text{La}_{0.1}\text{FeO}_3$ multiferroic in the low-frequency (LF) and microwave (MW) ranges.

Preparation of $\text{BiFe}_{1-x}\text{Mn}_x\text{O}_3$ solid solutions via low temperature sol-gel synthesis route

R. Diliautas¹, D. Karoblis¹, K. Mazeika², D. Baltrunas², A. Beganskiene¹, A. Kareiva¹

1- Faculty of Chemistry and Geosciences, Vilnius University, Naugarduko 24, LT-03225 Vilnius, Lithuania

2- State Research Institute Center for Physical Sciences and Technology, LT-02300 Vilnius, Lithuania

ramunas.diliautas@chgf.stud.vu.lt

Multiferroicity is regarded as very prominent property of materials due to possible applications in spintronics [1], sensors [2], data storage [3] etc. In materials, which show ferroelectricity and ferromagnetism at the same time, the magnetization can be handled by application electric field and polarization – by magnetic field [4]. Two of the most prominent multiferroic materials are bismuth ferrite (BiFeO_3) and bismuth manganite (BiMnO_3). While BiFeO_3 can be prepared by different synthetic approaches, synthesis of pure BiFeO_3 remain problematic. Similarly, preparation of BiMnO_3 at ambient conditions is still complex task. Previous studies show that substitution of Fe^{3+} to +4 valence ions or appearance of lattice defects can lead to improved magnetic properties and easier synthesis conditions [5].

In this study $\text{BiFe}_{1-x}\text{Mn}_x\text{O}_3$ solid solutions were prepared by low temperature sol-gel synthesis route. Metal nitrates were used as starting materials. Firstly, all required nitrates were dissolved in distilled water and ethylene glycol was added as complexing agent. The obtained precursor was homogenized under constant stirring at 90 °C for 1 h and the plate temperature was increased to 150 °C for gel formation. Thermal behavior of precursor gel was investigated by thermogravimetric and differential scanning calorimetry (TG-DSC) measurements. For the characterization of obtained samples X-ray diffraction (XRD) analysis, scanning electron microscopy (SEM), Fourier transform infrared spectroscopy (FTIR) and other methods were used.

The obtained results showed that monophasic samples form up to 25 mol%. Furthermore, it was observed that structure can be indexed by rhombohedral or orthorhombic unit cell depending upon Mn^{3+} concentration. Also smaller particles form when Mn^{3+} is present at the structure.

Acknowledgments

This work was supported by a Research grant BUNACOMP (No. SMIP-19-9) from the Research Council of Lithuania.

[1] H. Béa, M. Gajek, M. Bibes, and A. Barthélémy, Spintronics with multiferroics, *J. Phys. Condens. Matter*, vol. 20, no. 43, pp. 434221, (2008).

[2] H. Palneedi, V. Annareddy, S. Priya, J. Ryu, Status and perspectives of multiferroic magnetoelectric composite materials and applications, *Actuators*, vol. 5, pp. 9 (2016).

[3] M. Bibes and A. Barthélémy, Towards a magnetoelectric memory, *Nat. Mater.*, vol. 7, no. 6, pp. 425–426, (2008).

[4] G. Schileo, C. Pascual-Gonzalez, M. Alguero, I. M. Reaney, P. Postolache, L. Mitoseriu, K. Reichmann, A. Feteira, Yttrium iron garnet/barium titanate multiferroic composite, *J. Am. Ceram. Soc.*, vol. 99, pp. 1609-1614, (2016)

[5] V. R. Palkar, D. C. Kundaliya, and S. K. Malik, Effect of Mn substitution on magnetoelectric properties of bismuth ferrite system, *J. Appl. Phys.*, vol. 93, no. 7, pp. 4337–4339, (2003).

Synthesis and characterization of YMnO_3 - GdMnO_3 solid solutions via sol-gel method

D. Karoblis¹, A. Zarkov¹, A. Beganskiene¹, D. Baltrunas², K. Mazeika², G. Niaura³, A. Kareiva¹

1- Institute of Chemistry, Vilnius University, Naugarduko 24, LT-03225 Vilnius, Lithuania

2- Center for Physical Sciences and Technology, Vilnius LT-02300, Lithuania

3- Institute of Chemical Physics, Faculty of Physics, Vilnius University, Sauletekio Ave. 3, LT-10257, Vilnius, Lithuania

dovydas.karoblis@chgf.vu.lt

Recently, there has been a lot of interest in multiferroic materials, which exhibit two or more “ferroic” (ferromagnetism, ferroelasticity and ferroelectricity) properties at once. Those materials offer new range of applications like AC/DC magnetic field sensors, microwave resonators, new data storage media, gyrators etc [1]. One of those materials is YMnO_3 . It has a relative high Curie temperature ($T_C \sim 900$ K) and low Neel temperature ($T_N \sim 70$ K) [2, 3]. It was shown, that this material can couple both ferroelectric and antiferromagnetic properties. Other perovskite type material, where magnetic and ferroelectric orders coexist is GdMnO_3 [4]. It was demonstrated that synthesis of different composition solid solutions is a promising tool for tuning of physical properties of functional materials.

In this study, solid solutions of YMnO_3 - GdMnO_3 have been synthesized using an aqueous sol-gel method. The conditions for obtaining pure single-phase compounds were determined. The thermal behaviour of precursor gels was investigated by thermogravimetric and differential scanning calorimetry (TG-DSC) measurements. X-ray diffraction (XRD) analysis was performed for the characterization of phase purity and crystallinity. Rietveld analysis was employed to calculate lattice parameters of the synthesized species. For the investigation of structural properties of obtained solid solutions by Mössbauer spectroscopy, Mn ions were partially substituted with ^{57}Fe and XRD patterns of these samples are represented in Figure 1. Scanning electron microscopy (SEM) was employed for the estimation of morphological features. Moreover, YMnO_3 - GdMnO_3 specimens were also characterized by FT-IR, Raman spectroscopy. Also magnetization measurements were carried out for all samples.

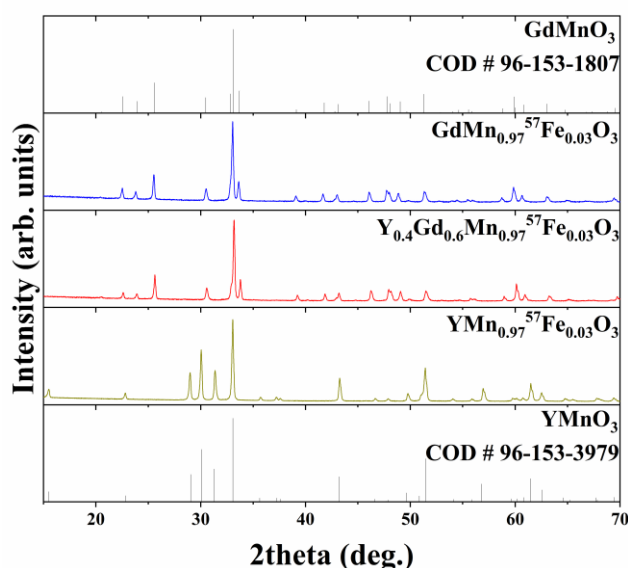


Figure 1. XRD patterns of $\text{Y}_x\text{Gd}_{1-x}\text{Mn}_{0.97}\text{Fe}_{0.03}\text{O}_3$ solid solutions.

Acknowledgments

This work was supported by a Research grant BUNACOMP (No. SMIP-19-9) from the Research Council of Lithuania.

- [1] M. M. Vopson Fundamentals of multiferroic materials and their possible applications, Critical Reviews in Solid State and Materials Sciences, vol. 40, pp. 223-250 (2015).
- [2] D. Khomskii, Classifying multiferroics: Mechanisms and effects, Physics 2, vol. 20 (2009).
- [3] A. S. Gibbs, K. S. Knight, P. Lightfoot, High-temperature phase transitions of hexagonal YMnO_3 , Physical Review B, vol. 83(9) (2011).
- [4] X. Li, C. Lu, J. Dai, S. Dong, Y. Chen, N. Hu, G. Wu, M. Liu, Z. Yan, J. M. Liu, Novel multiferroicity in GdMnO_3 thin films with self-assembled nano-twinned domains, Scientific Reports, vol. 4, pp. 7019 (2014).

In-plane lattice parameters and structural transitions on SrTiO₃ (001) surface at low temperatures

N. Krainyukova¹, V. Hamalii¹, A. Popov², E. Kotomin²

1- B. Verkin Institute for Low Temperature Physics and Engineering of the National Academy of Sciences of Ukraine, 47 Nauky Ave., Kharkiv 61103, Ukraine

2- Institute of Solid State Physics, University of Latvia, 8 Kengaraga St., Riga LV-1063, Latvia

Email: krainyukova@ilt.kharkov.ua ; popov@latnet.lv

The smooth (001) surfaces of SrTiO₃ (STO) single crystals were investigated by the reflection high-energy electron diffraction (RHEED) method in the temperature range from 5 to 300 K. The precisely measured lattice parameters are very sensitive to any structural transformations [1]. Five structural anomalies were found depending on temperature (Figure 1d). The antiferrodistortive (AFD) phase transition from the cubic structure to tetragonal (#3) observed in the STO bulk at 105 K on the surface extends from 70 to 120 K. The anomalies below 7 K (#1) and about 35 K (#2) are similar to those in the bulk considered as a crossover between the growth of the ferroelectric atomic displacements with decreasing temperature and quantum-mechanical stabilization of this growth due to the zero-point atomic motion. The other two anomalies (#4&5) are related only to a surface. Differentiation of lattice parameters depending on the depth from a surface revealed nonmonotonic changes (Figures 1a, 1b), which could be used for detecting the structural transformations.

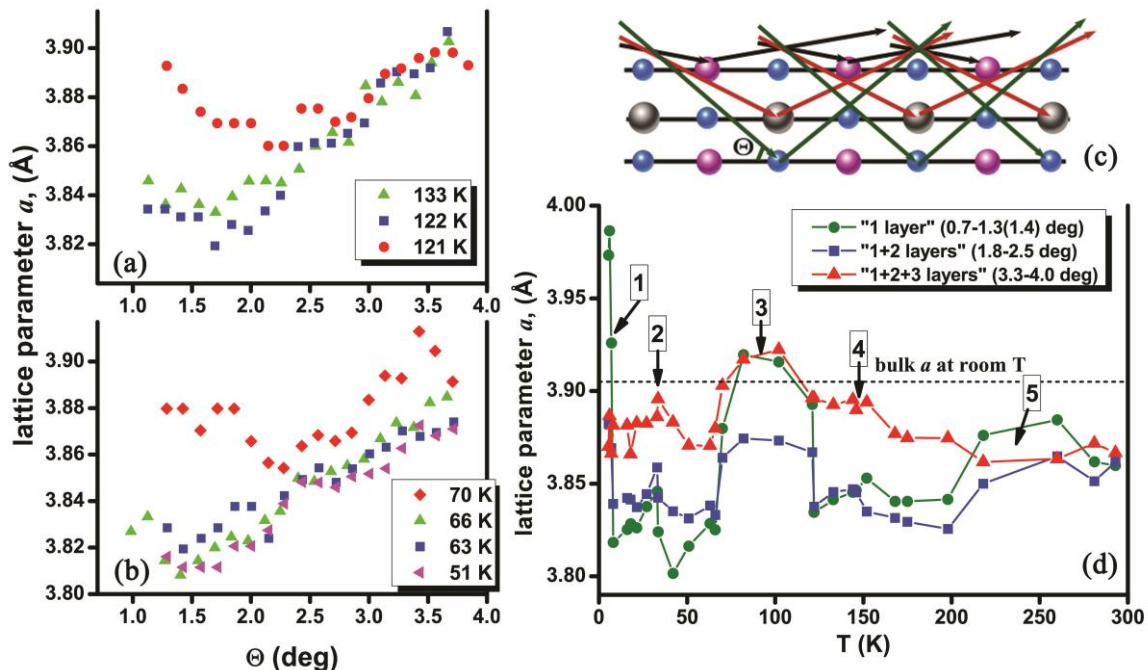


Figure 1 Surface in-plane lattice parameters as the functions of the electron incidence angle on the STO (001) surface or on the depth of electron penetration into a crystal at the beginning of the phase transition at ~ 120 K at decreasing temperatures (a), which is likely to be of the same AFD type as in the bulk at $T \approx 105$ K and at the end of the structural transformations at ~ 70 K (b). Dependence of the in-plane lattice parameters (parallel to the surface (001) STO) on the temperature (d). Using circles, squares, and triangles, we distinguish the data related solely to the first surface layer, to a mixture of the first and second layers and the averaged data over the three surface layers, respectively (d). This owes to the screening effect of the upper layers on the surface on the deeper electron penetration into a crystal (c). The numbers (#) are used for convenience of description of five structural transformations on the STO (001) surface (d).

Since the surface symmetry and energetics imposes differences in lattice parameters in parallel to a surface with respect to the bulk, this effect results in weak incommensurability between lattice parameters in surface layers and the bulk relaxed due to step edges and misfit dislocations [1,2].

This work was supported by the Ministry of Education and Science of Ukraine under the Contract No. M/22–2020 and by the Latvian–Ukrainian Grant LV-UA/2018/2.

[1] N.V. Krainyukova, V.O. Hamalii, A.V. Peschanskii, A.I. Popov, and E.A. Kotomin, Low temperature structural transformations on the (001) surface of SrTiO₃ single crystals, *Fiz. Nizk. Temp./Low Temp. Phys.*, 46, 877-888 (740-750), (2020).

[2] V.O. Hamalii, A.V. Peschanskii, A.I. Popov, and N.V. Krainyukova, Intrinsic nanostructures on the (001) surface of strontium titanate at low temperatures, *Fiz. Nizk. Temp./Low Temp. Phys.*, 46, N12, (2020).

Synthesis, structure, and dielectric properties of XPbBr_3 ($\text{X}=\text{MA}, \text{FA}, \text{Cs}$) and $\text{Cs}_2\text{AgBiBr}_6$ perovskite single crystals

A. Karabanov¹, M. Escobar¹, V. V. Shvartsman¹, Š. Svirskas², S. Balčiūnas², A. N. Salak³, J. Banys², D. C. Lupascu¹

1- Institute for Materials Science and Center for Nanointegration Duisburg-Essen (CENIDE), University of Duisburg-Essen, Universitätsstraße 15, 45141 Essen, Germany

2 - Faculty of Physics, Vilnius University, Sauletekio av. 9, LT-10222 Vilnius, Lithuania

3- Department of Materials and Ceramics Engineering, CICECO-Aveiro Institute of Materials, University of Aveiro, 3810-193 Aveiro, Portugal

andrei.karabanov@uni-due.de

In the last ten years, enormous efforts have been put into the research of hybrid perovskites as an absorbing material for solar cells. These materials show excellent photovoltaic properties not only in single, but also in tandem devices. However, the physical nature and the underlying mechanisms of such excellent photovoltaic performance are still unclear. Therefore, it is important to study the properties of these materials in single crystalline form.

Here we report on solution growth of XPbBr_3 ($\text{X} = \text{MA}, \text{FA}, \text{Cs}$) and $\text{Cs}_2\text{AgBiBr}_6$ single crystals. Concentration of the solution, temperature, heating and cooling rate were found for the successful growth of good quality single crystals with dimensions ranging from $5 \times 5 \text{ mm}^2$ to $10 \times 10 \text{ mm}^2$. XRD measurements prove that the single crystals do not show any other phases and have a proper stoichiometry. Temperature dependent dielectric impedance measurements were conducted to reveal phase transitions, one of the examples for CsPbBr_3 can be seen in the Figure 1. We have compared the results of dielectric measurements with calorimetry and structure data and discuss the effect of the A-site cations on dielectric response and polarization dynamics.

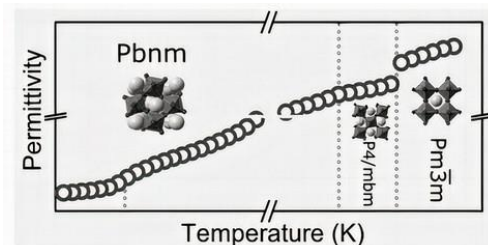


Figure 1 Temperature dependence of the permittivity of the CsPbBr_3 single crystal [1]

[1] Š. Svirskas, S. Balčiūnas, M. Šimėnas, G. Usevičius, M. Kinka, M. Velička, D. Kubicki, M. Escobar C., A. Karabanov, V. V. Shvartsman, M. de Rosário Soares, V. Šablinskas, A. N. Salak, D. C. Lupascu and J. Banys, Phase transitions, screening and dielectric response of CsPbBr_3 , J. Mater. Chem. A, 8, pp. 14015–14022, (2020).

Influence of sintering temperature on NBT ceramics

M. Duncce, E. Birks, M. Antonova, L. Bikshe, S. Dutkevica, O. Freimanis, A. Atvars

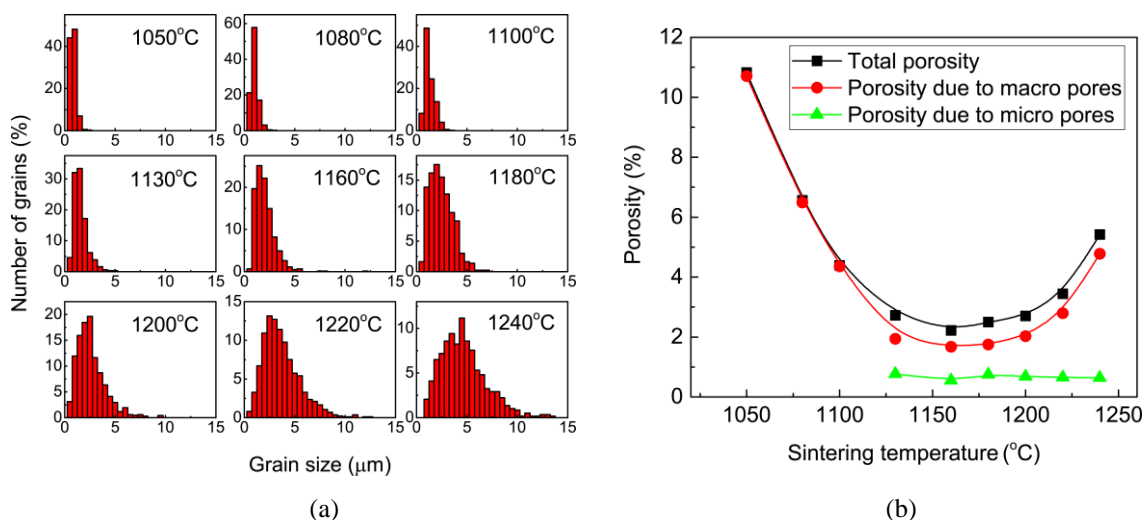
*Institute of Solid State Physics, University of Latvia,
Kengaraga 8, LV-1063, Riga, Latvia*

marija.duncce@cfi.lu.lv

$\text{Na}_{0.5}\text{Bi}_{0.5}\text{TiO}_3$ (NBT) is intensively studied in the last years due to being a good candidate for replacement of nowadays widely used lead-containing ferroelectrics, use of which is being gradually limited due to health and environmental considerations. Although research of modification of properties of NBT-based compositions is a hot topic, there is very little attention paid to their characterization from the aspect of ceramics and process of its producing. Apparently, it partly explains some discrepancies regarding the results of published studies, devoted to the same compositions, and reduces quality of their interpretation.

Here we have prepared and studied NBT compositions prepared by conventional ceramics sintering method from oxides and carbonates, varying the sintering temperature in a wide range from 1020oC to 1240oC. Content and homogeneity of the obtained NBT ceramic compositions were studied by means of XRD, SEM and EDX techniques.

Analysis of the SEM micrographs indicates smooth increasing of the average grain size and broadening of the grain size distribution, upon increasing of the sintering temperature. Whereas porosity as a function of sintering temperature has a minimum around 1160°C. Moreover, it is shown that macro-pores give the main contribution to porosity, while the contribution from micro-pores is comparatively very small and almost independent from sintering temperature. Thorough analysis of inhomogeneity of the NBT ceramics was also performed. A change



of inclusion character was detected, upon change of sintering temperature. The constituent elements and their concentrations in different inclusions, as well as in the matrix grains were locally analyzed, using EDX, and discussed in the context of change of the sintering temperature. For all compositions, it was shown that the concentrations of the constituent elements in the matrix grains is practically the same and does not change upon varying the sintering temperature. This indicates that compensation of the probable Bi-deficiency is realized more likely by means of composition and concentration of the inclusions than by change of composition of the matrix grains. Mutual connection between microstructure and ferroelectric properties of the NBT ceramics is recovered, involving measurements of dielectric permittivity and polarization.

This work has been funded by the European Regional Development Fund in the framework of the postdoctoral research project No. 1.1.1.2/VIAA/3/19/558.

First principles modelling of water adsorption and dissociation on flat and faceted SrTiO₃ surfaces

Yu. A. Mastrikov¹, G. Zvejnieks¹, L. L. Rusevich¹, E. A. Kotomin^{1,2}

1- Institute of Solid State Physics, University of Latvia, Riga, Latvia

2- Max Planck Institute for Solid State Research, Stuttgart, Germany

Yuri.Mastrikov@cfi.lu.lv

The search for novel materials promoting effective H₂O photodissociation with hydrogen production is fuelled by both environmental as well as scientific point of view. The engineering challenge is to find an efficient material that stays stable during repetitive catalytic reaction cycles without losing its properties.

In this work, we use first principles linear combination of atomic orbitals (LCAO) approach with hybrid density functional theory (DFT) formalism as implemented in CRYSTAL17 code [1] to model various H₂O adsorption and dissociation steps on SrTiO₃. In particular we consider molecular and dissociative H₂O adsorption on flat SrTiO₃ (001) surface in a low adsorbate coverage limit and compare our results with other theoretical simulations [2-4]. We extend our calculations to model H₂O on a faceted SrTiO₃ surfaces and analyze the surface stability during dissociation reaction. Finally, we have analyzed the initial step of H₂O dissociation reaction when water molecule is adsorbed next to an electron hole on a flat SrTiO₃ (001) surface.

[1] R. Dovesi, V. R. Saunders, C. Roetti, R. Orlando, C. M. Zicovich-Wilson, F. Pascale, B. Civalieri, K. Doll, N. M. Harrison and I. J. Bush, et al., CRYSTAL17 User's Manual, University of Torino, Torino, 2017.

[2] H. Guhl, W. Miller, K. Reuter Phys. Rev. B, 81, 155455 (2010).

[3] B. B. Hinojosa, T. van Cleve, A. Asthagiri, Mol. Simul., 36, 604 (2010).

[4] E. Holmström, P. Spijker, A. S. Foster, Proc. F. Soc. A, 472, 20160293 (2016).

Band gap engineering of SrTiO₃ photocatalyst for sunlight-driven water splitting: *ab initio* simulations

L.L. Rusevich¹, G. Zvejnieks¹, Yu.A. Mastrikov¹, E.A. Kotomin¹, M. Maček Krzmann²

1 – Institute of Solid State Physics, University of Latvia, Riga, Latvia

2 – Faculty of Chemistry, University of Ljubljana, Slovenia

Yuri.Mastrikov@cfi.lu.lv

The efficient solar-driven energy production continues to attract great interest in the last years. Sunlight-driven water splitting is one of the most promising pollution-free strategies for production of hydrogen. Photocatalytic water splitting consists of water decomposition into hydrogen and oxygen by a reaction with photo-generated charge carriers. Band engineering is one of the ways for development of the optimal photocatalytic material with both strong visible light absorption and high charge mobility. Band gap of efficient photocatalyst must be above 1.23 eV, to achieve water splitting, but less than 2.7 eV, to use efficiently a visible light. Moreover, the special conditions exist also for energy positions for boundaries of valence and conduction bands.

In this study, we used *ab initio* (first-principles) calculations, to investigate the structural and electronic properties of SrTiO₃ (STO) perovskite photocatalyst (band gap 3.25 eV) and to modify its electronic band structure in desired direction by means of defects and impurities. Unrestricted DFT (open-shell) calculations were performed with the CRYSTAL17 computer code within the linear combination of atomic orbitals (LCAO) approximation with using B1WC advanced hybrid functional. We considered first the bulk STO crystal and its (001) slabs, and then employed a supercell model to simulate point defects (neutral and charged oxygen vacancies, nitrogen and aluminum substitutional atoms). Our computations demonstrate that creation of defects indeed makes STO photocatalyst more efficient for sunlight-driven water splitting.

The calculated bandgap values of stoichiometric STO and reduced SrTiO_{3-δ} were compared with the optical bandgaps, determined experimentally by means of diffuse reflectance spectroscopy and Kubelka-Munk method.

Second Harmonic Generation in Generalized Ferroelectric Superlattices

Zafer Ozer¹, Selami Palaz², Amirullah M. Mamedov^{*3,4} Ekmel Ozbay³

1- Mersin Vocational High School, Mersin University, Mersin, Turkey, (+90) 324-4822221 ; zaferozzer@hotmail.com

2- Faculty of Science, Department of Physics, Haran University, Turkey, (+90) 414-3183541, spalaz@harran.edu.tr

3- Nanotechnology Research Center, Bilkent University, Bilkent, Ankara, Turkey, (+90) 312-2664042 ; mamedov@bilkent.edu.tr ;

ozbay@bilkent.edu.tr

4- Baku State University, International Scientific Center, Baku, Azerbaijan

*mamedov@bilkent.edu.tr

The goal of the work presented in this investigation is to achieve efficient parametric interaction of narrow beams (in particular second harmonic generation-SHG) using nonlinear (ferroelectric) photonic crystal tuned to self-collimation (nondiffractive) regimes. The first part concerns the fundamentals of this idea showing that simultaneously selfcollimation regimes for both fundamental and second harmonic waves can be obtained in an 1D and 2D superlattices and lead to an amplification of the nonlinear interaction. The second part is more applied, dedicated to analyze the realization of this idea in realistic materials and configurations (Fibonacci, Thue-Morse or Cantor-like). A large enhancement of up to 5 orders of magnitude in SHG efficiency was observed for superlattices made with a Cantor/Fibonacci like quasiperiodic assembly of a nonlinear material and a metamaterial. The enhancement was found to depend much more on the electric field amplitude along the structure because of self-similarity effects than on the amount of nonlinear material, which opens the way to design superlattices for tailored applications in broad-band tunable lasers. The thicknesses of the substrates are changed to obtain the maximum frequency conversion in different structures. Tuning the thicknesses causes the second harmonic waves generated in each LiTaO₃ layer to interfere constructively. Also, the fundamental and second-harmonic wavelengths are both located at the photonic band gap edges, where the density of electromagnetic modes and the nonlinear interaction time are enhanced. Our results show that the SHG efficiencies were increased in quasiperiodic photonic crystals with respect to the periodic structure with the same number of LiTaO₃ layers. In Fibonacci photonic crystal structures there are more geometrical parameters that can be tuned to obtain the highest efficiencies. Furthermore, we used a Bragg mirror at one side of each structure to control the propagation direction of the generated second-harmonic waves and to decrease the backward waves, which led to enhancement of the forward waves. In addition, we have theoretically calculated the photonic band structure and optical properties of LiTaO₃ based photonic crystal superlattices.

A numerical study of second harmonic generation (SHG) in one-dimensional nonlinear photonic crystals based on full nonlinear system of equations, implemented by a combination of the method of finite elements and fixed-point iterations, is reported. This model is derived from a nonlinear system of Maxwell's equations, which partly overcomes the known shortcoming of some existing models relied on the undepleted-pump approximation. We derive a general solution of SHG in one-dimensional nonlinear photonic crystals structures. The convergence of our method is fast. Numerical simulations also show the conversion efficiency of SHG can be significantly enhanced when the frequencies of the fundamental wave are located at the photonic band edges or are assigned to the designed defect states.

Keywords: Second harmonic generation; Photonic crystal; Ferroelectric; Finite element method

Phononic Crystals with Archimedean-like Tiling: Band Structure and Transformation of Sound

Zafer Ozer¹, Amirullah M. Mamedov^{*2,3}, and Ekmel Ozbay²

1 Mersin Vocational High School, Mersin University, Mersin, Turkey, (+90) 324-4822221 ; zaferozzer@hotmail.com
*2 Nanotechnology Research Center, Bilkent University, Bilkent, Ankara, Turkey, (+90) 312-2664042 ; mamedov@bilkent.edu.tr ;
ozbay@bilkent.edu.tr*
3 Baku State University, International Scientific Center, Baku, Azerbaijan
** mamedov@bilkent.edu.tr*

In this study, we investigate acoustic wave propagation in ferroelectric based 3D phononic crystal slabs, wherein scatterers have different cross sections, by using the finite element method. The phononic crystal consists of scatterers embedded in the host material arranged in a square lattice and honeycomb lattice in different patterns (bathroom and ladybug tiling in Archimedean-like tiling). By determining the eigenmodes and band gaps, complete and accurate band structures and transmission spectra are obtained. Compared to traditional square lattice phononic crystals, it has been observed that the bands obtained in pattern structures may have some advantages in terms of the width and position. It was also shown that the low frequency response of two Archimedean Archimedean-like structures was similar with respect to the traditional square lattice.

Keywords: Archimedean-like tiling; Phononic crystal; Finite element method

Influence of the Phase Transition on the Mechanical, Electronic and Optical Properties of Sn₂P₂X₆ Compounds

Husnu Koc*¹, Selami Palaz², Amirullah M. Mamedov^{3,4}, Ekmel Ozbay³

1 - Department of Physics, Siirt University, Turkey

2 - Department of Physics, Harran University, Turkey

3- Nanotechnology Research Center (NANOTAM), Bilkent University, 06800 Bilkent, Ankara, Turkey

4- Address International Scientific Center, Baku State University, Baku, Azerbaijan

**husnu_01_12@hotmail.com*

In present paper, the structural, mechanical, and electronic properties of the Sn₂P₂X₆ (X=S, Se) compounds under different pressures by the density functional methods in the generalized gradient approximation have been examined in the ferroelectric (Pc) and paraelectric (P2₁ / c) phases. The generalized gradient approximation (GGA) and local density approximation (LDA) has been used for modeling exchange-correlation effects. The lattice parameters have been calculated in the optimization process. The calculated lattice parameters are in agreement with the experimental values. The elastic constants have been calculated using the strain-stress method and the other related quantities have been derived. The electronic band structure and the total and partial density of states corresponding to the these band structures for both phases have been calculated. The forbidden energy band gap value (E_g) obtained for ferroelectric and paraelectric phases at zero pressure is 2.12 eV and 1.74 eV, respectively. The nonlinear optical properties and electro-optic effects of Sn₂P₂S₆-Pc have been studied by the density functional theory (DFT) in the local density approximation (LDA). Our structural estimation and some other results are in agreement with the available experimental and theoretical data.

Rational Sol-Gel-Based Synthesis Design and Magnetic and Dielectric Properties Study of Selected Nanocrystalline Double and Triple Perovskites

Igor Djerdj¹, Jelena Bijelić¹, Dalibor Tatar¹, Sugato Hajra², Manisha Sahu², Ákos Kukovecz³, Zvonko Jagličić^{4,5}, Bernd M. Smarsly⁶

1- Josip Juraj Strossmayer University of Osijek, Department of Chemistry, Cara Hadrijana 8/A, HR-31000 Osijek, Croatia

2- Institute of Technical Education and Research Siksha O Anusandhan (Deemed to be University), Department of Electrical and Electronics Engineering, Bhubaneswar-751030, India

3- University of Szeged, Interdisciplinary Excellence Centre, Department of Applied and Environmental Chemistry, Rerrich Béla tér 1, H-6720 Szeged, Hungary

4- University of Ljubljana, Faculty of Civil and Geodetic Engineering, Jamova 2, SI-1000 Ljubljana, Slovenia

5- University of Ljubljana, Institute of Mathematics and Physics & Mechanics, Jadranska 19, SI-1000 Ljubljana, Slovenia

6- Justus-Liebig-Universität, Physikalisch-Chemisches Institut, Heinrich-Buff-Ring 17, D-35392 Gießen, Germany

igor.djerdj@kemija.unios.hr

Complex perovskites have attracted extensive attention due to their fascinating physical properties and novel features owing to the coexistence of the ferro/ferri-magnetic ground state and semiconducting behavior in the single material. The triple perovskite $\text{Sr}_3\text{Co}_2\text{WO}_9$ (SCWO) has been successfully synthesized for the first time in the nanocrystalline form with an average crystallite size of 23 nm using a high yield (81 %) aqueous citrate sol-gel method [1]. At room temperature, the crystal structure of $\text{Sr}_3\text{Co}_2\text{WO}_9$ is cubic, space group $Fm\bar{3}m$, with lattice parameter $a = 7.9073(6)$ Å. The formation of SCWO triple perovskite was studied in situ by X-ray diffraction and subsequently analyzed by the Rietveld analysis. The detected hysteresis loops with non-zero remanent magnetization and rather large coercive field reveal ferrimagnetic ordering with a Curie temperature of 144 K. The measured effective magnetic moment of $3 \mu_B$ is close to the expected value for rarely observed intermediate spin $S = 1$. It is found that the compound exhibits semiconducting properties with the optical band gaps equal to 3.52 eV (indirect) and 3.76 eV (direct), respectively, further confirmed by the determination of the AC conductivity, which in the measured temperature range (25 -500 °C at 1 kHz) lies within the interval from 10^{-5} - $10^{-4} \Omega^{-1} \text{cm}^{-1}$. The Maxwell-Wagner model is employed to describe the frequency dependent dielectric constant. The frequency-dependent AC conductivity follows the universal Jonscher's power law. Double perovskites with Sr_2NiMO_6 (M = Te, W) structure type have been similarly synthesized [2]. The reaction yielded phase pure nanocrystalline powders of two compounds Sr_2NiWO_6 (SNWO) and $\text{Sr}_2\text{NiTeO}_6$ (SNTO). According to the Rietveld refinement of powder X-ray diffraction data at room temperature Sr_2NiWO_6 is tetragonal ($I4/m$) and $\text{Sr}_2\text{NiTeO}_6$ is monoclinic ($C12/m1$) with average crystallite sizes of 49 and 77 nm, respectively. Structural studies have been additionally performed by Raman spectroscopy revealing optical phonons typical for vibrations of $\text{Te}^{6+}/\text{W}^{6+}\text{O}_6$ octahedra. Both SNTO and SNWO possess high values of dielectric constants (341 and 308, respectively) with low dielectric loss (0.06 for SNWO) at frequency of 1 kHz. These values decrease exponentially with the increase of frequency to 1000 kHz, with dielectric constant being around 260 for both compounds and dielectric loss being 0.01 for SNWO and 0.04 for SNTO. The Nyquist plot for both samples confirms the non-Debye type of relaxation behavior and the dominance of shorter-range movement of charge carriers. Magnetic studies of both compounds revealed antiferromagnetic behavior with T_N being 57 K for SNWO and 35 K for SNTO. Since they possess both magnetic and semiconductor properties, these materials could be a promising candidates to use in devices where its semiconducting properties would be spin-controlled.

[1] Jelena Bijelić, Anamarija Stanković, Martina Medvidović-Kosanović, Berislav Marković, Pascal Cop, Yu Sun, Sugato Hajra, Manisha Sahu, Jelena Vukmirović, Dean Marković, Akos Kukovecz, Zvonko Jagličić, Bernd M. Smarsly, and Igor Djerdj, Rational Sol-Gel-Based Synthesis Design and Magnetic, Dielectric, and Optical Properties Study of Nanocrystalline $\text{Sr}_3\text{Co}_2\text{WO}_9$ Triple Perovskite, *J. Phys. Chem. C* 124 23, 12794-12807 (2020).

[2] Jelena Bijelić, Dalibor Tatar, Sugato Hajra, Manisha Sahu, Sang Jae Kim, Zvonko Jagličić and Igor Djerdj, Nanocrystalline Antiferromagnetic High- κ Dielectric Sr_2NiMO_6 (M = Te, W) with Double Perovskite Structure Type, *Molecules*, 25 17, 3996 (2020).

Charge carriers transport properties in PCPDTBT thin film transistor structures

Andrius Aukštuolis¹, Nerijus Nekrašas¹, Kristijonas Genevičius¹, Jūratė Jonikaitė-Švėgždienė², Giedrius Juška¹

1- Vilnius University, Faculty of Physics, Institute of Chemical Physics, Vilnius, Lithuania

2- Vilnius University, Faculty of Chemistry and Geosciences, Institute of Chemistry, Vilnius, Lithuania

Andrius Aukštuolis: andrius.aukstuolis@ff.vu.lt

In this study we investigated holes mobility in different directions in the organic field effect transistor structures with an active layer of PCPDTBT. Holes' mobility and its dependence on the temperature was measured by i-CELIV and current transient methods. The combination of both techniques allowed us to investigate properties of holes transport in different directions in the layer. Differential scanning calorimetry (DSC) measurements in the same temperature range were performed to investigate and explain morphological changes in the active layer of the field effect transistor structure. Accumulated results allowed to explain mechanisms how holes travel in the layer and to calculate energetic disorder parameter σ of Bäessler's Gaussian Disorder Model (GDM). DSC and holes' transport properties results let to outcome that the change in PCPDTBT's morphology strongly affects holes' mobility in the field effect transistor structure.

Keywords: PCPDTBT, OFET, i-CELIV, DSC, mobility, morphology.

Low frequency noise and resistivity characteristics of epoxy composites with variety of onion-like carbon

M. Tretjak¹, S. Pralgauskaitė¹, J. Matukas¹, J. Macutkevič¹, J. Banys¹,
V. Fierro², A. Celzard², S. Schaefer², O. Shenderova³

1- Institute of Applied Electrodynamics and Telecommunications, Vilnius University, Sauletekio 3, 10257 Vilnius, Lithuania

2- Université de Lorraine, CNRS, IJL, F-88000 Epinal, France

3- International Technology Center, Raleigh, NC 27715, USA

marina.tretjak@ff.vu.lt

The development of composite materials with different carbon fillers leads to the changes in many areas of human life. The great interest in these materials can be explained by their special mechanical, chemical and electrical properties, which allow fabrication of high quality, promising structures. Carbon nanoparticles, which can bind in aggregates and form micro and macromolecular systems, are currently being extensively studied. One of these are onion-like carbon (OLC) particles: a spherical multilayer structure belonging to the fullerene family [1]. OLC structures were discovered almost simultaneously with the well-known carbon nanotubes (CNTs). Nevertheless, much more attention was paid to the tubes. But, in 2000 interest in onion-like carbon returned due to the promising their applications in electronics, electrochemistry, nonlinear optics, biomedicine [2]. The main advantage of the OLC composites is that their fabrication is simpler and less expensive comparing to the above-mentioned CNTs. The electromagnetic properties of composites with OLC strongly depend on the particle size, density, distribution in the matrix. This allows fabrication of the material with desirable electrical, chemical, thermal, and other properties [3] and opens the way for versatile studies on the electrophysical properties of polymer composites. One of the informative study of the new composites with different fillers, evaluation of efficiency of their manufacturing methods is measurement of the low frequency noise. In this work, analysis of the low frequency noise and resistivity characteristics, which helps to clarify mechanisms of the charge carrier transport in the composites and structural changes of such materials caused by the temperature variation was carried out.

The set of investigated materials includes hybrid composites of epoxy resin with OLC fillers. Three groups of OLC particles of different size: 40 nm, 100 nm, and (200-250) nm, were used as filler. And materials of different filler concentration: 2 vol%, 5 vol%, 7 vol%, 10 vol%, 15 vol%, were investigated [4]. The measured noise signal (in the frequency range from 10 Hz to 20 kHz) was processed by a low-noise amplifier, a filter system and an analog-to-digital converter [5]. Noise spectra were obtained by the Fast Fourier Transform and the voltage noise spectral density was evaluated by comparing with the thermal noise of the load resistance.

The density of the OLC fillers and their size have direct effect on the conductivity of the composite: conductivity is larger for materials with larger concentration and larger particles. At low voltage (approximately up to 5 V (at fixed temperature)) the resistance of samples is constant, and at increasing voltage it decreases, what is typical for composites with conducting fillers, and this characteristic type does not depend on the particles size and their concentration. As temperature increases resistance of the sample decreases approximately up to 250 K. In this temperature range, the dominant induced tunnel transport of charge carriers can be observed. At higher temperature, the resistivity starts to increase due to the expansion of the epoxy matrix; and above 325 K, it decreases with onset of conductivity in the matrix.

Low-frequency fluctuations of the materials under study have $1/f^\alpha$ -type spectra. $1/f^\alpha$ -type fluctuations are result of the superposition of many generation and recombination processes of similar intensity and with widely distributed characteristic times. Some investigated samples exhibited the random telegraph noise at particular temperature. The voltage noise spectral density is approximately proportional to the voltage square. Consequently, the observed voltage fluctuations are caused by the resistance fluctuations resulting from the random processes of the charge carrier capture and release in the defects formed centers.

[1] O. Mykhailiv, H. Zubyk, M. E. Plonska-Brzezinska, Carbon nano-onions: Unique carbon nanostructures with fascinating properties and their potential applications, *Inorganica Chimica Acta*, 468, 49–66 (2017).

[2] D. M. Brus, O. Mykhailiv, L. Echevoyen, M. E. Plonska-Brzezinska, in: *Carbon Nanomaterials Sourcebook*, vol. 1, ed. K. D. Sattler (CRC Press, New York) pp. 275 – 295 (2016).

[3] V. L. Kuznetsov, S. I. Moseenkov, K. V. Elumeeva, T. V. Larina, V. F. Anufrienko, A. Romanenko, O. B. Anikeeva, E. N. Tkachev, Comparative study of reflectance properties of nanodiamonds, onion - like carbon and multiwalled carbon nanotubes, *Physica Status Solidi B*, 248, 2572–2576 (2011).

[4] E. Palaimiene, J. Macutkevic, J. Banys, A. Selskis, V. Fierro, A. Celzard, S. Schaefer, O. Shenderova, Ultra-low percolation threshold in epoxy resin–onion-like carbon composites, *Appl. Phys. Lett.*, 113, 033105, (2018).

[5] I. Zamaraitė, J. Matukas, S. Pralgauskaitė, Yu. Vysochanskii, J. Banys, A. Dziazugys, Low-Frequency Noise Characteristics of Lamellar Ferrielectric Crystal CuInP2S6 at the Phase Transition, *J. Appl. Phys.*, 122, 024101 (2017).

Electrical conductivity of superionic $(\text{Ag}_x\text{Cu}_{1-x})_7\text{GeS}_5\text{I}$ and $(\text{Ag}_x\text{Cu}_{1-x})_7\text{GeSe}_5\text{I}$ mixed crystals

I. Studenyak¹, O. Yamkovy¹, A. Pogodin¹, O. Kokhan¹, V. Kavaliukė², T. Šalkus², A. Kežionis²

1- Uzhhorod National University, 46 Pidhirna St., 88000 Uzhhorod, Ukraine

2- Vilnius University, Saulėtekio al. 9, LT-10222 Vilnius, Lithuania

Main author email address: tomas.salkus@ff.vu.lt

$\text{Cu}_7\text{GeS}_5\text{I}$ and $\text{Ag}_7\text{GeS}_5\text{I}$ compounds as well as their selenium-containing counterparts $\text{Cu}_7\text{GeSe}_5\text{I}$ and $\text{Ag}_7\text{GeSe}_5\text{I}$ belong to the family of the argyrodite-type superionic conductors [1]. This makes them, along with other copper- and silver-containing argyrodites, promising materials for solid electrolyte accumulators, supercapacitors, and electrochemical sensors [2, 3]. Growth processes, some physical and chemical properties of $\text{Cu}_7\text{GeS}_5\text{I}$ and $\text{Cu}_7\text{GeSe}_5\text{I}$ crystals were studied in several papers [2, 3]. The aim of this paper is to investigate the structure parameters and electrical conductivity of $(\text{Cu}_{1-x}\text{Ag}_x)_7\text{GeS}_5\text{I}$ and $(\text{Cu}_{1-x}\text{Ag}_x)_7\text{GeSe}_5\text{I}$ mixed crystals as well as to study the influence of cationic substitution on their electrical properties which are interesting both in fundamental and applied aspects.

$(\text{Cu}_{1-x}\text{Ag}_x)_7\text{GeS}_5\text{I}$ and $(\text{Cu}_{1-x}\text{Ag}_x)_7\text{GeSe}_5\text{I}$ ($x=0, 0.25, 0.5, 0.75, 1$) mixed crystals were obtained by the zone crystallization from the melt using a modified method. Specificity of the modified method for growing crystals in the case of individual compounds is that in the growth ampoule the starting simple substances Ag, Cu, Ge, S, Se and pre-synthesized CuI (AgI) are loaded in the corresponding stoichiometric ratios, further purified by vacuum distillation (CuI) and by directed melt crystallization (AgI). As a starting material for growing $(\text{Cu}_{1-x}\text{Ag}_x)_7\text{GeS}_5\text{I}$ and $(\text{Cu}_{1-x}\text{Ag}_x)_7\text{GeSe}_5\text{I}$ mixed crystals we used previously synthesized $\text{Cu}_7\text{GeS}_5\text{I}$ and $\text{Ag}_7\text{GeS}_5\text{I}$ as well as $\text{Cu}_7\text{GeSe}_5\text{I}$ and $\text{Ag}_7\text{GeSe}_5\text{I}$, respectively. Growing of $(\text{Cu}_{1-x}\text{Ag}_x)_7\text{GeS}_5\text{I}$ and $(\text{Cu}_{1-x}\text{Ag}_x)_7\text{GeSe}_5\text{I}$ mixed crystals includes forming monocrystalline "nucleus" by accumulative recrystallization in the lower conical part of the growth container (48 hours). The displacement rate of the crystallization front was 0.4 mm/h. After moving the ampoule with the crystal into the annealing region, homogenizing annealing is carried out for 3 days, which is necessary for removing the thermal stresses in the crystals. Thus, $(\text{Cu}_{1-x}\text{Ag}_x)_7\text{GeS}_5\text{I}$ and $(\text{Cu}_{1-x}\text{Ag}_x)_7\text{GeSe}_5\text{I}$ mixed crystals with $x=0, 0.25, 0.5, 0.75, 1$ of 20-40 mm in length and 10 to 15 mm in diameter were obtained.

The structural studies were carried out with powder method using diffraction patterns obtained on a DRON-3 diffractometer (conventional θ - 2θ scanning method, Bragg angle $2\theta \cong 10$ - 60° , Ni-filtered CuK_α radiation). It was determined that $(\text{Cu}_{1-x}\text{Ag}_x)_7\text{GeS}_5\text{I}$ and $(\text{Cu}_{1-x}\text{Ag}_x)_7\text{GeSe}_5\text{I}$ compounds crystallize in cubic crystal system. The compositional dependence of cubic lattice parameter at cation substitution was obtained. It is shown that the increase of Ag content leads to the increase of cubic lattice parameter in $(\text{Cu}_{1-x}\text{Ag}_x)_7\text{GeS}_5\text{I}$ and $(\text{Cu}_{1-x}\text{Ag}_x)_7\text{GeSe}_5\text{I}$ mixed crystals.

Electrical properties of $(\text{Cu}_{1-x}\text{Ag}_x)_7\text{GeS}_5\text{I}$ and $(\text{Cu}_{1-x}\text{Ag}_x)_7\text{GeSe}_5\text{I}$ mixed crystals with $x = 0, 0.25, 0.5, 0.75$ were investigated by the impedance spectroscopy. The measurements for $(\text{Cu}_{1-x}\text{Ag}_x)_7\text{GeS}_5\text{I}$ mixed crystals were performed in the temperature range 300 – 360 K and in the frequency range 10 Hz – 10 GHz while for $(\text{Cu}_{1-x}\text{Ag}_x)_7\text{GeSe}_5\text{I}$ mixed crystals were carried out in the temperature range 292 – 378 K and in the frequency range 20 Hz – 2 MHz. It is shown that the total electrical conductivity of $(\text{Cu}_{1-x}\text{Ag}_x)_7\text{GeS}_5\text{I}$ decreased at $T = 300$ K with the increase of stoichiometric parameter x . The highest electrical conductivity value $\sigma_{100\text{Hz}} = 4.3$ S/m (activation energy $\Delta E = 0.17$ eV) was observed for $\text{Cu}_7\text{GeS}_5\text{I}$. The complex impedance plots were fitted with Zview software. The temperature dependences of the real part of complex conductivity for $(\text{Cu}_{1-x}\text{Ag}_x)_7\text{GeS}_5\text{I}$ and $(\text{Cu}_{1-x}\text{Ag}_x)_7\text{GeSe}_5\text{I}$ mixed crystals were described by Arrhenius law.

For the separation into ionic and electronic components, a standard approach using electrode equivalent circuits and their analysis on Nyquist plots was used. It is shown that the compositional dependence of ionic conductivity is nonlinear with maximum, whereas the electronic conductivity for $(\text{Cu}_{1-x}\text{Ag}_x)_7\text{GeSe}_5\text{I}$ mixed crystals nonlinearly decreases without any anomalies with silver content increase. It should be noted that at the transition from $\text{Cu}_7\text{GeSe}_5\text{I}$ crystal, where electronic conductivity is 39 times greater than the ionic one, to $\text{Ag}_7\text{GeSe}_5\text{I}$, the ratio $\sigma_{\text{ion}}/\sigma_{\text{el}}$ trends to increase and in $\text{Ag}_7\text{GeSe}_5\text{I}$ crystal the ionic conductivity is 4.5 times greater than the electronic one.

[1] T. Nilges and A. Pfitzner, A structural differentiation of quaternary copper argyrodites: Structure – property relations of high temperature ion conductors, *Z. Kristallogr.*, vol. 220, pp. 281–294 (2005).

[2] I.P. Studenyak, M. Kranjčec, Gy.Sh. Kovacs et al, Electrical and optical absorption studies of $\text{Cu}_7\text{GeS}_5\text{I}$ fast-ion conductor, *J. Phys.Chem. Solids*, vol. 63, pp. 267–271 (2002).

[3] I.P. Studenyak, M. Kranjčec, V.V. Bilanchuk et al, Temperature variation of electrical conductivity and absorption edge in $\text{Cu}_7\text{GeSe}_5\text{I}$ advanced superionic conductor, *J. Phys.Chem. Solids*, vol. 70, pp. 1478–1481 (2009).

The manganese ferrite effect on dielectric properties of MWCNT-based epoxy resin composites

D. Meisak^{1,2}, J. Macutkevic¹, J. Banys¹, P. Kuzhir^{3,2}

1- Vilnius University, Physics Faculty, Sauletekio al. 9 LT-10222 Vilnius, Lithuania

2- Research Institute for Nuclear Problems BSU, Babruiskaya st. 11, 220030 Minsk, Belarus

3- Institute of Photonics, University of Eastern Finland, Yliopistokatu st. 7 FI-80101 Joensuu, Finland

email: dariameysak@gmail.com

In present work, the dielectric and electrical properties of epoxy resin composites materials based on multiwalled carbon nanotubes (MWCNT) and manganese ferrite (MnFe_2O_4) nanopowder were studied in broad frequency (20 Hz – 40 GHz) and temperature (20 - 500 K) ranges.

Commercial Epikote 828 epoxy resin was used as a polymer matrix. The MWCNT grown by the CVD method [1] and commercially available manganese ferrite (MnFe_2O_4) nanopowder with 28 nm spherical particle size [2] were used as fillers. The standard procedure for filler particles dispersing in a polymer matrix was used in order to prepare the composites [3]. Using the mentioned above procedure, two series of composites with a fixed MWCNT-concentration and various small amount of MnFe_2O_4 were prepared. The first one had a MWCNT-content of 0.09 vol.% (just below percolation state in corresponding monofiller composites [4]), while the second one had higher MWCNT-concentration of 0.58 vol.% (above percolation threshold). Manganese ferrite concentration varied up to 0.65 vol.%. The complex dielectric permittivity was measured using the dielectric spectroscopy methods.

MnFe_2O_4 -concentration dependences of the real part of dielectric permittivity and electrical conductivity for composites of both series at room temperature and 129 Hz before and after annealing at 500 K are presented in Figure 1(a,b). In the second series (see Figure 1b), with the addition of manganese ferrite to the initially conductive MWCNT-composite, the electrical conductivity decreases. While for first series (see Figure 1a), the dielectric permittivity and the electrical conductivity of composites are strongly dependent on MnFe_2O_4 concentration and the electrical conductivity has the maximum close to 0.025 vol%, which gave up to 10^3 larger conductivity than that of composite without MnFe_2O_4 . It means that certain small amounts of MnFe_2O_4 particles improve the electrical properties of initially non-conductive MWCNT/epoxy resin composites due to the better

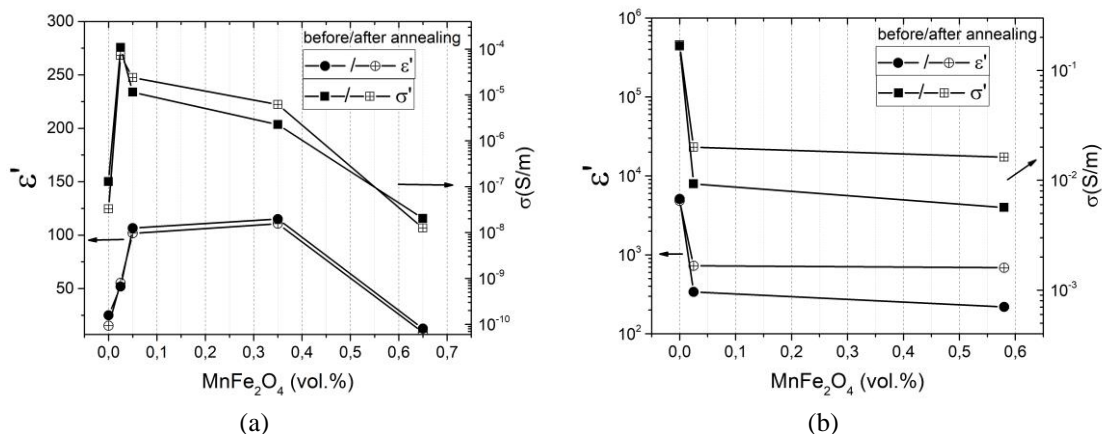


Figure 1 MnFe_2O_4 -concentration dependence of the real part of dielectric permittivity and electrical conductivity for composites with (a) 0.09 vol.% and (b) 0.58 vol.% of MWCNT at room temperature and 129 Hz before and after annealing at 500 K.

MWCNT dispersion inside polymer matrix.

The frequency and temperature dependencies of dielectric permittivity and electrical conductivity are presented. The electrical properties are discussed in terms of the complex impedance and distributions of relaxation times.

[1] A. Okotrub, L. Bulusheva, A. Kudashov et al., Arrays of carbon nanotubes aligned perpendicular to the substrate surface: Anisotropy of structure and properties, *Nanotechnologies in Russia*, vol. 3, pp. 191-200, (2008).

[2] <https://www.us-nano.com/inc/sdetail/7019>

[3] D. Meisak, J. Macutkevic, J. Banys et al., Dielectric properties and electrical percolation in MnFe_2O_4 /epoxy resin composites, *Physica Status Solidi A*, vol. 1900526, pp. 1-6, (2019).

[4] P. Bertasius, J. Macutkevic, J. Banys et al., Fine tuning of dielectric properties of epoxy/carbon nanotubes composites via magnesium oxide additives, *Polymers*, vol. 11, 2044, pp. 1-14, (2019).

DEVELOPMENT, CHARACTERISATION AND MODELING OF MECHANICAL PROPERTIES OF THE POLYPROPYLENE COMPOSITES WITH RENEWABLE FILLERS

J. Zicans¹, R. Merijs-Meri¹, T. Ivanova¹, M. Ziganova¹, A. Kovalov², P. Danilovas, A.K. Bledzki³, P. Franciszczak³

1- Institute of Polymer Materials, Faculty of Materials Science and Applied Chemistry, Riga technical University, 3 Paula Valdena street, Riga, LV-1048, Latvia

2- Institute of Materials and Structures, Faculty of Civil Engineering, Riga Technical University, 6B Kipsalas street, Riga, LV-1048, Latvia

3- Institute of Materials Science, West Pomeranian University of Technology, 19 Piastów Avenue, 70310, Szczecin, Poland

remo.merijs-meri@rtu.lv

Biobased polymer composites gain increased attention by considering the necessity of implementing Circular Economy principles. Consequently, the research is devoted to the development of polypropylene composites reinforced with spelt husks derived lignocellulosic microfibers. Spelt husk microfibers were obtained in a multiple-step process. Initially spelt husks were subjected to steam explosion treatment at various severity factors. Steam explosion treatment of spelt husk microfibers was performed at various combinations of 3 different temperatures (205°C, 220°C and 235°C) and 3 different times (1 min., 3 min. and 5 min.). After steam explosion treatment spelt husk microfibers were dried up to the constant mass and mechanically ground to yield suitable dimensions for extrusion processing. Compounding of polypropylene with spelt husk microfibers was performed using twin screw extruder. The content of spelt husk microfibers in the polypropylene matrix was fixed at 40 wt.%, thus making the composites suitable for processing by conventional injection moulding technique. Thus obtained polypropylene composites with spelt husk microfibers were characterised in respects to their structural, rheological, calorimetric, thermogravimetric, quasistatic (tensile, flexural) and dynamic (impact) mechanical properties. In addition, attention was paid to modeling of mechanical properties of the above mentioned polypropylene composites. Results of the investigation testify that elastic modulus and strength of the investigated ecocomposites increases by decreasing steam explosion treatment time and temperature. The relationships of strain and impact strength as functions of steam explosion treatment time and temperature were more complex. In the case of melt flow rate, the highest flowability was for the composites, containing spelt microfibers, obtained at higher treatment times and temperatures. In general, this testifies that high treatment temperatures and times should be avoided when preparing spelt husk microfibers by steam explosion treatment for compounding with polypropylene matrix.

Acknowledgment

This work has been financially supported by the M-ERA.NET Project HyBiCo

Dielectric/electric properties of the silver-PDMS nanocomposite

E. Palaimiene¹, J. Macutkevicius¹, J. Banys¹, A. Selskis²,
S. Schaefer³, V. Fierro³, A. Celzard³

1 - Institute of Applied Electrodynamics and Telecommunications, Vilnius University, Sauletekio 3, LT-10257 Vilnius, Lithuania

2 - Center for Physical Science and Technology, Sauletekio Ave. 3, Vilnius, Lithuania

3 - Université de Lorraine, CNRS, IJL, F-88000 Epinal, France

edita.palaimiene@ff.vu.lt

In the consumer technology market, there is a need for printed electronic devices for the manufacture of devices such as thin film transistors, sensors, radio frequency components and devices, transparent electrodes, electronic films, flexible personal healthcare sensors and more. The production and capabilities of these devices are topical issues in medicine, industry, and telecommunications. Currently, metal nanoparticles with a polymeric matrix have been studied and applied for these purposes [1]. One possible composite material is silver polydimethylsiloxane (Ag-PDMS) [2,3]. Therefore, the aim of present work is to investigate the dielectric properties of PDMS nanocomposites with different size Ag nanoparticles. The concentration dependence of the dielectric permittivity and the electrical conductivity at the frequency 129 Hz is presented in Fig. 1. It was established that the percolation threshold in the composites is close to 20 vol.% and it is dependent on the particles size. Above the percolation threshold values of the dielectric permittivity and the electrical conductivity are quite high $\epsilon' \approx 10^7$ and $\sigma \approx 0.1$ S/cm at room temperature and 129 Hz frequency. Therefore, composites with Ag nanoparticles can be used for various electronic applications. Moreover, the electronic transport mechanism in composites is discussed in the presentation.

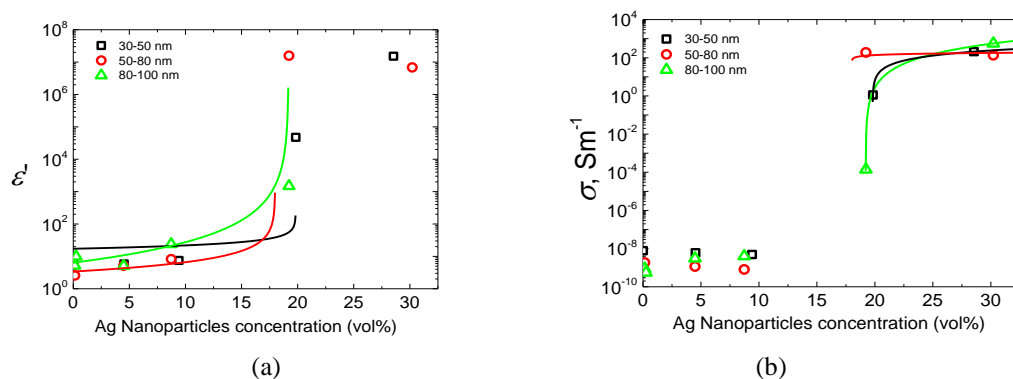


Figure 1 Dielectric permittivity (a) and the electrical conductivity (b) of Ag/PDMS composites vs Ag concentration and particle size at frequency 129 Hz and room temperature.

[1] J. Ozhikandathil, S. Badilescu, M. Packirisamy, Synthesis and characterization of silver-PDMS nanocomposite for the biosensing applications, Proc. SPIE 8007, Photonics North 2011, 800707 (2011).

[2] K.-H. Jung et al., Fabrication of Ag circuit embedded in PDMS substrate and its mechanical and electrical property with variations of photonic energy, Journal of Alloys and Compounds 748, 898-904, (2018).

[3] A. Larmagnac, S. Eggenberger, H. Janossy, J. Voros, Stretchable electronics based on Ag-PDMS composites, Scientific Reports 4, 7254 (2014).

Adsorption and desorption processes in the modified MgAl_2O_4 ceramics

H. Klym¹, I. Karbovnyk², I. Vasylyshyn¹, A.I. Popov³

¹-Lviv Polytechnic National University, 12 Bandera St., Lviv 79013, Ukraine

²-Ivan Franko National University of Lviv, 107 Tarnavskogo St., Lviv 79017, Ukraine

³-Institute of Solid State Physics, University of Latvia, 8 Kengaraga St., Riga, LV-1063, Latvia

klymija@yahoo.com; halyna.i.klym@lpnu.ua

It is known that spinel-type MgAl_2O_4 ceramics are one of the perspective materials for humidity sensors due to their advanced structure of grains, grain boundaries and open porosity [1]. In this work we study of absorption and desorption processes of water in the technologically modified MgAl_2O_4 ceramics sintered at 1300 °C and 1400 °C for 5 h and 9 h.

The MgAl_2O_4 ceramics were prepared from MgO and Al_2O_3 powders and sintered at maximal temperature (T_s) of 1300 °C and 1400 °C at duration (Δt) of 5 h and 9 h in respect to traditional ceramic technology [2]. For electrophysical investigations, the contact area with Ru paste and Pt contacts was formed. The electrical resistance was measured at 20 °C in the region of relative humidity (RH) from 20 % to 99 %. For study of stability in time, degradation test was performed at 40 °C and $RH = 95\%$ for 240 h.

It is shown that increasing of sintering duration of ceramics from 5 h and 9 h at 1300-1400 °C, the linearity dependence of electric resistance from RH in semi-logarithmic scale improves and the resistance continues to grow (Fig. 1). Along with this, investigated ceramic obtained at 1400 °C, $\Delta t = 5$ and 9 h are sensitive in the region of low RH (~ 25-40 %).

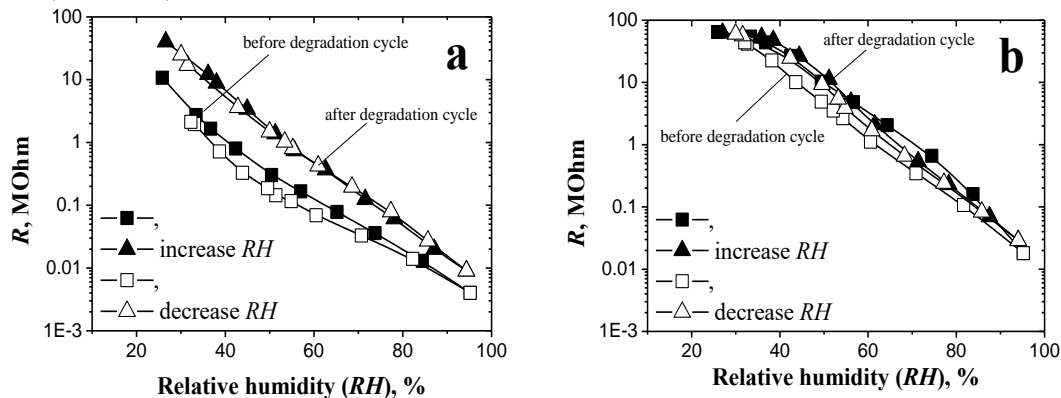


Figure 1 Dependence of electrical resistance from relative humidity for the MgAl_2O_4 ceramics sintered at 1300 °C, 5 h (a) and 1400 °C, 9 h (b) in adsorption-desorption cycles before and after degradation cycle

Most probably such changes are related to the evolution of porous structure of ceramics. Reducing the mesoporous range, whose radii are centered near 40-100 nm, leads to decrease in conductivity of the humidity in the investigated MgAl_2O_4 ceramics. It can be seen that the humidity sensitivity of ceramics, linearity of characteristics and minimal hysteresis in adsorption-desorption cycles are due to the three-dimensional pore size distribution. The loss of humidity-sensitivity in the low region of RH (25-40 %) is due to evolution of porous structure to bi-dimensional pore size distribution.

After degradation tests humidity-sensitivity is improved (sensitivity increases on the high region of $RH \approx 75-95\%$), as well the hysteresis of characteristics decreases. However, the change in electrical resistance changes for ceramic samples obtained at 1300 °C for 5 h and 9 h, while ceramics sintered at 1400 °C for 5 h and 9 h are well restored to their initial characteristics with practically complete absence of hysteresis. In ceramics obtained at 1300 °C, $\Delta t = 5$ h the area of humidity sensitivity is expanding to $\approx 25-95\%$. Increasing of sintering duration up to 9 h at 1300 °C and 1400 °C results in loss of sensitivity of samples in the region of $RH \approx 25-40\%$ (Fig. 1). Reducing the number of pores with a radius of 150 nm in ceramics obtained at 1300 °C, $\Delta t = 9$ h and their total absence in ceramics obtained at 1400 °C, $\Delta t = 9$ h leads to deterioration of conductivity of humidity.

This work was supported by the Ministry of Education and Science of Ukraine

- [1] A. Laobuthee, S. Wongkasemjit, E. Traversa, and R.M. Laine, MgAl_2O_4 spinel powders from oxide one pot synthesis (OOPS) process for ceramic humidity sensors, *J. Europ. Ceram. Soc.*, vol. 20(2), pp. 91-97 (2000).
- [2] H. Klym, I. Hadzaman, and O. Shpotyuk, Influence of sintering temperature on pore structure and electrical properties of technologically modified $\text{MgO-Al}_2\text{O}_3$ ceramics, *Materials Science*, vol. 21(1), pp. 92-95 (2015).

Electro-thermal properties of cross-linked carbon black (CB) and ethylene-vinyl acetate (EVA) composite

S. Eglite¹, A. Berzina¹, M. Knite¹

¹*Institute of Technical Physics, Faculty of Materials Science and Applied Chemistry, Riga Technical University, Riga, Latvia*

email: Sintija.eglite_3@rtu.lv

Self-regulating heating polymer materials are widely used in fields where flexible and safe temperature control is needed without overheating the main material. These are materials which have positive temperature coefficient of resistivity (PTC). When a voltage is applied to the material, the material heats up due to Joule heating. As the temperature of the material increases, the electrical resistance increases nonlinearly due to the PTC effect. At a particular temperature the material reaches an equilibrium state and does not overheat [1]. The aim of our research is to find a flexible material with self-regulating heating properties at a relatively low equilibrium temperature and which could be powered with a low voltage (USB charger (5V)). The best way how to create flexible, conductive materials is to use conductive polymer composites. Ethylene-vinyl acetate copolymer (EVA) starts to melt at around 70°C and in combination with highly structured carbon black nanoparticles the composite could have an equilibrium temperature around the human body comfort temperature.

In this research we investigated cross-linked carbon black and ethylene-vinyl acetate (VA content 40%) composites (EVA-CB). EVA was cross-linked using dicumyl peroxide (DCP) as cross-linking agent. The material was tested as a self-regulating heater so its electro-thermal properties were investigated, particularly the electrical resistance dependence from temperature externally (universal heating oven) and internally (applied voltage of 5 V) heating the material.

Samples were prepared by dissolving ethylene-vinyl acetate in chloroform and adding a mixture of 10 – 30 phr of CB ultrasonicated in chloroform. Different concentrations of dicumyl peroxide (1, 2 and 3 phr) were used to determine the most effective crosslinking degree. The acquired mixture is left to dry overnight in the fume hood for the solvent to evaporate. Next the composite is firstly melted into the desired form at 150°C under 30 kPa pressure for 5 minutes, secondly it is vulcanized at 150°C under 10 kPa for 25 minutes. For electrical resistance measurements silver glue electrodes are painted on opposite ends of the sample. The space between electrodes is 80 mm, but the total size of the samples is: width 100mm, length 69 mm and thickness 1,4 mm.

In this research, firstly we investigated the dependency of different carbon black concentrations for noncross-linked EVA-CB composites. These results show that with increasing concentration of CB, the equilibrium temperature increases, while the sample resistivity decreases. Noncross-linked EVA-CB composites in comparison to cross-linked EVA-CB composites show a lower equilibrium temperature and lower resistivity.

Secondly, we investigated DCP concentration dependence on the electro-thermal properties for samples with 30 phr of CB. Results show that cross-linked carbon black and ethylene-vinyl acetate composites exhibit positive temperature coefficient of resistivity. With increasing concentration of dicumyl peroxide, the equilibrium temperature decreases, while the overall resistivity of the samples increases. Samples with 2 phr dicumyl peroxide overall show the best results compared to samples with 1 or 3 phr dicumyl peroxide. Samples with 1 and 3 phr DCP are also difficult to obtain, because the formation process introduces cracks and other defects. We conclude that 2 phr of DCP is the optimal crosslinker concentration.

[1] Y. Liu, H. Zhang, H. Porwall, J. JC Bosfield, T. Peijs, E. Billoti, Pyroresistivity in conductive polymer composites: a perspective on recent advances and new applications, *Polym. Int.*, vol. 68, no. 3, pp. 299–305, (2019).

Fine Tuning of Electrical Transport and Dielectric Properties of Epoxy/Carbon Nanotubes Composites via Magnesium Oxide Additives

P. Bertasius¹, D. Meisak^{1,2}, J. Macutkevici¹, P. Kuzhir^{2,3},
A. Selskis⁴, E. Volnyanko⁵, J. Banys¹

1- Vilnius University, Sauletekio av. 3, Vilnius, Lithuania

2- Institute for Nuclear Problems, Belarusian State University, Minsk, Belarus

3- Institute of Photonics, University of Eastern Finland, Yliopistokatu 7, Joensuu, Finland

4- Center for Physical Science and Technology, Sauletekio Ave. 3, Vilnius, Lithuania

5- Metal Polymer Research Institute of the National Academy of Sciences of Belarus, Kirova str. 32a, Gomel, Belarus

Main author email address: pov.bertasius@gmail.com

The dielectric properties of epoxy resin/MWCNT (multi-walled carbon nanotubes)/MgO (40nm particle size) hybrid composites prepared by a solution mixing method with a fixed MWCNT amount of 0.12 vol.% (concentration at which frequency independent conductivity becomes visible in figure 1 (a) marking the percolation threshold) and varying up to 3 vol.% MgO concentrations were investigated in broad frequency (20–40 GHz) and temperature (20–500 K) ranges. The composites with up to 2 vol.% MgO concentration showed a significant increase of DC conductivity as can be seen in figure 1 (b). The optimal content of MgO was found to be 0.46 vol.%, which gave up to 2.5 orders of magnitude larger DC conductivity than of the samples prepared without MgO. Additionally, annealing at 500 K had a favorable effect on conductivity for MgO samples.

To see the change of macroscopic MWCNT distribution in composites with different MgO content, a panoramic SEM micrographs are presented in figure 1 (c,d). The 0.25 vol% MgO composite (figure 1 (c)) had a more pronounced MWCNT macro structure and a higher level of clustering than 1% MgO sample (figure 1 (d)) resulting in higher electrical conductivity (figure 1 (b))., This is in good agreement with previously reported results that the MWCNT clustering can decrease the percolation threshold value [1]. The smaller MgO clusters acts as separators of MWCNT clusters and support certain macroscopic structures.

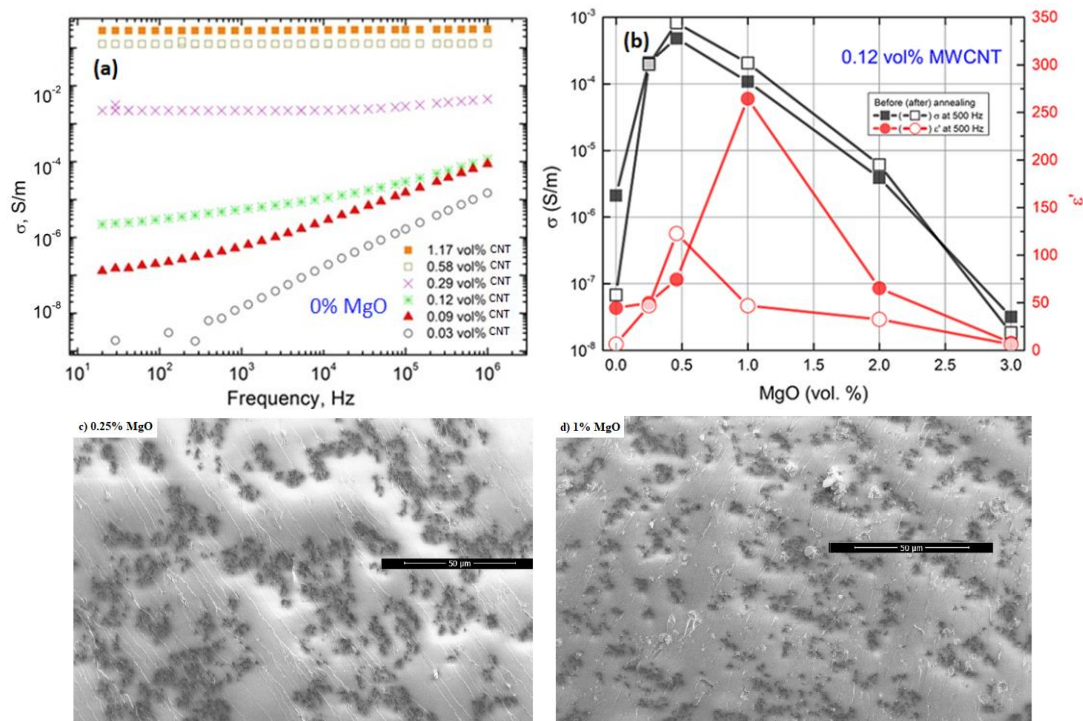


Figure 1 (a) frequency dependence of the electrical conductivity for epoxy composites with MWCNT inclusions without MgO (b) electrical conductivity and the real part of dielectric permittivity of composites with 0.12 vol% MWCNT and various MgO vol.% concentrations at room temperature, 500 Hz before and after annealing at 500 K. SEM micrographs of composites with 0.25% (c) and 1% (d) MgO content.

[1] J.O. Aguilar, J.R. Bautista-Quijano, F. Aviles, Influence of carbon nanotubes clustering on the electrical conductivity of polymer composites films, Express Polym. Lett. 2010, 4, 292–299 (2010).

Impedance spectroscopy study of some Argyrodite crystals

V. Kavaliukė¹, S. Balčiūnas¹, T. Šalkus¹, J. Banys¹, A.I. Pogodin², O.P. Kokhan², I.P. Studenyak²

1- Vilnius University, Saulėtekio av. 9/3, LT-10222, Vilnius, Lithuania

2- Uzhhorod National University, 46 Pidhirna St., 88000 Uzhhorod, Ukraine

Main author email address: vilma.kavaliuke@ff.vu.lt

(Cu_{1-x}Ag_x)₇GeS₅I (x = 0, 0.25, 0.5, 1) compounds belong to Argyrodite family and at room temperature they belong to cubic syngony (s.g. F4̄3m) [1-2]. Typically, Argyrodites are characterized by a disordered high-temperature phase (cubic F4̄3m) and an ordered low-temperature phase. The high temperature phase is characterized by high ionic or mixed ionic-electronic conductivity [1]. Cu₇GeS₅I and Ag₇GeS₅I argyrodites have high electrical conductivities: 2.9 S/m at T = 295 K, (activation energy E_a = 0.09 eV) [3] and 2.77·S/m at T = 298 K (E_a = 0.139 eV) [4], respectively. In this study electrical properties of (Cu_{1-x}Ag_x)₇GeS₅I (x = 0, 0.25, 0.5, 1) were investigated.

Single crystals of (Cu_{1-x}Ag_x)₇GeS₅I (x = 0, 0.25, 0.5, 1) were grown as described in [2]. Ag electrodes of the thickness of 300-400 nm were evaporated on the flat surfaces of the cylindrically shaped samples. Dielectric measurements in the frequency range from 10² to 10⁶ Hz and temperature interval from 300 K to 120 K were performed using precision LCR meter HP4284A capacitor method.

Relaxation dispersion of the real part of complex electrical conductivity was observed for all measured (Cu_{1-x}Ag_x)₇GeS₅I (x = 0, 0.25, 0.5, 1) crystals at T = 110 K. This dispersion shifts to higher frequencies as the temperature rises, and it disappears from the visible frequency range at higher temperatures and only plateau region remains in the conductivity spectrum. This relaxation dispersion can be attributed to Cu⁺ and/or Ag⁺ ions migration in the bulk of investigated crystals. In order to determine temperature dependences of electrical conductivity complex impedance plots were used.

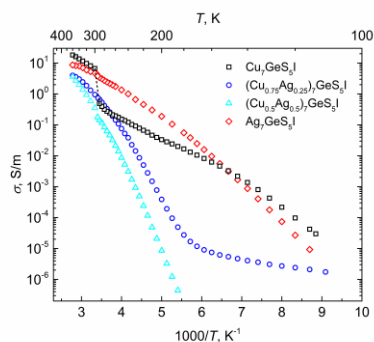


Figure 1 Arrhenius conductivity plots of (Cu_{1-x}Ag_x)₇GeS₅I (x = 0, 0.25, 0.5, 1) crystals.

Temperature dependencies of conductivities for all the investigated crystals are shown in Fig. 1 in Arrhenius representation. The abrupt change of Cu₇GeS₅I conductivity over one order of magnitude at about 295 K is visible. In the case of partial Cu⁺ ↔ Ag⁺ substitutions the obtained conductivity values of (Cu_{1-x}Ag_x)₇GeS₅I (x = 0.25 and 0.5) were found to be lower compared to the parent crystals Cu₇GeS₅I and Ag₇GeS₅I. This result can be associated with “mixed – ion effect” [5-6]. It is known that silver and copper ions occupy two positions 1 and 2, the position 2 being slightly different for Cu⁺ and for Ag⁺ [2]. Some substitution of Cu⁺ to Ag⁺ leads to the partially blocked pathways for Cu⁺ migration, so the conductivity is lower compared to both parent compounds and the activation energy is higher because of the higher potential barriers.

[1] W.F. Kuhs, R. Nitsche, K. Scheunemann, The argyrodites — A new family of tetrahedrally close-packed structures, *Mat. Res. Bull.* 14 241-248, (1979).

[2] I.P. Studenyak, A.I. Pogodin, O.P. Kokhan, V. Kavaliukė, T. Šalkus, A. Kežionis, A.F. Orliukas, Crystal growth, structural and electrical properties of (Cu_{1-x}Ag_x)₇GeS₅I superionic solid solutions, *Solid State Ion.* 329, 119-123, (2019).

[3] I.P. Studenyak, M. Kranjčec, V.V. Bilanchuk, O.P. Kokhan, A.F. Orliukas, A. Kežionis, E. Kazakevičius, T. Šalkus, *Solid State Ion.* 181 (2010) 1596. <https://doi.org/10.1016/j.ssi.2010.09.021>

[4] M. Laqibi, b. Cross, S. Peytavin, M. Ribes, *Solid State Ion.* 23 (1987) 21. [https://doi.org/10.1016/0167-2738\(87\)90077-4](https://doi.org/10.1016/0167-2738(87)90077-4)

[5] C. Karlsson, A. Mandanici, A. Matic, J. Swenson, and L. Borjesson, *Physical Review B* (2003) 064202. <https://doi.org/10.1103/PhysRevB.68.064202>

[6] J.E. Tsuchida, F.A. Ferri, P.S. Pizani, A.C.M. Rodrigues, S. Kundu, J.F. Schneider, E.D. Zanotto, *Phys. Chem. Chem. Phys.* 19 (2017) 6594. <https://doi.org/10.1039/C6CP07876A>

Temperature dependent structural changes of $\text{Na}_2\text{Mn}_3(\text{P}_2\text{O}_7)_2$ phase in $\text{NaLiMnP}_2\text{O}_7$ mixed phase compound

S. Daugela¹, T. Salkus¹, A. Kezionis¹, A. Dindune², D. Valdniece², T. Pietrzak³, A. Zalga⁴

1- Faculty of Physics, Vilnius University, Saulėtekio 9/3, LT-10222 Vilnius, Lithuania

2- Institute of Inorganic Chemistry, Riga Technical University, Paula Valdena 3/7, LV-1048 Riga, Latvia

3- Faculty of Physics, Warsaw University of Technology, Koszykowa 75, 00-662 Warsaw, Poland

4 - Faculty of Chemistry and Geosciences, Vilnius University, Naugarduko 24, LT-03225 Vilnius, Lithuania

saulius.daugela@ff.vu.lt

Alkali metal pyrophosphates are promising cathode materials for both lithium and sodium solid state secondary batteries. Pyrophosphate type electrolytes are attractive due to their rich crystal chemistry, chemically stable structure, convenient synthesis process and possible multidimensional ionic conduction pathways [1, 2]. XRD measurements revealed that the investigated $\text{NaLiMnP}_2\text{O}_7$ compound consists of two phases: $\text{Na}_2\text{Mn}_3(\text{P}_2\text{O}_7)_2$ and LiMnPO_4 . We found by XRD measurements that at 40 °C $\text{Na}_2\text{Mn}_3(\text{P}_2\text{O}_7)_2$ shows the triclinic symmetry of the compound (space group P-1) while LiMnPO_4 phase showed the orthorhombic crystal symmetry (space group Pnma). The phase change between 500 °C and 540 °C was proved by thermal XRD, impedance spectroscopy and DTA analysis. No evident changes of peak intensities in thermal XRPD were observed for LiMnPO_4 phase. The impedances of $\text{NaLiMnP}_2\text{O}_7$ ceramics was measured at different temperatures and the total ionic conductivity of the compound was found to be of $5.3 \cdot 10^{-9}$ S/m at 400 K temperature on heating stage and only vanishingly higher on cooling stage. The step-like phase transition determined the conductivity increase of about 3 orders of magnitude in a narrow range of temperature. The ionic transference number was found to be 0.91 at room temperature.

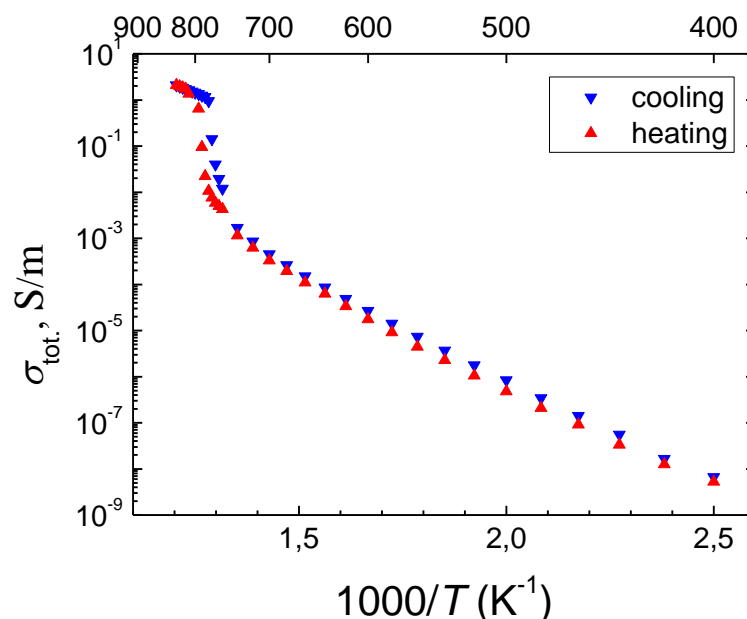


Figure 1. The plot of the total conductivity of $\text{NaLiMnP}_2\text{O}_7$ ceramics measured in ambient air on both heating and cooling stages. The increase of the conductivity at 760-810 K temperature was associated with the phase transition taking place in the ceramics.

- [1] P. Barpanda, T. Ye, S. Nishimura, S. C. Chung, Y. Yamada, M. Okubo, H. Zhou and A. Yamada, Sodium iron pyrophosphate: A novel 3.0 V iron-based cathode for sodium-ion batteries, *Electrochemistry Communications*, vol. 24, pp. 116-119, (2012).
- [2] J. M. Clark, P. Barpanda, A. Yamada and M. S. Islam, Sodium-ion battery cathodes $\text{Na}_2\text{FeP}_2\text{O}_7$ and $\text{Na}_2\text{MnP}_2\text{O}_7$: diffusion behaviour for high rate performance, *Journal of Materials Chemistry A*, vol. 2, no. 30, pp. 11807-11812, (2014).

Multiferroic perovskite $\text{BiFeO}_3\text{-BiZn}_{0.5}\text{Ti}_{0.5}\text{O}_3$ system with the morphotropic phase boundary

E. Čižmár¹, S. Vorobiov¹, A. Kliuikov¹, Yu.V. Radyush², A.V. Pushkarev², N.M. Olekhovich², K. Šul'ová³, K. Saksl³, A.N. Salak⁴, A. Feher¹

1- Institute of Physics, Faculty of Science, P.J. Šafárik University in Košice, Košice 04154, Slovakia

2- Scientific-Practical Materials Research Centre of NASB, Minsk 220072, Belarus

3- Institute of Material Science, Slovak Academy of Sciences, Košice 04001, Slovakia

4- Department of Materials and Ceramics Engineering, CICECO – Aveiro Institute of Materials, University of Aveiro, Aveiro 3810-193, Portugal

erik.cizmar@upjs.sk

Environmental requirements have stimulated the search for lead-free materials with piezo properties comparable to those of lead zirconate-titanate at the morphotropic phase boundary (MPB). BiFeO_3 (BF) is rhombohedral and $\text{BiZn}_{0.5}\text{Ti}_{0.5}\text{O}_3$ (BZT) is tetragonal and one can expect MPB in this system. BF can be prepared using the conventional solid-state reaction route, while BZT requires high-pressure synthesis. Some solid solutions of the BZ-BZT system were obtained earlier [1]. However, the localization of MPB was not determined with sufficient accuracy. Besides, due to the high conductivity of the samples, the piezoelectric properties of the BF-BZT- system ceramics were not investigated. The calculated estimates of spontaneous polarization turned out to be quite large, $\sim 110 \mu\text{C}/\text{cm}^2$.

The Fe-reach compositional range of the BF-BZT system is of particular interest owing to the recently disclosed phenomenon of conversion polymorphism [2]. It has been shown that annealing of the metastable phases can induce irreversible phase transformation into novel structural and/or magnetic structures [2,3].

Here we report structural, magnetic and calorimetric studies of $(1-x)\text{BiFeO}_3 - x\text{BiZn}_{0.5}\text{Ti}_{0.5}\text{O}_3$ system in the Fe-reach compositional range with $x = 0.05 - 0.25$. The Néel temperature for $x = 0.05$ should converge to 645 K as observed in pure BF system, interestingly, in the composition with $x = 0.25$, the magnetic ordering takes place at 460 K, which is higher than that observed for $\text{BiFe}_{1-y}\text{Sc}_y\text{O}_3$ series [3]. A differential-scanning calorimetry measurement revealed additional transitions above the Néel temperature that may be related to variation in the ferroelectric ordering.

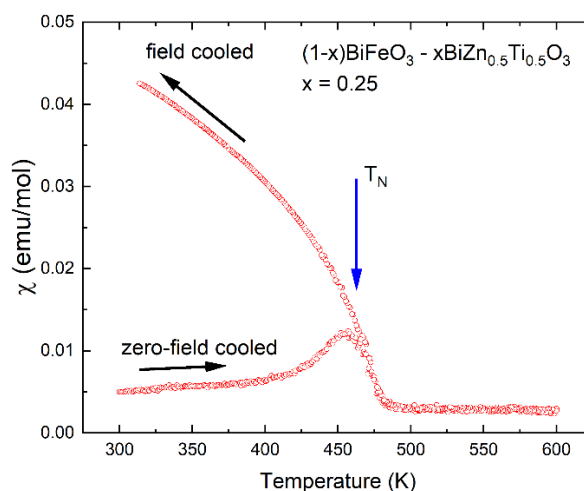


Figure 1 Temperature dependence of the magnetic susceptibility of $(1-x)\text{BiFeO}_3 - x\text{BiZn}_{0.5}\text{Ti}_{0.5}\text{O}_3$ with $x = 0.25$.

The authors acknowledge the financial support of the bilateral Slovakia-Belarus project APVV-SK-BY-RD-19-0008 and T20SLKG-001, respectively, as well as the support of P.J. Šafárik University in Košice through grant VVGS-2020-1403.

[1] Z. Pan, J. Chen, R. Yu, H. Yamamoto, Y. Rong, L. Hu, Q. Li, K. Lin, L. You, K. Zhao, L. Fan, Y. Ren, K.Kato, M. Azuma, X. Xing, Giant polarization and high temperature monoclinic phase in a lead-free perovskite of $\text{Bi}(\text{Zn}_{0.5}\text{Ti}_{0.5})\text{O}_3\text{-BiFeO}_3$, *Inorg. Chem.* 55, 9513-9516 (2016).

[2] D.D. Khalyavin, A.N. Salak, E.L. Fertman, O.V. Kotlyar, E. Eardley, N.M. Olekhovich, A.V. Pushkarev, Yu.V. Radyush, A.V. Fedorchenko, V.A. Desenko, P. Manuel, L. Ding, E. Čižmár, A. Feher, The phenomenon of conversion polymorphism in Bi- containing metastable perovskites, *ChemComm.* 55, 4683-4686 (2019).

[3] E.L. Fertman, A.V. Fedorchenko, E. Čižmár, S. Vorobiov, A. Feher, Yu.V. Radyush, A.V. Pushkarev, N.M. Olekhovich, A. Stanulis, A.R. Barron, D.D. Khalyavin, A.N. Salak, Magnetic diagram of the high-pressure stabilized multiferroic perovskites of the $\text{BiFe}_{1-y}\text{Sc}_y\text{O}_3$ series, *Crystals* 10, Art. No 00950 (2020).

Coats of Cerium, Boron and/or Magnesium Doped Garnets on Different Pallets and Their Luminescence Properties for Scintillators Application

G. Inkrataitė¹, R. Skaudžius¹

1- Institute of Chemistry, Faculty of Chemistry and Geosciences, Vilnius University, Naugardukas st. 24, LT-03225 Vilnius, Lithuania

Main author email address: greta.inkrataite@chgf.vu.lt

In recent years materials with luminescent properties have become very popular. In addition, these materials are very popular for usage in lamps and other light emitting devices, but nowadays scintillators and their research is becoming a very interesting subject for scientists. Scintillators are the basis for devices, that are used for radioactive contamination detection and measurement, nuclear material monitoring, also they are included in the computer detector composition of the tomography devices. There are various compounds that can be used as scintillators, but one of the most popular are those which have a garnet structure [1]. Amongst others, these can be yttrium or lutetium aluminum garnet, doped with different lanthanides (YAG:Ln; LuAG:Ln). These inorganics compounds have the required optical properties and radiation resistance and can, therefore, be used for thermal neutron and high energy radiation (X-ray, γ -radiation) detection [2, 3]. The development of new scintillators is important. However, not the materials which are used are important but also their form. The preparation of powder is the simplest, but they are not suitable for the construction of scintillator detectors. Best suited and used for the manufacture of various devices are single crystals. In addition to single crystals, coatings on various pallets or microfibers can be used [4]. Due to the possibility of using different substrates, different methods of coating, materials with different properties can be prepared, which makes this method widely used. Using the sol-gel method we can obtain homogeneous multicomponent coatings at low temperature, leaving the possibility of synthesizing compounds with emission intensity [5].

Improvement of luminescence is essential for getting the fastest scintillators properties. One way to do this is to additionally dope compounds with other elements. Replacing one element with another in the crystal lattice can influence the properties of the materials. The most common goal is to improve key parameters: compound emission intensity, quantum efficiency and decay times. One of the greatest scintillators drawbacks that is being addressed is that decay time is too long. When it is extremely long, then these second signal captured by the materials overlaps with the first, making the results unreliable and provides less data than it could. Scintillators such as YAG:Ce and LuAG:Ce doped with boron or magnesium can solve this problem. If a quick quench of decay time was obtained given result would be more accurate, and this method of synthesizing scintillators could be practically applicable [6, 7].

In this work cerium boron and/or magnesium doped YAG and LuAG are synthesized on silicon and quartz substrates using the dip-coating method. Boron and magnesium are expected to improve required luminescent properties, and with the sol-gel method, homogeneous compounds will be synthesized at low temperatures. Phosphor coatings were analyzed by x-ray diffraction (XRD), scanning electron microscopy (SEM) and atomic force microscopy (AFM). Of course, emission, excitation spectra and decay times have been investigated as well.

ACKNOWLEDGEMENTS:

This project has received funding from European Social Fund (project No [09.3.3-LMT-K-712-15-0151]) under grant agreement with the Research Council of Lithuania (LMTLT)

[1] D. S. McGregor, Materials for Gamma-Ray Spectrometers: Inorganic Scintillators, Annual Review of Materials Research, 48: 254-277 (2018)

[2] A.D. Sontakke, J. Ueda, J. Xu, et. al., A Comparison on Ce³⁺ Luminescence in Borate Glass and YAG Ceramic: Understanding the Role of Host's Characteristics, The Journal of Physical Chemistry C, 120, 31, 17683 – 17691 (2016)

[3] J. M. Ogieglo, A. Katelnikovas, A. Zych, T. Justel, et. al., Luminescence and Luminescence Quenching in Gd₃(Ga,Al)₅O₁₂ Scintillators Doped with Ce³⁺, The Journal of Physical Chemistry A, 117, 12, 8464 – 8474 (2012)

[4] S. Rawat, M. Tyagi, P. K. Netrakanti, et. al., Pulse shape discrimination properties of Gd₃Ga₃Al₂O₁₂:Ce,B single crystal in comparison with CsI:TI, Nuclear Instruments and Methods in Physics Research Section A: Accelerators, Spectrometers, Detectors and Associated Equipment, 840, 186 – 191 (2016)

[5] A. Potdevin, G. Chadeyron, D. Boyer, et. al., Sol-gel based YAG: Tb³⁺ or Eu³⁺ phosphors for application in lighting sources, Journal Of Physics D: Applied Physics, 3251 – 3260 (2005)

[6] C. Foster, Y. Wu, M. Koschan, et. al., Boron Codoping of Czochralski Grown Lutetium Aluminum Garnet and the Effect on Scintillation Properties, Journal of Crystal Growth, 486, 126 – 129 (2018)

[7] H. S. Yoo, W. B. Im, J. H. Kang, D. Y. Jeon, Preparation and photoluminescence properties of YAl₃(BO₃)₄:Tb³⁺, Bi³⁺ phosphor under VUV/UV excitation Optical Materials, 31, 2, 131 – 135 (2008)

Improving dosimetric properties of AlN by doping with rare earth metals.

J. Cipa¹, L. Trinkler¹, B. Berzina¹, V.Korsaks¹, J.Grabis²

1- Institute of Solid-State Physics, University of Latvia, Kengaraga St.8, Riga, Latvia

2- Riga Technical University, Faculty of Material Science and Applied Chemistry, P.Valdena St.6, Riga, Latvia

janis.cipa@cfi.lu.lv

AlN ceramic is a wide band gap material ($E=6.2$ eV), potentially applicable in TL/OSL dosimetry due to its high sensitivity to irradiation with UV light and ionizing radiation [1]. The pure AlN obtains a lot of advantages as TL and OSL material, but its disadvantage is its signal fading rate, which could be eliminated by doping. In this research the possible improvement of dosimetric properties is explored by doping AlN with different rare earth elements in order to get deep trap levels and efficient luminescence centres. Deep trap levels should provide more stable TL/OSL response during storage the irradiated material at room temperature.

AlN ceramics are produced from AlN powder (grain size around $10\ \mu\text{m}$) with admixture of metals/metal oxides by method of spark plasma sintering. The nominally pure the AlN powder contains the uncontrolled manganese impurities. For characterization of dosimetric properties of AlN ceramics Freiberg Instruments Lexsyg TL/OSL reader, conjugated with Andor spectrometer and CCD camera, was employed. The integrated X-ray lamp (40 KV, 0.5 mA) was used as a radiation source. After irradiation samples were transported to thermoluminescence measurement chamber where TL glow curves were measured and after a second identical irradiation run TL emission spectra were measured. To make sure that samples were fully bleached of the residual signal the repeated TL measurement was done in a separate sequence and nothing, but background was detected.

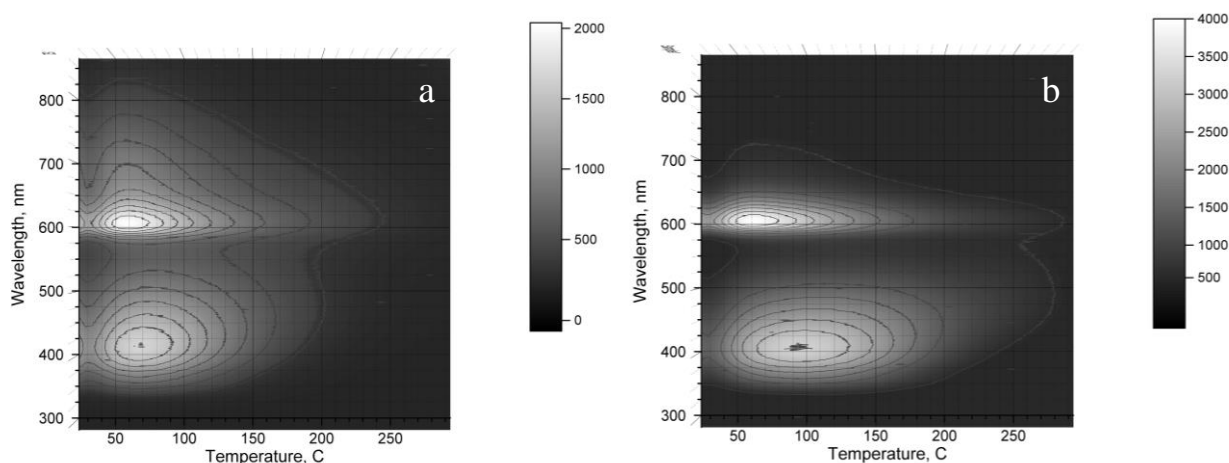


Figure 1. Thermoluminescence contour plot of AlN (a) and AlN doped with 2wt% Y_2O_3 (b).

An example of doping effect is shown by comparing properties of the X-ray induced TL in nominally pure AlN ceramics and AlN with Y_2O_3 (2 wt %). The thermoluminescence contour plot in Fig.1 shows that TL emission of both samples has 2 wide bands at around 400 and 600 nm due to recombination luminescence with participation of oxygen-related and manganese centres, correspondingly; while the TL curve reaches maximum at around 70-100 °C. Admixture of yttria to AlN ceramics seems to shift the TL peak to higher temperatures, thus making the stored signal more stable during storage of the irradiated sample at room temperature. The preliminary results show that doping with metal ions, providing deep trapping levels, gives the positive effect on dosimetric properties of AlN ceramics.

[1] A Trinkler L. and Berzina B., A chapter in book *Advances in Ceramics - Characterization, Raw Materials, Processing, Properties, Degradation and Healing*. (pp. 59-82) Publisher: InTech, 2011.

The present research has been sponsored from the Latvian Sciences Council Grant No. lzp-2018/1-0361.

Effect of a low-temperature deformation on E_x luminescence of KI single crystals

K. Shunkeyev¹, A. Maratova², A. Lushchik², L. Myasnikova¹, A. Lickevich³

1 - K. Zhubanov Aktobe Regional State University, Moldagulova Ave. 34, 030000 Aktobe, Kazakhstan

2 - Institute of Physics, University of Tartu, W. Oswald Str. 1, 50411 Tartu, Estonia

3 - Yanka Kupala State University of Grodno, Ozheshko str. 22, 230023, Grodno, Belarus

aida_m@list.ru

For KI single crystals, three exciton-related luminescence bands were reported in the literature: 3.0 eV (E_x) and two components of self-trapped exciton (STE) emission peaked at 3.31 eV (π) and 4.16 eV (σ) [1-2]. However, there is no consensus on the nature of E_x luminescence at the moment. In some studies, the E_x band is described as the intrinsic luminescence of a crystal (luminescence of a two-halide STE with weak off-configuration at regular lattice sites). In other papers, E_x band is referred to as the luminescence of bound excitons – luminescence of a two-halide exciton localized in a field of an impurity ion with a different ionic radius (for example, Na^+ or Br^-) or near some crystal lattice defect. It should be noted that the dependence of the E_x -luminescence intensity in KI on the concentration of impurities or lattice defects has not been established experimentally.

Under uniformed hydrostatic pressure applied to a KI crystal, the intensity redistribution between three above-mentioned luminescence bands was recorded: the enhancement of E_x luminescence was accompanied by the decreasing of the π - and σ -luminescence intensity. This result indicates the intrinsic nature of E_x luminescence [2]. It should be kept in mind that a uniformed hydrostatic compression of the crystal leads to changes in the energy of various electronic excitations (EEs) but does not change the lattice symmetry. Such external impact results in the enhancement of impurity and free exciton emissions, while the luminescence of STEs generally weakens.

The applied uniaxial deformation reduces the symmetry of the crystal lattice, but causes relatively weak changes of EE energy states. A uniaxial elastic deformation of the crystal results in the increase of STE luminescence intensity and the simultaneous weakening of the emission of both free excitons and different impurities. Note that the lowering of a potential barrier between the energy states of free excitons and STEs is the main reason of this effect. It should be emphasized that a significant rise of the σ -emission intensity in the X-ray luminescence spectrum of a KI crystal under applied uniaxial stress (at 100 K) is a result of the enhanced probability of the recombinational creation of anion excitons via the relaxation of electron-hole pairs formed by X-rays.

According to Ref. [3], a low-temperature uniaxial elastic deformation of KI-Tl crystals leads to a reduction in the free path of EEs before their localization. As a result, the redistribution of luminescence intensity in favor of the intrinsic σ - and π -emissions of STEs was recorded, while the intensity of the impurity thallium luminescence weakened significantly. Uniaxial deformation efficiently affects the intensity of E_x luminescence and its application allows to confirm the intrinsic origin of this luminescence in KI crystals (see also [3]).

Therefore, a permanent uniaxial elastic deformation (at 100 K) reduces the free path of EEs before their self-trapping. As a result, uncontrolled impurities (in case of their relatively low concentration) become "unattainable points" due to sufficiently rapid and small-distance migration of EEs before their self-trapping (anion excitons) at regular lattice sites. In other words, a low-temperature uniaxial deformation dramatically increases the probability of EE self-trapping and impedes the formation of so-called bound excitons (localized near impurities/defects, see, e.g., [4]) and appearance of the related luminescence.

[1] K.S. Song, R.T. Williams, Self-Trapped Excitons, 2nd ed., Springer, Berlin (1996).

[2] H. Nishimura, T. Tsujimoto, M. Nakayama, T. Horiguchi and M. Kobayashi, Effects of hydrostatic pressure on the self-trapped exciton luminescence in KI, J. Phys. Soc. Japan, 63, 2818-2824 (1994).

[3] K. Shunkeyev, N. Zhanturina, Z. Aimaganbetova, A. Barmina, L. Myasnikova, Sh. Sagymbaeva and D. Sergeev, The specifics of radiative annihilation of self-trapped excitons in a KI-Tl crystal under low-temperature deformation, Low Temp. Phys., 42, 580-583 (2016).

[4] Ch. Lushchik, A. Lushchik, Evolution of anion and cation excitons in alkali halide crystals, Phys. Solid State 60, 1487-1505 (2018) [Fiz. Tverd. Tela 60, 1478-1494 (2018)]

Templated synthesis and optical properties of multilayer porous anodized aluminium oxide – zinc oxide nanostructures for biosensing applications.

A. Dutovs¹, U. Maļinovskis¹, J. Prikulis¹, D. Jevdokimovs¹, R. Popļausks¹, O. Graniel², D. Erts¹

1- Institute of Chemical Physics, University of Latvia, Jelgavas str. 1, Riga, Latvia

2- European Institute of Membranes, University of Montpellier, 300 Avenue du Professeur Emile Jeanbrau, Montpellier, France

ad18122@edu.lu.lv

Zinc oxide (ZnO) is a well-known optically active semiconductor material with intense luminescence in ultraviolet and visible light spectral range [1]. ZnO nanostructures are widely used as an active element in optical sensing devices [2]. To archive lithography-free fabrication of nanoscale material, self-organized porous anodized alumina oxide (PAAO) templates on aluminum substrate can be used, with tunable parameters and well-established synthesis protocols [3].

In this study, 35 nm thin ZnO layer was synthesized by atomic layer deposition onto PAAO membranes (60-800 nm variable layer, pore diameter 40 - 50 nm) [3].

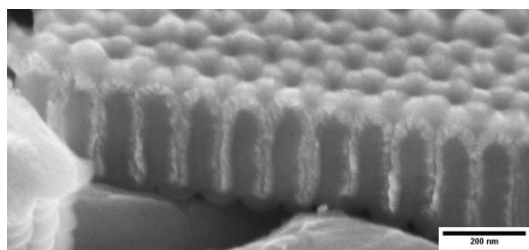


Figure 1. Scanning electron microscopy image of hybrid multilayer sample image. Aluminium oxide pores filled with zinc oxide. Zinc oxide layer on top.

Room temperature photoluminescence was studied by exciting hybrid sample with 3.3-3.8 eV energy and collecting spectral data in the visible light region. Acquired wide (1.5 – 3.0 eV) luminescence band was fitted to Gaussian constituents, which correspond to typical luminescence caused by both ZnO structural defects (surface defects at ~ 2.0 eV and oxygen vacancies at ~ 2.5 eV) and aluminium oxide defects (oxygen vacancies at ~2.8 eV) [1]. Comparing hybrid nanostructure luminescence to freestanding ZnO nanorods (produced by selective aluminium oxide dissolution in sodium hydroxide) luminescence, intensity decrease and red shift of central energies were observed in freestanding ZnO samples. Intensity of luminescence of hybrid nanostructure was several times higher, what makes use of PAAO membranes more suitable for ZnO-based sensing devices production, than use of freestanding ZnO nanostructures. For hybrid nanostructure layer thickness determination, we used light reflectance simulation model [4] and verified that method by scanning electron microscopy.

We observed correlation between hybrid nanostructure layer thickness and its luminescence.

[1] A. Author and B. Author, Title of paper, Journal Name, vol., pp. startpage-endpage, (year). O. Graniel, V. Fedorenko, V. Viter, I. Iatsunskyi, G. Nowaczyk, M. Weber, K. Załęski, S. Jurga, V. Smytyna, P. Miele, A. Ramanavicius, S. Balme, M. Bechelany, Optical properties of ZnO deposited by atomic layer deposition (ALD) on Si nanowires, *Materials Science & Engineering B*, vol. 236-237, pp. 139-146, (2018).

[2] U. Malinovskis, R. Poplausks, D. Erts, K. Ramser, S. Tamulvičius, A. Tamulevičiene, Y. Gu, J. Prikulis, High-Density Plasmonic Nanoparticle Arrays Deposited on Nanoporous Anodic Alumina Templates for Optical Sensor Applications, *Nanomaterials*, vol. 9(4), pp. 531, (2019).

[3] R. Poplausks, D. Jevdokimovs, U. Malinovskis, D. Erts, J. Prikulis, Variable Thickness Porous Anodic Alumina/Metal Film Bilayers for Optimization of Plasmonic Scattering by Nanoholes on Mirror, *ACS Omega*, vol. 3(5), pp. 5783–5788, (2018).

[4] J. Prikulis, T. Tamulevičius, R. Poplausks, G. Bergs, I. Apsite, U. Malinovskis, A. Actins, D. Erts, Optical properties of thin metal films with nanohole arrays on porous alumina–aluminum structures, *RSC Advances*, vol. 5(83), 68143–68150, (2015).

Structure and luminescent properties of YAG: Ce synthesized ceramic phosphors in radiation fields

V. Lisitsyn¹, D. Mussakhanov¹, G. Alpysova², Zh. Karipbayev², A. Akilbekov², A. Dauletbekova², Sh. Giniyatova²

1- National Research Tomsk Polytechnic University, 30 Lenin Ave., 634050 Tomsk, Russia

2- Eurasian National University, 2, Satpayev Str., 010008 Astana, Kazakhstan

Main author email address: Akilbekov_at@enu.kz

There are different approaches to creating optical ceramics, depending on the composition, but they can be distinguished in common features. To date, two main methods for obtaining optical YAG ceramics have been developed. These methods are the fundamental methods for obtaining optical ceramics. The first approach was developed by A. Ikesue from World-Lab Co, (Japan)[1] - a technology of reactive solid-phase sintering (SPS). The second is the process of forming ceramic materials from liquid and solid constituents (chemical coprecipitation technology), then filtration, washing, the precursor root. The resulting powder is passed for grinding a ball mill, forming and sintering. Here we present the results of the research in structural and luminescent properties of YAG:Ce ceramics synthesized in a radiation field [2].

One of the options is synthesis of ceramics in the field of high-power radiation fluxes. The synthesized test samples were two series of ceramics different in composition with a batch content: Al₂O₃(43%) + Y₂O₃(55%) + Ce₂O₃(2%) (YAG) and Al₂O₃(40%) + Y₂O₃(52%) + Ce₂O₃(2%) + Gd₂O₃(6%) (YAGG). The diffraction patterns

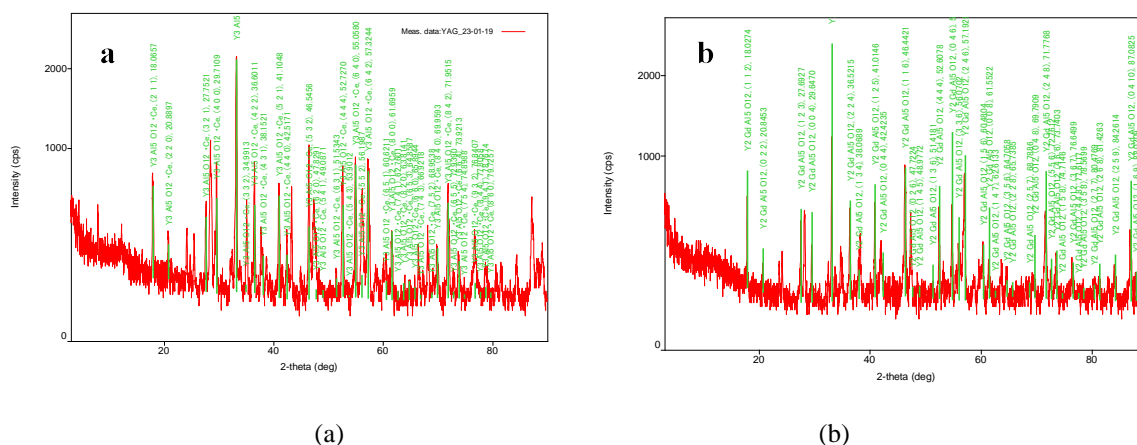


Figure 1 Spectra of XRD YAG (a) and YAGG (b) ceramic powders.

shown in Figure 4 completely correspond in position and ratio of peaks to those known for YAG:Ce crystals. All samples show an Ia-3d space symmetry group.

Luminescence is well excited by radiation at 340 and 460 nm. Effective luminescence can also be excited by radiation with $\lambda < 300$ nm. Luminescence in the region of 550 nm is observed to steady increase when the wavelength decreases. The excitation spectra of phosphors in the region of 250–300 nm differ in the samples before and after annealing. Annealing decreases, the efficiency of luminescence excited in this region.

[1] A. Ikesue, et al. Progress In Ceramic Lasers, Annu. Rev. Mater. Res., vol. 36, pp.397-429. 2006.

[2] D.A. Mussakhanov et al. Structural and luminescent characteristics of YAG phosphors synthesized in the radiation field, IOP Conf. Ser.: Mat. Sc. and Eng., Vo. 510, No. 1, 2019.

Luminescence of doped AlN powders

Rihards Ruska¹, Guna Kriekē¹, Andris Antuzevics¹, Baiba Berzina¹, Laima Trinkler¹, Janis Cipa¹

¹ - Institute of Solid State Physics, University of Latvia, 8 Kengaraga Str., LV-1063, Riga, Latvia

rihards.ruska@cfi.lu.lv

In search of new red-light-emitting materials, luminescence of AlN macro- and nano-sized powders doped with Tb, Mn and other dopants was studied. Methods of investigation included photoluminescence, its excitation spectra as well as luminescence kinetics at various temperatures and environments (vacuum and air).

For AlN:Mn nano materials the well-known Mn-caused red luminescence peaking at 600 nm appeared being dominant. Besides that, luminescence of unknown defects at 650 nm was observed. It was observed that for 600 nm luminescence there are two spectral regions where the red luminescence can be excited, forming a wide and complex excitation bands peaking at 520 nm and 260 nm. It was also found that excitation of AlN:Mn at both 520 nm and 260 nm PLE bands results in long-lasting luminescence.

Analysis of experimental results and their comparison with those obtained in undoped AlN materials allow conclusion that there are two defect-caused mechanisms originating Mn luminescence. One of them, most probably, complex intra-center mechanism, but other is recombination mechanism realizing at 520 and 260 nm excitations, respectively.

Luminescence of undoped ZnO and ZnO:In nanopowders

M. Senko¹, A. Spustaka¹, A.Zolotarjovs¹, D. Millers¹

1- Institute of Solid State Physics, University of Latvia, 8 Kengaraga Street, Riga

aleksejs.zol@gmail.com

Zinc oxide (ZnO) is a widely studied material due to its ease of production, many interesting nanoscale forms (powders, nanowires, nanotubes) and electrical, biological, optical and chemical properties. In addition, ZnO is easily doped with group 3 elements (boron, aluminium, gallium, indium) accompanied by drastic changes of properties thus enabling the fine-tuning of a structure for a particular task. One of the most interesting applications of doped ZnO is the use of the material as a scintillator. Two complex luminescence bands are usually present in ZnO – near band edge (NBE) luminescence concentrated in near UV range ($\approx 380\text{nm}$) and intrinsic defect luminescence – wide band centered around 500nm . NBE luminescence usually exhibits short decay time constants (in order of picoseconds [1]) – a good candidate for effective use as a fast scintillation material; however, the intrinsic defect luminescence is much slower, which hinders the practical use. Based on that, research on increasing the NBE luminescence while quenching intrinsic defects is critically important, and indium was proven to influence the relative intensity of NBE and intrinsic defect luminescence bands [2].

In this study, different aspects of ZnO:In for use as a scintillator will be explored. Photoluminescence and decay kinetics measurements will be used to validate the relative intensity and decay time of luminescence bands for ZnO nanopowders synthesised via different methods (sol-gel, hydrothermal, microwave assisted hydrothermal) and with different In concentrations (0-1at%). Furthermore, ceramic samples will be sintered from different ZnO:In nanopowders and correlation between powders and ceramics will be evaluated.

[1] L. Grigorjeva, J. Grube, I. Bite, A. Zolotarjovs, K. Smits, D. Millers, P. Rodnyi, K. Chernenko, Sub-nanosecond luminescence in ZnO:In nanocrystals, *Radiation Measurements*, vol. 123, pp. 69-73, (2019)

[2] K.A. Chernenko, E.I. Gorohova, S.B. Eron'ko, A.V. Sandulenko, I.D. Venevtsev, H. Wiczorek, P.A. Rodnyi, Structural, optical and luminescent properties of ZnO:Ga and ZnO:In ceramics, *IEEE Transactions on Nuclear Science*, 65 (8), pp. 2196-2202, (2018).

Luminescence properties of ZnMgO with different magnesium composition

S. Miasojedovas¹, P. Sčajev¹, L. Trinkler², L. Chang³, M. Chou³

1- Institute of Photonics and Nanotechnology, Vilnius University, Lithuania

2- Institute of Solid State Physics, University of Latvia, Latvia

3- Center of Crystal Research, Department of Materials and Optoelectronic Science, National Sun Yat-sen University, Kaohsiung, Taiwan

saulius.miasojedovas@ff.vu.lt

Knowledge on optical and electrical properties of novel $Zn_{1-x}Mg_xO$ materials grown on low lattice mismatched substrates are necessary to understand and implement for UV-solar blind photodetector fabrication. Characterization of epilayers via tuneable wavelength, excitation intensity and ambient temperature will allow to reveal grown structure spectral responsivity relations to excitation dependent electrical material parameters. The investigated samples were grown on $ScAlMgO_4$ substrate with different magnesium concentrations. Samples differ not only by layer thickness but also by structural phase (rock salt and wurtzite). $Zn_{1-x}Mg_xO$ samples were excited via nanosecond pulse wavelength tunable YAG laser. Luminescence properties were investigated in broad range of excitation intensities and various ambient temperatures. Samples showed band-to-band luminescence that blue-shifts with increase of magnesium concentration. This band showed linear dependence with increase of excitation intensity. Wide luminescence band at 400 nm can be ascribed to the defects that are formed during growth of ZnO phase. Opto-electrical measurements revealed dependency of induced current on magnesium concentration.

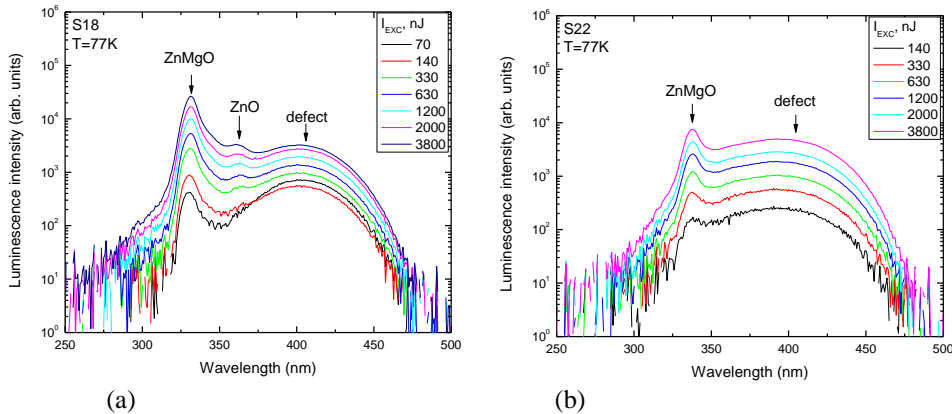


Figure 1 Luminescence spectra of ZnMgO layer with 20% (a) and 15% (b) of magnesium measured at 77 K and various excitation intensities of YAG laser. Excitation wavelength $\lambda = 230$ nm.

Analysis of correlations between the structural, optical, and photoelectrical properties will allow evaluation of optimal growth conditions, providing the advice for growth of the $Zn_{1-x}Mg_xO$ layers and heterostructures. We acknowledge support of M.ERA-NET project S-M-ERA.NET-19-2.

Luminescence and upconversion luminescence properties of $\text{K}_2\text{Yb}_{0.2}\text{Bi}_{0.8-x}(\text{PO}_4)(\text{MoO}_4): x \text{Er}^{3+}$

J. Grigorjevaite¹, A. Katelnikovas¹

¹ Institute of Chemistry, Faculty of Chemistry and Geosciences, Vilnius University,

Naugarduko 24, LT-03225 Vilnius, Lithuania;

Main author email address: julija.grigorjevaite@chf.vu.lt

The absorption of two or more photons leading to the emission of light at a wavelength shorter than the excitation wavelength is described as the upconversion (UC) process. UC materials possess many outstanding optical features and these materials are widely used in many devices such as solid-state lasers, temperature sensors, optical fibers or displays technologies [1].

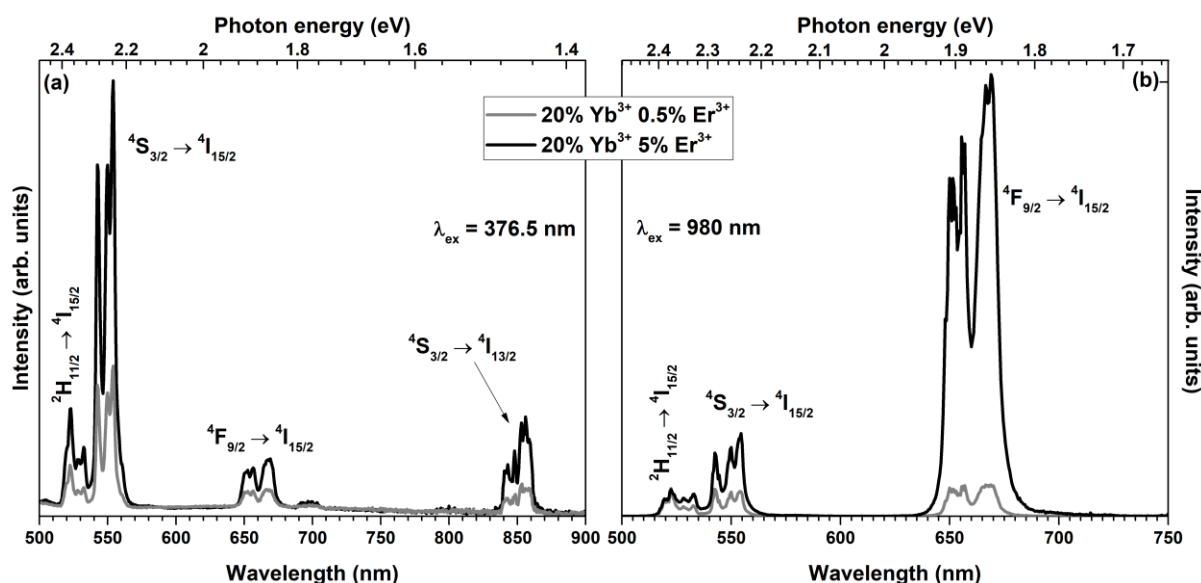


Figure 1. (a) Emission spectra of $\text{K}_2\text{Bi}(\text{PO}_4)(\text{MoO}_4):20\% \text{Yb}^{3+}$ doped with Er^{3+} under 376.5 nm excitation (b) upconversion emission spectra of $\text{K}_2\text{Bi}(\text{PO}_4)(\text{MoO}_4):20\% \text{Yb}^{3+}$ doped with Er^{3+} under 980 nm laser excitation.

A series of upconverting materials $\text{K}_2\text{Yb}_{0.2}\text{Bi}_{0.8-x}(\text{PO}_4)(\text{MoO}_4)$ doped with $x\text{Er}^{3+}$ ions was synthesized by solid state reaction method. All of the synthesized materials have shown similar emission spectra except different intensity (see Figure 1). The most intense peaks are centered in the green spectral region and can be attributed to the $^2\text{H}_{11/2} \rightarrow ^4\text{I}_{15/2}$ and $^4\text{S}_{3/2} \rightarrow ^4\text{I}_{15/2}$ transitions under 376.5 nm excitation [2], while synthesized materials show different features under 980 nm laser excitation. The most intense sample was doped with 5% Er^{3+} and the main emission peaks are centered in the orange-red region. These peaks can be attributed to the $^4\text{F}_{9/2} \rightarrow ^4\text{I}_{15/2}$ transitions of Er^{3+} ions.

The downconversion and upconversion luminescence emission of these materials have been studied and will be presented and discussed in the poster.

This research was funded by a grant (No. D-2018-0703 “Controlling the upconversion emission by tuning band gap of the host matrix”) from the Research Council of Lithuania.

[1] Bayart, A., Szczepanski, F., Blach, J. F., Rousseau, J., Katelnikovas, A., Saitzek, S., Upconversion luminescence properties and thermal quenching mechanisms in the layered perovskite $\text{La}_{1.9}\text{Er}_{0.1}\text{Ti}_2\text{O}_7$ toward an application as optical temperature sensor, *Journal Alloys and Compounds*, 744, 2018, 516-527.

[2] Liu, Y., Liu, Y., Liu, G., Dong, X., Wang, J., Up/down conversion, tunable, photoluminescence and energy transfer properties of $\text{NaLa}(\text{WO}_4)_2:\text{Er}^{3+}$, Eu^{3+} phosphors, *RSC Adv.* 5, 2015, 97995-98003.

Chromium doped alumina usability in dosimetry

E. Einbergs, A. Zolotarjovs, K. Smits, I. Bite, L. Trinkler

Institute of Solid State Physics, University of Latvia, Riga, Latvia

E-mail: ernestse@cfi.lu.lv

Study of radiation induced electronic processes in materials precipitated a now widespread material science field called dosimetry, which specializes in ionizing radiation detection and quantification. The performance of most materials used for dosimetry applications is mainly governed by the impurity ions in the crystalline lattice coupled with lattice imperfections around them (with a meaningful difference in size or oxidation state compared to host ions). In this study, we explored augmentation of luminescent properties of alumina caused by chromium ion doping, with a goal of increasing the quantity of charge carrier traps in the crystalline lattice. Porous $\text{Al}_2\text{O}_3:\text{Cr}$ microparticles synthesized with sol-gel method displayed higher thermoluminescent response compared to that of a single crystalline ruby. We have found that 0.2 wt% of Cr_2O_3 yielded the highest XRL and TSL readout of all studied additive concentrations. Our results display a promising use case for Cr doped alumina. Conducted study provides information on a new alternative to already existing ionizing radiation dosimetric materials with desirable physical and chemical properties as well as relatively lower manufacturing cost.

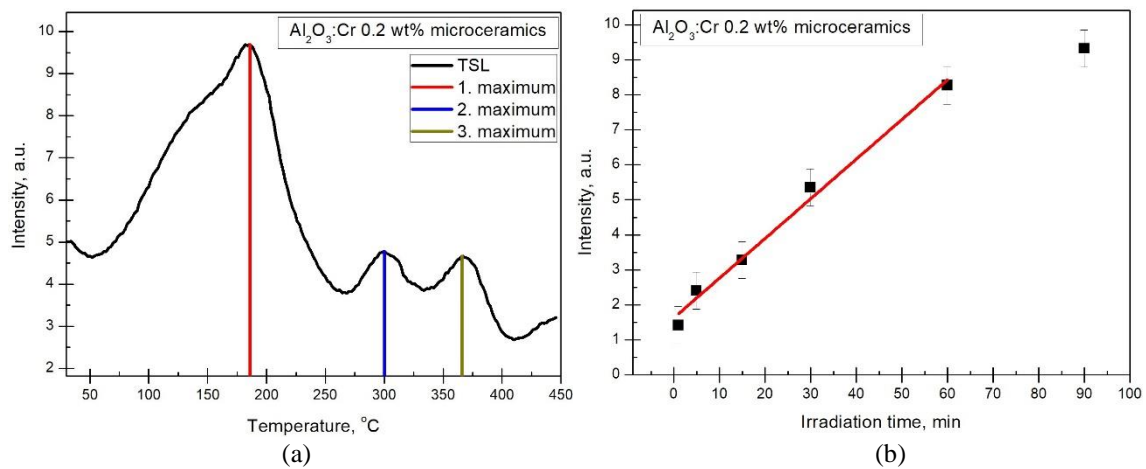


Figure 1. (a) Single TSL measurement of $\text{Al}_2\text{O}_3:\text{Cr}$ with 0.2 wt% Cr_2O_3 . (b) TSL intensity dependence on irradiation time with a linear fit for $\text{Al}_2\text{O}_3:\text{Cr}$ with 0.2 wt% Cr_2O_3 .

The financial support of LZP 2018/1-0361 project is greatly acknowledged.

Phase Stability and Luminescence Properties of $\text{ZrO}_2:\text{Pr}^{3+}$ and $\text{ZrO}_2:\text{Pr}^{3+},\text{Nb}^{5+}$ Nanophosphors

Laurits Puust¹, Valter Kiisk¹, Ivita Bite², Jaan Aarik¹, Ilmo Sildos¹

¹Institute of Physics, University of Tartu, W.Ostwaldi 1, 50411 Tartu, Estonia

² Institute of Solid State Physics, University of Latvia, Kengaraga street 8, Riga, LV-1063, Latvia

e-mail of presenting author: laurits.puust@ut.ee

Transparent metal oxides, such as ZrO_2 , constitute the basis for many functional optical materials. Optical properties (e.g. absorption and luminescence) of these materials are strongly affected by intrinsic defects, mainly anion vacancies, acting as chromophores, luminescence centres and charge carrier traps. It has been shown that high-temperature annealing of ZrO_2 in reducing or oxidizing ambient can distinctively modify its intrinsic photoluminescence (PL) and thermoluminescence (TL) [1]. Doping with certain heterovalently substituted impurities, such as rare earth (RE) ions, is also expected to result in significant alteration of vacancy concentration due to local charge compensation [2].

Hereby we synthesized various praseodymium (Pr) doped and Pr-niobium (Nb) doped ZrO_2 nanopowders by sol-gel and microwave-assisted hydrothermal methods, annealed the powders at different temperatures and comparatively evaluated their optical properties and phase compositions to understand the optical effects of vacancy formation and neutralization. As can be seen in Figure 1, the increase of Pr^{3+} concentration caused marked changes in PL emission spectra and also transition of ZrO_2 from the monoclinic to tetragonal phase followed by the transition of ZrO_2 back to the monoclinic phase when a corresponding amount of Nb^{5+} was added [2]. The local charge compensation led also to the most pronounced PL transitions from $^3\text{P}_0$ level to $^3\text{F}_2$ rather than to $^3\text{H}_6$ [3].

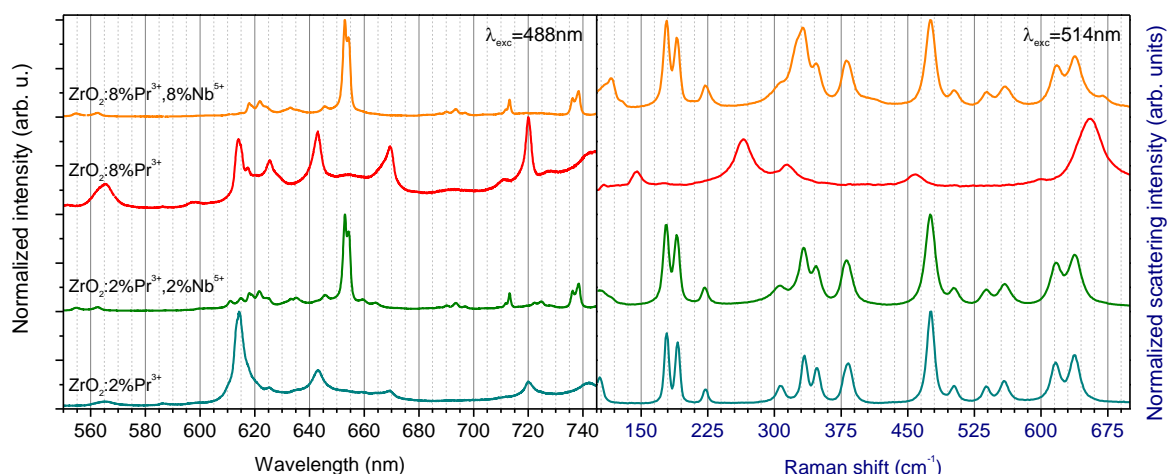


Figure 1. Luminescence spectra (left panel) and corresponding Raman spectra (right panel) of differently doped ZrO_2 nanopowders synthesized by sol-gel method and annealed at 1200°C .

[1] V. Kiisk, L. Puust, K. Utt, A. Maaroos, H. Mändar, E. Viviani, F. Piccinelli, R. Saar, U. Joost, I. Sildos, Photo-, thermo- and optically stimulated luminescence of monoclinic zirconia, *Journal of Luminescence*, 174, 49-55, (2016).

[2] L. Puust, V. Kiisk, M. Eltermann, H. Mändar, R. Saar, S. Lange, I. Sildos, L. Dolgov, L. Matisen, R. Jaaniso, Effect of ambient oxygen on the photoluminescence of sol-gel-derived nanocrystalline $\text{ZrO}_2:\text{Eu}$, Nb, *Journal of Physics D: Applied Physics*, 50, 21530, (2017).

[3] A. Čirić, S. Stojadinović, Photoluminescence properties of Pr^{3+} doped ZrO_2 formed by plasma electrolytic oxidation, *Journal of Alloys and Compounds*, 803, 126-134, (2019).

In-situ luminescence measurements for advanced ceramic breeder pebbles under the influence of X-rays and β -rays

A. Zariņš^{1,2}, A. Ansonē¹, J. Čīpa^{1,3} and G. Kizāne¹

1 – University of Latvia, Institute of Chemical Physics, Laboratory of Radiation Chemistry of Solids, 1 Jelgavas street, LV-1004, Riga, Latvia

2 – Daugavpils University, Faculty of Natural Science and Mathematics, Department of Environmental Science and Chemistry, 1a Parādes street, LV-5401, Daugavpils, Latvia

3 – University of Latvia, Institute of Solid State Physics, Laboratory of Spectroscopy, 8 Kengarāga street, LV-1063, Riga, Latvia

Main author email address: arturs.zarins@lu.lv

Advanced ceramic breeder (ACB) pebbles consisting of monoclinic lithium orthosilicate (Li_4SiO_4) as the primary phase and monoclinic lithium metatitanate (Li_2TiO_3) as the secondary phase are suggested as a potential solid-state candidate material for the tritium breeding in future thermonuclear fusion reactors [1]. In this study, the behaviour of luminescence emission for the Li_4SiO_4 pebbles with various nominal contents of Li_2TiO_3 was analysed under the influence of X-rays and β -rays using *in-situ* luminescence measurement technique and thermally stimulated luminescence method. The analysed samples were produced using a high-temperature melt jet break-up process, KALOS (KARlsruhe Lithium OrthoSilicate), at the Karlsruhe Institute of Technology (Germany) [2]. Figure 1 shows typical X-ray induced luminescence spectrum and thermally stimulated luminescence glow curve of the Li_4SiO_4 pebbles with additions of Li_2TiO_3 , respectively.

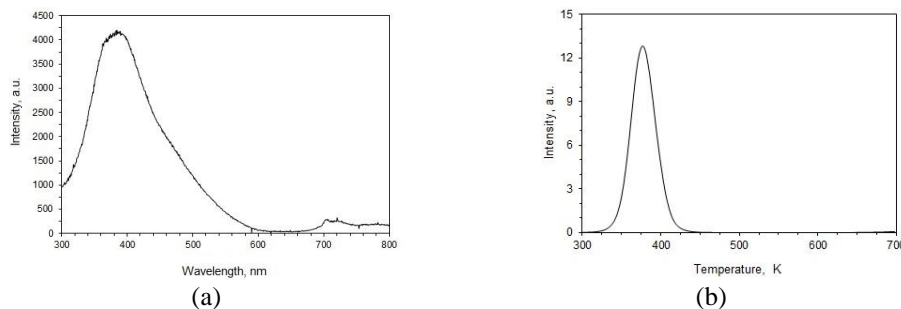


Figure 1. (a) X-ray induced luminescence spectra and (b) thermally stimulated luminescence glow curve of the Li_4SiO_4 pebbles with 10 mol% Li_2TiO_3

The X-ray and β -ray induced luminescence spectra of the Li_4SiO_4 pebbles with additions of Li_2TiO_3 are complex and consist of several overlapped bands with maxima between 300 nm and 800 nm. The luminescence band with a wavelength around 450 nm was attributed to the formation of E' centres (SiO_3^{3-}) or some variants of oxygen deficiency centres (ODCs) in the monoclinic Li_4SiO_4 phase [3,4]. The band with a relatively small intensity and a wavelength around 700 nm was attributed to the monoclinic Li_2TiO_3 phase [5]. The luminescence band with a wavelength around 380 nm has been detected in lithium oxide (Li_2O) and thereby can be attributed to F^+ centres (i.e. one localised electron in oxygen vacancy) [6]. In the thermally stimulated luminescence glow curves of the X-ray and β -ray irradiated Li_4SiO_4 pebbles with additions of Li_2TiO_3 , one main peak with a maximum at around 360 K was detected. This TSL peak is not stable during sample storage at room temperature, and the intensity of this peak decreases rapidly after the irradiation. The ACB pebbles are biphasic without solid solutions [2], and consequently the generation mechanism and the structure of primary RD during irradiation with X-rays and β -rays is similar to the single-phase ceramics. The minor excess of Li_2O can be added in the ACB pebbles during the fabrication process and thereby form additional LiO_4 tetrahedral groups in the primary phase.

[1] F. Cismondi et al., Progress of the conceptual design of the European DEMO breeding blanket, tritium extraction and coolant purification systems, *Fusion Engineering and Design*, 157, 111640 (2020).

[2] R. Knitter et al., Fabrication of modified lithium orthosilicate pebbles by addition of titania. *Journal of Nuclear Materials*, 442, S433-S436 (2013).

[3] K. Moritani et al., Production behavior of irradiation defects in lithium silicates and silica under ion beam irradiation. *Journal of Nuclear Materials*, 281, 106-111 (2000).

[4] H. Moriyama et al., In-situ luminescence measurement of irradiation defects in lithium silicates, *Nuclear Instruments and Methods in Physics Research Section B: Beam Interactions with Materials and Atoms*, 91, 317-321 (1994).

[5] V. Correcher and M. González. Preliminary results on the relationship between luminescence and crystalline structure of lithium metatitanate, *Nuclear Instruments and Methods in Physics Research Section B: Beam Interactions with Materials and Atoms*, 326, 86-89 (2014).

[6] Y. Asaoka et al., In-situ luminescence measurement of irradiation defects in lithium oxide, *Journal of Nuclear Materials*, 183, 174-179 (1991).

Nanoindentation and fracture characteristics of doped ZnO:In and ZnO:Ga luminescent ceramics

**F. Muktepavela¹, A. Zolotarjovs¹, K. Kundzins¹, P. Rodnyi², E. Gorokhova³,
E. Tamanis⁴, I. Venevcev²**

¹University of Latvia, Institute of Solid State Physics, 8 Kengaraga str., LV-1069, Riga, Latvia

²St.Petersburg State Polytechnic University, 29 Polytekhnicheskaja str., 195 251, Saint-Petersburg, Russia

³Scientific and Production Association S.I.Vavilov State Optical Institute, 36-1 Babushkina str., 192171, Saint Petersburg, Russia

⁴Daugavpils University, 13 Vienibas str., Daugavpils, LV-5401 Latvia

famuk@latnet.lv

ZnO as a wide-band-gap (band gap of 3.37 eV) multifunctional semiconductor possesses excellent optical properties and has a variety of applications which do not lose their relevance. Due to its luminescent characteristics the ZnO is a promising material for scintillators. With the recent advances in hot press sintering technology transparent ZnO ceramics based on nanopowders have aroused great interest for its use in fast and high-efficient photo- or X-ray luminescence scintillators. Despite many studies on the structural, electrical and optical properties of the ZnO ceramics its mechanical characteristics remain practically unexplored. It is known that mechanical properties are highly structure sensitive [3] and, thus, they will determine not only the technological properties of ceramics, but also reveal the influence of the doped elements on the structural phase state of ceramics. In this regard, the most applicable to ZnO ceramics (in form of thin discs) is nanoindentation (NI) as a fast and accurate method to measure the localized modulus of elasticity and hardness.

In the present research comparative analysis of the fracture modes and nanoindentation characteristics of the hot pressed ZnO: 0.13 wt% In and ZnO: 0.1 wt% Ga ceramics as promising materials for scintillators are investigated. Basing on results of nanoindentation, optical, atom force and scanning electron microscopy as well as energy dispersive X-ray spectra measurements different locations of gallium and indium in the microstructure (gallium within grains but indium in grain boundaries of ceramics) and their different effect on the mechanical properties of ZnO were found.

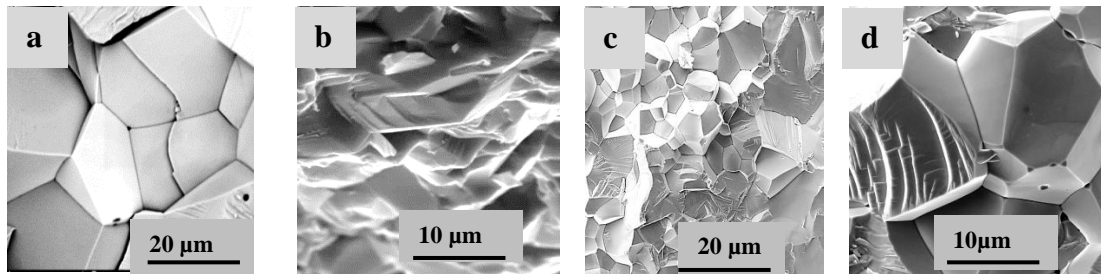


Figure 1. SEM images of the fracture surfaces in undoped (a), In-doped (b) and Ga-doped (c,d) ZnO ceramics.

The ZnO:Ga ceramics has increased modulus of elasticity ($E = 175$ GPa) within the grain, decreased hardness ($H = 2.5$ GPa) with cracking near grain boundaries (GBs) and exhibits brittle intercrystalline fracture mode. The ZnO:In ceramics is characterized by indium induced serrated GBs forms, transcrystalline fracture mode, modulus of elasticity ($E = 140$ GPa), hardness ($H = 4.5$ GPa) values close to those of the single crystalline ZnO and absence of GBs brittleness due to the presence of indium on GBs. Results evidence that the ZnO:In ceramics has a greater stress relaxation potential than the ZnO:Ga ceramics.

1. M. Ivor, D. Medved, M. Vojtko, A. Naughton-Duszova, L. Marciniak, J. Dusza. Nanoindentation and tribology of ZrB₂ based luminescent ceramic. J. Eur. Ceram. Soc., 40 (14) 2020 pp 4901-09.

This research is supported by the Project ERANET RUS_ST#2017-051 (Latvia) and #18-52-76002 (Russia);

Institute of Solid State Physics, University of Latvia as the Center of Excellence has received funding from the European Union's Horizon 2020 Framework, Programme H2020-WIDESPREAD -01-2016-2017-Teaming Phase 2 under grant agreement No 739508, project CAMART².

Fine structure of luminescence spectra of RE³⁺ ions in single crystals Gd₃Ga₅O₁₂

N. Mironova-Ulmane¹, A.I. Popov¹, G. Kriekle¹, I. Sildos², L. Puust², S.B. Ubizskii³, D. Sugak^{3,4}, E. Elsts¹, A. Sarakovskis¹

1-Institute of Solid State Physics, University of Latvia, 8 Kengaraga Str., Riga, , Latvia

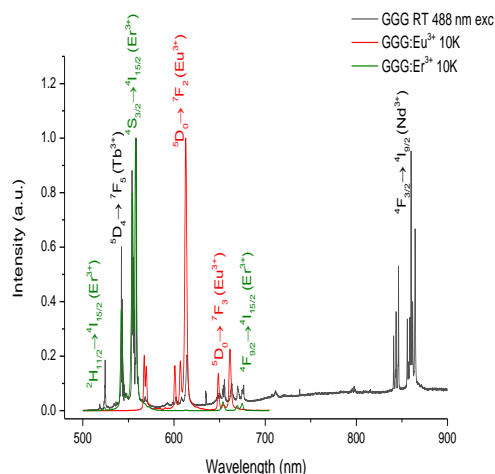
2-Institute of Physics, University of Tartu, W. Ostwald Str. 1, 50411 Tartu, Estonia

3-Lviv Polytechnic National University, 12, Bandera srt., Lviv 79013, Ukraine

4-Scientific Research Company „Electron-Carat”, 202 Stryjska Str., 79013 Lviv, Ukraine

Main author email address: Nina.Mironova-Ulmane@cfi.lu.lv

In the last decade, much effort has been directed towards studying the luminescence properties of Gd₃Ga₅O₁₂ (GGG) doped with rare earth elements (RE), especially in the development of laser elements, 3D optical imaging for display development, bio-imaging and neutron scintillator detectors. As it was established, the RE³⁺ ions replace Gd³⁺ ions located at a site of orthorhombic D₂ symmetry in the lattice GGG during crystal growth [1].



In this work we studied Gd₃Ga₅O₁₂ single crystals grown by the Czochralski method from the melt at a temperature about 1750°C in an N₂ atmosphere with 2% addition of O₂ [2]. The PL spectra were obtained upon excitation by a wavelength tunable pulsed solid state laser Ekspla NT342/3UV. The corresponding luminescence was recorded by Andor iStar DH734 CCD camera coupled to the spectrometer Andor SR-303i-B spectrometer, equipped with grating 2400 lines/mm (resolution at list 0.1 nm) using CCD camera.

Low temperature measurements were performed using Advanced Research Systems DE202 N cold finger type He cryostat. The photoluminescence (PL) spectra were also measured at RT in the spectral range of 500–1000 nm with the use of 1400 grooves/mm gratings onto Peltier-cooled CCD detectors under Argon laser 488 nm excitation.

In this work we have observed and analyzed the photoluminescence (PL) spectra of Er³⁺, Eu³⁺, Tb³⁺, Nd³⁺ ions in GGG in visible spectral range. Some PL spectra of Er³⁺, Eu³⁺, Tb³⁺, Nd³⁺ ions observed in GGG under 488 nm excitation at room temperature and 10 K are shown in Figure, where the corresponding electronic transitions of Er³⁺, Eu³⁺, Tb³⁺, Nd³⁺ ions are indicated.

In addition, the excitation spectrum of Er³⁺ ions for 558 nm photoluminescence was measured. It is concluded, that the overall Stark structures of the excitation spectrum bands of Er³⁺ (transition 4I_{15/2} → 4F_{3/2}, 4F_{5/2}, 4F_{7/2}, 2H_{11/2}, 4S_{3/2}) in the GGG are identical.

In conclusion, the corresponding scheme of splitting of the Stark energy levels of the investigated transitions of ions in the GGG is constructed.

1. A. Speghini, F. Piccinelli, M. Bettinelli Synthesis, characterization and luminescence spectroscopy of oxide nanopowders activated with trivalent lanthanide ions: The garnet family. *Optical Materials* 33, pp. 247-257, (2011).

2. I.M. Solskii, D.Yu Sugak, M.M. Vakiv. Growing Large Size Complex Oxide Single Crystals by Czochralski Technique for Electronic Devices. *Acta Phys. Pol., A*, 124, pp. 314-320, (2013)

Structural Characterization of Thermally Reduced Graphene Oxide in the Presence of Malonic Acid and Phosphorus Pentoxide

Rūta Aukštakojytė¹, Justina Gaidukevič¹, Jurgis Barkauskas¹

¹ Institute of Chemistry, Faculty of Chemistry and Geosciences, Vilnius University, Naugarduko 24, LT-03225 Vilnius, Lithuania

ruta.aukstakojyte@chgf.vu.lt

Graphene is a two dimensional (2D) material with sp^2 hybridized carbon atoms configured in a honeycomb-like structure. Unique thermal, electrical, optical, physical and mechanical properties make it highly promising energetic material for various applications in electronics or electrochemical power sources such as fuel or solar cells and supercapacitors [1]. Today thermal reduction of graphene oxide (GO) is one of the potential synthesis methods to obtain graphene in a simple, low-cost, high yield and time-saving way. However, high volume of carbon dioxide, carbon monoxide and H_2O is released due to the deoxygenation of functional groups in GO lattice. The vigorous process of deoxygenation generates topological defects and C vacancies in the final product and causes poor electrical conductivity of graphene prepared this way. Also, high temperature of exfoliation leads to the fragmentation of graphene structure [2]. To overcome these drawbacks, efficiency recovery of conjugated π -electron system could be achieved by using lower temperature of reduction and suitable source of elemental carbon. According to the literature, reaction between malonic acid (MA) and phosphorus pentoxide gives carbon suboxide (C_3O_2) that decomposes into carbon atoms at low temperatures [3]. By addition of these compounds in reduction of GO lower defects concentration and better structural properties of thermal reduced graphene can be achieved.

In this work, we present a new approach of thermal reduction of GO in the presence of additives. Three GO samples were prepared using different oxidizing agents and exfoliated by adding various amounts of MA and P_2O_5 . The thermal annealing under Ar gas atmosphere was performed for 30 min at different temperatures: 100 °C, 150 °C, 250 °C and 500 °C. Reduced GO products were analyzed by Fourier Transform infrared (FTIR) and Raman spectroscopy, scanning electron microscopy (SEM) and X-ray diffraction (XRD) analysis. Furthermore, measurements of electrical conductivity have also been carried out.

ACKNOWLEDGEMENTS:

This project has received funding from European Social Fund (project No 09.3.3-LMT-K-712-16-0154) under grant agreement with the Research Council of Lithuania (LMTLT).

[1] Q. Ke, J. Wang, Graphene-based materials for supercapacitor electrodes – A review, *Journal of Materiomics* 2, 37-54 (2016).

[2] S. Pei, H. Cheng, The reduction of graphene oxide, *Carbon* 50, 3210-3228 (2012).

[3] A. Ganguly, *Fundamentals of Inorganic Chemistry* (Pearson Education India) (2011).

EPR SPECTROSCOPY OF MANGANESE DOPED FERROELECTRIC $[\text{NH}_4][\text{Zn}(\text{HCOO})_3]$ FORMATE FRAMEWORK

M. Navickas¹, L. Giriūnas¹, V. Kalendra¹, T. Biktagirov², U. Gertsmann², W. G. Schmidt², M. Maćzka³, A. Pöppel⁴, J. Banys¹, M. Šimėnas¹

1- Faculty of Physics, Vilnius University, Saulėtekio 9, LT-10222 Vilnius, Lithuania

2- Department of Physics, Paderborn University, Warburger 100, D-33098 Paderborn, Germany

3- Institute of Low Temperature and Structure Research, Polish Academy of Sciences, P.O. Box-1410, PL-50-950 Wroclaw, Poland

4- Felix Bloch Institute for Solid State Physics, Leipzig University, Linnestrasse 5, D-04103 Leipzig, Germany

marius.navickas@ff.vu.lt

Metal-organic frameworks (MOFs) are extensively studied hybrid materials due to their potential applications in gas storage and separation systems and multiferroic memory devices [1, 2]. These coordination networks are formed from various organic linker molecules and metal centers that constitute porous structures. In the so called dense MOFs, the pore system inherently confines molecules, which are tightly bound to the framework. The most popular class of dense MOFs is metal-formate frameworks, which often exhibit interesting ferromagnetic and ferroelectric properties. These compounds consist of transition metal ions linked by formate linkers into porous frameworks, where each pore confines a molecular cation. Many members of these frameworks exhibit structural phase transitions, related to molecular cation ordering and metal-formate framework deformation. A useful method to study local changes in formate frameworks is electron paramagnetic resonance (EPR) spectroscopy.

In this work we present X-band and Q-band continuous wave (CW), pulse EPR and electron nuclear double resonance (ENDOR) study of manganese doped $[\text{NH}_4][\text{Zn}(\text{HCOO})_3]$ (AmZnF) hybrid formate framework, which exhibits ferroelectric phase transition at 190 K. The temperature dependent EPR spectra of AmZn:Mn²⁺ powder are typical Mn²⁺ powder patterns of the 3d⁵ electronic configuration. The obtained non-zero value of the zero-field splitting at low temperature shows the deformation of the MnO₆ octahedra. CW EPR results are supported by the density functional theory calculations.

In order to study the broader environment of the Mn²⁺ probe ion, we performed pulse EPR experiments [3]. As expected, the low temperature electron spin echo-detected field sweep spectrum corresponds to the powder pattern of the Mn²⁺ ions, indicating the uniform distribution of Mn²⁺ centers in crystal lattice. The two and three-pulse electron spin echo envelope modulation (ESEEM) (spectra presented in Fig 1) measurements data indicates the interaction between Mn²⁺ center and protons. ENDOR spectrum shows the interactions of different protons with Mn²⁺ center. The two-dimensional hyperfine sublevel correlation (HYSCORE) EPR spectrum also indicates proton interactions and demonstrates the signal of ¹³C. Longitudinal relaxation measurements of low temperature phase shows that the longitudinal relaxation is dominated by the direct process of the acoustic lattice phonons at lower temperature and the two-phonon Raman process at higher temperatures.

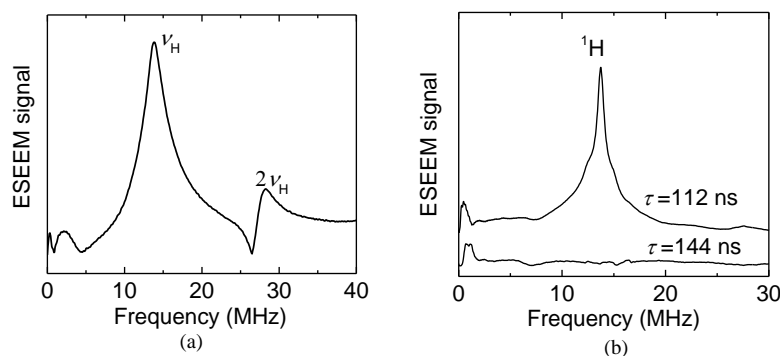


Figure 1 X-band 2 pulse (a) and 3 pulse (b) ESEEM spectra obtained at 15 K. The 3 pulse ESEEM spectrum demonstrates the blind spot on proton Larmor frequency at $\tau = 144$ ns.

[1] B. Li and H.-M. Wen, Porous metal-organic framework for gas storage and separation: what, how and why?, *The journal of physical chemistry letters*, 5., pp. 3468-3479, (2014).

[2] P. Jain and A. Stroppa, Switchable electric polarization and ferroelectric domains in a metal-organic-framework, *Npj Quantum Materials*, 1., pp. 1-6, (2016).

[3] A. Schweiger, *Principles of Pulse Electron Paramagnetic Resonance* (Oxford University Press), (2001).

X-ray defect formation in rare-earth ion doped oxyfluoride glasses

A. Antuzevics, G. Krieke, E. Pavlovskā

Institute of Solid State Physics, University of Latvia, Kengaraga Str. 8, Riga, Latvia

Andris.Antuzevics@cfi.lu.lv

X-ray induced defects in glasses are typically responsible for absorption bands in the visible part of the electromagnetic spectrum, which leads to a coloration of the sample [1]. Additionally, in rare-earth ion activated glasses changes in the oxidation state of the activator and thereby – luminescence properties – can be expected [2]. For optical applications both effects may be undesirable and should be controlled.

In this study formation and stability of x-ray induced defects is analyzed in different oxyfluoride glass systems with emphasis on generation of paramagnetic species and electron paramagnetic resonance (EPR) investigations. Different defect centres can be created depending on the chosen composition, which produce EPR signals in the vicinity of $g = 2.0$ (in X-band EPR at $B \approx 3370$ G). It is demonstrated in Figure 1 that defect formation can be suppressed by doping the composition with europium.

The financial support of Latvian Council of Science grant LZP-2018/1-0335 “Novel transparent nanocomposite oxyfluoride materials for optical applications” is greatly acknowledged.

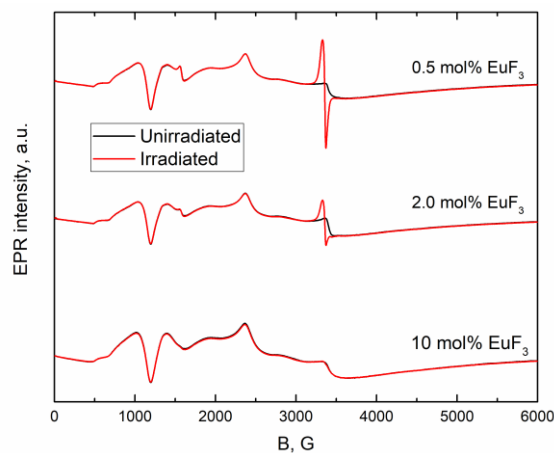


Figure 1. EPR spectra of oxyfluoride glasses with different content of europium prior and after irradiation with X-rays.

[1] J. Sheng, K. Kadono, Y. Utagawa, T. Yazawa, X-ray irradiation on the soda-lime container glass, *Applied radiation and isotopes*, 56(4), 621-626, (2002).

[2] G. Okada, J. Ueda, S. Tanabe, G. Belev, T. Wysokinski, D. Chapman, D. Tonchev, S. Kasap, Samarium-doped oxyfluoride glass-ceramic as a new fast erasable dosimetric detector material for microbeam radiation cancer therapy applications at the Canadian synchrotron, *Journal of the American Ceramic Society*, 97(7), 2147-2153, (2014).

Cr³⁺ paramagnetic probe in LaOCl

Haralds Ozols, Andris Antuzevics, Guna Kriekle

Institute of Solid State Physics, University of Latvia

haralds.ozols@cfi.lu.lv

Doped LaOCl can be used as a luminophore material with luminescent properties highly dependent on the type and concentration of the doped elements. For electron paramagnetic resonance (EPR) studies of materials, activators such as Gd³⁺ or Mn²⁺ are typically used, however while studying different activators in LaOCl, an atypical EPR spectrum was observed for Cr³⁺ (Figure 1 (a)).

In this work LaOCl:Cr³⁺ samples have been studied with different concentrations of Cr³⁺: 0.01 mol%, 0.1 mol% and 0.5 mol%. La_xY_{1-x}OCl:Cr³⁺ with different La-Y proportions in increments of 10% were also studied.

EPR spectrum of LaOCl:Cr³⁺ consists of a superhyperfine structure (shfs) which can be explained with electron-nucleus interactions between Cr³⁺ and the surrounding Cl or La nuclei. In Cr³⁺ doped YOCl no shfs structure is observed, despite the similarities of crystalline structures of LaOCl and YOCl. This suggests that the shfs structure originates from Cr³⁺ - La electron-nucleus interactions, however the interaction between Cr³⁺ and Cl is also considered. The intensity of the EPR spectrum of LaOCl:Cr³⁺ increases with increasing the Cr³⁺ concentration in the sample without shifting the shfs structure. Luminescence study of LaOCl:Cr³⁺ shows that there is virtually no luminescence at room temperature, however at lower temperatures luminescence intensity greatly increases (Figure 1 (b)).

Based on the EPR and luminescence experimental data and EPR spectra simulations, the properties of Cr³⁺ as an activator in LaOCl are discussed.

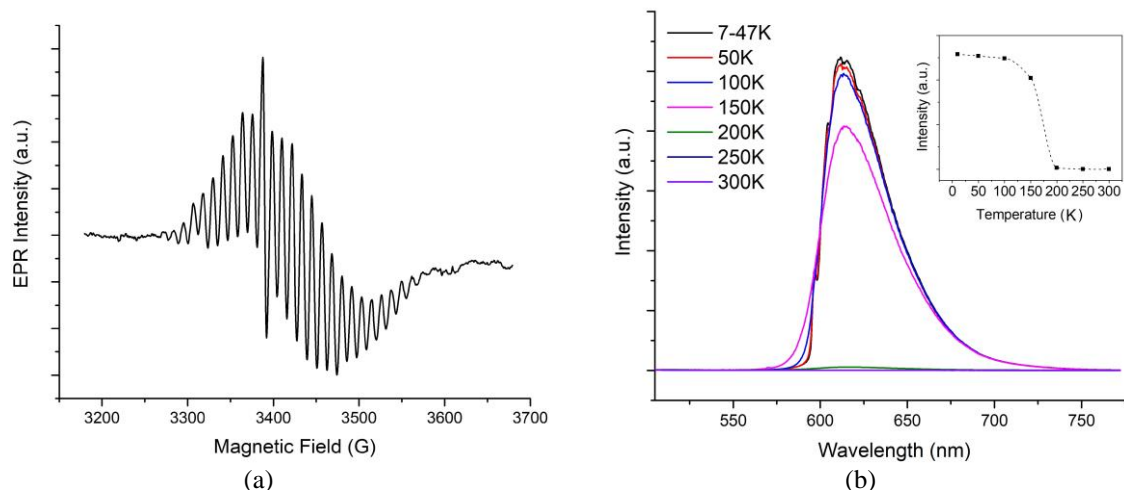


Figure 1 (a) EPR spectrum of Cr³⁺ doped LaOCl with Cr³⁺ concentration 0,5 mol% (b) luminescence of Cr³⁺ doped LaOCl with Cr³⁺ concentration 0,5 mol% depending on temperature.

The financial support of Latvian Council of Science grant LZP-2018/1-0335 “Novel transparent nanocomposite oxyfluoride materials for optical applications” is greatly acknowledged.

Gadolinium ion incorporation in CaF₂ oxyfluoride glass ceramics.

Jekabs Cirulis, Andris Antuzevics, Guna Kriekle

Institute of Solid State Physics, University of Latvia

Jekabs.Cirulis@cifi.lu.lv

Transparent rare earth doped oxyfluoride glass ceramics are potential alternative for high efficiency luminescent materials. Crystalline phase in ceramics is the reason for increased luminescence over glass. So it is of interest to control the incorporation of activator ions in the crystalline phase of glass ceramics.

Following glass compositions were synthesized: 46SiO₂ – 20Al₂O₃ – 8CaCO₃ – 25.9CaF₂ – 0.1GdF₃ (STD) and STD – 20.9CaF₂ – 5XF where X is Li, K, Na. Samples were treated at different temperatures and for each sample electron paramagnetic resonance (EPR) and x-ray diffraction (XRD) analysis was carried out.

The EPR spectra contain quantitative information about incorporation of Gd³⁺ ions in CaF₂ crystalline phase. In addition, measurements for polycrystalline CaF₂ samples were made to characterize Gd³⁺ incorporation dynamics depending on the composition and annealing temperature of glass ceramics.

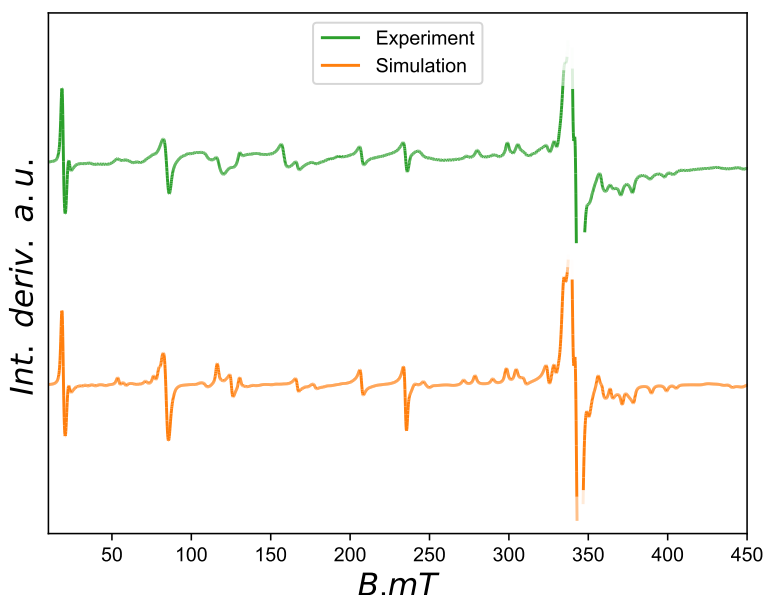


Figure 1 Example spectrum of standard sample annealed at 750 °C.

The financial support of Latvian Council of Science grant LZP-2018/1-0335 Novel transparent nanocomposite oxyfluoride materials for optical applications is greatly acknowledged.

Thermal annealing of oxygen-related structural defects in fast-neutron-irradiated aluminium oxide crystals

G. Prieditis¹, A. Lushchik¹, A.I. Popov², V. Seeman¹, E. Shablonin¹

1- Institute of Physics, University of Tartu, W. Ostwald Str. 1, 50411 Tartu, Estonia

2- Institute of Solid State Physics, University of Latvia, Kengaraga Str. 8, Riga LV-1063, Latvia

Main author email address: prieditisgatis@gmail.com

Because of fascinating mechanical and physicochemical properties, aluminum oxide single crystals and transparent ceramics are used for various applications in science and technology. In particular, Al₂O₃ is involved in the list of attractive candidates with optical/diagnostics window capabilities for future fusion devices (PROTO and other deuterium-tritium reactors). Accumulation of stable structural defects determines the radiation damage and strongly influences the functionality of optical materials. Therefore, the investigation of the creation of interstitial-vacancy Frenkel pairs and their aggregates under fission neutron irradiation as well as the processes of subsequent thermal annealing of radiation defects (i.e. material recovery) is of a special importance. It is generally accepted that the universal knock-on mechanism (elastic collisions of incident particles with crystal atoms/ions) of Frenkel defect creation is a dominant mechanism of radiation damage under metal oxide irradiation by fast neutrons.

The process of radiation damage caused by ~1-MeV fission neutrons (Oak Ridge National Laboratory, fluence of 6.9×10^{18} n/cm²) has been studied in Czochralski-grown Al₂O₃ single crystals from Union Carbide Corporation by means of the optical spectroscopy and EPR methods. The similar studies have been recently performed for magnesium aluminate spinel and MgO crystals [1, 2]. The EPR spectra were measured by Bruker X-band (9.8 GHz) EPR spectrometer ELEXSYS E500. The spectra of optical absorption were measured at room temperature (RT) in a spectral region of 1.5-6.5 eV using a high-absorbance spectrometer JASCO V-660 with a double monochromator, while measurements in near-vacuum UV region (up to 9 eV) were performed using a vacuum monochromator and the hydrogen discharge light source. The annealing of radiation-induced optical absorption (RIOA, absorption of a virgin crystal is subtracted) was performed in a stepwise regime in a flowing argon atmosphere up to 1300 K. The main emphasis was paid to oxygen-related defects: F^+ and F centers (an oxygen vacancy with one to two trapped electrons, respectively) and their simplest aggregates – two spatially close anion vacancies in different charge states (F_2 , F_2^+ , F_2^{2+} – see, e.g., [3]). Subsequent comparison of the temperature dependences of elementary absorption bands related to different F -type defects as well as the pulse annealing of the EPR signal of F^+ centers (under the same annealing procedure conditions) has been performed. The elementary bands were obtained via decomposition of RIOA spectra (after irradiation and each subsequent preheating) into Gaussian components with the maximum position in brackets: F (6.1 eV) and F^+ (4.8 eV and 5.3 eV), F_2 (4.1 eV), F_2^+ (3.4 eV) and F_2^{2+} (2.7 eV).

The experimental decay kinetics has been analyzed in terms of the diffusion-controlled bimolecular reactions (see for details [4, 5]) between the F^+ , F centers and complementary interstitial oxygen ions – the most “invisible/hidden” primary Frenkel defect in wide-gap metal oxides. Rather complicated transformation between tree types of F_2 aggregates at temperatures above 600 K has been analyzed as well. The obtained results are compared with the literature data (see [4, 5] and references therein). The EPR signal of a trapped-hole center revealed for the first time in a neutron-irradiated Al₂O₃ and the corresponding RIOA band around 5.6 eV are tentatively ascribed to oxygen interstitials, while further study and modelling of this important Frenkel defect still lies ahead. A tentative scenario of the irreversible annealing of neutron-induced defects in Al₂O₃ single crystals has been considered

- [1] V. Seeman, E. Feldbach, T. Kärner, A. Maaros, N. Mironova-Ulmane, A.I. Popov, E. Shablonin, E. Vasil'chenko, A. Lushchik, Fast-neutron-induced and as-grown structural defects in magnesium aluminate spinel crystals with different stoichiometry, *Opt. Mater.* 91, 42-49 (2019).
- [2] G. Baubekova, A. Akilbekov, E.A. Kotomin, V.N. Kuzovkov, A.I. Popov, E. Shablonin, E. Vasil'chenko, M. Zdorovets, A. Lushchik, Thermal annealing of radiation damage caused by swift ¹³²Xe ions in MgO crystals, *Nucl. Instrum. Meth. B* 462, 163-168 (2020).
- [3] B.D. Evans, A review of the optical properties of anion lattice vacancies, and electrical conduction in α -Al₂O₃: their relation to radiation-induced electrical degradation, *J. Nucl. Mater.* 219, 202-223 (1995).
- [4] E.A. Kotomin, V.N. Kuzovkov, A.I. Popov, R. Vila, Kinetics of F center annealing and colloid formation in Al₂O₃, *Nucl. Instrum. Meth. B* 374, 107-110 (2016)
- [5] A.I. Popov, A. Lushchik, E. Shablonin, E. Vasil'chenko, E.A. Kotomin, A.M. Moskina, V.N. Kuzovkov, Comparison of the F-type center thermal annealing in heavy-ion and neutron irradiated Al₂O₃ single crystals, *Nucl. Instrum. Meth. B* 433, 93-97 (2018).

Paramagnetic defects in neutron irradiated Al₂O₃

A. Antuzevics, M. Kemere, A. I. Popov

Institute of Solid State Physics, University of Latvia, Kengaraga Str. 8, Riga, Latvia

Andris.Antuzevics@cfi.lu.lv

It is fundamentally important to understand, control and predict the effect of radiation on structure and optical properties of functional materials. Al₂O₃ is an important technological material with a wide array of applications such as solid-state lasers, substrates for microelectronics and optical windows. In this work formation and thermal stability of neutron irradiation induced defects is investigated in single crystalline and sintered Al₂O₃ samples.

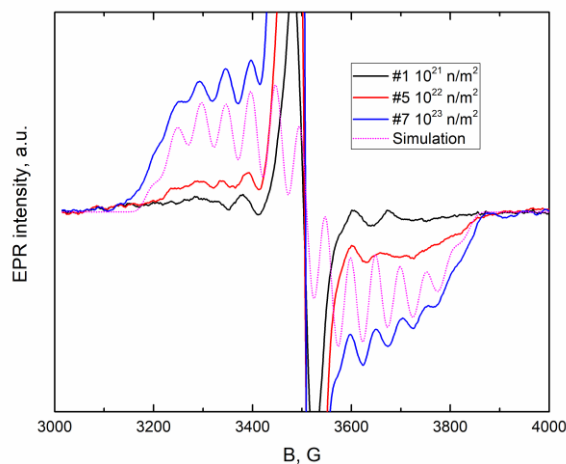


Figure 1. EPR spectra of sintered samples subjected to different fluences of neutron irradiation. Simulation curve represents the F⁺ center signal in Al₂O₃.

Electron paramagnetic resonance (EPR) spectroscopy investigations reveal the presence of Cr³⁺ and Fe³⁺ ions in the single crystals, while no impurities can be detected in the sintered samples. EPR signals in the vicinity of $g = 2$ (≈ 3500 G, see Figure 1) correlate with the neutron dose received by the samples and are assigned to F⁺ and trapped hole centers. Based on EPR and photoluminescence analysis creation and thermal stability of radiation-induced defects will be discussed in single crystal and sintered Al₂O₃.

FTIR spectra of neutron irradiated CVD diamonds

G. Chikvaidze¹, T.A. Scherer², G. Aiello², A.I. Popov¹

1- Institute of Solid State Physics University of Latvia, Riga, 8 Kengaraga, 1069 Riga, Latvia

2 - Karlsruhe Institute of Technology, Institute for Applied Materials, Eggenstein-Leopoldshafen, 76344 Germany,

Email address: georgc@cfi.lu.lv

Chemical vapor deposition (CVD) diamond windows are important components of electron cyclotron heating and current drive systems used in tokamaks for a diverse range of applications including plasma heating and control of plasma magneto-hydrodynamic instabilities [1]. Although in order to understand and predict their performance in harsh radiation environment, numerous radiation tests have already been carried out for various diamond samples, nevertheless, there is still a lot of ambiguity regarding damage to diamond materials by fast neutrons.

In this work, using FTIR spectroscopy, we present the results of a comparative analysis of two CVD diamond disks, which were irradiated with two different fluences of fast neutrons with one similar non-irradiated CVD diamond disk.

All spectra were recorded using FTIR vacuum spectrometer Vertex 80v (Bruker, Germany) in spectral range of 50 – 10000 cm^{-1} with spectral resolution of 2 cm^{-1} . All spectra were measured in transmission mode at room temperature, using LNT-cooled MCT detector.

An unirradiated diamond sample shows a spectrum, which is common to synthetic diamonds. In particular, only spectral lines characteristic for the diamond are observed in the spectral region of 1900 - 2500 cm^{-1} (lines belong to the C - C vibrations).

Significant changes were found in the spectrum of irradiated CVD diamond, which are directly dependent on the radiation dose.

In particular, new bands at 1007 cm^{-1} , 1116 cm^{-1} , 1194 cm^{-1} , related to nitrogen (N) were observed. Furthermore, another new bands at 1390 cm^{-1} and 1416 cm^{-1} also arose. Finally, new bands at 1528 cm^{-1} and 1566 cm^{-1} , which are tentatively assigned to local defect modes also appeared. No such bands are found in the unirradiated samples. Note, that the intensity of all these bands increases with increasing dose from 10^{21} n/m^2 to 10^{22} n/m^2 . We also note that only small changes were observed in the region of 1800–2300 cm^{-1} .

It was also found that the intensities of characteristic of C - C bonds do not change monotonously with neutron fluence.

All these changes indicate, in particular, the appearance of lattice disorder in the sample irradiated with a dose of 10^{22} n/m^2 .

[1] Aiello, G., Scherer, T., Avramidis, K. et al. Diamond Window Technology for Electron Cyclotron Heating and Current Drive: State of the Art. Fusion Science and Technology, 75(7), pp. 719-729, (2019).

Case analysis of self-trapped hole V_k center mobility in metal fluorides and fluoroperovskites

A. I. Popov^{1,2}, I. Makarenko³, Yu. Mastrikov¹, E.A. Kotomin¹,

1- Institute of Solid State Physics, University of Latvia, 8 Kengaraga, LV-1063, Riga, Latvia

2- Institute of Physics, University of Tartu, 1 W. Ostwald Str., Tartu 50411, Estonia

3- Kryvyi Rih State Pedagogical University, Gagarina Avenue, 54, Kryvyi Rih, Ukraine

popov@latnet.lv, popov@cfi.lu.lv

The self-trapped hole polarons (called also V_k centres) where a hole is shared by two nearest halogens, X_2^-) are very common color centers created in alkali halides and alkaline-earth halides under all kinds of irradiation (UV light, electrons, gamma rays, neutrons, heavy swift ions). The hole polarons start to migrate and recombine above certain critical temperatures. Their thermally induced decay has been observed by different experimental techniques (optical absorption, EPR, thermostimulated luminescence and etc) in almost all alkali halides, as well as in some halides and more complex halides, such as perovskite halides, ammonium halides, halide sodalites etc [1].

In this report, we review and analyse the self-trapped hole center migration temperatures for a series of alkali fluorides (LiF, NaF, KF, RbF, CsF), alkaline-earth fluorides (CaF₂, SrF₂, BaF₂), MgF₂, CdF₂ and some fluoroperovskites such as KMgF₃, RbMgF₃, BaLiF₃ as a function of halogen-halogen distance in a regular crystalline lattice as well as of halogen-halogen distance in isolated molecular ions. We will discuss similar situation in some other fluorides, such as CeF₃ or PbF₂, where V_k have not been observed.

[1] A.I. Popov, E.A. Kotomin, J. Maier. Solid State Ionics, 302 (2017) 3-6.

LAMOX functional materials as promising oxygen-ion electrolytes

N. Porotnikova^{1,2}, A. Khrustov^{1,2}, A. Farlenkov^{1,2}, A. Khodimchuk^{1,2}, M. Vlasov^{1,2}, G. Partin², I. Animitsa², M. Ananyev^{1,2}

1- Institute of High-Temperature Electrochemistry UB RAS, Russia;

2- Ural Federal University, Russia.

Porotnikova@ihte.uran.ru

Recently researches of SOFC with a high working temperature are aimed at its reduction. Therefore, it is of great importance to search for novel oxide-ion conductors with high ionic conductivity at intermediate temperatures (600–800 °C). The rare-earth molybdates $\text{La}_2\text{Mo}_2\text{O}_9$ have high oxygen-ion conductivity, the value of which at 800 °C is comparable with zirconium yttrium electrolyte.

Introduction of an inert additional phase $\text{La}_2\text{Mo}_3\text{O}_{12}$ to form $\text{La}_2\text{Mo}_2\text{O}_9$ – $\text{La}_2\text{Mo}_3\text{O}_{12}$ composite results in an increase of conductivity by approximately one order of magnitude. This increase is associated with the appearance of a composite effect in oxygen-ion conductors [1]. This study is aimed to identify the nature of the composite effect in $\text{La}_2\text{Mo}_2\text{O}_9$ – $\text{La}_2\text{Mo}_3\text{O}_{12}$ materials.

The X-ray diffraction study was carried out on Rigaku D/MAX-2200 diffractometer using Cu K α radiation: no peaks corresponding to impurity phases were observed. Morphology of the samples was investigated using the Tescan MIRA 3 LMU scanning electron microscope with the X-ray energy-dispersive microanalysis system (EDX). Microphotograph clearly shows the contrast of two different phases $\text{La}_2\text{Mo}_2\text{O}_9$ and $\text{La}_2\text{Mo}_3\text{O}_{12}$, which made it possible to mathematically calculate the grains distribution of each phases, length of the two-phase boundary and the porosity of the material. The electron backscatter diffraction (EBSD) analysis allowed estimation of the primary orientation of every grain for the considered surface area.

It was revealed that the composite effect in oxygen-ion diffusivity is caused by the formation of a new phase between grains of $\text{La}_2\text{Mo}_2\text{O}_9$ and $\text{La}_2\text{Mo}_3\text{O}_{12}$ in $\text{La}_2\text{Mo}_2\text{O}_9$ – $\text{La}_2\text{Mo}_3\text{O}_{12}$ composite, Fig. 1a. This new phase was detected for the first time by means of EBSD method to be La_2MoO_6 , Fig. 1b.

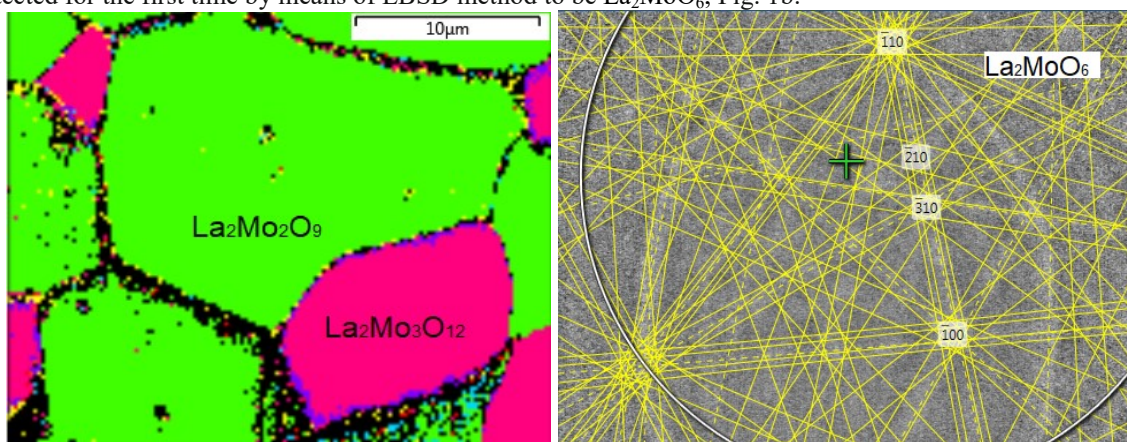


Figure 1 An EBSD map of the $\text{La}_2\text{Mo}_2\text{O}_9$ – $\text{La}_2\text{Mo}_3\text{O}_{12}$ surface (a) Kikuchi lines for La_2MoO_6

The oxygen isotope exchange method was used to study kinetics in the temperature range 850–950 °C and oxygen pressure 10^{-2} atm in the LAMOX system. The ^{18}O profiles for individual oxides consist of two regions corresponding to two processes: the rate of heterogeneous oxygen exchange (r_H) and the oxygen diffusion coefficient (D). But two relaxation processes for $\text{La}_2\text{Mo}_2\text{O}_9$ – $\text{La}_2\text{Mo}_3\text{O}_{12}$ materials are observed: the “fast” process of oxygen diffusion and the “slow” the oxygen isotope equilibration.

It was shown that the addition of the low-conducting phase $\text{La}_2\text{Mo}_3\text{O}_{12}$ leads to an increase in the heterogeneous exchange rate with maximum on 30mol% $\text{La}_2\text{Mo}_3\text{O}_{12}$. The length of the two-phase boundary $\text{La}_2\text{Mo}_2\text{O}_9$ and $\text{La}_2\text{Mo}_3\text{O}_{12}$ in the composite probably makes a significant contribution to the oxygen exchange process.

[1] G. Partin, N. A. Kochetova, I. E. Animitsa, Electrical Properties of $(1-x)\text{La}_2\text{Mo}_2\text{O}_9-x\text{La}_2\text{Mo}_3\text{O}_{12}$ ($x = 0.15$) Composite System, Sino-Russian ASRTU Conference Alternative Energy, 8–13, (2018)

LATTICE DYNAMICS CALCULATIONS FOR $\text{Mg}_{1-x}\text{Zn}_x\text{O}$ SOLID SOLUTIONS

Ciro F. Tiplaldi, Jevgenijs Gabrusenoks

Institute of Solid-State Physics, University of Latvia, Riga, Latvia

e-mail: tipaldi@cfi.lu.lv

In the course of this work MgO, ZnO and the $\text{Mg}_{1-x}\text{Zn}_x\text{O}$ solid solutions are studied by modelling lattice dynamics, using the methods of classical molecular dynamics. The main program used is General Utility Lattice Program (*GULP*). The Buckingham potential is used for modelling interatomic forces. The parameters for this potential are found for different effective ionic charges by using lattice parameters and vibrational frequencies obtained from *ab initio* calculations performed in the program *CRYSTAL*. With these potentials the dispersion relations and densities of states have been calculated for MgO, ZnO and $\text{Mg}_{1-x}\text{Zn}_x\text{O}$. Calculations have been made for different Mg and Zn contents in the wurtzite and cubic phase solid solutions respectively, using the supercell method and a large number of Brillouin zone sampling points.

The obtained potential parameters of the interatomic forces have been verified and the phonon dispersion curves and DOS for MgO and ZnO utilizing these potential parameters have been compared to previous work done by other researchers, both experimental and theoretical. By adding more Zn in the c-phase solution, no local vibrational modes are observed, however, there is a clear spectral widening and a noticeable change in the low frequency region ($100\text{-}300\text{ cm}^{-1}$) of the DOS. Adding more Mg in w-phase solution, on the other hand, results in local vibrational modes in the mid (350 cm^{-1}) and high frequency (650 cm^{-1}) regions. The calculation method used in this work allows for large crystalline structures and many different impurity concentrations.

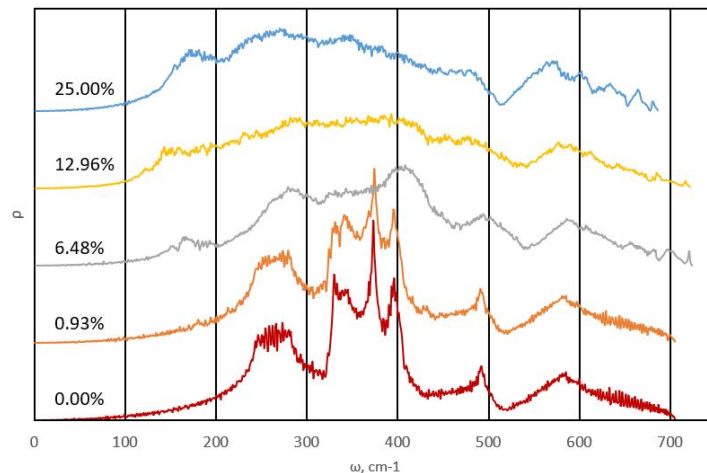


Fig. 1. Phonon density of states for $\text{Mg}_{1-x}\text{Zn}_x\text{O}$ at concentration values $x = 0.0; 0.0093; 0.0648; 0.1296; 0.25$.

This work is supported by the M-Era.net research project ZMOMUVS.

Theoretical calculation and spectroscopic measurements of electrocatalytic Cu and Cu/C thin films for CO₂ reduction

A. Knoks¹, S. Piskunov¹, G. Chikvaidze¹, J. Kleperis¹, R. Kalendarjovs¹, P. Lesnicenoks^{1,2}, I. Lukosevics¹, L. Jekabsons¹, G. Vaivars¹, L. Grinberga¹,

1- Institute of Solid state physics, University of Latvia, Kengaraga street 8, LV-1063

2-Faculty of Materials science and Applied Chemistry, Riga Technical University

Main author email address: knoks@cfi.lu.lv

Research on selective CO₂ reduction catalysts that can be used in large-scale, low-cost and environmentally friendly ways is on the rise for some time. Especially with potential of capturing and reforming anthropogenic CO₂ into useful materials. Thus, a clear mechanism determination is necessary, which is still missing. Theoretical and experimental methods are used to find it, i.e. grain boundaries of Cu₇ cluster investigated for electrocatalytic ability for the C₂H₄ formation through CH₂ dimerization or direct FTIR spectroscopy investigation for molecular-level information using an electrolysis cell with a thin film of copper cathode on the ATR crystal. It is known from theoretical calculations that electrochemical CO₂ reduction on Cu-decorated graphene electrode has attracted attention, because of its potential to generate significant amounts of hydrocarbon intermediates at high reaction rates over sustained periods of time. In fact, the first intermediate for ethylene is -CO₂⁻, which can be further reduced via protonation to generate the -COOH intermediate that can be further reduced by one electron with one proton to form CO. But clear participation of graphene is not known. In addition large-scale CO₂ reduction electrodes will be of composite structure not pure metal such as copper. Clear investigation of graphene material influence on the electrocatalytic CO₂ reduction process. Thus, semitransparent Cu and Cu/C thin films electrodes are deposited on the ATR crystal and spectroscopic investigation was done. The theoretical calculations are compared with spectroscopic data and conclusions on Cu and Cu/graphene role are made.

Funding from European Union`s Horizon 2020 Research and Innovation Program project under grant agreement No 768789 is greatly acknowledged.

First-principles calculations and spectral characterization of $\text{Zn}_{1-x}\text{Mg}_x\text{O}$ epilayers

S. Piskunov, O. Lisovskij, G. Kriekle, L. Trinkler, B. Berzina, R. Ruska

Institute of Solid State Physics, University of Latvia, Kengaraga 8, LV-1063 Riga, Latvia

piskunov@cfi.lu.lv

Deep UV photon sensors based on wide bandgap semiconductors can be used as biological and chemical sensors for ozone detection, detectors for water purification, determination of pollution levels in any biological agent. The aim of this project is to perform first principles modelling of the ZnO-MgO pseudobinary system, which has tunable bandgap from 3.3 eV to 7.8 eV, that can significantly enhance the ability of the sensor to detect signals at different energies simultaneously. The recent results indicated that the limitation of ZnO and MgO mutual solubilities can be broken by stabilizing the high MgO-content wurtzite (wz) $\text{Zn}_{1-x}\text{Mg}_x\text{O}$ and high ZnO-content rocksalt (rs) $\text{Zn}_{1-x}\text{Mg}_x\text{O}$ epilayers by using low lattice mismatch substrates such as ScAlMgO_4 , MgO and Cu_2O . Both $\text{Zn}_{1-x}\text{Mg}_x\text{O}$ p-n junction and Schottky photodiodes with cut-off wavelength < 320 nm, < 280 nm, < 240 nm is expected to be fabricated for deep UV photosensing. Such devices for deep UV solar-blind detection will have advantages of small size, low operating voltage, and low cost. However, the success of the devices relies on a thorough understanding of the basic microstructural, optical and electric properties of the materials and the heterojunctions. To reach this goal the thorough large-scale computer modelling of $\text{Zn}_{1-x}\text{Mg}_x\text{O}$ heterostructures has been performed by means of density functional theory as implemented in commercial total energy code CRYSTAL. The electronic band structure of $\text{Zn}_{1-x}\text{Mg}_x\text{O}$ has been calculated. The effects of the substrate, dopants, and point defects on $\text{Zn}_{1-x}\text{Mg}_x\text{O}$ heterostructures have been assessed.

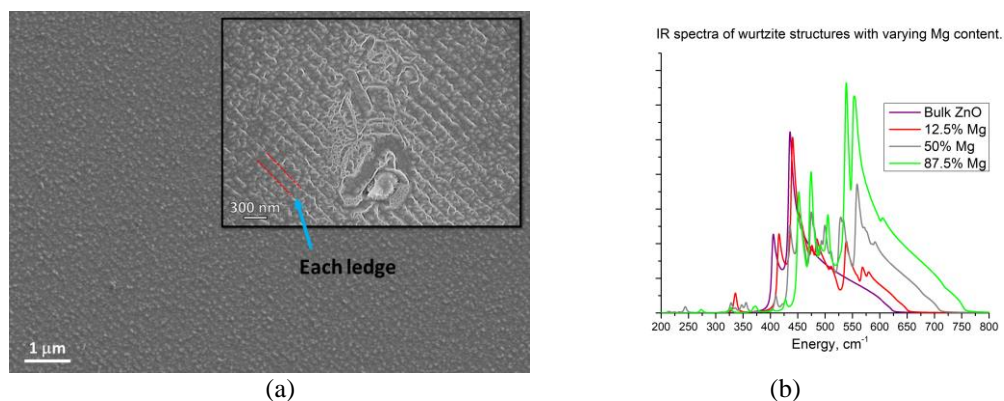


Figure 1. (a) Secondary electron image: ZnO epilayer on ScAlMgO_4 substrate. (b) IR spectra of a number of wz $\text{Zn}_{1-x}\text{Mg}_x\text{O}$ structures with varying Mg content.

Within the framework of our study we have elaborated the reliable models to simulate both rs and wz structures of $\text{Zn}_{1-x}\text{Mg}_x\text{O}$. In agreement with experiment we predict that the increase of Mg in $\text{Zn}_{1-x}\text{Mg}_x\text{O}$ leads to increase of the band gap of the material. Calculated IR spectra shows that the peaks are shifted toward larger frequencies when Mg content is increased at wz $\text{Zn}_{1-x}\text{Mg}_x\text{O}$. Predicted absence of imaginary frequencies allows us to predict stability of wz structure independently of Mg concentration value.

The samples of wurtzite structure ZnO epilayers (pure and doped with copper) on ScAlMgO_4 substrate have been characterized using the spectroscopic methods. At low temperatures the photoluminescence spectra of all studied samples reveal edge luminescence with fine structure typical for ZnO crystals. Replicas of exciton line due to presence of longitudinal optical phonon $\text{LO} \approx 85$ meV have been observed. Exciton excitation spectrum also reveals phonon structure and is symmetrical to the luminescence spectrum.

The financial support of m-era.net project “ZnMgO materials with tunable band gap for solar-blind UV sensors” (ZMOMUVS) is greatly acknowledged.

Engineering of surface electrical charge of HAp due to its structural imperfections

A. Bystrova^{1,2}, V. Bystrov², Y. Dekhtyar¹

1- Riga Technical University, Latvia, Riga LV 1658, 1 Kalku street

2- Institute of Mathematical Problems of Biology– the Branch of Keldysh Institute of Applied Mathematics of Russian Academy of Sciences (IMPB RAS - Branch of KIAM RAS), Russia, 142290, Moscow district, Puschino, 1 Prof Vitkevicha street

Main author email address: bystrova@physics.msu.ru

Hydroxyapatite (HAp) is the most widely used material for the production of bone implants. The bone cells that regenerate the bone tissue and are compatible with an implant, have to be adhered on the implant's surface [1]. To adhere living cells, it is necessary to adjust the electrical potential on HAp surface [2, 3].

HAp contains structural defects and has non-stoichiometric composition. Defects induce the heterogeneity of the surface electrical potential [4]. To adjust the electrical potential on HAp surface is possible by changing the value of surface charge. To change the surface charge is possible by charge insertion or charge transfer. The charge transfer is possible by the insertion of an atom (H) into OH-channel in HAp structure. The charge insertion is possible by the formation of hydroxyl group, oxygen, hydrogen vacancies or filling of unsaturated hydrogen bonds in HAp structure.

The treatment types used to generate defects are considered in Table 1.

Table 1. Treatment types and induced defects.

Defect type	Treatments type
Vacancy OH	Annealing 500 - 900 ^o C
Vacancy O	Gamma-ray irradiation
Vacancy H	
Interstitial H	Hydrogenation + Microwave irradiation

The induction of defects was controlled by measuring of electron work function before and after treatments. The methods of photoelectron (PE) emission spectroscopy was used to measure the output of electrons, which in the case of semiconductors and dielectrics is directly related to the surface charge.

The results obtained allow suggesting a recommendation to engineer the surface potential of HAp samples to improve the cells' adhesion – to anneal the sample in temperature 542 - 546^oC for 30 minutes, and after to hydrogenate for 6 hours at settings 60 ± 2 atmospheres under $t = 23^{\circ}\text{C}$ or/and apply microwave irradiation (power 800 W) for 6,5 minutes for deeper penetration of protons in the samples. However, this depends on presence of different types of defects in the initial HAp sample structure.

The following equipment was employed to process HAp:

1. Annealing was provided in a vacuum condition 10^{-4} Pa using the custom made equipment [5].
2. Gamma-ray irradiation: linear accelerator CLINAC, Varian Medical Systems Inc., USA.
3. Hydrogenation: autoclave, HPM-P, PREMEX, Switzerland.
4. Microwave (MW) irradiation: microwave oven, SAMSUNG, South Korea.

[1] Yu. Dekhtyar, V. Bystrov, A. Bystrova, A. Dindune, A. Katashev, I. Khlusov, E. Palcevskis, E. Paramonova, N. Polyaka, M. Romanova, R. Sammons, D. Veljović, Engineering of the Hydroxyapatite Cell Adhesion Capacity, IFMBE Proceedings, vol. 38, pp. 182-185, (2013).

[2] Yu. Dekhtyar, I. Khlusov, N. Polyaka, R. Sammons, F. Tyulkin, Influence of Bioimplant Surface Electrical potential on osteoblast Behaviour and Bone Tissue Formation, IFMBE Proceeding, vol. 29, pp. 800-803, (2010).

[3] V.S. Bystrov, E. Paramonova, Yu. Dekhtyar, A. Katashev, A. Karlov, N. Polyaka, A.V. Bystrova, A. Patmalnieks, A.L. Kholkin, Computational and experimental studies of size and shape related physical properties of hydroxyapatite nanoparticles, Journal of Physics: Condensed Matter, vol. 23(6), article number 065302, (2011).

[4] V.S. Bystrov, J. Coutinho, A. V. Bystrova, Y.D. Dekhtyar, R.C. Pullar, A. Poronin, E. Palcevskis, A. Dindune, B. Alkan, C. Durucan, E.V. Paramonova, Computational study of hydroxyapatite structures, properties and defects, J. Phys. D: Appl. Phys., vol. 48, pp. 195302-195322, (2015).

[5] R.J. Akmene, A.J. Balodis, Y.D. Dekhtyar, G.N. Markelova, J.V. Matvejevs, L.B. Rozenfelds, G.L. Sagalovich, J.S. Smirnovs, A.A. Tolkachovs, A.I. Upmins, Exoelectron emission spectrometer complete set of surface local investigation, Surface, physics, chemistry, mechanics (In Russian: Poverhn. Fiz. Him. Meh.), vol. 8, pp. 125-128, (1993).

Modelling of the pedestal growth of silicon crystals

K. Surovovs¹, A. Kravtsov², J. Virbulis¹

1 – Institute of Numerical Modelling, University of Latvia, Jelgavas street 3, LV-1002, Riga, Latvia

2 - KEPP EU, Carnikavas street 5, LV-1034, Riga, Latvia

kirils.surovovs@lu.lv

To measure impurity level in polycrystalline rods (e.g., with Fourier-transform infrared spectroscopy), they must be melted and recrystallized as single crystals. To ensure that the addition of dopants is as low as possible, a crucible-free method should be used. The pedestal method is an alternative to well-known floating zone method and is also performed with high-frequency electromagnetic (HFEM) heating. Unlike floating zone method, single crystal is pulled upwards from the melt. It allows to lower feed rod quality requirements and simplify the process control due to absence of open melting front [1].

As the pedestal method has not been widely used in industry for silicon crystals, the development of it requires extensive numerical modelling. The present work describes verification of the previously created mathematical model and application of the model for crystals with the diameters higher than it is currently possible in the experimental setup [2]. Gradient optimization method was used to find the HFEM inductor shape that creates the deepest melting front and reduces the experimentally observed risk of melt freezing [3]. For the model verification purposes, the shape of the melting front was compared to the experiment, as shown in Figure 1. Due to model approximations (axial symmetry, simplified side heating) and the unsteadiness of the experiment, melting interface depth is overestimated in the model.

Nevertheless, further simulations of crystals with larger diameter (see Figure 2) were performed to assist the development of experimental prototype. The previous model [3] was supplemented with calculations of low-frequency EM heating of the pedestal side surface instead of pre-defined fixed heat flux. Another addition is supplementary free surface heating, that prevents melt center freezing during the seeding phase. Numerous calculations were performed to describe not only cylindrical, but also cone phase of crystal growth.

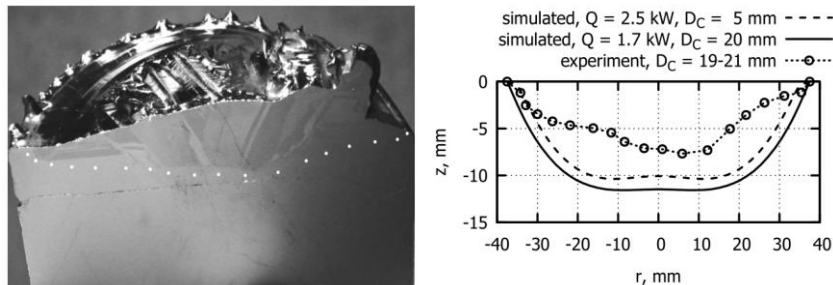


Figure 1. Left – vertical slice of the pedestal after the process with 20 mm crystal and 75 mm pedestal, white points denote melting interface measurements (etching with KOH). Right – comparison between experimentally measured and simulated interface shapes.

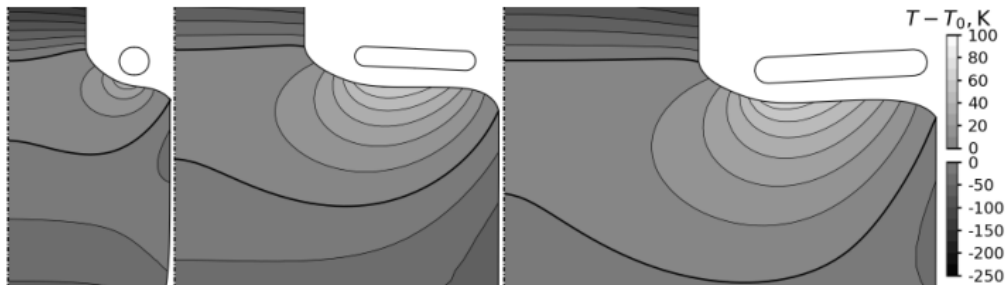


Figure 2. Temperature of solid and molten silicon, calculated for the systems with crystal diameter $D_C = 36$ mm (left), $D_C = 60$ mm (middle) and $D_C = 90$ mm (right).

[1] W. C. Dash, Improvements on the Pedestal Method of Growing Silicon and Germanium Crystals, Journal of Applied Physics, vol. 31, p. 736, (1960).

[2] A. Kravtsov, K. Surovovs, J. Virbulis, Float zone single crystals for testing rods, pulled under electron beam heating. IOP Conference Series: Materials Science and Engineering, vol. 503, (2019).

[3] K. Surovovs, A. Kravtsov, J. Virbulis, Optimization of the shape of high-frequency inductor for the pedestal growth of silicon crystals, Magnetohydrodynamics Vol. 55, pp. 353-366, (2019).

First-principles calculations on stability, electronic and phonon properties of monolayers and nanotubes based on gallium monochalcogenides

V.V. Karpov¹, A.V. Bandura¹, R.A. Evarestov¹

1- Saint-Petersburg State University, 7/9, Universitetskaya Embankment, St Petersburg, 199034, Russia

Main author e-mail address: valerkarp@mail.ru

Gallium monosulfide and monoselenide belong to A^{III}B^{VI} type compounds. Their technological applications are connected with semiconducting properties. Layered crystals of GaS and GaSe are used in optoelectronics, non-linear optics and as an anode material for lithium anode batteries. It is known that a conversion of bulk crystals (3D systems) to monolayers (2D) and nanotubes (1D) can modify the useful properties of these semiconductor materials. This was confirmed for GaS-based nanotubes, which recently have been synthesized. Particularly, they can be produced from powders of gallium and sulfur [1].

We performed quantum chemical calculations of both GaS and GaSe monolayers and achiral nanotubes obtained by rolling up these layers. The hybrid density functional method within the CRYSTAL17 computer code [2] was used. Our results indicate the absence of imaginary frequencies in the phonon spectrum of considered systems thus confirming a stability of monolayers and nanotubes (with diameter larger than ~ 30 Å). We also present the results of the electronic structure calculations, e.g. band gap and strain energy (the total energy difference of a tube and a monolayer). The estimated characteristics depend mainly on the nanotube diameter. The nanotube chirality dependence is weaker. On the basis of the results obtained the dependences of the strain energy and band gap on the system size were established (see Figure 1). Particularly, we found that the strain energies of GaSe nanotubes are greater than those of GaS nanotubes, but both do not depend on the chirality type. The obtained values of strain energy and band gap are in a good agreement with earlier Density Functional-Tight Binding (DFTB) study on GaS-based nanotubes [3, 4].

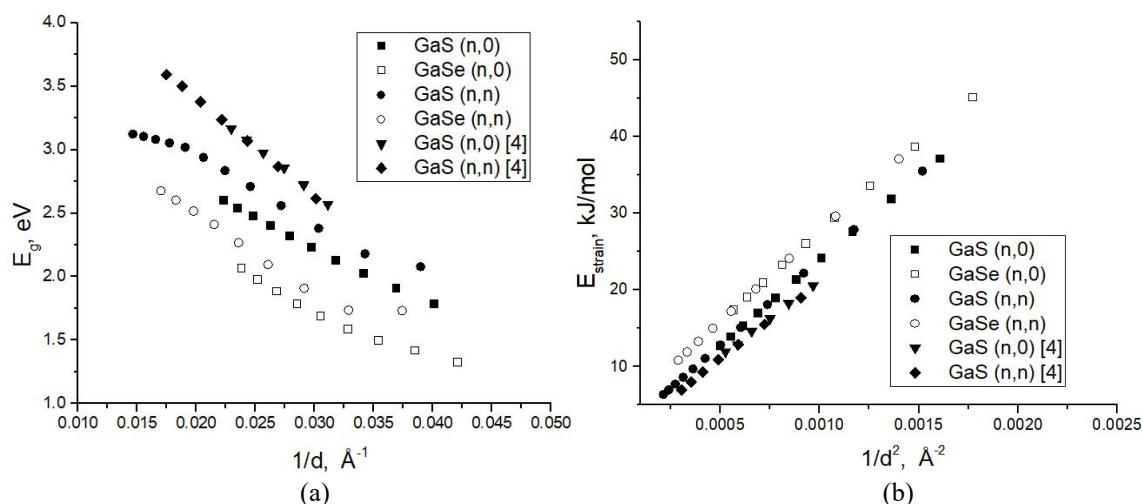


Figure 1 Energy characteristics of nanotubes. (a) Dependence of band gap on reverse diameter. (b) Dependence of strain energy on reverse square diameter.

Acknowledgments: The reported study was funded by RFBR, project number 20-03-00271. The authors also acknowledge the assistance of the Computer Center of the St. Petersburg State University on performing the computations.

- [1] P.A. Hu, Y.Q. Liu, L. Fu, L.C. Cao, D.B. Zhu, GaS multi-walled nanotubes from the lamellar precursor, *Appl. Phys. A*, 80, 1413–1417, (2005).
- [2] R. Dovesi, A. Erba, R. Orlando, C.M. Zicovich-Wilson, B. Civalleri, L. Maschio, M. Rerat, S. Casassa, J. Baima, S. Salustro, B. Kirtman, Quantum-Mechanical Condensed Matter Simulations with CRYSTAL, *WIREs Comput. Mol. Sci.*, 8, e1360, (2018).
- [3] A.N. Enyashin, O. Brontvein, G. Seifert, R. Tenne, Structure and Stability of GaS Fullerenes and Nanotubes, *Isr. J. Chem.*, 57, 529–539, (2017).
- [4] T. Köhler, T. Frauenheim, Z. Hajnal, G. Seifert, Tubular structures of GaS, *Phys. Rev. B*, 69, 193403, (2004)

Effect of the dipole moment on the formation of trap states in CdS and CdSe quantum dots

A. Aldongarov¹, A. Assilbekova¹, I. Irgibaeva²

1- Department of Technical Physics, L.N. Gumilyov Eurasian National University, 2 Satpaev str., 010008, Nur-Sultan, Kazakhstan

2- Luminescent Materials Research Center LLP, 13 Kazhymukan str., 010008, Nur-Sultan, Kazakhstan

enu-2010@yandex.kz

The consideration of the trap states formation in semiconducting nanoparticles is of great importance for developing quantum dots with the desired optical properties. Despite of many years of theoretical and experimental studies of sources of trap states in the band gap region there is no widely accepted point of view on this problem [1,2].

Based on the results we obtained previously we may say that dipole moment plays significant role on formation of trap states. Therefore we used DFTB method for large CdS and CdSe clusters (number of atoms up to 1000) to show correlation between dipole moment and trap states.

We have tested effect of variation of structures of the large CdS and CdSe clusters with the same stoichiometry formula on the electronic transitions and dipole moments using DFTB method. The results show that the variations of structures with the same stoichiometry may provide significant change of dipole moment and electronic transitions at the same time. Usually increase of dipole moment correlates with the decrease of energy of first electronic transition.

DFTB calculations for very large clusters (300–1000 atoms) have also demonstrated that the location of surface defects play important role in formation of trap states. We have created surface defects by removing SH groups in directions along and against the dipole moment. The results show that probability of formation of trap states increases if the termination of SH group provided increase of dipole moment and vice versa.

[1] A. Houtepen, Z. Hens, J. Owen, I. Infante, On the Origin of Surface Traps in Colloidal II–VI Semiconductor Nanocrystals, *Chem. Mater.*, 29(2), pp 752–761, (2017).

[2] C. Giansante, I. Infante, Surface Traps in Colloidal Quantum Dots: A Combined Experimental and Theoretical Perspective, *J. Phys. Chem. Lett.*, 8, pp 5209–5215 (2017).

CHARACTERIZATION OF Co ION OXIDATION STATE AND LOCAL STRUCTURAL DISTORTIONS IN BaCoO_{3-δ}

D. Zavickis, G. Zvejnieks, E. Kotomin, D. Gryaznov

Institute of Solid State Physics, University of Latvia, Latvia

e-mail: davis.zavickis@gmail.com

Protonic ceramic fuel cells (PCFCs) represent an important alternative to oxide conducting solid oxide fuel cells demonstrating higher ionic conductivity. In contrast to an electrolyte material, the optimal cathode material still has to be found, by identifying solid solution compositions with sufficiently high electronic and proton conductivity. Recent experimental observations in the literature optimized complex (Ba, Sr, La)(Fe, Co, Zn, Y)O_{3-δ} perovskites as promising cathode materials for PCFC [1].

In this work we used density functional theory (DFT) calculations and supercells to analyze properties of barium cobalt oxide (BCO) with and without oxygen vacancies (Vo's) with the focus on atomic and electronic structure. We were able to identify the low symmetric monoclinic structure for perfect BCO without Vo's and obtain the low spin state of cobalt ion. The Vo formation energy was estimated depending on its position in the supercell. Results obtained allow us to characterize local structural distortions and oxidation state of cobalt ion in the presence of Vo's. A complexity comes from the fact that the magnetic moment of Co³⁺ varies with the Co-Vo distance smoothly. Furthermore, the Co³⁺ and Co⁴⁺ ions prefer intermediate spin states unlike the Fe ions [3] in the defective supercells. Two separate BCO space groups are considered in the calculations to ascertain the model correctness. Supercell calculations were performed with CRYSTAL17 code [2] within the linear combination of atomic orbitals (LCAO) approximation, using advanced hybrid B1WC density functional.

The financial support of LZP-2018/1-0147 grant is greatly acknowledged.

[1] R. Zohourian, R. Merkle, G. Raimondi, J. Maier, Mixed-conducting perovskites as cathode materials for protonic ceramic fuel cells: Understanding the trends in proton uptake, *Advanced Functional Materials*, vol 38., no 35., (2018).

[2] R. Dovesi, V. R. Saunders, C. Roetti, et al., *CRYSTAL17 User's Manual*, University of Torino, Italy, (2017)

[3] D. Gryaznov, R. Merkle, E. A. Kotomin, J. Maier, *Journal of Materials Chemistry A* 4, 13093 (2016); M. Hoedl, D. Gryaznov, R. Merkle, E. A. Kotomin, J. Maier, *Journal of Physical Chemistry C* 124, 11780 (2020).

Theoretical simulation of electron-phonon interaction in the indium selenides from the first principles

L.Yu.Kharkhalis, K.E.Glukhov, T.Ya.Babuka, M.V.Liakh

*Institute of Physics and Chemistry of Solid State, Uzhhorod National University,
54 Voloshin St., 88000 Uzhgorod, Ukraine,*

E-mail: lkharkhalis@gmail.com

Nowadays, the indium selenides have attracted considerable interest since they are potential candidates for the applications of their physical properties in many devices. In particular, the In_4Se_3 semiconductor is known as a good thermoelectric material. In this crystal, it was revealed a high thermoelectric figure of merit [1] that opens its perspective for thermoelectrics. It was supported that the reason for the sharp increase in thermoelectric efficiency in In_4Se_3 may be due to the Peierls ordering or charge density states [1], or condensation states [2,3] which are connected with electron-phonon interaction. Recently, in [4] it was shown that electron-phonon coupling in the single-layer InSe is anomalously strong owing to the peculiar character of hole states and their interaction with phonons. As it is followed from our investigations the electron spectra of the In_4Se_3 crystal is also characterized by the dispersive dependence by the “Mexican hat” type [5] similar to one of InSe monolayer [6]. Therefore, for the bulk In_4Se_3 and $\beta\text{-InSe}$ crystals, it is of considerable interest to study the electron-phonon coupling which can play an important role in the transport phenomena and optical properties of considered materials. Both crystals demonstrate the layered structure but the layers in In_4Se_3 have the warped form and are more closely interconnected.

In our work, we present the calculations of the interaction between the electron and phonon subsystems for the In_4Se_3 and $\beta\text{-InSe}$ crystals in the framework of the program packet ABINIT with the application of the updated methodology of the density functional perturbation theory (DFPT). We calculated the phonon spectra, density of phonon states, the Eliashberg spectral function $\alpha^2F(\omega)$ and electron-phonon coupling strength λ . The phonon linewidths $\Gamma_{\text{el-ph}}$ for phonon wavevectors along high symmetry directions in the Brillouin zone are obtained too. According to our estimations, the parameters of electron-phonon interaction for In_4Se_3 are higher than for $\beta\text{-InSe}$ that indicates an increase in energy exchange between vibrational and electronic states. This fact is connected with the stronger interaction between the corrugated layers and more complicated chemical bonding topology in In_4Se_3 in comparison with the $\beta\text{-InSe}$ layered crystal. In accordance, a big number of the vibrations takes part in the interaction of the electron and phonon states in the In_4Se_3 . As it follows from the analysis of the frequency bandwidths and the distribution and intensity of spectral function $\alpha^2F(\omega)$ the main contribution in these characteristics is due to the high-frequency optical vibrations which are responsible for the oscillations in the perpendicular direction to the planes of the layers. The vectors of atom displacements corresponding to the normal vibrations active in the high-frequency region are constructed both for In_4Se_3 and $\beta\text{-InSe}$ crystals. Thus, based on the first principles investigations we obtain the increase in the intensity of electron-phonon interaction in bulk crystals In_4Se_3 with a complex crystalline structure, and this stimulates the search for new effects of optical and transport properties, similar to those found in InSe monolayer [4].

[1] J.-S. Rhyee, K.H. Lee, S.M. Lee, E. Cho, S. I. Kim, E. Lee, Y.S. Kwon, J.H. Shim, G. Kotliar. Peierls distortion as a route to high thermoelectric performance in In_4Se_3 , Nature, vol.459, pp. 965-968 (2009).

[2] Y.S. Lim, M. Jeong, W.-S.Seo, J.-H.Lee, C.H.Park, M. Sznajder, L.Yu.Kharkhalis, D.M. Bercha, J.Jang J. Condensation state and its effects on thermoelectric properties in In_4Se_3 , J.Phys.D.: Appl.Phys., vol.46, pp. 275304-275308. (2013),

[3] M.Jeong, Y.S.Lim, W.-S.Seo, J.-H.Lee, Ch.-H. Park, M.Sznajder, L.Yu.Kharkhalis, D.M.Bercha, J.Yang, Condensation-related thermoelectric properties and formation of coherent nano-inclusions in Te-substituted In_4Se_3 , Journ. of Materials Chemistry A., vol. 1, pp. 15342-15347. (2013).

[4] A.V.Lugovskoi, M.I.Katsnelson, A.N.Rudenko. Strong electron-phonon coupling and its influence on the transport and optical properties of hole-doped single-layer InSe., Physical Review Letters, vol.123, p. 176401 (2019)

[5] D.M.Bercha, L.Yu.Kharkhalis, A.I.Bercha, M.Sznajder M. Band Structure and Condensation States in In_4Se_3 Crystals, Phys. Stat. Sol. (b), vol.203, pp. 427 – 440 (1997)

[6] M. J. Hamer, J. Zultak, A. V. Tyurnina, V.Zolyomi Indirect to Direct Gap Crossover in Two-Dimensional InSe Revealed by Angle-Resolved Photoemission Spectroscopy, ACS Nano, vol. 13, pp.2136-2142 (2019)

Electronic and vibrational properties of $\text{TlIn}(\text{S}_{0.75}\text{Se}_{0.25})_2$ crystal: theoretical and experimental study

**T. Babuka^{1,2}, O.O. Gomonnai^{3,4}, K.E. Glukhov¹, L.Yu. Kharkhalis¹, A.V. Gomonnai^{3,5},
D.R.T. Zahn⁵, M. Makowska-Janusik²**

1- Institute for Physics and Chemistry of Solid State, Uzhhorod National University, 54 Voloshin St., 88000 Uzhhorod, Ukraine
2- Institute of Physics, Faculty of Mathematics and Natural Science, Jan Dlugosz University in Czestochowa, Al. Armii Krajowej 13/15,
42-200 Czestochowa, Poland
3- Optics Department, Uzhhorod National University, 46 Pidhima Str., 88000 Uzhhorod, Ukraine
4- Vlokh Institute of Physical Optics, 23 Dragomanov Str., 79005 Lviv, Ukraine
5- Institute of Electron Physics, Ukr. Nat. Acad. Sci., 21 Universytetska Str., 88017 Uzhhorod, Ukraine
6- Semiconductor Physics, Chemnitz University of Technology, D-09107 Chemnitz, Germany

E-mail: tanya.babuka@gmail.com

Recently, layered crystals have attracted research interest due to their structural and physical properties promising for different applications. A possibility to create new multifunctional artificial materials obtained through the arrangement of several layered crystals became a new subject of studies. One of the representatives of such a class of layered materials is TlInS_2 [1].

The electronic and vibrational properties of $\text{TlIn}(\text{S}_{0.75}\text{Se}_{0.25})_2$ crystal were investigated using first-principle calculations and experimental measurements. TlInS_2 crystallizes in a centered monoclinic lattice structure with $C2/c$ (C_{2h}^6) space symmetry group and exhibits four formula units per primitive cell, that contains 32 atoms and has a prominent layered structure with two layers in the unit cell which is characterized by the so-called van der Waals (vdW) gap [1]. In this case, first-principle calculations of vibrational properties of the TlInS_2 crystal have been carried out using a combination of the density functional theory (DFT) supplied with dispersion correction (D).

In our previous work [2], we investigated the electronic properties of pure TlInS_2 crystal. In this work, for the correct description of the values of bandgap, the Hubbard parameters for p -orbitals of S atoms were applied. In the present investigation, for the correct description, the electronic properties of solid solutions of $\text{TlIn}(\text{S}_{1-x}\text{Se}_x)_2$ ($x=0.25$) the Hubbard parameters for p -orbitals of S and Se atoms were used. As a result of this calculations the values of bandgap close to experimental data were obtained ($E_{\text{exp}}=2.1$ eV [3]).

For a detail description of the impact of the Hubbard correction on the physical properties of $\text{TlIn}(\text{S}_{0.75}\text{Se}_{0.25})_2$ material the energy band spectra, band gap values, the partial density of states and Mulliken populations were obtained. Also, the vibrational properties of the considered material were investigated. The phonon dispersion curves and partial density of phonon states using density functional theory were calculated. The phonon frequencies of $\text{TlIn}(\text{S}_{0.75}\text{Se}_{0.25})_2$ crystals was studied experimentally by Raman spectroscopy. Unpolarized Raman spectra were measured using a Dilor XY 800 spectrometer equipped with a CCD camera. A Kr^+ (647.1 nm) laser was used for excitation. The measurements were performed in the frequency range of 16–340 cm^{-1} in the temperature range of $30 \text{ K} \leq T \leq 293 \text{ K}$. To determine the nature of the experimental Raman scattering spectra it was compared to the eigenfrequencies of phonon modes calculated by DFT-D+U methodology. We obtained good agreement between experimental and theoretically calculated data. It was proved that the DFT-D+U methodology leads to correct optimization of the structure of the $\text{TlIn}(\text{S}_{0.75}\text{Se}_{0.25})_2$ crystal.

[1] V. Grivickas, P. Scajev, V. Bikbajevs, O. V. Korolik and A. V. Mazanik. Carrier dynamics in highly excited TlInS_2 : evidence of 2D electron-hole charge separation at parallel layers, *Phys. Chem. Chem. Phys.*, 1, 1 – 13, (2018)

[2] T. Babuka, O.O. Gomonnai, K.E. Glukhov, L.Yu. Kharkhalis, M. Sznajder and D.R.T. Zahn, Electronic and Optical Properties of the TlInS_2 Crystal: Theoretical and Experimental Studies, *Acta Physica Polonica a*, 136, 4, 640-644, (2019)

[3] N. M. Gasanly, Effect of temperature and isomorphous atom substitution on optical absorption edge of $\text{TlInS}_2\text{Se}_{2(1-x)}$ mixed crystals ($0.25 \leq x \leq 1$), *Cryst. Res. Technol.*, 45, 5, 525 – 528, (2010)

Conductivity and percolation in carbon nanotubes filled materials: numerical simulations

A. Plyushch^{1,2}, D. Lyakhov³, M. Šimėnas¹, D. Bychanok², J. Macutkevič¹,
D. Michels³, J. Banys¹, P. Lamberti⁴, P. Kuzhir^{5,2}

1- Faculty of Physics, Vilnius University, Sauletekio 9, LT-10222 Vilnius, Lithuania

2- Institute for Nuclear Problems, Belarusian State University, 220006 Minsk, Belarus

3- Computer, Electrical and Mathematical Science and Engineering Division, 4700 King Abdullah University of Science and Technology, Thuwal 23955-6900, Kingdom of Saudi Arabia

4- Department of Information and Electrical Engineering and Applied Mathematics, University of Salerno, Via Giovanni Paolo II 132, Fisciano (SA), 84084, Italy

5- Institute of Photonics, University of Eastern Finland, Yliopistokatu 7, FI-80101 Joensuu, Finland

artyom.plyushch@ff.vu.lt

The numerical simulation of the macroscopic properties of the composite materials filled with the carbonaceous fillers, like carbon nanotubes (CNT), or graphene nanoplatelets (GNP) is the important pre-experimental step. It allows rapidly and cost effectively predicting the properties of the composite systems taking into account the microscopic parameters, such as aspect ratio, the homogeneity of the distribution of the inclusions. Despite the significant progress in the studied area, several aspects are still under investigation both experimentally and numerically.

We report on the developing the numerical model for the computation of the conductivity and percolation threshold of the CNT-filled composites. CNTs are modeled as the ellipsoids of revolution with high aspect ratio. The composites after mechanical deformation of the hybrid composites are investigated. The deformation was introduced as the non homogeneity in angular distribution of the CNTs. Conductive or non conductive spherical particles were considered as a second filler for the hybrid composites.

The computed conductivity for the stretched composite along z -direction is presented in figure 1.

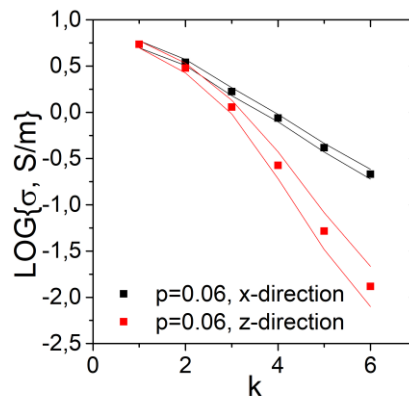


Figure 1 Dependence of the conductivity of the composite filled with 6 vol. % nanotubes on the relative deformation.

The significant anisotropy (more than the order of magnitude) was observed for the deformed composite. It was also shown, that the z -direction is preferable for the percolation in the deformed composites in comparison with x . But, being percolated, the composite has lower conductivity along z , than one along the perpendicular direction. In contrast to the percolation, where the appearance of only one conductive path is necessary, the conductivity strongly depends on the number of conductive paths through the unit cell and the total tunnelling distance.

KNbO₃ Based Space-Time Crystal and Dispersion Near Dirac Point

Zafer OZER¹, Amirullah M. Mamedov^{2,3}, Ekmel Ozbay²

1- Mersin Vocational High School, Electronic and Automation Department, Mersin University, Turkey

2- Nanotechnology Research Center (NANOTAM), Bilkent University, 06800 Bilkent, Ankara, Turkey

3- Address International Scientific Center, Baku State University, Baku, Azerbaijan

mamedov@bilkent.edu.tr

Photonic time crystal (PTC) have been introduced which exhibit photonic properties complementary to their conventional spatial photonic crystal analogs. While spatial photonic crystals induce forbidden bands in the frequency spectrum of photons, photonic time crystals create forbidden regions in the momentum spectrum of photons. This effect allows for enhanced control over many optical processes that require both photonic energy and momentum conservations such as nonlinear harmonic generation.

In present paper we analyzed a spatially homogeneous material with permittivity $\varepsilon(t)$, which is modulated in time, such that $\varepsilon(t)$ changes periodically, with period T , in a step-like manner. This results in a binary PTC with two time segments. In the first time-segment (t)= ε_1 for a duration of t_1 seconds, followed by a second time-segment in which $\varepsilon(t)=\varepsilon_2$ for $t_2=T-t_1$ seconds. The field is polarized in the x direction, and propagates in the z direction. With every modulation of $\varepsilon(t)$, a time reflection occurs, causing waves to partially reflect to their time reversed pair, while preserving the momentum k due to the homogeneity of space. The time reversed partner of a wave is a wave with the same momentum but with opposite spatial frequency. This is analogous to a wave conserving its energy, and scattering backwards in space in a PC. We proposed the concept of the PTC, and simulated electromagnetic wave propagation in 1D, and 2D PTC, the simulated results indicate that the scatter fields in PTC are more intensive than those in conventional PC, and the band gaps in PTC are larger than those in conventional PC.

Ab initio molecular dynamics simulations of transition metal dichalcogenides

Dmitry Bocharov¹, Inga Pudža¹, Alexei Kuzmin¹ and Matthias Krack²

1 - Institute of Solid State Physics, University of Latvia, Riga, Latvia

2 - Paul Scherrer Institute, Villigen, Switzerland

Main author email address: bocharov@latnet.lv

Two-dimensional (2D) layered materials include transition metal dichalcogenides. They have attracted considerable interest during last decades due to their extraordinary electronic, optical, transport and tribological properties [1]. The structure of these materials is characterized by strong in-plane chemical bonds and weak coupling between layers.

Understanding of the 2D material properties requires accurate knowledge of their atomic structure, including anisotropy of thermal expansion, as well as of intralayer and interlayer lattice dynamics closely related to their thermodynamics [2-4]. The obtaining of such information experimentally is challenging, and should be supported by theoretical simulations based on reliable and validated models. An example of the first-principles studies of the phonon properties and anharmonic effects in MX₂ materials can be found, for example, in [3, 4]: they addressed the role of ion masses, structure and bond strengths using the experimental Raman and infrared phonon frequencies and the lattice thermal expansion. At the same time, molecular dynamics simulations using empirical interatomic potentials (force-fields) opened possibility to follow the anisotropic nature of thermal conductivity in parallel and perpendicular directions to the 2D layers [5, 6]. However, the main problem caused by the use of the empirical interatomic potentials is related to the determination of their parameters, which is conventionally solved within quasiharmonic approximation by fitting to static structure, elastic constants and, more recently, phonon dispersion curves. Therefore, the optimization and validation of existing empirical interatomic potentials using the result of *ab initio* molecular dynamics (AIMD) simulations and additional experimental data, e.g. extended X-ray absorption fine structure (EXAFS) spectra, are crucial for an estimation of their reliability. Our previous MD-EXAFS studies of different materials such as Cu₃N, ZnO, UO₂ and ScF₃ [7-10] suggest that the use of molecular dynamics simulations provides reliable and detailed information on the thermal disorder as far as up to 6-7 Å from the absorber.

In the framework of this study, we apply this methodology to the above-mentioned layered materials performing AIMD simulations of MoS₂ and WS₂ compounds in the temperature range from 300 K to 1200 K using the CP2K code [11] in order to elucidate the details of thermal disorder and structural anisotropy on the lattice dynamics of layered structures. Analysis of Mean-Square Relative Displacement (MSRD) shown the strong anisotropy in atomic vibrations (interlayer MSRD differ from intralayer MSRD) for both compounds. In addition, we validated the obtained AIMD results by a direct comparison with the W L₃-edge and Mo K-edge absorption spectra using the MD-EXAFS approach developed in [12].

Financial support provided by project No. 1.1.1.2/VIAA/I/16/147 (1.1.1.2/16/I/001) under the activity "Post-doctoral research aid" realized at the Institute of Solid State Physics, University of Latvia is greatly acknowledged. We acknowledge that the results of this research have been achieved using the DECI resource BESKOW based in KTH Royal Institute of Technology, Sweden with support from the PRACE aisbl.

- [1] K.S. Novoselov, A. Mishchenko, A. Carvalho, A.H.C. Neto, 2D materials and van der Waals heterostructures, *Science* **353**, 461 (2016)
- [2] H. Wang, J. Bang, Y. Sun, L. Liang, D. West, V. Meunier, and S. Zhang, The role of collective motion in the ultrafast charge transfer in van der Waals heterostructures, *Nature Commun.* **7**, 11504 (2016)
- [3] L.-F. Huang and Z. Zeng, Roles of mass, structure, and bond strength in the phonon properties and lattice anharmonicity of single-layer Mo and W dichalcogenides, *J. Phys. Chem. C* **119**, 18779 (2015)
- [4] B. Peng, H. Zhang, H. Shao, Y. Xu, X. Zhang, and H. Zhu, Thermal conductivity of monolayer MoS₂, MoSe₂, and WS₂: interplay of mass effect, interatomic bonding and anharmonicity, *RSC Adv.* **6**, 5767 (2016)
- [5] V. Varshney, S. S. Patnaik, C. Muratore, A. K. Roy, A. A. Voevodin, and B. L. Farmer, MD simulations of MoS₂: Force-field parameterization and thermal transport behavior, *Comput. Mater. Sci.* **48**, 101 (2010)
- [6] J.-W. Jiang, H. S. Park, T. Rabezuk, Molecular dynamics simulations of single-layer molybdenum disulphide (MoS₂): Stillinger-Weber parametrization, mechanical properties, and thermal conductivity, *J. Appl. Phys.* **114**, 064307 (2013)
- [7] D. Bocharov, M. Chollet, M. Krack, J. Bertsch, D. Grolimund, M. Martin, A. Kuzmin, J. Purans, and E.A. Kotomin, Analysis of the U L₃-edge X-ray absorption spectra in UO₂ using molecular dynamics simulations. - *Progr. Nucl. Energy*, **94**, 187 (2017)
- [8] A. Kuzmin, A. Anspoks, A. Kalinko, J. Timoshenko, The use of x-ray absorption spectra for validation of classical force-field models, *Z. Phys. Chem.* **230**, 537 (2016)
- [9] D. Bocharov, M. Krack, Yu. Rafalskij, A. Kuzmin, J. Purans, Ab initio molecular dynamics simulations of negative thermal expansion in ScF₃: The effect of the supercell size, *Comput. Mater. Sci.*, **171**, 109198 (2020).
- [10] D. Bocharov, A. Anspoks, J. Timoshenko, A. Kalinko, M. Krack, A. Kuzmin, Interpretation of the Cu K-edge EXAFS spectra of Cu₃N using *ab initio* molecular dynamics, *Radiat. Phys. Chem.*, **175**, 108100 (2020).
- [11] CP2K developers team, <http://www.cp2k.org>
- [12] A. Kuzmin, R. A. Evarestov, Quantum mechanics–molecular dynamics approach to the interpretation of x-ray absorption spectra, *J. Phys.: Condens. Matter* **21** 055401(2009)

Spectroscopic study of water clusters in nanostructured materials

I. Doroshenko¹, A. Vasylieva¹, Ye. Hrabovskyi¹, G. Podust¹, P. Teselko¹, J. Stocka², V. Balevicius²

1- Faculty of Physics, Taras Shevchenko National University of Kyiv, Volodymyrska str., 64/13, Kyiv, 01601, Ukraine

2- Institute of Chemical Physics, Vilnius University, Saulėtekio av. 9, III bld., Vilnius, LT-10222, Lithuania

email: dori11@ukr.net

Structure and spectral properties of hydrogen-bonded water clusters in different environments – low-temperature matrices of inert gases, nanostructured calcium hydroxyapatite and lyotropic chromonic liquid crystals – were investigated by means of vibrational spectroscopy and quantum-chemical simulation.

Infrared absorption spectra of water trapped in an argon matrix were registered at different temperatures from 9 K to 50 K (see Figure 1). Using results of quantum-chemical calculation the observed spectral bands were assigned to water clusters consisting of different numbers of molecules. The temperature dependence of the registered spectra gives the possibility to construct a model of structure transformations occurring in water during the phase transition from gas to condensed state [1, 2]. Influence of cryogenic argon environment on small water clusters was investigated by quantum-chemical simulation of structure and vibrational spectra of water clusters consisting of different numbers of molecules [2, 3].

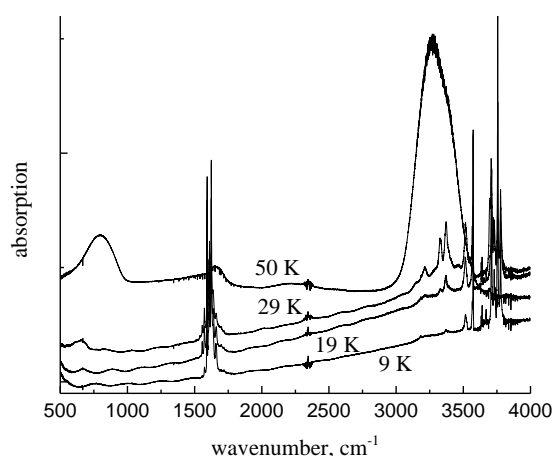


Figure 1 Infrared absorption spectra of water clusters trapped in an Ar matrix at different temperatures.

Water clusters were revealed in nano-structured calcium hydroxyapatite FTIR spectra [4]. The cluster structure and size depends on the hydration level of CaHA. Hexamers or higher structures were observed only in the samples containing significant amount of adsorbed water.

Temperature and composition effects in Sunset Yellow FCF (SSY) aqueous solutions were studied by NMR and Raman spectroscopy [5] passing through all phase transitions between isotropic phase (I) and chromonic phases – nematic (N) and columnar (M). The temperature dependences of H₂O chemical shift and Raman O–H stretching band shape show that water confined in the intercolumnar areas behaves as in the neat substance. When the sample is heated and the transition from M phase to N phase occurs, the molecular motion of water is seen to change in a manner similar to that when water is melting.

[1] V. Pogorelov and I. Doroshenko, Vibrational spectra of water clusters, trapped in low-temperature matrices, *Low Temperature Physics*, vol. 42, pp. 1163-1166, (2016).

[2] I. Doroshenko, A. Vasylieva. Cluster structure of water (Scholars' Press), (2019).

[3] A. Vasylieva, I. Doroshenko, O. Doroshenko, V. Pogorelov, Effect of argon environment on small water clusters in matrix isolation, *Low Temperature Physics*, vol. 45, pp. 736-743, (2019).

[4] K. Kristinaitytė, L. Dagys, J. Kausteklis, V. Klimavicius, I. Doroshenko, V. Pogorelov, N. Valevičienė, V. Balevicius, NMR and FTIR studies of clustering of water molecules: from low-temperature matrices to nano-structured materials used in innovative medicine, *Journal of Molecular Liquids*, vol. 235, pp. 1-6, (2017).

[5] K. Kristinaitytė, A. Maršalka, L. Dagys, K. Aidas, I. Doroshenko, Ye. Vaskivskyi, Ye. Chernolevska, V. Pogorelov, N. Valevičienė, V. Balevicius, NMR, Raman and DFT study of lyotropic chromonic liquid crystals of biomedical interest: tautomeric equilibrium and slow self-assembling in sunset yellow aqueous solutions, *Journal of Physical Chemistry. Part B*, vol. 122, pp. 3047–3055, (2018).

Radiation defects in a NaCl matrix with lowered lattice symmetry due to light cation doping and elastic uniaxial deformation

K. Shunkeyev¹, Zh. Ubaev¹, A. Lushchik², L. Myasnikova¹, A. German³

1- K. Zhubanov Aktobe Regional State University, Moldagulova av. 34, 030000 Aktobe, Kazakhstan

2- Institute of Physics, University of Tartu, W. Oswald Str. 1, 50411 Tartu, Estonia

3- Yanka Kupala State University of Grodno, Ozheshko str. 22, 230023, Grodno, Belarus

nczhiger@mail.ru

The main reasons for the instability of anionic electronic excitations (EEs) in alkali halide crystals (AHCs) are their nonradiative decay with the formation of Frenkel defects and radiative annihilation, and both these processes are important for the developing of functional optical materials. Local deformation of the AHC lattice by introducing small-radius homologous cations as well as via applying elastic uniaxial stress have an impact on relaxation processes of EEs [1-3]. It was found [1-3] that the lowering of the lattice symmetry of AHCs causes the reduction of EE free path length and the enhancement of EE (exciton) probability self-trapping in regular lattice regions. On the example of a NaCl crystal, the mechanisms of formation, recombination, and thermal annealing of radiation defects were studied using absorption and thermoactivation spectroscopy as well as light lithium cation doping and low-temperature elastic deformation.

The irradiation of a NaCl-Li crystal with X-rays at 90 K leads to the appearance of optical absorption bands peaked at 3.35 eV and 4.6 eV, which undergo simultaneous annealing to 130 K with the increase of the number of the F and F' centers and, therefore, are attributed to $H_A(\text{Li})$ centers. Thermal destruction of the $H_A(\text{Li})$ centers causes rearrangement of a crystal lattice and the formation of halogen centers responsible for the absorption band peaked at 5.35 eV, while further heating to 300 K results in the formation of more complex centers with absorption at 5.8 eV and stability up to ~400 K.

Intense peaks of thermally stimulated luminescence (TSL) at 110 K, 125 K, 165 K, 200 K, and 250 K were registered in a NaCl crystal doped with Li ions. After applying a low-temperature elastic deformation, the intensity of 110 K and 165 K peaks, attributed to the formations of F' and V_K centers, respectively, sharply increases. On the other hand, the TSL peak at 125 K, which belongs to the $H_A(\text{Li})$ centers, remains virtually unchanged as it is typical for impurity centers.

Analysis of spectral composition of the TSL peaks in NaCl-Li crystals shows that an electron released at thermal ionization of an F' center recombines with a localized hole center and forms an exciton-like excitation – $(e^-+V_K)\text{Li}$ – in the field of a light impurity ion. Radiative decay of such EEs gives emissions with the maxima at 2.7 eV. Recombination of a mobile hole, formed due to thermal ionization of a V_K center (165 K), with an electron from an F center is accompanied by the luminescence of self-trapped excitons (3.4 eV) or exciton-like emission in the field of an anion vacancy (unresolved emission bands peaked at about 2.9 and 4.0 eV).

Recombination of a mobile hole released from a V_F -center (200 K) with an electron from an F center is accompanied by luminescence with a maximum at 4.0 eV, similar to the emission of a bound anion exciton near a divacancy.

In conclusion, a low-temperature (100 K) elastic deformation ($\varepsilon = 1.2\%$) increases the concentrations of F and V_K centers as it is evidenced by tunnel and thermally stimulated luminescence of NaCl-Li crystals.

[1] L. Myasnikova, K. Shunkeyev, N. Zhanturina, Zh. Ubaev, A. Barmina, S. Sagimbaeva and Z. Aimaganbetova, Luminescence of self-trapped excitons in alkali halide crystals at low temperature uniaxial deformation, Nucl. Inst. Meth. B 464, 95-99 (2020).

[2] K. Shunkeyev, N. Zhanturina, Z. Aimaganbetova, A. Barmina, L. Myasnikova, Sh. Sagymbaeva and D. Sergeev, The specifics of radiative annihilation of self-trapped excitons in a KI-Tl crystal under low-temperature deformation, Low Temp. Phys., 42, 580-583 (2016).

[3] A. Bekeshev, E. Vasil'chenko, A. Dauletbekova, K. Shunkeyev and A. Élango, Radiation-stimulated impurity yield in interstitial sites in KBr-Li and KCl-Li crystals, Physics of the Solid State, 38(3), 425-429 (1996).

INDEX

- Aarik, Jaan 154
Abdulhadi, H. 103
Acik, I. Oja 62
Agafonov, V. 56
Aiello, G. 165
Akhmatkhanov, A. R. 69
Akilbekov, A. 148
Akylbekova, A. 74
Akopdzhanyan, T. G. 58
Al-Ashouri, A. 80
Albrecht, S. 80
Aldongarov, A. 174
Aleksandravicius, E. 16
Alpysova, G. 148
Ananyev, M. 167
Ananyev, Maxim 26
Andronikova, Daria 70
Animitsa, I. 167
Ansona, A. 155
Antonova, M. 125
Antuzevics, A. 36, 160, 164
Antuzevics, Andris 149, 161, 162
Anulyte, J. 59
Ardaravicius, L. 105
Arlauskas, K. 59
Artsiukh, E. 67
Assilbekova, A. 174
Ašmontas, S. 105
Atvars, A. 125
Auffray, E. 27
Aukštakojytė, Rūta 158
Aukštuolis, Andrius 132
Babayigit, C. 37, 38
Babichenko, Sergey 43
Babkin, R. Yu. 29
Babuka, T. 45, 177
Babuka, T. Ya. 109, 176
Baimukhanov, Z. 74
Baitimirova, M. 88
Bajars, G. 92
Bajars, Gunars 76
Balciunaite, A. 21
Balciunas, S. 124, 141
Balevicius, V. 181
Baltrunas, D. 121, 122
Ban, H. 108
Bandura, A. V. 173
Banys, J. 64, 65, 84, 114, 115, 118, 119, 124, 133, 135, 137, 140, 141, 159, 178
Banys, Juras 112
Barkane, A. 101
Barkauskas, Jurgis 158
Barvainiene, B. 80
Beganskiene, A. 121, 122
Belotserkovskiy, M. 91
Belousova, E. 103
Beluns, S. 102
Bertasius, P. 140
Berzina, A. 90, 139
Berzina, B. 20, 36, 170
Berzina, Baiba 149
Berzina145
Bychanok, D. 84, 178
Biciunas, A. 56
Bijelic, Jelena 131
Bikshe, L. 116, 125
Biktagirov, T. 159
Birks, E. 115, 116, 125
Birks, Eriks 113
Bystrov, V. 171
Bystrova, A. 171
Bite, I. 99, 153
Bite, Ivita 154
Bledzki, A. K. 136
Bocharov, Dmitry 180
Bockute, Kristina 94
Bogdanov, E. V. 106
Boiprav, O. 103
Bosak, Alexei 70
Brett, C. M. A. 33
Bronwald, Iurii 70
Bubniene, G. 80
Bukauskas, V. 56
Bulusheva, L. 84
Buntkowsky, Gerd 17
Burkovsky, R. G. 70
Butkus, R. 41
Butkute, R. 56
Cardoso, J. P. 64
Cechavicius, B. 56
Celzard, A. 133, 137
Chang, L. 42, 151
Chang, Liuwen 52
Chashin, D. 96, 107
Chen, Z. 62
Cheng, H. H. 60
Chesnokov, A. 35
Chikvaidze, G. 79, 165, 169
Chizhov, A. 34
Chou, M. 151
Chou, M. C. M. 52
Chou, M. M. C. 42
Chou, Mitch M. C. 20
Chuvakova, M. A. 69
Cipa, J. 20, 36, 145, 155
Cipa, Janis 149
Cirulis, Jekabs 162
Constantin, V. 72
Covarrubias, Monica Susana Campos 94
Cresta, V. 61
Čižmár, E. 29, 143
Danilenko, I. A. 120
Danilovas, P. 136
Daskeviciene, M. 80, 81, 82
Daskeviciute, S. 82
Daškevičienė, Marytė 83
Daugela, S. 142
Dauletbekova, A. 74, 148
Dec, J. 68
Dedova, T. 62
Dekhtyar, Y. 171
Demidenko, O. 72
Derets, N. K. 61
Devižis, Andrius 54
Didenko, Y. V. 120
Diliautas, R. 121
Dindune, A. 142
Djerdj, Igor 131
Dobele, Galina 76
Doke, G. 36
Domenici, V. 61
Donath, C. 72
Doroshenko, I. 181
Drevilkauskaitė, A. 82
Dunce, M. 115, 116, 125
Dutkevica, S. 125
Dutovs, A. 147
Dziaugys, A. 65, 118
Eglite, S. 139
Eglitis, R. I. 47
Einbergs, E. 153
Elsts, E. 157
Erts, D. 88, 147
Escobar, M. 124
Esin, A. A. 69
Evans, D. R. 110
Evarestov, R. A. 22, 173
Farlenkov, A. 167
Fedorchenko, A. V. 29, 64
Fedotovs, A. 36
Fedulov, F. 107
Feher, A. 29, 143
Feldbach, E. 40
Ferreira, M. G. S. 33
Fertman, E. L. 29, 64

Fetisov, Y. 96, 107
 Fetisov, L. 96, 107
 Fierro, V. 133, 137
 Filimonov, Alexey 70
 Flerov, I. N. 106
 Franciszczak, P. 136
 Freimanis, O. 125
 Fröhlich, K. 24
 Gabrusenoks, Jevgenijs 168
 Gaidukevic, J. 78
 Gaidukevic, Justina 158
 Gaidukovs, S. 101, 102
 Gailevicius, D. 16, 38
 Gal, D. 89, 108
 Gallet, Jean - Jacques 25
 Gao, Feng 54
 Gaskov, M. 34
 Gazda, Maria 94
 Genevicius, Kristijonas 132
 Gerasimov, V. 89
 German, A. 182
 Germane, L. 93
 Gertsman, U. 159
 Getautis, V. 80, 82
 Getautis, Vytautas 83
 Giniyatova, Sh. 74, 148
 Giriunas, L. 159
 Glukhov, K. 45, 108, 110, 119
 Glukhov, K. E. 109, 176, 177
 Gomonnai, A. V. 177
 Gomonnai, O. O. 177
 Gorban, O. A. 120
 Gorev, M. V. 106
 Gorodetskiy, D. 84
 Gorokhov, G. 84
 Gorokhova, E. 34, 156
 Govor, G. 44, 75
 Grabar, A. 110
 Grabis, J. 36, 145
 Graniel, O. 147
 Grazulevicius, J. V. 95
 Gryaznov, D. 35, 55, 175
 Gribauskaite, V. 64
 Grigalaitis, R. 64
 Grigonis, R. 41
 Grigoraviciute-Puroniene, I. 73, 104
 Grigorjevaite, J. 152
 Grinberga, L. 90, 169
 Grineviciute, L. 37, 38
 Gruodis, A. 82
 Gruszka, I. 114
 Gudeika, D. 95
 Gulbinas, Vidmantas 54
 Gureviciene, V. 78
 Habbibi, Y. 101
 Haborets, V. 119
 Hajra, Sugato 131
 Hallén, Anders 28
 Hamalii, V. 123
 Hammar, Mattias 18
 Harmatha, L. 24
 Hasynets, S. 110
 Horvat, A. 111
 Hrabovskyi, Ye. 181
 Hušeková, K. 24
 Yamkovy, O. 134
 Yang, Chih - Cheng 52
 Yanushkevich, K. 44, 72, 75
 Yevych, R. 118
 Iliciukaite, Aiste 83
 Ilina, T. S. 63
 Inkraitaite, G. 144
 Irgibaeva, I. 174
 Iskhakova, L. D. 39
 Yun, Mung 120
 Ivanova, T. 136
 Jablonskas, Džiugas 112
 Jaglicic, Zvonko 131
 Jankauskas, V. 80, 81, 82
 Jankauskas, Vyintas 83
 Janulevicius, M. 39
 Jasinskas, A. 56
 Jasiunas, Rokas 54
 Jakobsons, L. 169
 Jevdokimovs, D. 147
 Jonikaitė-Švēgždienė, Jūratė 132
 Joost, Urmas 25
 Juodenas, Mindaugas 19
 Juodkazyte, J. 55, 77
 Jurinovs, M. 101
 Jurjans, Miks 113
 Juška, G. 59
 Juška, Giedrius 132
 Käämbre, Tanel 25
 Kalendarjovs, R. 169
 Kalendra, V. 159
 Kaleva, G. M. 63
 Kamarauskas, E. 80, 81, 82
 Kamarauskas, Egidijus 83
 Kamarauskas, M. 56
 Kanarbik, Rait 25
 Kanda, H. 82
 Kaparkalejs, R. 87
 Kaprans, Kaspars 76
 Karabanov, A. 124
 Karbovnyk, I. 117, 138
 Kareiva, A. 73, 104, 121, 122
 Karipbayev, Zh. 148
 Karoblis, D. 121, 122
 Karpov, V. V. 173
 Katelnikovas, A. 152
 Katerski, A. 62
 Kavaliauskas, V. 86, 97
 Kavaliuke, V. 134, 141
 Kemere, M. 36, 164
 Kezionis, A. 142
 Kežionis, A. 134
 Khalyavin, D. D. 64
 Kharkhalis, L. Yu. 109, 176, 177
 Khodimchuk, A. 167
 Khrustov, A. 167
 Kiisk, Valter 154
 Kiprijanovic, O. 105
 Kirm, M. 40, 43, 46
 Kiselev, D. A. 63
 Kivi, Indrek 25
 Kizane, G. 155
 Kleperis, J. 79, 85, 90, 169
 Kleperis, Janis 76
 Klym, H. 117, 138
 Klimavicius, V. 66
 Kliuikov, A. 143
 Knite, M. 93, 139
 Knoks, A. 85, 90, 169
 Koc, Husnu 49, 130
 Kodu, Margus 25
 Kohutych, A. 110
 Kojima, Seiji 112
 Kokhan, O. 134
 Kokhan, O. P. 141
 Kook, Mati 25
 Kooser, Kuno 25
 Korjik, M. 27
 Korjus, Ove 25
 Korsaks, V. 145
 Kostiv, Yu. 117
 Kotomin, E. 123, 175
 Kotomin, E. A. 127
 Kotomin, E. A. 48, 57, 126, 166
 Kotomin35
 Kovalov, A. 136
 Kozlova, A. P. 58
 Kozlovskiy, A. 74
 Krack, Matthias 180
 Krainyukova, N. 123
 Krauze, A. 51
 Kravtsov, A. 51, 172
 Krieke, G. 36, 157, 160, 170

Kriekē, Guna 149, 161, 162
 Krikis, K. E. 90
 Krunks, M. 62
 Krzmann, M. Macek 127
 Kucinskis, G. 92
 Kucinskis, Gints 76
 Kudrevicius, T. 115
 Kudryavtseva, I. 40
 Kuk, Edwin 25
 Kukovecz, Ákos 131
 Kulda, J. 31
 Kulmatova, D. 88
 Kundzins, K. 116, 156
 Kundzins, Maris 113
 Kurenya, A. 84
 Kuzhir, P. 84, 135, 140, 178
 Kuzmin, Alexei 22, 180
 Lamberti, P. 178
 Lapcinskis, L. 50, 93, 100
 Larin, A. 75
 Laukaitis, Giedrius 94
 Laurinavicius, K. 86
 Leimane, M. 99
 Lengyel, K. 41
 Lesnicenoks, P. 85, 90, 169
 Levchenko, G. G. 120
 Li, Quanjun 120
 Liakh, M. V. 176
 Lyakhov, D. 178
 Lickevich, A. 146
 Liedienov, N. A. 120
 Linarts, A. 100
 Lisitsyn, V. 148
 Lisovskij, O. 170
 Lityagin, Georgiy 70
 Liubachko, V. 65
 Lomach, M. 91
 Luizys, P. 81
 Lukosevics, I. 85, 90, 169
 Lukša, A. 56
 Lupascu, D. C. 124
 Lushchik, A. 30, 146, 163, 182
 Lust, Enn 25
 Macutkevicius, J. 84, 114, 133, 135, 137, 140, 178
 Maczka, M. 159
 Magomedov, A. 80
 Majchrowski, Andrzej 70
 Makarenko, I. 166
 Makoed, I. I. 120
 Makowska-Janusik, M. 177
 Malinauskas, M. 16
 Malinovskis, U. 88, 147
 Malnieks, K. 50, 100
 Mamedov, A. M. 49
 Mamedov, Amirullah M. 128, 129, 130, 179
 Maratova, A. 146
 Mastrikov, Yu. 166
 Mastrikov, Yu. A. 48, 126, 127
 Matukas, J. 133
 Mazeika, K. 121, 122
 Medulych, M. 108
 Medvids, A. 60
 Mehta, N. 111
 Meisak, D. 135, 140
 Mekys, A. 60
 Merijs-Meri, R. 136
 Myasnikova, L. 146, 182
 Miasojedovas, S. 151
 Michels, D. 178
 Mikhaleva, E. A. 106
 Mikla, V. 111
 Mikolášek, M. 24
 Milavec, J. 61
 Milianas, Armantas 54
 Millers, D. 150
 Minkovich, V. 111
 Mironova-Ulmane, N. 157
 Molak, A. 114
 Möller, Priit 25
 Molnar, A. 89, 108, 110, 111
 Mosunov, A. V. 63
 Mukhurov, N. 103
 Muktepavela, F. 156
 Muktepavela, Faina 34
 Mussakhanov, D. 148
 Nagyné-Kovács, T. 62
 Nagirnyi, V. 40, 41
 Nargelas, S. 27
 Navickas, M. 159
 Nazeeruddin, M. K. 82
 Neacsu, E. I. 72
 Nedzinskas, R. 42
 Nekrašas, Nerijus 132
 Nesterova, I. 92
 Niaura, G. 98, 122
 Nikitina, J. 37, 38
 Norkus, M. 98
 Novickovas, A. 86
 Nurk, Gunnar 25
 Okotrub, A. 84
 Oleaga, A. 65
 Olekhovich, N. M. 64, 143
 Olins, R. 85, 90
 Olšauskaitė, V. 97
 Omelkov, S. 40
 Ondrejka, P. 24
 Onufrijevs, P. 60
 Opuchovic, O. 64
 Orlovskii, Yu. V. 39
 Ozbay, Ekmel 49, 128, 129, 130, 179
 Ozer, Zafer 128, 129
 OZER, Zafer 179
 Ozols, Haralds 161
 Padarauskas, A. 97
 Pakalniškis, A. 104
 Palaimiene, E. 64, 114, 137
 Palaz, Selami 128, 130
 Pankratov, V. 20
 Pankratov, Vladimir 58
 Partin, G. 167
 Pashchenko, A. V. 120
 Pashkevich, Yu. G. 29
 Pavlovskaya, E. 160
 Peckus, Domantas 19
 Petruleviciene, M. 77
 Piecha, Julita 70
 Pietrzak, T. 142
 Pilipavicius, J. 55, 77
 Piskunov, S. 169, 170
 Pištšev, Aleksandr 39
 Pleckaityte, G. 77
 Plyushch, A. 115, 178
 Podust, G. 181
 Pogodin, A. 134
 Pogodin, A. I. 141
 Pogrebnyak, V. G. 120
 Politova, E. D. 63
 Popescu, A. M. 72
 Poplauskas, R. 147
 Popov, A. 123
 Popov, A. I. 57, 117, 138, 157, 163, 164, 165, 166
 Pöppel, A. 159
 Poryvkina, Larisa 43
 Porotnikova, N. 167
 Pralgauskaite, S. 133
 Prieditis, G. 163
 Prikulis, J. 88, 147
 Prudnik, A. 103
 Pudža, Inga 180
 Pukiene, S. 56
 Purans, J. 35, 47
 Pushkarev, A. V. 64, 143
 Puust, L. 41, 157
 Puust, Laurits 154
 Radyush, Y. V. 64
 Radyush, Yu. V. 143
 Rakstys, K. 82
 Ramalis, L. 38
 Razumiene, J. 78

Rebane, O. 46
 Rebane43
 Řeháček, V. 24
 Rekštytė, S. 16
 Rešetič, A. 61
 Rimkute, G. 78
 Rodnyi, P. 34, 156
 Roy, S. 40
 Roleder, Krystian 70
 Romet, I. 40, 41
 Rubanik, jr. V. 91
 Rubanik, V. 91
 Rudskoy, Andrey 70
 Rupasov, S. I. 58
 Rusevich, L. L. 126, 127
 Ruska, R. 36, 170
 Ruska, Rihards 149
 Saaring, J. 40
 Sadovskaya, N. V. 63
 Sahoo, P. P. 24
 Sahu, Manisha 131
 Saksl, K. 143
 Salak, A. N. 29, 33, 64, 124, 143
 Salazar, A. 65
 Salkus, T. 142
 Sanghyun, P. 82
 Sarakovskis, A. 36, 157
 Sassenberg, U. 46
 Saveliev, D. 96
 Scajev, P. 151
 Schaefer, S. 133, 137
 Scherer, T. A. 165
 Schmidt, W. G. 159
 Sedelnikova, O. 84
 Seeman, V. 163
 Selskis, A. 115, 137, 140
 Senko, M. 150
 Shablonin, E. 163
 Shenderova, O. 133
 Shibayama, N. 82
 Shilin, A. 91
 Shunkeyev, K. 146, 182
 Shur, V. Ya. 69
 Shvartsman, V. V. 64, 124
 Sildos, I. 41, 157
 Sildos, Ilmo 154
 Sirutkaitis, V. 41
 Skaudžius, R. 98, 104, 144
 Skliutas, E. 16
 Skorodumova, N. V. 35
 Skuja, L. 99
 Sluban, M. 61
 Smarsly, Bernd M. 131
 Smits, K. 153
 Smits, Krishjanis 34
 Snarskis, G. 55
 Solomon, A. 111
 Solovjovas, Arnoldas 112
 Souliou, Sofia - Michaela 70
 Sprugis, E. 87
 Spustaka, A. 150
 Sriubas, Mantas 94
 Staliunas, K. 37, 38
 Stefanovich, S. Yu. 63
 Sternberg, Andris 113
 Sternbergs, A. 116
 Stocka, J. 181
 Strugovshchikov, Evgenii 39
 Studenyak, I. 134
 Studenyak, I. P. 141
 Stulnikov, A. 34
 Subacius, L. 60
 Suchanek, G. 67
 Suchodolskis, A. 42
 Sugak, D. 157
 Sun, Li - Chuan 52
 Surovovs, K. 172
 Sutka, A. 100
 Svirskas, Š. 112, 115, 118
 124
 Szilágyi, I. M. 62
 Šakinytė, I. 78
 Šalkus, T. 134, 141
 Ščajev, P. 60
 Šetkus, A. 56
 Šimenas, M. 159, 178
 Šul'ová, K. 143
 Šulskus, Juozas 54
 Šutka, A. 50, 93
 Tagantsev, Alexander 70
 Tamanis, E. 156
 Tamošiūnas, V. 86
 Tamulaitis, G. 27
 Tamulevicius, Sigitas 19
 Tamulevicius, Tomas 19
 Tatar, Dalibor 131
 Tatarchuk, D. D. 120
 Teselko, P. 181
 Tichy-Rács, É. 41
 Timoshkov, Yu. 75
 Timpmann, K. 41
 Tipaldi, Ciro F. 168
 Tolenis, T. 38
 Tretjak, M. 133
 Trinkler, L. 20, 36, 42, 145, 151, 153, 170
 Trinkler, Laima 149
 Trukhin, A. 20
 Tsai, Tsung - Ming 52
 Tsyhyka, M. 110
 Tsukada, Shinya 112
 Ubaev, Zh. 182
 Ubizskii, S. B. 157
 Umek, P. 61
 Urpelainen, Samuli 25
 Usseinov, A. 74
 Vagapova, E. A. 39
 Vaitkevicius, A. 27
 Vaitukaityte, D. 80
 Vaivars, G. 79, 87, 169
 Valdniece, D. 142
 Valeikiene, L. 73
 Vanetsev, A. 40
 Vanetsev39
 Varapnickas, S. 16
 Vasylychshyn, I. 138
 Vasylieva, A. 181
 Venevcev, I. 156
 Venevtsev, I. 34
 Vengris, M. 41
 Vestli, Mihkel 25
 Vetcher, A. 44, 75
 Vieira, D. E. L. 29, 33
 Vieira, J. M. 29, 33, 64
 Vilciauskas, L. 55, 77
 Virbulis, J. 51, 172
 Vysochanskii, Yu. 45, 65, 108, 110, 118, 119
 Višniakova, S. 59
 Vlasov, M. 167
 Volyniuk, D. 95
 Volnyanko, E. 140
 Volperts, Aleksandrs 76
 Vorobiov, S. 143
 Vosylius, Ž. 86
 Wang, Qin 23
 Wei, Ziyu 120
 Winiarz, Piotr 94
 Zahn, D. R. T. 177
 Zalar, B. 61
 Zalga, A. 142
 Zamaraitė, I. 65, 118
 Zarin, A. 155
 Zarkov, A. 104, 122
 Zavickis, D. 175
 Zelca, Z. 101
 Zhang, Huotian 54
 Zhyvulka, A. 72
 Zicans, J. 136
 Ziganova, M. 136
 Zolotarjovs, A. 150, 153, 156
 Zvejnieks, G. 126, 127, 175
 Žilinskas, A. 59